Author:
Maheri, M. R

Title:
Vibration damping in composite/honeycomb sandwich beams.

VIBRATION DAMPING

IN

COMPOSITE/HONEYCOMB SANDWICH BEAMS

by

M. R. MAHERI

A dissertation submitted for the Degree of Doctor of Philosophy at the University of Bristol,
Department of Mechanical Engineering
March 1991

Errata

Page 24

The second term in **Eqn. (3.1.b)** should be

$$k(\frac{\partial^2 w}{\partial x^2})$$

Page 25

The second term in **Eqn. (3.5.b)** should be

$$b^2 s^2 W$$

Page 28

The last term in **Eqn. (3.18)** should be

$$\frac{P}{\alpha} C_3 \sin(b\beta\zeta)$$

Page 34

Middle of the page, the reference "Mead, 1968" should be changed to "Mead and Markus, 1969"

Page 50

In the last sentence of the first paragraph, the expression "...in the second mode..." should be changed to "...in higher modes...".

Page 83

In the third sentence of the fourth paragraph, the expression "... with the core thickness **(Eqns. (3.23))**." should be changed to "...with the core thickness **(Eqn. (3.42))**."

Page 96

The correct form of **Eqns. (6.31)** and **(6.32)** are, respectively, as follows

$$\Psi_y = \frac{8\Psi_t}{C_{11}^* N^3} \sum_{k=1}^{N/2} n^2 (n^2 C_{11}^* + m^2 C_{12}^* - mnC_{16}^*)(C_{11}^* Q_{11}^k + C_{12}^* Q_{12}^k + C_{16}^* Q_{16}^k)(k^3 - (k-1)^3)$$

$$\Psi_{xy} = \frac{8\Psi_h}{C_{11}^* N^3} \sum_{k=1}^{N/2} mn(2mnC_{11}^* - 2mnC_{12}^* - (m^2 - n^2)C_{16}^*)(C_{11}^* Q_{11}^k + C_{12}^* Q_{12}^k + C_{16}^* Q_{16}^k)(k^3 - (k-1)^3)$$

Page 137

The correct form of **Eqns. (B.13)** and **(B.14)** are, respectively, as follows

$$k_1 = \frac{1}{3}(1 - \frac{192}{\pi^5}\frac{h}{w} \sum_{n=1,3,5,\ldots}^{\infty} \frac{1}{n^5} \tanh(n\pi w/2h))$$

$$G = \frac{4\pi^2 f_n^2 J_{bar}}{k_1 w h^3} \times L$$

The sentence in between **Eqns. (B.13)** and **(B.14)** should be changed to "Then, **Eqns. (B.1), (B.4)** and **(B.12)** give..."

Manohar 20/9/1994

Memorandum

The accompanying dissertation entitled "Vibration damping in composite/honeycomb sandwich beams" is submitted in support of an application for the degree of Doctor of Philosophy in Engineering at the University of Bristol.

The dissertation is based on independent work by the candidate - all contributions from others have been fully acknowledged within the dissertation. The supervisor's contribution was that normally made at a British University.

None of the work described has been, or is being, submitted for any other degree or diploma to this or any other University.

I hereby declare that the statements in this memorandum are true.

Mohammad Reza Maheri

March 1991

Acknowledgements

I wish to express my sincere gratitude to Prof. R.D. Adams for his invaluable supervision and assistance throughout the course of this work.

I am also grateful to the other academic and technical staff of the Department of Mechanical Engineering for their advice and assistance and in particular, to Mr. B. Smith and Mr. J. Skinner for their considerable effort in developing the test-rigs and preparing the specimens.

Thanks are also due to Mrs. M. Singh for her interest in the subject and many helpful discussions, and to Mr. J. Bishopp of Ciba-Geigy for his general assistance and providing some of the specimens.

I would like to acknowledge the assistance always readily offered by the staff at the Computer Centre, especially Dr. I. Stewart.

Finally, I wish to acknowledge with gratitude the financial support of the Iranian Ministry for Higher Education for the duration of this work.

Summary

The Timoshenko beam equations have been extended to account for flexural vibration of a shear-sensitive beam carrying a mass, thus enabling steady-state damping measurements to be made when the drive and pick-up mechanisms are attached to the beam. These equations have been subsequently adapted to account for simple bending/shearing of a shear soft sandwich beam. Experimental verifications, regarding the frequencies and mode shapes, have been carried out.

A method has been devised for measuring the dynamic properties of honeycomb in shear. The orthotropic shear properties of a number of aluminium and composite honeycombs have been investigated.

The basic laminated plate theory and the Adams-Bacon damping criterion, have been utilised to predict, from constitutive data, the modulus and the specific damping capacity of unidirectional laminated composite beams with respect to fibre orientation. The necessary experimental verifications have been carried out.

Using the constitutive data of the laminated skins, and the dynamic data of the core, the modified Timoshenko beam equations have been utilised to predict the proportions of the skin/core contribution to the overall damping of a shear soft symmetric sandwich beam with respect to the skin fibre orientation. The necessary experimental verifications regarding the overall damping have been carried out.

List of Contents

List of Tables

List of Illustrations

List of Figures

Nomenclature

N.B. - Most symbols have been defined in the text where they first appear. Otherwise, the following definitions apply.

A	Cross sectional area of solid beam
	Cross sectional area of sandwich beam core
b	Frequency number
c	Thickness of sandwich core
E	Dynamic Young's modulus
f_n	Natural frequency
G	Dynamic shear modulus
h	Total depth of beam or plate
I	Moment of inertia
J	Polar moment of inertia
K	Stiffness
k	Dynamic shear shape factor
L	Beam length
M	Bending moment
	Total mass attached to each end of shear test piece
M_c	Total central mass attached to beam
M_e	Total end mass attached to beam
m	Beam mass
Q	Shearing force
r	Rotary inertia parameter
s	Shear flexibility parameter
t	Thickness of sandwich skin
	Time
U	Maximum strain energy
W	Total lateral deflection
w	Width of beam
	Time dependent total lateral deflection
V_f	Volume fraction of fibre in pre-preg
x	Distance along the beam

ΔU	Energy dissipation per cycle
ε	Normal strain
Γ	Coil sensitivity
γ	Shear rotation
τ	Shear stress
Φ	Bending slope
ϕ	Time dependent bending slope
θ	Angle w.r.t. lay of fibre
ρ	Mass density
σ	Normal stress
υ	Poisson's ratio
ω	Angular velocity
ψ	Specific damping capacity (SDC)

Chapter 1

INTRODUCTION

1.1 General introduction

Earlier sandwich structures were often made from non-metallic skins with corrugated or foam cores; the work on these was mainly focused on the static loading characteristics, and specially on the core stability under lateral load. More modern sandwich structures, made mostly from aluminium and incorporating a honeycomb core, proved to be adequately stiff in that respect but posed problems in dynamic loading, namely, vibration, noise and fatigue. These problems, of particular concern in aerospace applications, are frequently realised only subsequent to some in-service period, and the necessary modifications are usually costly, difficult to implement and often unsatisfactory. Tremendous interest has, therefore, been shown in different aspects of sandwich damping as a means of minimising the resonant vibrations. In aerospace applications particularly, an important consideration has been in the efficient incorporation of damping into the sandwich such that an acceptable weight/stiffness ratio is realised. This task has been made easier with the advent of polymer-based fibrous composites, which provide the designer with a greater degree of flexibility in material selection and even the material design, the so called "tailoring" of properties.

Work on the mechanisms of vibration damping[1] in a sandwich, in so far as the proportion of the contribution of the constituent parts to the overall damping is concerned, has been usually confined to the one-dimensional case, *i.e.* a 'beam'. Initial work on sandwich damping was carried out around 1960 in the U.S.A. The earlier works seem to have suffered

---

[1] By the term 'damping', the specific damping capacity, defined as the ratio of energy dissipation per cycle to maximum strain energy, is meant. Any reference to the 'damping energy', or alternatively the 'energy dissipation', will be made specifically in those terms.

from the lack of a systematic analytical tool. It is, therefore, not surprising to see that, for example, some investigations on the sandwich beam took into consideration one or both of the second order parameters, namely rotary inertia and shear flexibility, but simply assumed an elementary (Bernoulli-Euler) type of mode shape. From the pioneering works of Keer and Lazan [1961] to the work by Bert *et al* [1967] continuous refinements were made to, or utilised in, the theory.

In this last work [Bert *et al*, 1967], the Timoshenko beam equations, uncoupled into the bending slope and total deflection through Huang's procedure [1961], were adapted for a sandwich configuration. Characteristically, the Timoshenko equations stem from an attempt to refine the classical (Love-Kirchhoff) bending theory by adding the deflection due to transverse shear when it no longer can be ignored. Of course, 'exact' analyses have been introduced which, by definition, have their basis not so much in refinements or corrections of simple existing theories, but in a wholesome application of the elasticity theory following, more or less strictly, the patterns developed by the stresses, strains and displacements. As such, these analyses can be expected to offer correct, or more correct, predictions as well as providing an insight into the actual deformations. Inevitably, however, they are also very complex and generally difficult, if not impossible, to apply to other than simple idealised situations. Moreover, these difficulties are not usually matched by the improvements they afford on the 'corrected' theories.

Measurement of damping is a somewhat involved procedure, demanding a great deal of time, care and patience. Repeatability has seldom been the virtue of damping tests, particularly when different test-methods, mathematical models, units *etc*. have been used. Indeed, the *ad hoc* approach to sandwich damping is a characteristic of the early works. Quoting figures for 'facing damping coefficient', having units (in.^{3}/lb-cycle), or 'core damping coefficient', here of units (in.^{2}/lb-cycle), are not uncommon. For that reason,

throughout this work the specific damping capacity, a non-dimensional measure of damping, is used.

Furthermore, in the early works the method for damping measurement was almost exclusively by the free-decay of the resonant amplitude. Although this method is a quick and convenient way of assessing the vibration damping, but compared to the steady-state damping measurement, the free-decay suffers several drawbacks [Adams, 1967]. The chief limitation is the fact that, similar to the bandwidth method, the damping is measured over a varying stress amplitude, making it difficult to quote measurements at a particular stress level for a material with stress dependent damping. The problem becomes more acute for high damping materials where the decay rate is relatively short, and the material non-linearity is large. A further problem may arise in testing composites which show some degree of anisotropy in flexure, where the free vibration is more prone to coupled modes.

Damping measurement in steady-state vibration, on the other hand, can be expected to offer a higher degree of repeatability. Moreover, it can provide a convenient means to measure damping at different stress amplitudes, thereby providing an insight into the material behaviour with respect to stress variation. Indeed, it has been used as a means of non-destructive testing of structural integrity of the material [Adams and Cawley, 1985]. The method's shortcomings include the fact that the shape of the cyclic deformation needs to be explicitly determined, and that forced vibration could, and often does, introduce additional extraneous damping due to the excitation system.

1.2 Objectives

The basic objective of this work was to investigate the mechanisms by which the constituent parts of a symmetric composite-honeycomb-composite sandwich beam contribute to the overall damping in flexural vibration and, by a wider implication, the possibility of predicting the damping properties of such a beam at a given skin fibre orientation from the constituent data based on elasticity and damping properties of the unidirectional composite, and those of the honeycomb. A second, concurrent, objective of the work was to measure the damping of the sandwich in steady-state vibration. These general objectives involved the following

a) extending the modified Timoshenko-Huang beam equations to account for flexural vibration of a loaded shear-soft beam, thus enabling the assessment of the bending/shearing proportion in the beam when the latter is required to be loaded with the drive and pick-up mechanisms,

b) devising a method for measuring the dynamic properties of honeycomb in shear, and

c) verification of the Adams-Bacon damping criterion in predicting the damping properties of a multilayer unidirectional fibrous composite with respect to fibre orientation from the orthotropic elastic data and the damping data of the composite.

Chapter 2

A SURVEY OF LITERATURE

Scope - Given the great volume and the diversity of the work on the dynamics of sandwich structures, one cannot afford but to be very selective regarding the past work. In this chapter, an outline of the work reported on those aspects of the dynamics of sandwich beams which are deemed to be of relevance to the present work, is considered.

2.1 Application of Timoshenko beam equations

Timoshenko [1921] proposed to add the shear effect in the transverse vibrations of prismatic bars. In so doing, he derived the well known and often used equation incorporating both the rotary inertia, which had been introduced earlier by Lord Rayleigh, and the shear effects. Beam analyses which include both these so called 'secondary effects', are generally referred to as Timoshenko beams.

It was not, however, until the lapse of another thirty years or so that the Timoshenko beam analyses were gradually utilised to their best effect. Much of the earlier work on vibration of the Timoshenko beams seems to have suffered complexity or inaccuracy of analysis. The Uflyand analysis, for example, of a semi-infinite Timoshenko beam subjected to a concentrated load has incorrect boundary conditions [Dengler and Goland, 1951], although Miklowitz [1953] shows that Uflyand's solutions are meaningful subject to 'proper interpretation'.

Kruszowski in 1949 was reported to be the first to have applied the correct boundary conditions for use with Timoshenko beam equations [Bert *et al*, 1967] although the correctness of his boundary conditions are not universally acknowledged [Nordby *et al*,

1965][1]. There is, however, agreement [Miklowitz, 1953; Nordby *et al*, 1965; Bert *et al*, 1967] on the validity of another form of the boundary conditions derived by Dengler and Goland [1951]. In analysing the problem of the instantaneous stresses produced in transverse impact of long beams, Dengler and Goland used the Timoshenko beam equations using time dependent boundary conditions. They point out, however, the limitations of the Timoshenko theory ('and in this way achieves its simplicity') inasmuch as, unlike the solutions obtained by the elasticity theory, they do not account for the presence of the higher modes at each wavelength, which are of significance in impact.

Forced vibration of the Timoshenko beams is discussed by Herrmann [1955], who utilised the method first used by Mindlin and Goodman in 1950 in dealing with time dependent boundary conditions.

The first explicit use of Timoshenko's original coupled equations and the associated boundary conditions was probably due to Anderson [1953]. As stated by Anderson and reiterated by Miklowitz [1953], the coupled equations approach results in simplified associated expressions and well defined boundary conditions. Using the classical mode superposition method, Anderson proceeds to solve the Timoshenko beam equations in a series form, in the same way as the solutions of the elementary (Bernoulli-Euler) equations are usually presented. In this, he shows the convenience for routine numerical calculations. Although this view is shared by such as Dengler [1954], Anderson's series solutions have also been subject to criticism as 'cumbersome' [Nordby *et al*, 1965] and somewhat superficial compared to the exact solution [Dengler, 1954].

In his paper, Huang [1961] mentions the complexity and limitations of the analysis by Kruszowski. The latter obtains the frequency equations for clamped-free and free-free beams by solving a complete differential equation in lateral deflection with prescribed

---

[1] Nordby *et al* [1965] state that these incorrect boundary conditions will be discussed in a later section, but no further reference to this point is made.

boundary conditions. Huang, however, proceeds in obtaining two complete differential equations in bending slope and total deflection from the original coupled equations due to Timoshenko [1955 - a slightly modified version of Timoshenko, 1921]. Two solutions are therefore obtained with the constants in the solutions being related through the original coupled equations. The 'novel' features of his approach include homogeneous prescribed boundary conditions. Frequency equations and normal mode functions are obtained for all combinations of fixed, free and simply supported end conditions.

Kobayashi's analysis in 1954 of the vibration of a sandwich beam was reportedly the first of its kind [Nordby *et al*, 1965] but his analysis was based on the elementary equations. Kimel *et al* in 1959 used an energy approach and included both shear and rotary inertia effects but again based their mode shapes on the elementary theory. Raville *et al* [1961] also used an energy approach and included both shear and rotary inertia effects. They derived the frequency equation for a fixed-fixed beam in the form of a series which would converge to a 'good accuracy' with the number of terms used only slightly higher than the number of frequencies required. They attributed the consistently lower experimental values to the difficulty in achieving complete fixity at the ends. Clary and Leadbetter in 1963 were reportedly the first to apply the Timoshenko beam theory to a sandwich beam [Nordby *et al*, 1965] but used the same boundary conditions as Kruszowski.

Nordby *et al* [1965] were apparently the first to apply correctly the Timoshenko-Huang[2] beam equations to a sandwich beam. To this end, they assumed the direct stresses and shear strains were limited to the skins and the core respectively. Their use of the equations so obtained was, however, limited to predicting the natural frequencies and mode shapes of a free-free sandwich beam. Their prediction of the fundamental frequency and the nodal locations of various samples is fairly good with almost all the values within a difference of +1% to +6% from the experimental values.

---

[2] Although not specifically using Huang's method, they arrived at the same equations using the Lagrangian method.

Similar use of the Timoshenko-Huang equations together with what is said to be the Dengler-Goland boundary conditions was made later by Bert *et al* [1967]. Their prediction of the fundamental frequencies and the nodal locations of aluminium and GFRP sandwich beams, with free-free boundary conditions, are generally good with a difference from experimental values of mostly below 5% in frequencies and -2% to +5% in nodal locations[3].

2.1.1 The shear correction factor

From the onset of the derivation of Timoshenko's beam equations, controversy has existed about the characteristic nature of what is usually known as the shear correction (or shape) factor. The shear correction factor, usually represented by k, is defined as the ratio of the mean shear stress over the beam cross section to the maximum shear stress occurring at the neutral axis, and stems from the assumption of uniformity of shear stress distribution over the cross section in deriving the Timoshenko beam equations. In the static analysis of the deflection of a solid and uniformly loaded beam with rectangular cross section it is readily shown that the parabolic nature of the shear distribution will require that k be 2/3 [4]. Initially, it was simply assumed that this value also applied to the dynamic problems [Timoshenko, 1921], only to be modified later to an empirical value of 8/9 [Timoshenko, 1922]. The inadequacy of the static value of k for dynamic problems has been mentioned in several works [Mindlin, 1951; Goodman and Sutherland, 1951; Mindlin and Deresiewicz, 1953; Dengler and Goodman, 1954; Cowper, 1966; Whitney, 1973 *etc.*] where it is generally pointed out a more complicated nature of shear distribution, especially at higher frequencies, due to the presence of inertia forces. There is, however, less unanimity in an alternative definition for the shear correction factor. Roughly speaking, there seem to be two general approaches in tackling the factor k. Expressions have been derived which find k either

---

[3] A persistent misrepresentation of the expressions for α and β has been noticed in the paper by Bert *et al*, as well as in Wilkins [1965] which is believed to be the original source for this paper. In both cases the term (r^2-s^2) in the expressions appears with the first power while this term should be of the second power.

[4] Even this definition of the static value of k has been subject to criticism. See [Cowper, 1966].

through equating the shear dominant frequencies of vibration [Mindlin, 1951] or relate k to the Poisson's ratio through the application of the elasticity theory [Mindlin, 1951; Goodman, 1951; Cowper, 1966].

Mindlin's approach to the problem seems to have been the most popular of all, and many workers who subsequently used the Timoshenko beam equations followed this approach in one way or another. In a paper [1951] concerning the two dimensional analysis of plate vibration, analogous to the one dimensional Timoshenko beam analysis, he postulated to find the factor k in such a way that the first pure thickness-shear frequency predicted by the Timoshenko beam (or in his case plate) equations equals the frequency of the first pure shear mode of vibration according to the exact three-dimensional theory of elasticity. For a beam with rectangular cross section, these frequencies are, respectively, given as

$$\omega_s^2 = kAG/\rho I$$

$$\omega_s^2 = (\pi/h)^2 (G/\rho)$$

where A, G, ρ, I and h are the cross sectional area, shear modulus, density, second moment of area and depth of the beam respectively. The first frequency is readily obtained by setting to zero the lateral displacement amplitude, $w_{(x,t)}$, in the Timoshenko beam equations (*Appendix (C)*), while the second frequency follows from the equations of the waves of distortion in an elastic medium [Timoshenko and Goodier, 1951]. Equating these frequencies will result in $k=\pi^2/12$ (=0.822), which is also the value obtained by Mindlin for a simply supported plate.

Mindlin's reasoning for this procedure was based on the fact that at the frequencies of the first thickness-shear mode, there is a strong coupling between the flexural and thickness-shear modes [Mindlin and Deresiewicz, 1955]. In the same paper [1951], using classical plate theory, he derives an expression relating the k factor to Poisson's ratio in which the former ranges from 0.76 to 0.91 for a range of the latter from 0 to 0.5. Mindlin restates Rayleigh's observation that the classical plate theory gives better results for long

waves and that its departure from the three-dimensional theory of elasticity at shorter wavelengths is almost entirely due to the transverse shear deformation.

In a somewhat similar way to Mindlin's first method, Goodman [1951] derived a cubic equation for the case of a simply supported beam in which k is found in terms of Poisson's ratio. For a Poisson's ratio of 0.33, this equation yields $k = 0.869$.

As noted by Goodman [1954] and Mindlin [1955], at lower frequencies the shear stress distribution is not much different from the parabola of statics but, as the frequency increases, owing to inertia forces a "skin effect" dominates in such a way that the shear distribution tends to revert, maximising near the surface and diminishing towards the mid-depth **(Fig. 2.1)**.

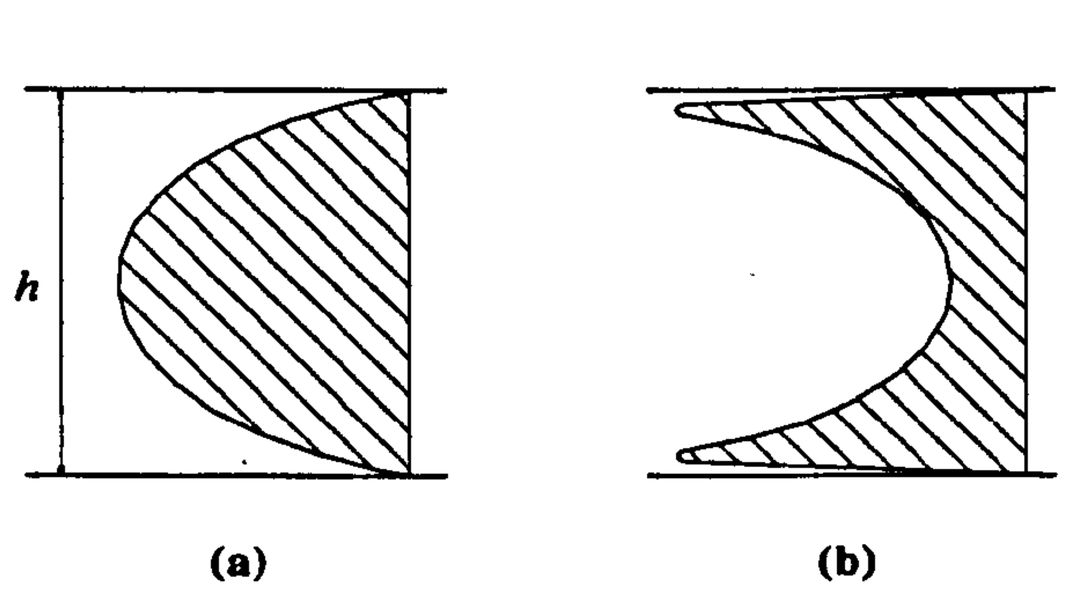

Fig. 2.1 *Schematic shear distribution in solid beams*
a) *static*, **b)** *high frequency dynamic*

In a three-dimensional elasticity analysis of beams, Cowper [1966] derived expressions in terms of Poisson's ratio for various cross-sections which were 'most satisfactory for static and...low-frequency' situations. Cowper's value for k for a rectangular section beam with a Poisson's ratio of 0.33 is 0.851, which is somewhat lower than the corresponding figure obtained by Goodman. The expressions used for shear stress and displacement are said to be applicable to both uniformly loaded beams as well as to end loaded cantilever beams, since in both cases the shear stress distribution is exactly the same. Based on this, Cowper

concludes that the k values would be valid approximations for general loading, including dynamic loading.

It will be noted that whichever method is used regarding the determination of k, the latter will be frequency dependent owing to the inertia effects and therefore, as advocated by most writers and in particular by Mindlin [1951], a choice should be made or compromised depending on the 'relative importance of the two modes of motion' (*i.e.* flexural and thickness-shear).

There seem to be only a few investigators who have undertaken to find the shear correction factor for a skin/core sandwich configuration [Yu, 1959-a, b; Nordby *et al*, 1965; Bert *et al*, 1967], although the shear factor for thick solid laminated beams and plates has been the subject of several investigations [Whitney and Pagano, 1970; Chow, 1971; Kulkarni and Pagano, 1972; Whitney, 1972, 1973; Sun and Whitney, 1973 *etc.*]. In an elaborate analysis in which no otherwise customary assumptions were made, Yu [1959-a] developed stress-strain and displacement equations of motion for the flexure of a symmetric sandwich plate. His method was, in fact, an extension of Mindlin's earlier work on plate theory and reduces to Mindlin's results for a continuum plate as a special case. Similarly, the one-dimensional case is reducible to that of a Timoshenko beam. In much the same way as Mindlin's method, Yu [1959-b] then proceeds to find the thickness-shear frequency equation and equates the frequencies to those obtained from the exact theory of elasticity. His expression for the factor k so obtained involves the skin/core ratios of thickness and density. In the limiting case of very thin skins, k becomes unity, thereby removing the need for a shear correction factor.

Nordby *et al* [1965] applied Mindlin's method in its entirety to a sandwich beam, that is, they adapted the expression for pure shear frequency given by the three-dimensional theory of elasticity for a solid beam by replacing the density with the effective density of a sandwich. Through this procedure, they arrive at an expression for k in terms of the mass, the mass

moment of inertia of the beam, and depth of the core. For a typical sandwich beam, their expression gives a value for k of the order 2. This method was subsequently used by Wilkins [1965].

Bert *et al* [1967], while acknowledging the 'very simplified' nature of the earlier analysis by Nordby *et al*, proceed to replace the expression for the pure shear frequency in that work by the one they obtain through treating the core and the skins as a two degree of freedom system consisting of a shear-type spring bounded between two longitudinally vibrating masses. Their expression for k is a function of mass moment of inertia and width of the beam, density of the skin and depth of the core. They report k values in the range of 1 to 1.4 for typical sandwich constructions. They further propose a second method, based on elasticity analysis, in which the core is treated as a continuous medium. From symmetry, the half depth of the core and one skin are considered as a "shear cantilever" subjected to the lateral vibration of the end mass. The expression for the factor k involves the mass moment of inertia and width of the beam, the depth of the core and the densities of the skin and the core. No typical value for k is reported.

2.2 Damping of composite and sandwich structures

2.2.1 Undamped analysis

Although a considerable amount of work has been carried out on damping of composites, relatively fewer works have been produced specifically on the damping of honeycomb sandwich structures. The earliest reported investigation on the damping properties of these structures was due to Keer and Lazan in 1961 [Bert *et al*, 1967]. They used the elementary theory for their analysis and for this reason the apparently close agreement between the theoretical predictions and experimental results has been subject to scepticism [Nordby *et al*, 1965; Wilkins, 1965].

In a sizeable work on the damping of aluminium honeycomb sandwich beams, James [1962] undertook to demonstrate the feasibility of predicting the damping of the compound beam from that of the constituent parts[5]. He used an energy method to find the frequency and in this he included both rotary inertia and shear effects. Nonetheless, he used a mode shape based on the elementary theory. Basically, his method for predicting the specific damping capacity (SDC) of the compound beam may be written as

$$(\Delta U / U) = (\Delta U_s / U) + (\Delta U_c / U) ,$$

where ΔU and U are the damping energy per cycle and the maximum strain energy respectively, and the suffixes s and c refer to the skin and the core. Assuming the damping energy to be proportional to the square of the stress amplitude (the 'linear damping' mechanism), then all the terms in this equation will have the square of the displacement amplitude of vibrations as a factor and this is cancelled out. The SDC will then be a function of the beam geometries, Young's modulus of the skin, the shear modulus of the core, and the damping properties of the skin and of the core. An assumed logarithmic decrement, that of

---

[5] As acknowledged by James [1962], the method is originally due to C.W. Norris of the Forest Products Laboratory, U.S.A.

soft aluminium (0.00052, equivalent to a SDC of 0.1%) was used throughout. The damping of the compound beam was then found experimentally by the free-decay method.

James' predictions of the fundamental frequency are only fair (within -0.8% to +12% of the experimental values) but the damping predictions are generally poor (mostly with a difference of between 30 to 70%, and as high as +134%, from the experimental values). James attributes the poor damping predictions to the 'simple theory' used.

Nordby *et al* [1965] used the free-decay method to measure the damping of honeycomb sandwich beams. All their samples had GFRP skins. The honeycomb cores were either GFRP or aluminium. They present their damping results as a function of stress amplitude in the skins which they measured using strain gauges.

Bert *et al* [1967] used the same basic method as James [1962] in order to predict the damping of a honeycomb sandwich beam. However, they followed the method of Nordby *et al* [1965] (as outlined in **2.1**), to derive the frequency equation and mode shape of a free-free beam. They further used the mode shape equation to derive expressions for maximum strain energy as well as the damping energy per cycle for the skins and the core, and thus proceeded in predicting the damping of the beam from those of the constituent parts. All their samples consisted of GFRP skins and either GFRP or aluminium honeycomb core. They used reported values for the damping coefficients of the skin and the core, although they measured the skin modulus at compatible frequencies. They found a difference of mostly above 20% and as high as -37% between the predicted and the measured damping of the compound beam. Nonetheless, in comparison, their predictions are an improvement on James' results.

2.2.2 Damped analysis

The flexural vibration of another sandwich configuration, that of a beam consisting of alternate layers of elastic and viscoelastic material, was analysed by DiTaranto [1965]. As such, DiTaranto's analysis involved the concept of complex notation where the elastic and viscous behaviour of a linearly viscoelastic material are modelled as separable quantities and are treated as real and imaginary components of a complex set. DiTaranto derived a sixth-order linear homogeneous differential equation of motion in terms of the longitudinal displacements. Expressions were subsequently obtained for the natural frequencies and loss factor of a freely vibrating beam. These expressions implied that the variation of the loss factor with natural frequency was independent of the end conditions and mode shapes but dependent on the cross-sectional geometry and material properties of the elastic and viscoelastic materials.

It is noted that in DiTaranto's analysis, all the damping is attributed to the viscous shearing of the viscoelastic layer. Furthermore, unlike the 'undamped' analyses in which the equations of motion are derived for materials assumed to be Hookean elastic, in analyses such as DiTaranto's the viscoelastic nature of the modulus will lead to equations of motion for a damped material, and consequently to damping dependent frequencies.

In a later work [DiTaranto and Blasingame, 1967], the results of the earlier analysis [DiTaranto, 1965] were used to obtain generalised plots, presenting loss factors and various eigenvalues as functions of a parameter in terms of the average mass density of the composite beam, the Young's modulus of the elastic layer, the elastic component of the viscoelastic shear modulus, the thickness of the elastic layer, and the reduced natural frequency.

Agbasiere and Grootenhuis [1968] question the notion of a complex shear modulus since it 'presupposes' a definite stress-strain law. Their own analysis of a damped sandwich beam concerns a general stress-strain relation applicable to both linear and non-linear materials.

This approach, however, resulted in a complex set of four simultaneous equations of the twelfth order which were cumbersome to solve in a closed form and therefore they resolved to a numerical method (Finite Differences). Nonetheless, their expressed confidence in the analysis is backed by some experimental results which they obtained from tests on a three and a five layer beam. These results indicate fairly accurate predictions of resonance curves and mode shapes especially for the three layer and the lower modes of the five layer beam.

Mead and Markus [1969] derived a sixth order differential equation of flexural motion, analogous to that of DiTaranto's, in terms of the transverse displacements (the DTMM, DiTaranto-Mead-Markus equation as it was subsequently called by Mead [1982]). The equation in terms of the transverse displacements, they argue, will allow a better physical understanding of the problem, especially in the presence of transverse loading. Furthermore, they challenge DiTaranto's use of the complex stiffness notation for free vibration and state that DiTaranto's resonant frequencies and modes can, in fact, be attributed to a special class of forced vibration. All the other conclusions of DiTaranto, and in particular his assertion that the curve of the loss factor versus frequency is independent of the end conditions, are reiterated in this work; although one particular result in a later work [Mead and Markus, 1970] seemed to imply otherwise. In their analysis, Mead and Markus [1969] make the usual simplifying assumptions which include no through thickness straining and negligible normal stresses in the core and shear strains in the skin compared to the same quantities in the skin and in the core respectively. In these analyses, the rotary inertia effects are also ignored. In fact, for a sandwich beam with a shear stiff core, the DTMM equation will reduce to the elementary Bernoulli-Euler equation [Mead, 1982]. The DTMM equation is refined in a later work [Mead, 1982] by including the shear and longitudinal inertia effects in the skins. The rotary inertia effects were still ignored.

In an analytical work much reminiscent of the earlier one [1961], Huang and Huang [1971] incorporated viscoelastic damping in the Timoshenko beam equations. The viscoelastic

response was based on the standard viscoelastic model. Here, too, the frequency equations and mode functions for different combinations of end conditions were obtained.

Mead [1972] undertook a theoretical study of the effect of imposing elastic boundary conditions, such as stiffeners and rivets, on the damping of a three layer damped sandwich plate. A constant loss factor (0.3), representing a highly damped viscoelastic layer, is assumed throughout but a wide range of the shear moduli[1] are considered. Computed results are mostly presented as plots of the loss factor of the plates with different boundary conditions versus the shear parameter, the latter being a non-dimensionalised function of the complex shear modulus, Young's modulus of the elastic layer, the plate geometry and Poisson's ratio. Among the conclusions made from these results one is that in the absence of torsional edge constraints, preventing local shearing through riveting would substantially reduce the damping but the latter would increase when torsional constraints are also imposed. Furthermore, torsional constraints on their own would reduce the damping of a soft core sandwich, but would increase that for a stiff core.

A similar analytical study, but this time concerning the effect of boundary conditions on eigensolutions of a sandwich beam, was carried out by Markus and Valaskova [1972]. Frequency equations are obtained for the case of the unrestrained and that of the riveted free end of a cantilever beam. Results showed that, for a relatively soft core sandwich beam, certain nodal shifts relative to Bernoulli-Euler beam occurred in both cases. As expected, no such shifts resulted for a beam with a very rigid core. Analogous effects were deduced from eigenvalues.

Soovere [1973] investigated the dynamic response and sonic fatigue resistance of honeycomb sandwich panels with graphite fibre skins. In all cases, Nomex cores were used. A coil attached to the panel and a magnet provided the means of excitation, while strain

---

[1] The expression for the complex shear modulus on the second page should read $G^*(1+i\beta)$, according to the definitions in the appendix.

gauges attached to the panel were used to measure the response. Results showed that the damping in the fundamental mode of the graphite sandwich panel was of about the same order as that in an aluminium sandwich panel or in a graphite fibre solid beam. Increased damping in other modes was attributed to the acoustic radiation. Free-free tests on PRD-49 (Kevlar) panels showed a five fold increase in damping of these panels compared to the graphite panels. Apart from the possibility of higher material damping, it was concluded that the increase in damping was possibly due to different fibre orientations (woven and unidirectional respectively) and the methods of fabrication (hand-lay-up and pre-cured sheets).

Similar conclusions were reported in a later work [Soovere, 1984]. It was found that acoustic radiation was the major contributor to damping in stiffened honeycomb panels. The material damping was found to be very low in CFRP sandwich honeycomb panels. On the other hand, damping in Kevlar sandwich honeycomb panels was found to be quite significant and it was shown to be resin dominated. The damping due to fasteners was shown to be small.

2.3 Works of Adams *et al*

Much of the present work has been based, directly or otherwise, on the earlier works by Adams and co-workers . In this section, the relevant works are outlined.

Adams and Bacon [1973-a] described an apparatus suitable for measurement of material damping in steady-state flexural vibration. The apparatus, it is reported, can be used to measure accurately specific damping capacities as low as 0.1% over a frequency range of 100 to 800 Hz and a temperature range of -50 to +200° C. A pair of coils attached to opposite surfaces in the mid-span of a free-free beam and placed in magnetic fields provide the means for excitation and measurement of displacement. The Bernoulli-Euler beam equations with the appropriate boundary conditions are used to derive expressions for the frequency equation, mode shape function, and maximum strain energy. These equations, together with a knowledge of the displacement amplitude and the excitation energy per cycle were then used to compute the SDC, maximum surface stress and the dynamic Young's modulus of the beam. Tests were carried out in air and in a vacuum, and over a range of temperatures. The results showed that air damping was of significance for low damping high modulus materials such as Duralumin and CFRP along the fibre direction, and that it increased linearly with displacement amplitude. The mode shapes were accurately predicted.

Guild and Adams [1981] developed a new technique for the measurement of the SDC of beams in flexure. This technique was basically a rearrangement of the earlier method of Adams and Bacon [1973-a] in that here the two coils were attached to the beam ends. Unlike the centrally driven arrangement in which only symmetric modes can be attained, this technique can produce both symmetric as well as anti-symmetric modes. The relevant expressions, based on Bernoulli-Euler beam equations, are derived for the new boundary conditions. Good agreement was obtained between theoretical and experimental mode shapes for the fundamental mode and it was shown that the rotary inertia of the end coils did not have any significant effect on the mode shapes. However, compared to the results

obtained by Adams and Bacon [1973-a], their results of tests on Duralumin seems to indicate a relatively significant increase in extraneous damping (from 0.1% to 0.5%). This result is somewhat unexpected since, as will be shown in the present work (*Chapter 5*), the end driven arrangement should lead to reduced extraneous damping.

Theoretical predictions and experimental results of the variation of dynamic properties in flexure as well as torsion of unidirectional composites with respect to fibre volume fraction are presented by Adams and Bacon [1973-b]. They adopt Hashins's expression for the complex moduli as a function of fibre volume fraction for their prediction of axial and longitudinal shear damping. The damping is assumed to be stress independent and due to the matrix only. A torsion pendulum apparatus was used to find the longitudinal shear damping of the matrix. Their prediction of the flexural damping involves first finding the damping due to interlaminar shear from a knowledge of the longitudinal shear damping of the matrix and the Bernoulli-Euler mode shape. Their flexural damping is then given by the sum of the axial and interlaminar shear damping. Attempts were made to compare their predictions of damping in longitudinal shear with those of Hashin and the results, normalised with respect to the matrix damping and presented as functions of fibre volume fraction, show that although both theories overestimate the damping, the predictions of Adams and Bacon are closer to the experimental points. Flexural damping results are presented as functions of aspect ratio of the beam. As expected, predictions based on the law of mixtures alone do not account for the variation of damping with aspect ratio and also they underestimate the damping by a large margin. However, predictions which do take into account the interlaminar shearing closely follow the trend of the experimental results but still generally underestimate them by a significant margin.

The effect of fibre orientation and laminate geometry on the dynamic properties of free-free composite beams are discussed by Adams and Bacon [1973-c]. They postulate a criterion for damping in which the damping energy in an elastically deformed element of the material is a

function of three independent components of energy dissipation in the x, y and xy directions. Hence, with respect to the fibre direction, x, of a unidirectional layer of composite, the total damping would be a function of longitudinal, transverse and longitudinal shear damping. Using the constitutive equations of flexure of a laminated plate, they derived expressions for the effective Young's modulus and flexural damping of a free-free laminated beam. For simplicity of solution, stress independent damping across the beam thickness was assumed. The bending-twisting coupling was ignored and tests on the off-axis unidirectional CFRP beams showed that the induced torsion due to the above mentioned coupling was relatively small. The Young's modulus and flexural damping results are presented as functions of fibre orientation. The predictions of modulus and damping in the case of unidirectional beams are reasonably good, but for the angle plied laminates they generally overestimate the damping, increasingly so towards the 45° orientation. It was shown that neither the modulus nor the damping was significantly affected by the width of the beam.

In a similar but more refined work, Ni and Adams [1984] obtained expressions for predicting the dynamic Young's modulus and specific damping capacity of laminated fibrous beams in flexure. Using the Adams-Bacon apparatus, tests were carried out on both CFRP and GFRP free-free beams in the fundamental mode. Beam samples were either cut at different orientations from a unidirectional laminate ('off-axis' beams), or cut at different orientations from cross and angle ply laminates ('general ply' beams). Experimental results were closely predicted. Comparing their damping results with those of Adams and Bacon [1973-c], Ni and Adams attribute their improved predictions to the fact that, unlike the former work, they did take into account the bending-twisting coupling.

Based on Adams-Bacon [1973-c] damping criterion, Lin *et al* [1984] included the 'damped element' in a Finite Element program originally due to Cawley [1978]. The analysis is basically the plate equivalence of that of Ni and Adams [1984] for beams, although the

Adams-Bacon damping criterion was extended to five terms including the two transverse shears (the *xz* and *yz* shears, *x* and *y* being the in-plane co-ordinates). Parabolic variation of transverse shear over the thickness was assumed. Flexural frequencies, mode shapes and damping of various free-free angle plied symmetric composite plates were both measured and computed. Damping measurements were obtained from the frequency domain transient response using a dynamic analyser capable of 'zooming' on a resonance peak, a method developed earlier by Lin and Adams [1984]. Both GFRP and CFRP plates were tested for up to the sixth flexural mode. An examination of their results show that the frequencies were predicted to within a range of -14% to +20% of experimental values but mostly less than 6%. The damping results were predicted to within a range of -34% to +18%, but again mostly much lower. They further produced plots for prediction of frequencies and damping from the geometry of the plate.

The work of Ni *et al* [1984] concerns the prediction of dynamic properties of hybrid layered composite beams and plates. They adapted the earlier analysis [Ni and Adams, 1984] for the damping prediction of beams, and used the damped element Finite Element program of Lin *et al* [1984] for prediction of the plate modal damping. In both cases the test pieces were made up of symmetrically oriented layers of GFRP sandwiched between CFRP. The predictions of the effective Young's modulus and the SDC of the beams are in most cases in good correlation with the experimental results. They attribute the few deviations to the lack of perfect fibre alignment. The predictions of the first six flexural frequencies of the plates are mostly within 5% of experimental values, while the damping results fall within an error range of -45% to +9%.

Chapter 3

FLEXURAL VIBRATION OF A TIMOSHENKO BEAM

Scope - In this chapter, equations are developed for flexural vibration of a centrally loaded free-free beam using Timoshenko beam equations. The developed equations are then adapted for prediction and measurement of damping in a free-free sandwich beam. Theoretical and experimental results, regarding frequencies and mode shapes of both solid and sandwich beams, will be presented. The case of a symmetrically end loaded beam will also be considered. Application of these equations with regard to damping of sandwich beams is considered in later chapters.

3.1 Loaded beams[1]

The flexural vibration of both centrally loaded and end loaded beams is of particular interest in steady-state measurement of damping, since in forced vibration of the beam, it may be required that the latter is point-loaded in the centre, or loaded symmetrically at both ends, by the drive and/or pick-up mechanisms [Adams and Bacon, 1973-a; Guild and Adams, 1981]. Depending on the load, this would change the frequency and mode shape of the beam, which should be taken into account when computing the kinetic or strain energies. Moreover, whereas for a monolithic beam within the limits of linear damping, the damping is theoretically independent of any load carried by the beam (also verified experimentally by Wren and Kinra [1989-a]), for a hybrid structure such as a shear-soft sandwich beam the load will have an influence on the proportion of the skin/core contribution to the overall damping of the beam.

---

[1] The terms 'load' and 'loaded' are somewhat loosely used in this work; but they are used for conciseness and are meant to merely refer to a mass attached to a point on the beam.

The case of the centrally loaded Timoshenko beam applies to the present work and its analyses will be considered here in some detail. The analyses of a symmetrically end loaded Timoshenko beam are given in *Appendix (C)*.

Explicit representations of the developed equations will be extremely lengthy and therefore unwarranted; substitutions will have to be used.

3.2 Constitutive equations

The coupled equations for the total deflection, w, and the bending slope, ϕ, of a uniform beam in harmonic flexural vibration are given as [Timoshenko, 1955]

$$EI \frac{\partial^2 \phi}{\partial x^2} + k\left(\frac{\partial w}{\partial x} - \phi\right) AG - \rho I \frac{\partial^2 \phi}{\partial t^2} = 0 \qquad \textbf{(3.1.a)}$$

$$\rho A \frac{\partial^2 w}{\partial t^2} - k\left(\frac{\partial^2 w}{\partial^2 x} - \frac{\partial \phi}{\partial x}\right) AG = 0 \qquad \textbf{(3.1.b)}$$

where

$$w = W e^{i\omega t} \qquad \textbf{(3.2)}$$

$$\phi = \Phi e^{i\omega t} \qquad \textbf{(3.3)}$$

and W and Φ are normal functions of x.

Eliminating, in turn, ϕ and w from **Eqns. (3.1)**, the following two uncoupled differential equations of flexure are obtained [Huang, 1961] [2]

$$EI \frac{\partial^4 w}{\partial x^4} + \rho A \frac{\partial^2 w}{\partial t^2} - \left(\rho I + \frac{E\rho I}{kG}\right) \frac{\partial^4 w}{\partial x^2 \partial t^2} + \frac{\rho^2 I}{kG} \frac{\partial^4 w}{\partial t^4} = 0 \qquad \textbf{(3.4.a)}$$

$$EI \frac{\partial^4 \phi}{\partial x^4} + \rho A \frac{\partial^2 \phi}{\partial t^2} - \left(\rho I + \frac{E\rho I}{kG}\right) \frac{\partial^4 \phi}{\partial x^2 \partial t^2} + \frac{\rho^2 I}{kG} \frac{\partial^4 \phi}{\partial t^4} = 0 \qquad \textbf{(3.4.b)}$$

---

[2] See *Appendix (C)* for a complete derivation.

Substituting for ϕ and w in **Eqns. (3.1)** and **(3.4)**, the latter are respectively reduce to

$$s^2 \frac{\partial^2 \Phi}{\partial \zeta^2} - (1 - b^2 r^2 s^2)\ \Phi + \frac{1}{L}\frac{\partial W}{\partial \zeta} = 0 \qquad \textbf{(3.5.a)}$$

$$\frac{\partial^2 W}{\partial \zeta^2} + b^2 s^2 \Omega - L\frac{\partial \Phi}{\partial \zeta} = 0 \qquad \textbf{(3.5.b)}$$

$$\frac{\partial^4 W}{\partial \zeta^4} + b^2 (r^2 + s^2) \frac{\partial^2 W}{\partial \zeta^2} - b^2 (1 - b^2 r^2 s^2) W = 0 \qquad \textbf{(3.6.a)}$$

$$\frac{\partial^4 \Phi}{\partial \zeta^4} + b^2 (r^2 + s^2) \frac{\partial^2 \Phi}{\partial \zeta^2} - b^2 (1 - b^2 r^2 s^2) \Phi = 0 \qquad \textbf{(3.6.b)}$$

where

$$\zeta = \frac{x}{L} \qquad \textbf{(3.7)}$$

$$b^2 = \frac{\rho A L^4 \omega^2}{EI} \qquad \textbf{(3.8)}$$

$$r^2 = \frac{I}{AL^2} \qquad \textbf{(3.9)}$$

$$s^2 = \frac{EI}{kAGL^2} \qquad \textbf{(3.10)}$$

The solutions to the uncoupled **Eqns. (3.6)** are given as

$$W = C_1 \cosh(b\alpha\zeta) + C_2 \sinh(b\alpha\zeta) + C_3 \cos(b\beta\zeta) + C_4 \sin(b\beta\zeta) \qquad \textbf{(3.11.a)}$$

$$\Phi = C_1' \sinh(b\alpha\zeta) + C_2' \cosh(b\alpha\zeta) + C_3' \sin(b\beta\zeta) + C_4' \cos(b\beta\zeta) \qquad \textbf{(3.11.b)}$$

where

$$\alpha, \beta = \frac{1}{\sqrt{2}} \left\{ -, + \ (r^2+s^2) + \left[(r^2-s^2)^2 + \frac{4}{b^2} \right]^{1/2} \right\}^{1/2} \qquad \textbf{(3.12)}$$

Only one half of the coefficients C_i , C_i' $_{(i = 1..4)}$ are independent since W and Φ are coupled by **Eqns. (3.1)**. The dependent coefficients are found by substituting **Eqns. (3.11)** in either one of the coupled **Eqns. (3.5)** and equating the coefficients of individual hyperbolic and trigonometric terms. The following are found from **Eqn. (3.5.b)**

$$C_1' = \frac{b}{L}\left(\frac{\alpha^2+s^2}{\alpha}\right) C_1 \quad ; \quad C_2' = \frac{b}{L}\left(\frac{\alpha^2+s^2}{\alpha}\right) C_2$$

$$C_3' = -\frac{b}{L}\left(\frac{\beta^2-s^2}{\beta}\right) C_3 \quad ; \quad C_4' = \frac{b}{L}\left(\frac{\beta^2-s^2}{\beta}\right) C_4 \qquad \textbf{(3.13)}$$

Equations **(3.11)** and their first derivatives may now be written as

$$W = C_1 \cosh(b\alpha\zeta) + C_2 \sinh(b\alpha\zeta) + C_3 \cos(b\beta\zeta) + C_4 \sin(b\beta\zeta) \qquad \textbf{(3.14.a)}$$

$$\frac{\partial W}{\partial x} = \frac{b}{L}\left[C_1 \alpha \sinh(b\alpha\zeta) + C_2 \alpha \cosh(b\alpha\zeta) - C_3 \beta \sin(b\beta\zeta) + C_4 \beta \cos(b\beta\zeta)\right] \qquad \textbf{(3.14.b)}$$

$$\Phi = \frac{b}{L}\left[\frac{\alpha^2+s^2}{\alpha}\left(C_1 \sinh(b\alpha\zeta) + C_2 \cosh(b\alpha\zeta)\right)\right.$$

$$\left. - \frac{\beta^2-s^2}{\beta}\left(C_3 \sin(b\beta\zeta) - C_4 \cos(b\beta\zeta)\right)\right] \qquad \textbf{(3.14.c)}$$

$$\frac{\partial \Phi}{\partial x} = \left(\frac{b}{L}\right)^2 \left[(\alpha^2+s^2)\left(C_1 \cosh(b\alpha\zeta) + C_2 \sinh(b\alpha\zeta)\right)\right.$$

$$\left. - (\beta^2-s^2)\left(C_3 \cos(b\beta\zeta) + C_4 \sin(b\beta\zeta)\right)\right] \qquad \textbf{(3.14.d)}$$

3.3 Centrally loaded beam

A free-free Timoshenko beam with a point load at the mid-span **(Fig. 3.1)** vibrating in a symmetric normal mode is subjected to the following conditions

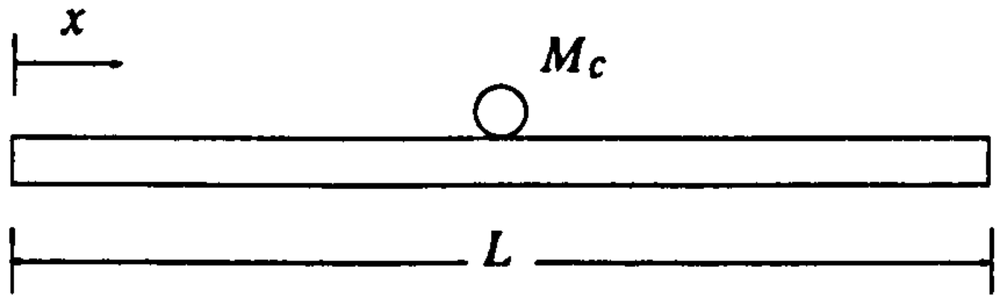

Fig. 3.1 *Centrally loaded beam*

i) at $x = 0$, $EI \dfrac{\partial \Phi}{\partial x} = 0$ (zero bending moment)

$$\text{so,} \quad \frac{\partial \Phi}{\partial x} = 0 \tag{3.15.a}$$

ii) at $x = 0$, $kAG\gamma = 0$ (zero shearing force)

$$\text{so,} \quad \left(\frac{\partial W}{\partial x} - \Phi \right) = 0 \tag{3.15.b}$$

iii) at $x = \dfrac{L}{2}$, $\Phi = 0$ (zero bending slope) **(3.15.c)**

iv) at $x = \dfrac{L}{2}$, $kAG\gamma - \dfrac{M_c}{2} \omega^2 W = 0$ (shear force induced due to M_c)

$$\text{so,} \quad kAG \left(\frac{\partial W}{\partial x} - \Phi \right) - \frac{M_c}{2} \omega^2 W = 0$$

$$\text{or} \quad kAG \left(\frac{\partial W}{\partial x} \right) - \frac{M_c}{2} \omega^2 W = 0 \tag{3.15.d}$$

In **Eqns. (3.15)**, the local effects due to the point load [Timoshenko and Goodier, 1951] have been neglected.

Equations (3.15) will respectively give the following four equations

$$C_1(\alpha^2+s^2) - C_3(\beta^2-s^2) = 0 \qquad \textbf{(3.16.a)}$$

$$-C_2\,\beta\,s^2 + C_4\,\alpha\,s^2 = 0 \qquad \textbf{(3.16.b)}$$

$$\beta(\alpha^2+s^2)(C_1\sinh(H) + C_2\cosh(H)) - \alpha(\beta^2-s^2)((C_3\sin(T) + C_4\cos(T)) = 0 \qquad \textbf{(3.16.c)}$$

$$\frac{mL}{b^2s^2}\;\frac{b}{L}\;[C_1\,\alpha\sinh(H) + C_2\,\alpha\cosh(H) - C_3\,\beta\sin(T) + C_4\,\beta\cos(T)]$$

$$-\frac{M_c}{2}\;[C_1\cosh(H) + C_2\sinh(H) + C_3\cos(T) + C_4\sin(T)] = 0 \qquad \textbf{(3.16.d)}$$

where

$$H = b\alpha/2 \qquad ; \qquad T = b\beta/2$$

Equations (3.16) may be written in the form

$$[A]\,\{C_i\} = 0 \qquad (i = 1,4)$$

For a non-trivial solution, the determinant of the matrix of coefficients *[A]* is set to zero. This will give the following frequency equation for the centrally loaded free-free Timoshenko beam

$$\frac{(\alpha^2+\beta^2)}{\beta^2(\beta^2-s^2)}\;\frac{m}{b}\;\cosh(H)\sin(T) - \frac{(\beta^2-\alpha^2)}{\alpha\beta^2}\;\sinh(H)\sin(T)\;\frac{M_c}{2} +$$

$$\frac{(\alpha^2+\beta^2)}{\alpha\beta(\alpha^2+s^2)}\;\frac{m}{b}\;\sinh(H)\cos(T) + \frac{(\alpha^2+s^2)^2+(\beta^2-s^2)^2}{\beta(\alpha^2+s^2)(\beta^2-s^2)}\;\cosh(H)\cos(T)\;\frac{M_c}{2} + \frac{M_c}{\beta} = 0 \qquad \textbf{(3.17)}$$

From **Eqns. (3.16)**, three of the constants C_i may be found in terms of the fourth one, for example C_3, giving, from **Eqn. (3.14.a)**, the total deflection, W, as

$$W = \frac{\beta^2-s^2}{\alpha^2+s^2}\;C_3\cosh(b\alpha\zeta) + \frac{P}{\beta}\;C_3\sinh(b\alpha\zeta) + C_3\cos(b\beta\zeta) + C_3\sin(b\beta\zeta) \qquad \textbf{(3.18)}$$

where

$$P = \frac{(\beta^2-s^2)(\alpha\sin(T) - \beta\sinh(H))}{(\beta^2-s^2)\cos(T) + (\alpha^2+s^2)\cosh(H)} \qquad \textbf{(3.19)}$$

Now, if W is known at some positive x, then C_3 can be found from **Eqn. (3.18)**. Consequently, the constants C_1, C_2, C_4 will be known, and the quantities W, $\partial W/\partial x$, Φ and $\partial\Phi/\partial x$ can be found explicitly for any x.

3.3.1 Strain energy

The total strain energy stored in flexure of a Timoshenko beam is assumed to consist of two separable strain energies, one due to bending about the y axis **(Fig. 3.2)**, and the other due to shearing between the xy planes.

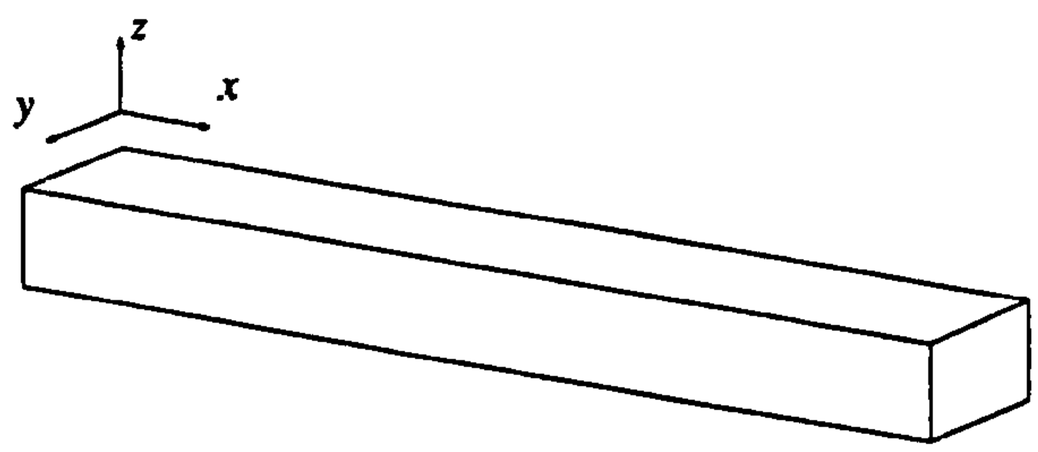

Fig. 3.2 *Beam co-ordinate system*

Thus

$$U = U_b + U_s = \int_0^L \frac{EI}{2} \left(\frac{\partial\Phi}{\partial x}\right)^2 dx + \int_0^L \frac{kAG}{2} \left(\frac{\partial W}{\partial x} - \Phi\right)^2 dx \qquad (3.20)$$

To avoid complex algebra in the above integration, it will be convenient to rewrite **Eqns. (3.14)** in the same general form, *viz*

$$W = A\cosh(b\alpha\zeta) + B\sinh(b\alpha\zeta) + C\cos(b\beta\zeta) + D\sin(b\beta\zeta) \qquad (3.21.a)$$

$$\frac{\partial W}{\partial x} = \frac{b}{L}\left[A\cosh(b\alpha\zeta) + B\sinh(b\alpha\zeta) + C\cos(b\beta\zeta) + D\sin(b\beta\zeta)\right] \qquad (3.21.b)$$

$$\Phi = \frac{b}{L}\left[A\cosh(b\alpha\zeta) + B\sinh(b\alpha\zeta) + C\cos(b\beta\zeta) + D\sin(b\beta\zeta)\right] \qquad (3.21.c)$$

$$\frac{\partial\Phi}{\partial x} = \left(\frac{b}{L}\right)^2 \left[A\cosh(b\alpha\zeta) + B\sinh(b\alpha\zeta) + C\cos(b\beta\zeta) + D\sin(b\beta\zeta)\right] \qquad (3.21.d)$$

where the coefficients A, B, C and D are only locally defined within each individual equation. In terms of C_3 , these coefficients are found as follows

In **Eqn. (3.21.a)**

$$A = \frac{\beta^2 - s^2}{\alpha^2 + s^2} C_3 \quad ; \quad B = \frac{1}{\beta} P \; C_3$$

$$C = C_3 \quad ; \quad D = \frac{1}{\alpha} P \; C_3 \quad , \qquad \textbf{(3.22.a)}$$

in Eqn. (3.21.b)

$$A = \frac{\alpha}{\beta} P \; C_3 \quad ; \quad B = \alpha \frac{\beta^2 - s^2}{\alpha^2 + s^2} C_3$$

$$C = \frac{\beta}{\alpha} P \; C_3 \quad ; \quad D = -\beta \; C_3 \quad , \qquad \textbf{(3.22.b)}$$

in Eqn. (3.21.c)

$$A = \frac{1}{\alpha\beta} (\alpha^2 + s^2) P \, C_3 \quad ; \quad B = \frac{\beta^2 - s^2}{\alpha} C_3$$

$$C = \frac{1}{\alpha\beta} (\beta^2 - s^2) P \, C_3 \quad ; \quad D = -\frac{\beta^2 - s^2}{\beta} C_3 \quad , \qquad \textbf{(3.22.c)}$$

and in **Eqn. (3.21.d)**

$$A = (\beta^2 - s^2) C_3 \quad ; \quad B = \frac{1}{\beta} (\alpha^2 + s^2) P \, C_3$$

$$C = -(\beta^2 - s^2) C_3 \quad ; \quad D = -\frac{1}{\alpha} (\beta^2 - s^2) P \, C_3 \qquad \textbf{(3.22.d)}$$

3.3.1.1 Strain energy of bending

Strain energy of bending of a Timoshenko beam is given by

$$U_b = \int_0^L \frac{EI}{2} \left(\frac{\partial \Phi}{\partial x}\right)^2 dx \qquad (3.23)$$

Substituting for $\partial\Phi/\partial x$ from **(3.21.d)** and integrating will give

$$\begin{aligned} U_b = EI \left(\frac{b}{L}\right)^3 \Bigg\{ & \frac{b}{4}(A^2 - B^2 + C^2 + D^2) \\ & + \frac{A^2+B^2}{4\alpha} \sinh(2H) + \frac{C^2-D^2}{4\beta} \sin(2T) \\ & + \frac{AB}{2\alpha} \cosh(2H) - \frac{CD}{2\beta} \cos(2T) \\ & + \frac{2}{\alpha^2+\beta^2} \Big[(\alpha AC - \beta BD) \sinh(H) \cos(T) \\ & + (\alpha BD + \beta AC) \cosh(H) \sin(T) \\ & + (\alpha AD + \beta BC) \sinh(H) \sin(T) \\ & + (\alpha BC - \beta AD) \cosh(H) \cos(T) \Big] \\ & - \frac{AB}{2\alpha} + \frac{CD}{2\beta} - \frac{2}{\alpha^2+\beta^2} (\alpha BC - \beta AD) \Bigg\} \end{aligned} \qquad (3.24)$$

where A, B, C and D are given by **Eqns. (3.22.d).**

3.3.1.2 Strain energy of shearing

Strain energy of shearing of a Timoshenko beam is given by

$$U_s = \int_0^L \frac{kAG}{2} \left(\frac{\partial W}{\partial x} - \Phi \right)^2 dx \tag{3.25}$$

Substituting for $\partial W/\partial x$ and Φ from **Eqns. (3.21.b)** and **(3.21.c)**, and integrating will give

$$\begin{aligned} U_s = kAG \left(\frac{b}{L} \right) \Bigg\{ & \frac{b}{4} \left(\hat{A}_{12}^2 - \hat{B}_{12}^2 + \hat{C}_{12}^2 + \hat{D}_{12}^2 \right) \\ & + \frac{\hat{A}_{12}^2 + \hat{B}_{12}^2}{4\alpha} \sinh(2H) + \frac{\hat{C}_{12}^2 - \hat{D}_{12}^2}{4\beta} \sin(2T) \\ & + \frac{A_{12}B_{12}}{2\alpha} \cosh(2H) - \frac{C_{12}D_{12}}{2\beta} \cos(2T) \\ & + \frac{2}{\alpha^2+\beta^2} \Big[(\alpha A_{12}C_{12} - \beta B_{12}D_{12}) \sinh(H) \cos(T) \\ & + (\alpha B_{12}D_{12} + \beta A_{12}C_{12}) \cosh(H) \sin(T) \\ & + (\alpha A_{12}D_{12} + \beta B_{12}C_{12}) \sinh(H) \sin(T) \\ & + (\alpha B_{12}C_{12} - \beta A_{12}D_{12}) \cosh(H) \cos(T) \Big] \\ & - \frac{A_{12}B_{12}}{2\alpha} + \frac{C_{12}D_{12}}{2\beta} - \frac{2}{\alpha^2+\beta^2} (\alpha B_{12}C_{12} - \beta A_{12}D_{12}) \Bigg\} \end{aligned} \tag{3.26}$$

where

$$A_{12}\,,\ B_{12}\,,\ C_{12}\,,\ D_{12} = A_1 - A_2\,,\ B_1 - B_2\,,\ C_1 - C_2\,,\ D_1 - D_2$$

and

$$A_1\,,\ B_1\,,\ C_1\,,\ D_1 = A\,,\ B\,,\ C\,,\ D$$

as given by **Eqns. (3.22.b)**; and

$$A_2\,,\ B_2\,,\ C_2\,,\ D_2 = A\,,\ B\,,\ C\,,\ D$$

as given by **Eqns. (3.22.c)**.

3.3.2 Bending and shearing stresses

For the first mode of vibration, the maximum bending moment of a free-free Timoshenko beam is given by

$$M_{mx} = EI \left(\frac{\partial \Phi}{\partial x}\right)_{(x=L/2)} \tag{3.27}$$

where $\partial\Phi/\partial x$ is given by **Eqn. (3.21.d)**, in which the constants A, B, C and D are given by **Eqns. (3.22.d)**.

The maximum bending stress is then given by

$$\sigma_{mx} = \frac{M_{mx}}{I} \frac{h}{2} \tag{3.28}$$

The shearing stress is given by

$$\tau = kG \left(\frac{\partial W}{\partial x} - \Phi\right) \tag{3.29}$$

where $\partial W/\partial x$ is given by **Eqn. (3.21.b)**, in which the constants A, B, C and D are given by **Eqns. (3.22.b)**; and Φ is given by **Eqn. (3.21.c)**, in which the constants A, B, C and D are given by **Eqns. (3.22.c)**.

3.3.3 Bernoulli-Euler simplification

The Timoshenko beam equations are readily simplified to the elementary Bernoulli-Euler beam equations by setting the rotary inertia and the shear parameters to zero. Thus

$$r = s = 0$$

and **Eqn. (3.12)** will now give

$$\alpha = \beta = 1 / \sqrt{b}$$

The following relationship is then established between the quantity b in this work and λ in [Bacon, 1973]

$$\sqrt{b} = \lambda \tag{3.30}$$

Once relevant substitutions are made, **Eqns. (3.17)** and **(3.18)** will be identical to **Eqns. (18)** and **(19)** in [Bacon, 1973]. The total strain energy in **Eqn. (3.20)** will now reduce to the strain energy due to bending, U_b , and the latter will reduce to the corresponding **Eqn. (21)** in [Bacon, 1973].

3.3.4 Sandwich beam

By making certain simplifying assumptions, it is possible to adapt the Timoshenko beam equations for a symmetric skin-core-skin sandwich beam [Bert *et al*, 1967]. To that end the following usual assumptions are made

1 - the in-plane modulus of the core is negligible compared to that of the skin

2 - transverse shearing of the skin is negligible compared to that of the core

Both assumptions have been almost universally accepted as justified and have been utilised in sandwich analyses [James, 1962; DiTaranto, 1965; Mead, 1968; Donnell, 1976 *etc.*] By virtue of the assumption 1, the bending stiffness *EI* in **Eqns. (3.8)** and **(3.10)** will be that of the skins only. In accordance with the Timoshenko beam equations, this implies the skins bend about the sandwich neutral axis and, therefore, undergo uniaxial tension or compression. Also implicit within this assumption is that the mass of the beam is concentrated in the skins, which is a justifiable assumption since the skins are usually several times heavier than the core. From assumption 2, the area *A* will be the cross sectional area of the core only. The rotary inertia parameter, *r*, is now expressed in terms of $I_{s\,c}$, the effective moment of inertia of the whole beam cross section. Based on these assumptions, **Eqns. (3.8)** to **(3.10)** can be written as follows

$$b^2 = \frac{mL^3\omega^2}{(EI)_s} \tag{3.31}$$

$$r^2 = \frac{I_{s\,c}}{A_c L^2} \tag{3.32}$$

$$s^2 = \frac{(EI)_s}{(kAG)_c L^2} \tag{3.33}$$

where suffixes s and c indicate skin and core respectively, and I_{sc} is given by

$$I_{sc} = I_s + \frac{\rho_c}{\rho_s} I_c \tag{3.34}$$

In the above formulae, the contribution from the adhesive layer[3] to the overall stiffness has been considered negligible. Furthermore, as Mindlin [1951] showed, the rotary inertia is almost entirely negligible 'over the whole wave-length spectrum'. For a typical sandwich beam, the shear parameter, s , is of the order of ten times or more of the rotary inertia parameter, r . In view of this and the fact that, unlike the skin and the core, the geometry of the adhesive layer is not well defined, the rotary inertia due to the adhesive layer has also been ignored.

The question arises as to the value of the factor k (**Eqn. (3.33)**), following the above procedure. Unfortunately, the equations so developed for a sandwich configuration throw little light on the actual shear distribution over the beam cross section, even more so than their original counterparts intended for a solid beam. The first of the above assumptions implies that the shear distribution over the core cross section is uniform [Mead and Markus, 1969], which in turn leads to a shear correction factor of unity. However, the notion of unity of the factor k which follows the assumed uniformity of shear distribution over the core cross section would be somewhat misleading, for it ignores the shearing stresses which must exist in the skins if the implication of shear discontinuity at the interface is to be avoided [Chow, 1971]. On the other hand, if it is assumed that the shear stress over the whole sandwich cross section is uniform, then this implies that the shear stress in the skin is of the same order as that in the core, regardless of the core shear rigidity. As pointed out by Mead [1981], this cannot be the case when the core is soft, in which case the skins tend to bend independently of the core and about their own neutral axis. Moreover, as was already pointed out, when the beam is subjected to dynamic loading, the inertia effects could

---

[3] In this work, the 'adhesive layer' refers specifically to the adhesive used in the skin/core interface.

become the determining factors in the shear distribution, although this is expected to occur only at high frequencies.

An assumption which is implicit within the Timoshenko beam equations is that no through thickness straining in the beam occurs, such that the outmost planes, for example, remain plane and at the same fixed distance regardless of the state of the stress. This assumption, however, is not exclusive to the Timoshenko equations and follows from the classical theory of bending; it is another 'almost universal' assumption in sandwich analyses. Even in solid beams there is a variation in this distance due to the Poisson's effect alone [Donnell, 1976; Whitney, 1987]. For a sandwich configuration in particular, where the core is of relatively small elastic modulus, this assumption imposes a constraint on the deformation, in that it allows no localised bending of the skins which can be expected to occur because of such as point loads. By the same token, the state of stress within the skins is assumed to be unaffected by any compressive stresses which may develop in the core [Benjamin, 1969].

When the beam is point loaded in the mid span, the situation becomes somewhat more complicated. From symmetry, there cannot be shearing in the mid span while, immediately beyond this point, an abrupt change in the shear stress should take place. Timoshenko and Goodier [1951] elaborate on local effects at the point of loading and show that the shear deflection for a length along the beam approximately equal to half of the depth of the beam is slightly less than when assuming a uniform stress distribution.

It is apparent from the foregoing that an analytical determination of the shear correction factor for a sandwich configuration becomes extremely difficult and subject to the particular circumstances. Subsequently, the determination of the factor k in the present work was approached from a different view point, *i.e.* , that its value be such that the experimentally determined natural frequencies are accurately predicted. It is suggested that this procedure is justifiable as far as the damping of a shear soft sandwich is concerned since, in effect, the

factor k is manipulated so that the correct ratio of the bending/shearing stiffness, as indicated by the sandwich natural frequency, is achieved.

However, in so doing, the physical meaning of the factor k will be somewhat removed from its original definition. A more appropriate definition for k would now be 'a correction factor' taking into account mainly the assumption of the uniformity of the shear distribution, but also the extent of the validity of the assumptions made for the particular test piece, as well as the extent of the idealisation of the test piece, that is, such factors as the accuracy of the skin and core moduli, the structural integrity of the sandwich, the degree of the contribution of the adhesive layer to the overall stiffness and, as correctly pointed out by James [1962], the uniformity of the adhesive distribution since, depending on the particular mode shape and nodal locations, a non-uniform distribution would lead to overrating or underrating the experimental natural frequency.

3.3.5 Computation of the specific damping capacity

By definition of the SDC, the damping energy in the skins undergoing uniaxial tension/compression is given by

$$\Delta U_s = \int_{v_s} \sigma_x \varepsilon_x \psi(\sigma_x)\, d(v_s) \tag{3.35}$$

where v_s is the skin volume and $\psi(\sigma_x)$ indicates the stress dependency of damping, ψ. For a uniform beam in flexure, the integration over the width is trivial. However, the stress varies over both depth as well as length in the beam. Hence, in order to take the stress dependency of SDC into account, it will be necessary to establish the relationship between the SDC and σ_x for the particular material under test. Adams and Bacon [1973-a] outlined a method in which this relationship may be established through the use of a polynomial of a suitable degree fitting the experimentally determined SDC versus stress points, the coefficients of which are determined experimentally. Such a procedure would subsequently involve numerical integration of the integral in **Eqn. (3.35)**. White and Abdin [1985] postulated a

similar approach. However, most workers in the past have assumed a damping mechanism in which the damping energy is proportional to the square of the stress amplitude [Keer and Lazan, 1961; Bert *et al*, 1967; Adams and Bacon, 1973-a, b, c; Ni and Adams, 1984 *etc.*]. In this case, the SDC will be independent of the stress amplitude and the so called 'linear' damping mechanism applies. Keer and Lazan [1961] reported that stress independency of the SDC was recorded in all their tests on aluminium honeycomb sandwich beams. This assumption can be justified only for the lower regions of stress amplitude where many materials show a constant damping with the variation of stress. Lazan [1968] showed that for metals, the linear damping existed for amplitudes of cyclic stresses up to 80% of the fatigue limit, at which point the material showed both nonlinear and stress-history-dependent damping.

For most engineering purposes, a low stress amplitude and, therefore, linear damping may be assumed. In this case, **Eqn. (3.35)** may be written as

$$\Delta U_s = \psi_s \int_{v_s} \sigma_x \varepsilon_x \, d(v_s) \tag{3.36}$$

where ψ_s is the flexural damping of the skin as determined experimentally from a uniform beam of the same material. The integral has already been evaluated as **Eqn. (3.24)**, in which for a sandwich beam, **Eqns. (3.31)** to **(3.34)** apply.

Similarly, the energy dissipation in the core is given by

$$\Delta U_c = \int_{v_c} \sigma_{xz} \varepsilon_{xz} \psi(\sigma_{xz}) \, d(v_c) \tag{3.37}$$

As mentioned earlier, the assumption of negligible direct stresses in the core will lead to the assumption of uniform shear distribution over the core cross section. Therefore, the integration over both width and depth of the core becomes trivial, and the stress dependency of the SDC is integrated over the length only. The experiments of Keer and Lazan [1961],

however, showed that the linear damping mechanism was also present in the core. With this assumption, **Eqn. (3.37)** may be written as

$$\Delta U_c = \psi_c \int_{v_c} \sigma_{xx}\, \varepsilon_{xx}\, d(v_c) \qquad (3.38)$$

where ψ_c is the core shear damping. The integral has already been evaluated as **Eqn. (3.26)** where, for a sandwich beam, the quantity kAG will be that of the core.

The SDC of the beam is, therefore, given by

$$\psi = \frac{\psi_s U_b + \psi_c U_s}{U_b + U_s} \qquad (3.39)$$

where U_b and U_s are given by **Eqns. (3.24)** and **(3.26)** respectively. It is noted that both U_b and U_s have the square of the displacement amplitude as a factor and, therefore, ψ will be independent of the amplitude of vibration.

For measuring the SDC in steady-state flexural vibration, **Eqn. (3.39)** may be re-written as

$$\psi = \frac{\Delta U}{U_b + U_s} \qquad (3.40)$$

In *Appendix (A)*, a method is described for measuring the energy dissipation per cycle ΔU, as well as the displacement amplitude of vibration at mid-span, thereby obtaining the values of U_b, U_s and the maximum bending stress, σ_{mx} **(Eqn. (3.28))**, for a given mid-span displacement amplitude.

For a slender solid beam of the Bernoulli-Euler type, **Eqn. (3.40)** is reduced to

$$\psi = \frac{\Delta U}{U_b} \qquad (3.41)$$

where U_b is found following the arguments given in section **3.3.3**. This equation may be used for measuring the SDC of the thin skins bending on their own.

For predicting the individual contributions of the skin and of the core to the total SDC of the sandwich beam, **Eqn. (3.39)** may be rearranged as

$$\psi = \frac{\psi_s U_b}{U_b + U_s} + \frac{\psi_c U_s}{U_b + U_s} \tag{3.42}$$

where the first term is the contribution to damping of the skins in bending, and the second term is the contribution to damping of the core in shearing. In *Chapter 4*, a method for measuring the core shear damping, ψ_c , will be described.

3.3.6 Computer implementation

The above analyses were put into computer code using *FORTRAN 77*. One program, *BEAM4.FOR*, was written for the computation of the SDC using either the Adams-Bacon or the Adams-Guild test rigs. Both solid as well as sandwich beam options have been implemented. A second program, *BEAM6.FOR*, was written specifically for the eigen solution of either beam.

The roots are found successively, and are first roughly located by a simple scanning of the frequency equations ((3.17), (C.11) (*Appendix (C)*) and (C.15)), detecting the change of sign. A sufficiently small sampling interval, found by experience, is used. In the case of the end loaded beam, the frequency equation is discontinuous and the roots are situated at alternate occurrence of the change of sign. Subsequent pin-point location of the root is carried out using the secant iterative method.

On request, both programs can provide the user with a file containing a detailed description of a data file, thereby avoiding the need for a separate 'user-guide'. A desk-top computer can be conveniently used to run either one of the programs.

3.4 Experimental verifications

Few explicit experimental investigations of the Timoshenko beam analysis have been reported in the literature. Huang [1961] presented a graph of the ratio of the Timoshenko to Bernoulli-Euler frequencies as a function of the rotary inertia for the first five modes of a clamped-free beam. He noted that the eigen solution of a Timoshenko beam was 'highly transcendental'. Such a frequency chart would, therefore, allow corrections to be made to the frequencies obtained by the elementary analysis. Bert *et al* [1967] carried out a series of theoretical investigations on the effect of the beam length on the fundamental frequency and nodal locations of different sandwich beams.

Here, the Timoshenko beam equations were subjected to a series of experimental investigations. Frequency and mode shape tests were carried out on solid as well as on honeycomb sandwich beams. Only free-free end conditions, which are the only end conditions applicable to this work, were considered. Both loaded as well as unloaded beams were tested. Solid beams of two different cross sections and materials were investigated. The specifications of the solid beams are tabulated in **Table (3.1)**.

Table (3.1) *Solid beams specifications*

Material	Designation	m (g)	L (mm)	w (mm)	h (mm)
Duralumin	AL1	257.2	600.0	12.65	12.65
Duralumin	AL2	292.1	600.5	19.00	9.50
Mild steel	MS1	748.4	600.0	12.65	12.65
Mild steel	MS2	858.6	600.0	19.10	9.60

where m, L, w and h are mass, length, width and thickness of the beams respectively.

The Young's modulus of the solid beams was found dynamically. First, the fundamental frequency in flexure was found for a slender beam sample. Using the Bernoulli-Euler option

in the program *BEAM4.FOR*, and hence avoiding the need for a shear correction factor at this stage, the dynamic Young's modulus was computed according to **Eqn. (3.8)**. It will be noted that, for a sufficiently slender beam, the elementary and improved analysis give almost identical results for the first frequency. The Poisson's ration, υ , for aluminium and for mild steel was assumed to be 0.35 and 0.28 respectively. The shear modulus, G, was calculated from $E = 2\,G\,(1 + \upsilon)$. The elastic properties of the solid beams are tabulated in **Table (3.2)**.

Table (3.2) *Elastic properties of solid beams*

Designation	E (GPa)	G (GPa)	υ
AL1	67.34	24.94	0.35
AL2	69.88	25.88	0.35
MS1	207.36	81.00	0.28
MS2	207.08	80.89	0.28

The sandwich beams were pre-fabricated symmetric all-aluminium beams using identical skin, core and adhesive (Ciba-Geigy's 'Aerolam M-Board'). The specifications of the sandwich beams are tabulated in **Table (3.3)**.

Table (3.3) *Aluminium sandwich beams specifications*

Designation	m (g)	L (mm)	w (mm)	c (mm)	t (mm)	*cell size* (mm)
2SB1-X	72.2	400.0	40.0	12.5	0.57	6.25
2SB2-X	87.2	400.0	40.0	25.0	0.57	6.25
2SB3-X	67.4	270.0	39.5	33.5	0.57	6.25
2SB4-X	120.9	400.0	40.0	50.0	0.57	6.25

where c and t are the thicknesses of the honeycomb core and the skin respectively, and *cell size* refers to the diameter of the inscribed circle of the hexagonal honeycomb cell.

No raw material was available for the skin of the sandwich beam and the manufacturer's figure for the Young's modulus had to be used. The shear modulus of the core (Ciba-Geigy's Aeroweb 5.2,1/4,25-3003) was found using the honeycomb shear test-rig (*Chapter 4*). The shear modulus was found along the ribbon, or *X'*, direction since this was the orientation of the core in the sandwich beam tested. The elastic properties of the sandwich beams are tabulated in **Table (3.4)**.

Table (3.4) *Elastic properties of sandwich beams*

Designation	E_f (GPa)	G_c (GPa)
2SB1,2,3,4-X	69.0	0.285

3.4.1 Natural frequencies

The roots of the frequency **Eqns. (3.17), (C.11)** (*Appendix (C)*) and **(C.15)** will give the frequencies of the centrally and end loaded Timoshenko beam. The frequencies of the unloaded beam are obtained by simply setting $M_c, M_e = 0$ in these equations.

The frequency tests were carried out to within the sensitivity of the equipments available. As far as it was possible, the steady-state technique was used for greater accuracy. An electrodynamic shaker was used for excitation and the amplified signal from a microphone was fed to a voltmeter and an oscilloscope. The resonance frequency was then noted at the maximum reading of the voltmeter. Beyond the limit of the shaker (about 5 kHz), the transient technique was used, taking particular care to tap the sample on the centre so that not to excite any torsional frequencies. The test set-up for the latter method is shown in **Fig. 3.3.**

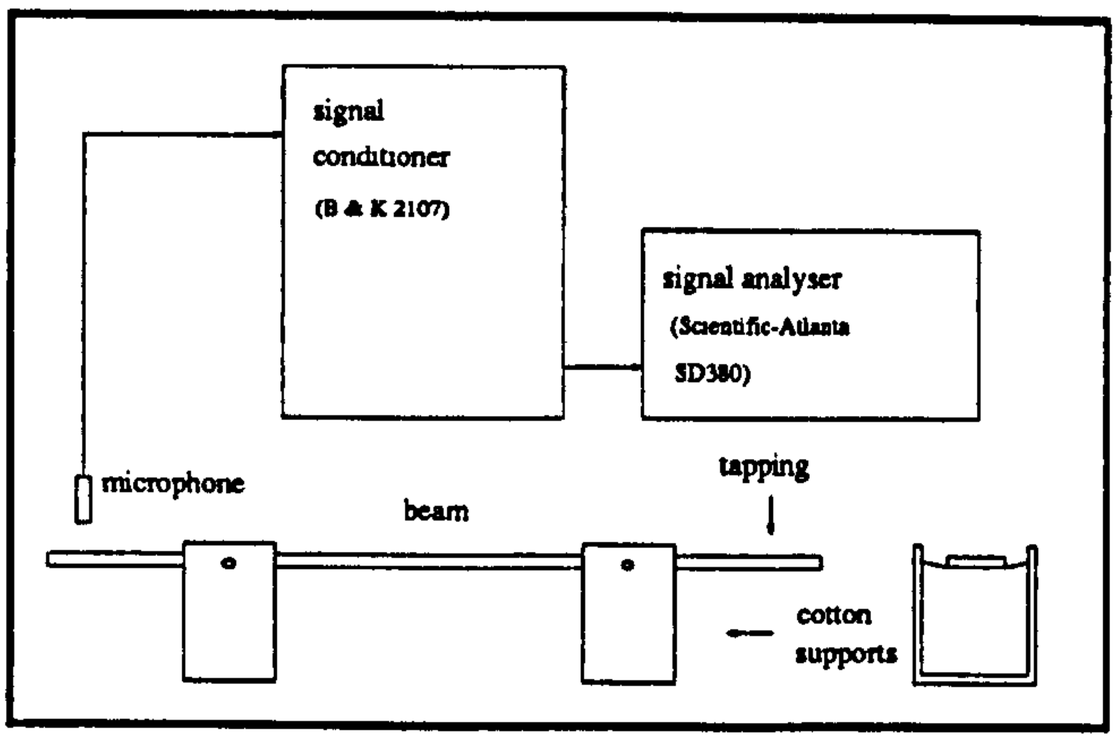

Fig. 3.3 *Transient measurement of natural frequencies*

The test procedure for the transient tests was as follows. The first 25 frequencies were initially computed for the particular beam under test using the 'Timoshenko' option on the *BEAM6.FOR* program, at this stage ignoring the shear correction factor (*i.e. k=1*). The lower frequencies were determined without any filtration. At higher frequencies, the 'Freq. Analysis' option on the signal conditioner was used to filter out the noise at the expected frequency, thus giving a cleaner signal. For some range beyond the range of the signal conditioner (20 kHz), still a reasonable signal could be gained using the 'Auto.' option.

The frequency results are presented in **Figs. 3.5** to **3.19**. For the solid beams, the predicted frequencies were obtained for a shear correction factor of 0.82. For the sandwich beams, the frequencies were obtained for a correction factor which would predict the highest test frequency within ±0.5% (see below). Comparison is also made with the predictions according to the elementary theory. With negligible rotary inertia effects, this theory may be conceived as that for a Timoshenko beam with a shear factor tending to infinity. For both the solid as well as the sandwich beams, the frequency results with unit correction factor are also included. These results, $F_{(k=1)}$, have also been used as basis for normalising the frequencies, F, according to the following criterion

$$\frac{F - F_{(k=1)}}{F_{(k=1)}} \tag{3.43}$$

As such, this quantity represents the percentage error with respect to the frequencies $F_{(k=1)}$. The choice of a theoretical rather than the test frequency as the normalising basis was made to keep any scatter in the test results within the latter. The specific choice of $F_{(k=1)}$ was made on the basis of its significance as the case for 'no shear correction'. All the frequencies are presented as functions of the mode number, the latter being the only common factor as far as the elementary and the improved theories are concerned.

Referring to the results, generally with or without a correction factor, excellent frequency predictions are made by the improved theory. Moreover, it can be seen that the accuracy of predictions are maintained over the whole frequency range. Comparing the results obtained through the two theories, the mainly shear effects which are accounted for in the improved theory are clearly manifested at higher frequencies and in the shorter beams.

As can be seen (**Figs. 3.5** to **3.12**), in the case of the solid unloaded beams, the difference between the predicted frequencies and the test results for either value of k is of any significance only at the top range of frequency. However, there does not seem to be any particular trend in the predictions regarding the two values of the shear factor. For the square section Duralumin beam (**Fig. 3.5**), the $k=0.82$ tends to underestimate the predictions while $k=1$ seems to overestimate the predictions. This trend is seen to be repeated for the rectangular section mild steel beam (**Fig. 3.8**). On the other hand, for the rectangular section Duralumin beam (**Fig. 3.6**) and the square section mild steel beam (**Fig. 3.7**), the $k=1$ and $k=0.82$ frequencies are, respectively, seen to give very accurate predictions, although, as is best shown in the normalised frequencies of **Fig. 3.7**, within each set of these two results, a constant fluctuation between the theoretical and test frequencies occurs, a possible indication of slight frequency dependence of the shear distribution. As expected, for the same mode, the elementary theory leads to a higher percentage of error for the thicker, square section beams, as these experience more shearing (*cf.* elementary results of **Figs. 3.5** and **3.6**, and of **Figs. 3.7** and **3.8**).

In comparing the test results with those obtained with the two values of the shear factor, the impression should be avoided that any one value of k is necessarily a 'better' representation of the shear distribution. Certain assumptions have been made regarding the elastic properties. A value for the Poisson's ratio, for example, has been assumed, and the shear modulus has been found accordingly. Furthermore, it has been assumed that the moduli remain independent of the frequency. A more rigourous investigation, if warranted, would require that both moduli are found at each test frequency, and the theoretical frequencies are found accordingly, a procedure which would bring about further complexities. Clearly then, a limit emerges as to the capacity of the test results in accurate determination of the shear distribution at any particular frequency.

Theoretically, the influence of the decrease in the wavelength on the second order effects should be the same regardless of how the decrease is realised. Then, when increasing the frequencies by progressively shortening the beam, the same trend in the predicted frequencies should be observed regarding different values of k. However, unlike the results of the frequency as a function of mode number, the scatter of the test results observed regarding the frequency as a function of the beam depth/length (**Figs. 3.9** to **3.12**) makes the emergence of any particular trend difficult; although in one particular case (square section mild steel beam, **Fig. 3.11**), a value of unity for the shear factor gives more accurate predictions at high frequencies. However, since the difference between the two results is only marginal and within the range of the experimental errors, again, no firm conclusions can be drawn.

As expected, compared to the results for the unloaded beams, there are some discrepancies in the frequency results of the loaded solid beams (**Figs. 3.13** and **3.14**), more so in the case of the end loaded beam. The discrepancies are believed to be almost entirely due to the extraneous inertia effects. The central load on the Duralumin beam was in the shape of a cylinder with a mass ratio to that of the beam of 0.38. This was bonded along its length

across the width of the beam so that point-loading condition could be achieved. As can be seen from the last few results (**Fig. 3.13**), the theoretical predictions generally overestimate the frequency. However, while the overestimate is consistently larger for the symmetric modes (**Fig. 3.13(a)**), it is relatively small for the anti-symmetric modes (**Fig. 3.13(b)**). The reason for this seems to be due to the fact that in the latter case, the mid-span is laterally stationary. Hence, the extraneous inertia effects brought about by any off-set between the centre of the mass and the mid-span will be smaller for the anti-symmetric modes. It will be noted that, neglecting the in-plane rotary inertia effects of the centre mass, the anti-symmetric frequencies of the centrally loaded and those of the unloaded beam will be the same since in either case the mid-span is laterally stationary. This can be verified by comparing the anti-symmetric frequency results in **Figs. 3.6** and **3.13(b)**. Up to the onset of the discrepancies (mode 12, **Fig. 3.13(b)**), the two frequencies are found to be almost identical.

In the case of the end loaded beam, two identical cubic masses having a total mass ratio to the beam of 0.26 were bonded to the beam at either ends with the edge of the beam positioned half way on the cube surface (**Fig. 3.4**).

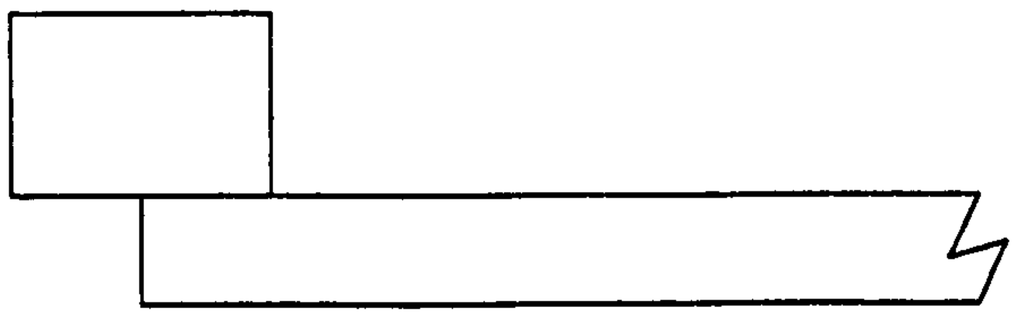

Fig. 3.4 *End loaded beam*

The results (**Fig. 3.14**) indicate much larger discrepancies, and are somewhat inconsistent. There is a fluctuation of test results across the frequency spectrum, initially falling below the predictions, before overtaking the predictions for the higher modes. Dynamically, the end loaded beam is less stable than the centrally loaded beam because of the presence of two loads which makes the achievement of perfect symmetry that much more difficult. To this

must be added the difficulty in achieving point-loading at the beam end and, similarly, in determining the effective length of the beam. At one stage it was noted that a slight misalignment of one end load dropped the third frequency by 8% (from 594 to 545 Hz).

As is evident from **Figs. 3.13** and **3.14**, unlike the unloaded beams, with the loaded beams the fundamental frequency is generally underestimated by both values of $k=1$ and 0.82, a likely indication of a major difference in shear distribution, at least in the fundamental mode, between the loaded and unloaded beams.

The shear effect is much more profound on the frequencies of the sandwich beams, as can be seen by comparing the frequencies obtained by the elementary and the improved theories in **Figs. 3.15** to **3.19**. This is, of course, due to the relative shear softness of the sandwich core. Comparing a typical aluminium honeycomb sandwich with a solid aluminium beam, such as 2SB1-X and AL1 beams specified in section **3.4**, the shear modulus of the former is some 93 times less than the latter. For the same reason, the frequencies are much more sensitive to the shear factor, k . For example, at the highest frequency which could be attained for the unloaded 2SB1-X beam (mode 9, **Fig. 3.15**), a change of k from 1.77 to 1.0 decreases the frequency by some 25% while, in a solid beam and at a comparable frequency number, a change of the same order in the value of k bears almost no consequence on the frequency.

As mentioned earlier, k was selected to predict the highest test frequency which could be attained within ±0.5%. The reason for setting this criterion was based on the argument that the higher modes are more representative of the dynamic shear distribution in the beam since, as advocated by Goodman [1954] and Mindlin [1955], the nature of the shear distribution is different for lower and higher frequencies owing to the inertia effects (section **2.1.1**). Nonetheless, the results here indicate a remarkable accuracy of the predictions over the entire frequency range, especially for thicker beams (**Figs. 3.17** to **3.19**). The persistently close predictions may be due to the lower inertia effects of the sandwich, since these are

primarily due to the skins, and therefore a more stable shear distribution with respect to the frequency.

The frequencies of the centrally loaded beam (**Fig. 3.16**) are also accurately predicted, although slightly more scatter of results is observed here (*cf.* **Figs. 3.15** and **3.16**).

From these results, it is clear that the assumption of unity of k due to the assumed uniformity of transverse shear distribution over the core cross section of the sandwich cannot account for the sandwich frequencies. The test results for the four sandwich beams varying only in thickness of the core (**Figs. 3.15** to **3.19**) suggest that the value of k is sensitive to the core thickness. In **Fig. 3.20**, the optimum value of k , obtained from earlier results, has been considered as a function of the skin/core thickness ratio. These results suggest that a linear variation of k with the ratio of skin/core thickness exists. It is of interest to note (**Fig. 3.20**) that a value of *1.0* for k occurs only at infinitely small skin/core thickness ratio.

3.4.2 Mode Shapes

The stored energy in a vibrating structure at any instant depends on the shape of the deformation of the structure at that instant. By definition, therefore, the accuracy of the prediction, or steady-state measurement, of the SDC is directly related to the accuracy of the function defining the mode shape.

A series of tests was conducted on the 2SB1-X sandwich beam. All the tests were carried out in the first mode and on different lengths of the free-free beam which was supported on cotton threads at the nodal points. The latter were detected by sensing the vibration through a thin rod lightly held on the beam. Both unloaded and loaded beams were tested. In the latter case, the beam was either loaded at the mid-point with the drive and pick-up coil assembly (of 134 g mass) or loaded at the ends with the drive and pick-up magnets (each of 40 g mass). In the case of the unloaded beams, an electrodynamic shaker was used to excite the beam at one end, and a microphone held over the mid-point was used to detect

and tune the resonance frequency as well as to check and maintain a constant displacement amplitude. In the case of the loaded beams, the drive coils were used for excitation. For each test, the beam was marked at equal intervals (10 mm) along its length and on the edge of the upper skin. An image-shearing optical device (WISE) was used to measure the displacement amplitude at the marked points. With the forced vibration arrangement (centrally or end driven), steady-state vibration was maintained throughout the test duration. However, using the shaker as a means of excitation proved to be troublesome and the current to the shaker had to be constantly readjusted to maintain a constant amplitude of vibration. Furthermore, only the longer beams could be tested in the unloaded or end loaded set ups. This was because, unlike the centrally driven arrangement, in these cases the displacement amplitude was too small to be measured with certainty. Attempts were also made to carry out tests in the second mode, but for the same reason these proved to be futile even with the centrally driven arrangement.

The theoretical predictions were obtained following the arguments given at the end of section 3.3, which have been implemented in the program *BEAM4.FOR*. In the centrally and end driven cases, the voltage induced in the pick-up coil was used to measure the local displacement amplitude while, with the unloaded cases, the central displacement amplitude was measured using the WISE. In this procedure of predicting the mode shape, it is important to measure the single displacement amplitude accurately since, depending on the particular mode shape, its value will to a lesser or greater extent influence the predictions. This concept will be explained in more detail below with reference to some illustrative examples.

The flexural mode shape (lateral displacement amplitude) results are shown in Figs. 3.21 to 3.26. As Fig. 3.21 indicates, with the 400 mm unloaded beam no appreciable difference exists between the predictions of the two analyses and the test results, although a slight overestimation of the Bernoulli-Euler predictions towards the beam ends is noticeable. As is

indicated by **Fig. 3.22**, the deviation of displacement amplitude according to the elementary theory from the actual displacement amplitude is more pronounced as the beam becomes shorter. For the beams carrying a central load (**Figs. 3.23, 3.25** and **3.26**), this effect is increased even further, since the elementary (Bernoulli-Euler) analysis does not account for the shearing of the core which increases with the shorter beams and with the beams which carry a load. The nature of the actual deformation is illustrated even more positively in **Fig. 3.26**, where the extent of the shearing in the centrally loaded shorter beam is such that the beam curves in, a process which is in sharp contrast to the prediction of the elementary theory where, as expected, a convex curve is resulted through the assumption of pure bending of the beam. The Timoshenko beam analysis on the other hand closely predicts the mode shape. The slight deviation of the Timoshenko predictions from the actual results in **Fig. 3.26** could be either due to the underrating of the core shear modulus or the onset of a discrepancy between the theoretical predictions and the experimental results. However, since there is no apparent reason to question the accuracy of the measurement of the core shear modulus it seems therefore that the latter case is true. Referring to the same figures **3.23, 3.25** and **3.26**, it can be seen that as the nodal lines move towards the mid-point, the central displacement amplitude and its ratio to the end displacement amplitude decreases. In the case of the centrally driven 200 mm beam, for example (**Fig. 3.26**), this ratio is of the order of nearly 1:10 for the experimental results. Hence, any error occurring in the measurement of the central displacement amplitude will be magnified by 10 times when computing the end displacement amplitude. For this reason and in the absence of the means for accurate measurement of the central displacement amplitude for the prediction of the mode shape, it may be advantageous to use a curve fitting procedure whereby the mode shape is computed from a displacement amplitude which would bring the theoretical and experimental results as close together as possible. This procedure was used by Ritchie [1973].

The mode shape results for the end loaded 400 mm beam are shown in **Fig. 3.24**. No appreciable difference exists between the predictions of the elementary and the improved

theories. The shift between the predicted and actual displacement amplitudes in the middle portion of the beam is believed to be due to the overrating of the end displacement amplitude from which the mode shapes were predicted. As mentioned previously, the end loaded beams are less stable than the centrally loaded beams due to the difficulties in achieving perfect alignment of the two end masses. The scatter of the test results in this figure, compared to the results of the centrally driven beams, seems to have been caused by the instability of the vibrating system.

3.5 Conclusions

On the basis of the Timoshenko beam equations, the theoretical frequencies and mode shapes of both solid as well as sandwich beams were computed, and these were shown to follow closely the experimental results for both loaded and unloaded free-free beams. Certain assumptions were made in adapting the Timoshenko equations for a shear soft sandwich beam. On the basis of the high correlation between the results, these assumptions, within the context of the shear correction factor, seem to be justified. The particular relevance of these equations to the shear flexible sandwich beams was clearly shown.

In the case of the solid beams, two special values for k , $\pi^2/12$ and 1.0, were considered. The difference in results was found to be marginal and well within the limitations of an experimental verification; no trend could be detected as to the superiority of one value or the other in prediction of frequencies. With the loaded beams, both values were found to underrate the fundamental frequency.

It was further concluded that, at least in the case of aluminium honeycomb sandwich, the shear factor was a linear function of the relative thickness of the skin and of the core, and that in practical situations its value was more than unity. Moreover, it was shown that for both solid beams and aluminium sandwich beams, any deviation from the experimental results could be attributed solely to the value chosen for the shear correction factor, k , such

that for a 'correct' factor, the accuracy of frequency predictions was maintained over the entire frequency range.

Owing to unnecessary complexities involved in an analytical approach to the determination of the factor k in a sandwich beam, specially when, as in the damping tests in the present work, the beam is to be subjected to mid-span forced vibration, an empirical approach to its determination was suggested.

Generally, owing to shear, there is a shift of the nodal lines towards the centre of the beam and a partial translation of the total lateral displacement amplitude into the shear rotation, a process which was found to be closely followed by the Timoshenko theory.

Chapter 4

HONEYCOMB DYNAMIC SHEAR PROPERTIES

Scope - In this chapter, a device is described for measuring the dynamic shear properties, namely dynamic modulus and the SDC, of honeycomb. Results of shear tests are then presented and these are compared with those reported in the literature. Some of these results will be used in a subsequent chapter.

4.1 Measurement of honeycomb dynamic shear properties

Very few works have been reported on the measurement of the honeycomb dynamic properties in shear. The first attempt in this field seems to have been due to James and Norris in 1958 [James, 1962]. Their work was followed by the work of Keer and Lazan [1961]. Except for a schematic diagram, reproduced here in **Fig. 4.1**, no details are given of the apparatus used in this latter work.

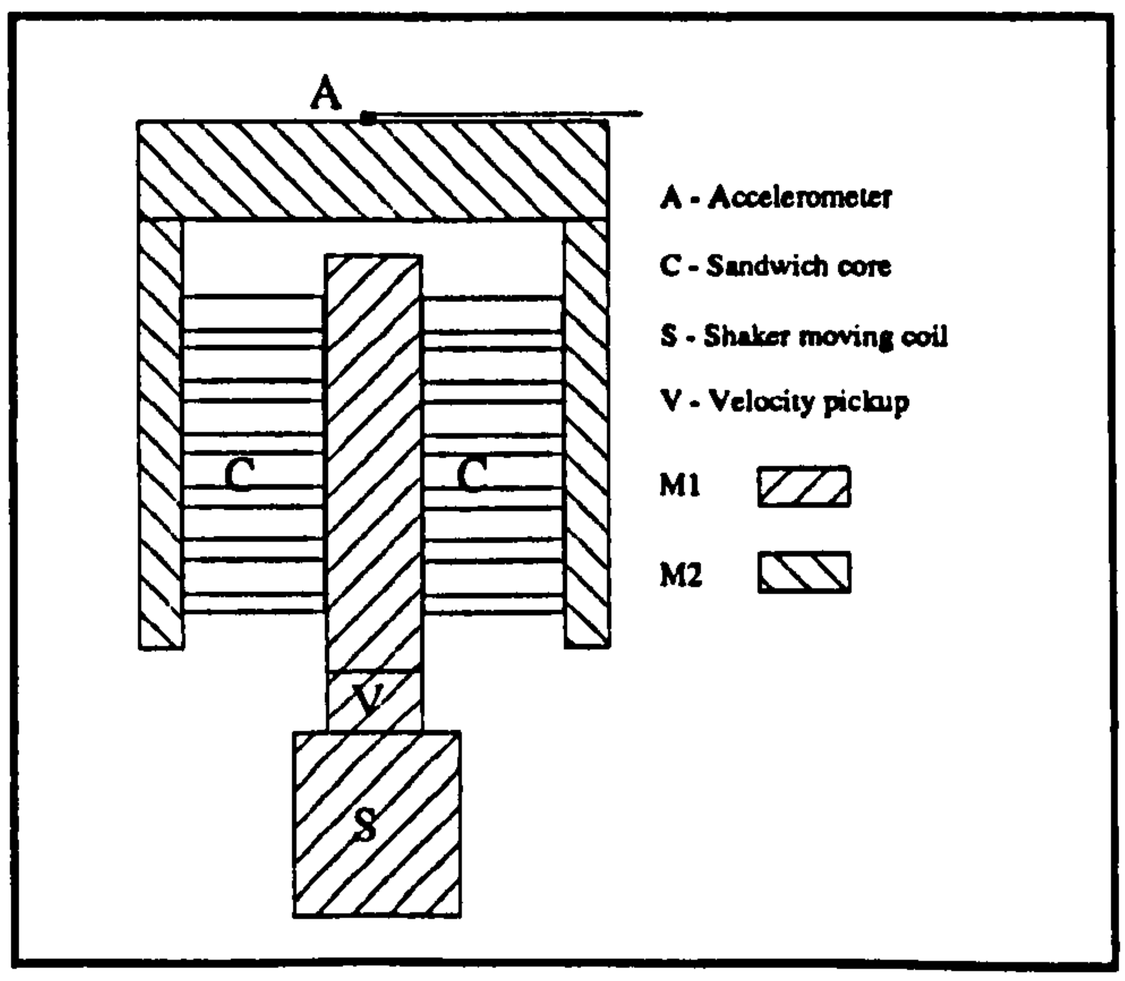

Fig. 4.1 *Keer-Lazan honeycomb shear test-rig*
(After Keer and Lazan [1961])

Evidently, the test-rig constitutes a two DOF vibrating system due to lateral anti-phase vibration of the masses *M1* and *M2* (indicated by hatchings in the diagram). From their assumption that the core damping energy was proportional to the square of the transverse shear stress amplitude, Keer and Lazan sought to find the constant of proportionality, the so called 'core damping coefficient', J_c , in

$$D_c = J_c \tau^2$$

where

$$D_c = 2 \pi W_0 / A_r$$

in which W_0 is strain energy which, for small damping, may be assumed as equal to kinetic energy, and therefore

$$W_0 = 0.5 (M_1 \dot{x}_1^2 + M_2 \dot{x}_2^2) ,$$

and A_r is the amplification factor at resonance, which is obtained from the frequency band-width, $\Delta\omega$, at $\sqrt{2}$ of the resonance amplitude according to the relationship

$$A_r = \omega_n / \Delta\omega$$

where ω_n is the natural frequency. Having obtained the shear modulus of the core from

$$G = \omega_n^2 \quad \frac{M_1 M_2}{M_1 + M_2} \frac{c}{A}$$

in which c and A are thickness of the core and the total area under shear respectively, they proceed to find the total displacement amplitude of vibration by adding the deflections x_1 and x_2 as measured by the accelerometer and the velocity pick-up. The shear strain, and subsequently the shear stress are found from the total deflection.

The results are presented as values of J_c for a number of honeycomb core materials including aluminium and fibreglass. Contrary to their assertion, no explicit results are presented in this work in support of the assumption of proportionality of damping energy to the square of the stress amplitude. In a later work, however, James [1962] presented results showing that

linear damping mechanism existed in the case of aluminium honeycomb for a stress amplitude up to about 140 kPa. At higher stresses, the power of the stress proportionality increased, reaching a value of 4.5 at about 700 kPa.

The honeycomb damping results reported by these experimenters are dimensionalised with respect to the particular samples. However, from the definition of the SDC as

$$SDC = \frac{\Delta U}{U}$$

where

$$\Delta U = D_c \qquad \text{and} \qquad U = 0.5\,\tau^2/G\,,$$

then the following relationship may be established between the SDC and the core damping coefficient

$$SDC = 2\,J_c\,G \tag{4.1}$$

Nordby *et al* [1965] proposed to utilise the modified Timoshenko-Huang beam equations in order to compute the dynamic shear modulus of the core, as well as the dynamic Young's modulus of the skin, from the fundamental natural frequency and nodal locations determined by a single test on a sandwich specimen. To this end, they showed that the natural frequency depends on both E and E/G, and that nodal locations depend on E/G only. Since there is only one unique set of values of E and G which satisfy a unique value of E and the ratio E/G, then they can both be explicitly determined. Their tests in the fundamental mode showed that for both fibreglass skin and aluminium core, the dynamic moduli were 'the same as' their static values.

4.2 A new method for measurement of dynamic shear properties

In this work, a new method was used to measure the dynamic properties of the sandwich honeycomb core in shear. The basic requirement was for an arrangement whereby the honeycomb could be put into shear vibration with the least extraneous damping. The shear modulus could then be computed from the natural frequency, and the SDC could be obtained by the free-decay method or, in a steady-state test, computed from the measurement of maximum strain energy and the damping energy per cycle, in much the same way as in the flexural tests. The latter method offers the possibility of measuring damping as a function of stress amplitude. The double-lap joint arrangement, described below, proved to be adequate for this purpose.

Initially, two identical aluminium sandwich beams were bonded together on the skin and a slot was cut through the middle section, leaving the single skin on each side (**Fig. 4.2**). A length of the single skin and the honeycomb was then removed at both ends on each face, leaving the double skin protruding out at the ends.

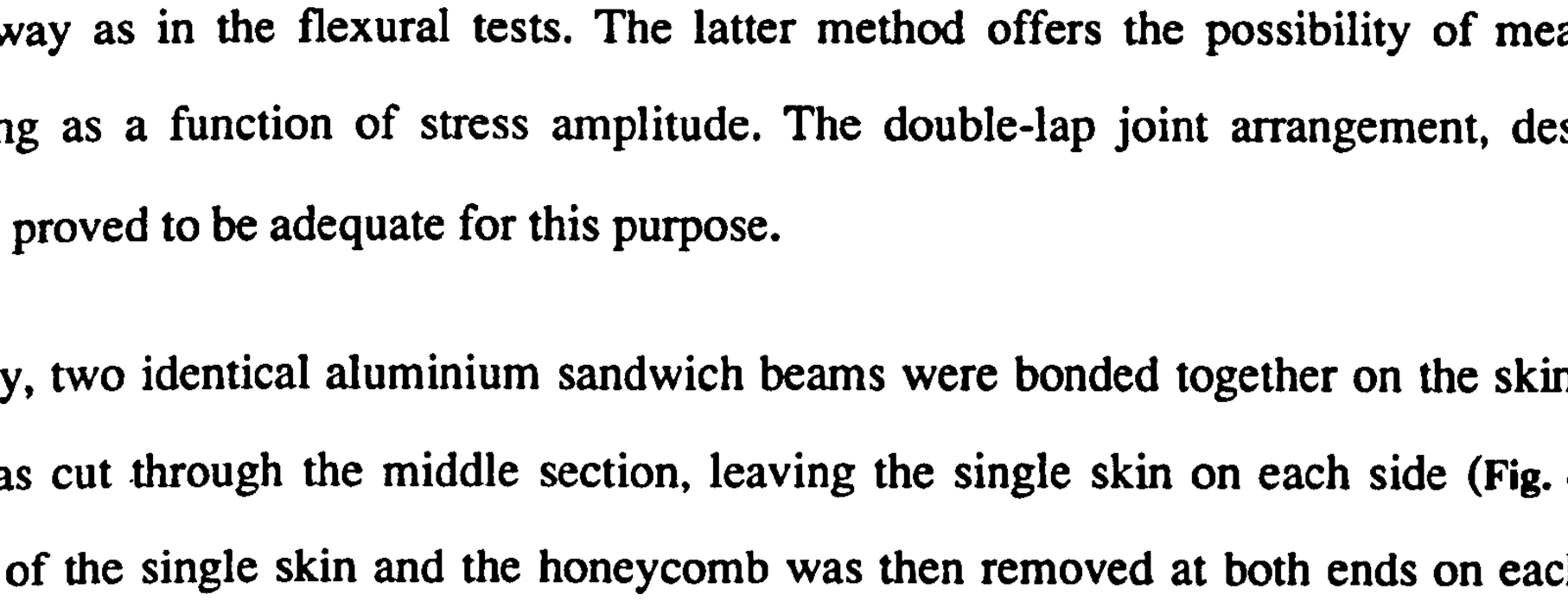

Fig. 4.2 *Original honeycomb shear test-rig*

This arrangement is basically a double-lap joint which allows for the application of an axial force at the ends to be-translated into mainly shearing of the honeycomb. The test piece is symmetric about the mid-plane as well as the mid-section.

Two equal masses were clamped at either ends with a permanent U magnet attached to each mass. Using cotton threads, the test piece was then suspended horizontally, from the end masses, inside an aluminium frame and two coils, attached to the frame, were positioned inside the magnets' poles. The instrumentation used was the same as that used for the flexural test-rig (fully described in *Chapter 5*), with one coil driving the end mass, and the other sensing the displacement amplitude of vibration.

Initial difficulties, not dissimilar to those reported by Bacon [1973], were experienced concerning the pick-up signal. In developing the flexural test-rig, Bacon reported an interference of the drive magnetic field with the pick-up signal when the drive and pick-up coils were positioned in the same plane. The voltage across the pick-up coil is expected to rise linearly as the frequency approaches resonance. However, Bacon observed a sharp non-linear fall of the pick-up signal as the beam approached resonance. He attributed the cause to the cutting of the drive magnetic flux by the pick-up coil. Since at resonance the drive current falls to a minimum, so does the intensity of the drive coil magnetic field and therefore any induced voltage across the pick-up coil due to the drive system. The nature of the problem in the honeycomb shear test was somewhat different from that experienced by Bacon in that the pick-up signal was not responsive to resonance to any appreciable extent. The distance between the drive and pick-up points was about 15 in., some five times that in the flexural test-rig. Moreover, the flux intensity of the permanent magnet used here was much lower than the flux intensity of the electromagnet used in the flexural rig. These may explain the fact that pick-up was not responsive to the changes in the drive magnetic flux. The remedy, however, was found to be the same as that reported by Bacon. At resonance, the pick-up coil/magnet set were rotated through 90° so that the plane of the pick-up coil

was perpendicular to the plane of the drive coil. As the coil was rotated, the pick-up signal intensified, reaching a maximum at 90°. The most likely explanation seems to be the sensitivity of the pick-up coil to the electromagnetic radiation from the drive coil. When the two coils are positioned at right angles, the drive/pick-up interaction reaches a minimum allowing the voltage induced in the pick-up by cutting the magnetic flux to prevail.

In the double-lap joint arrangement, because of the eccentricity of the forces in the mid-plane and the outer faces, bending moments are induced which tend to distort the outer skins specially in the middle. As a result, the skins undergo a complex cyclic deformation. These deformations have an adverse affect in two ways. First, they are expected to increase extraneous damping and secondly a number of frequencies are excited which make the detection of the shear frequency that much more difficult. Clearly, a more rigid test piece was needed. To that end, two thick Duralumin plates were stuck to the outer skins using a thermoset adhesive. This reduced the non-shear frequencies but at the same time seemed to have slightly increased damping, most likely due to deformation of the additional adhesive layer.

At this point, it was decided to fabricate the test piece from the constituent parts, replacing the skins with thick plates. A schematic diagram of the new test piece is shown in **Fig. 4.3.**

Fig. 4.3 *Honeycomb shear test piece*

Four honeycomb slices of equal size were cut from stock and, using a hot-press, were adhered to Duralumin plates following the manufacturer's moulding instructions and specifications. The same adhesive film used in the beams, was used for this purpose. Using the sandwich beams is a simple and convenient way to fabricate the shear test piece. Also, it has the merit that tests can be carried out on the manufacturer's end product. However, tests on the new test piece showed that the former method was inadequate for honeycomb shear assessment. For the same honeycomb, the SDC as measured by the second arrangement was reduced by almost a half (from 2.1% to 1.1%). The non-shear frequencies were not totally eliminated but compared to the shear frequency, these were of negligible amplitude. The vibration in the poles supporting the coils was still a cause for concern. The possibility of reducing these was explored by first placing the test piece horizontally on a solid platform

with the coils fixed to two brackets which were rigidly secured in position (**Fig 4.4**). With this arrangement, the damping due to the suspension, which at the time could not have been assessed, would be avoided. The vibration in the coils was almost entirely eliminated but the damping increased slightly (1.1% to 1.3%). Clearly the new source of extraneous damping was due to the contact between the test piece and the platform. The fact that the two overhung end masses were now imposing a bending moment of their own on the structure could also have been a contributory factor.

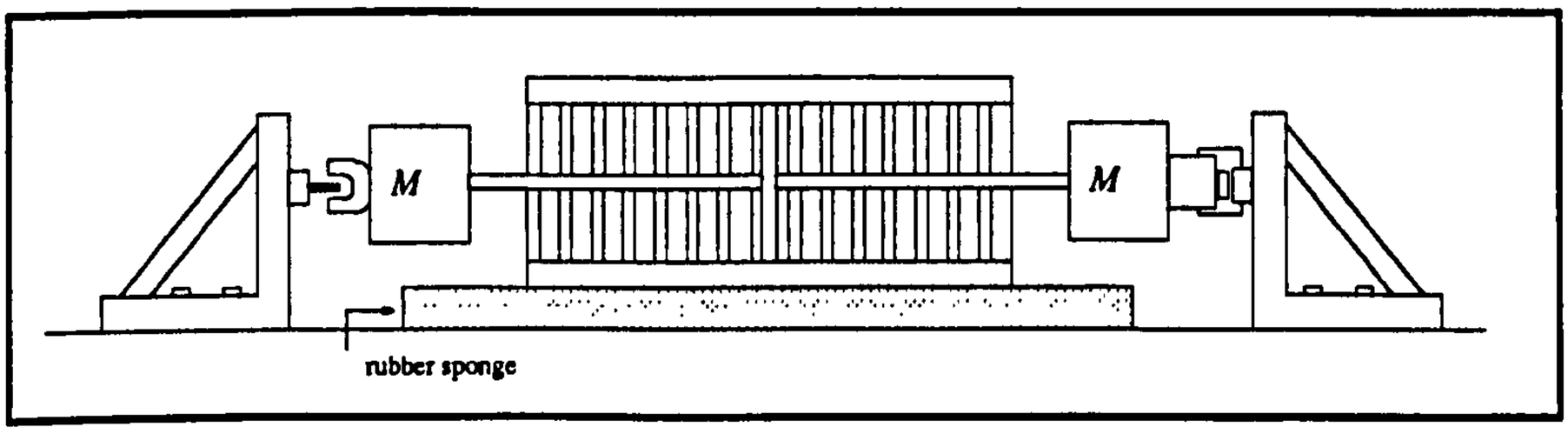

Fig. 4.4 *Rearrangement of the honeycomb shear test*

An alternative method which would avoid the problem of overhung end masses as well as the damping due to the vibration of the suspension was to suspend the test piece vertically from the outer plates (**Fig 4.5**). A new frame was build for this purpose with particular emphasis put on the rigidity of the coil supports. Tests on the same honeycomb sample showed that this arrangement was a good improvement on the horizontal suspension, reducing the SDC from 1.1% to 0.7%. All subsequent honeycomb shear tests were carried out using this test-rig.

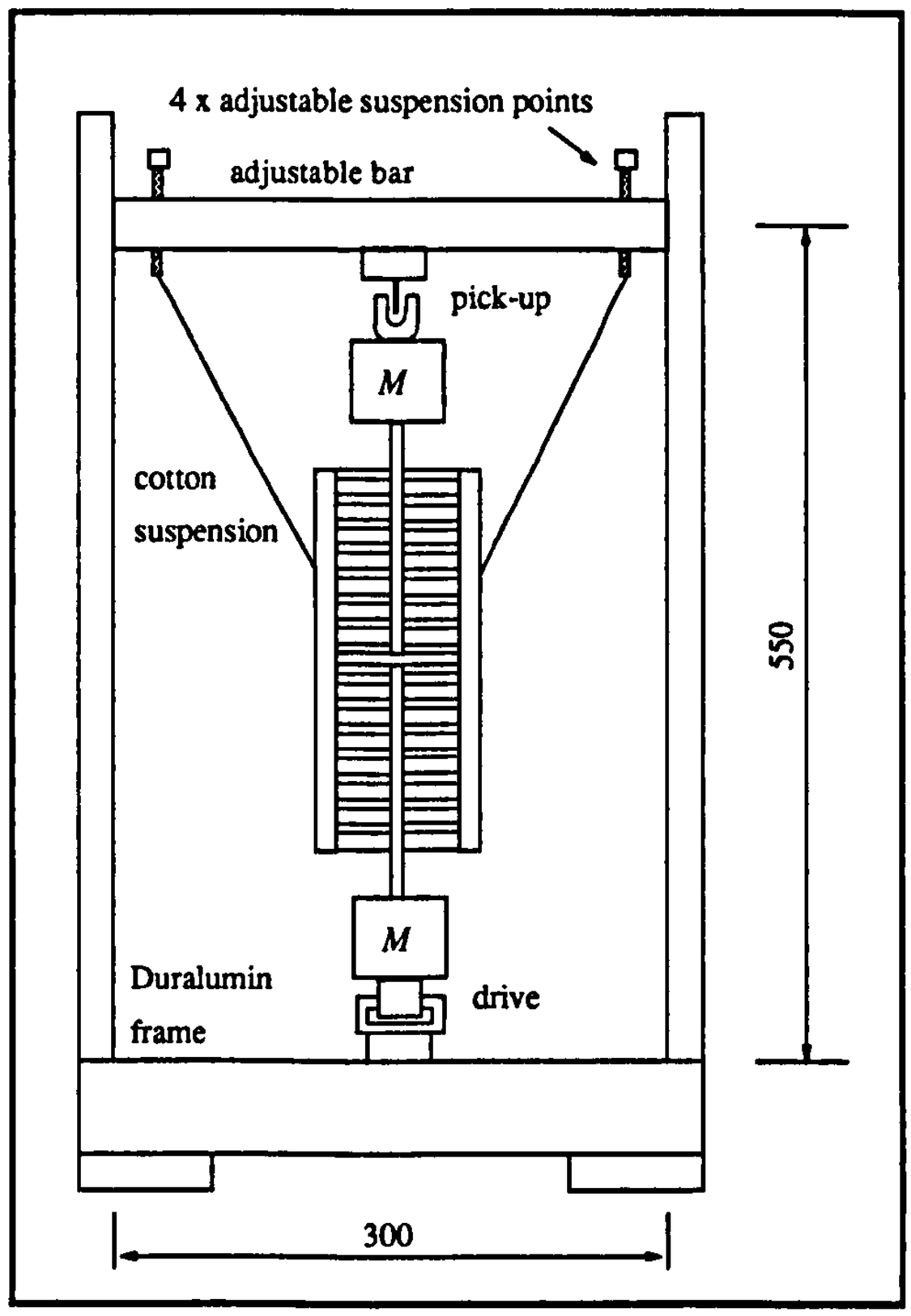

Fig. 4.5 *Honeycomb shear test-rig*

The vibration system is basically a two DOF system which with a symmetrical test piece will give two symmetric frequencies. Then, the only non-rigid-body motion is when the end masses vibrate in opposite directions. The relative motion of the end masses was verified experimentally by attaching an accelerometer, in turn, to the outer end of each mass and comparing the two signals.

Some extraneous damping due to the vibration of the outer Duralumin plates is inevitable, although this is expected to be insignificant. Generally, the outer plates are subjected to a complex system of forces, but provided the plates are sufficiently rigid the resulting vibrations and therefore any air-damping will be of negligible magnitude. The plates used in the shear test piece were 1/2 in. thick Duralumin plates and as expected, it was found that the

largest displacement amplitude was due to the flexure at the mid-section where the plate is subjected to the maximum bending moment. However, compared to the shear displacement amplitude this was of insignificant value (less than one tenth).

4.2.1 Analysis of honeycomb dynamic shear properties

4.2.1.1 Shear modulus

From symmetry, the mid-section is axially stationary and only one half of the test piece need be considered, as shown in **Fig 4.6**. The undamped spring-mass mathematical model is shown in the same figure, in which the two parallel springs, each of stiffness K, are subjected to longitudinal vibration of the mass M, where M is the total mass attached at either end of the shear test piece, including mass of the central plate.

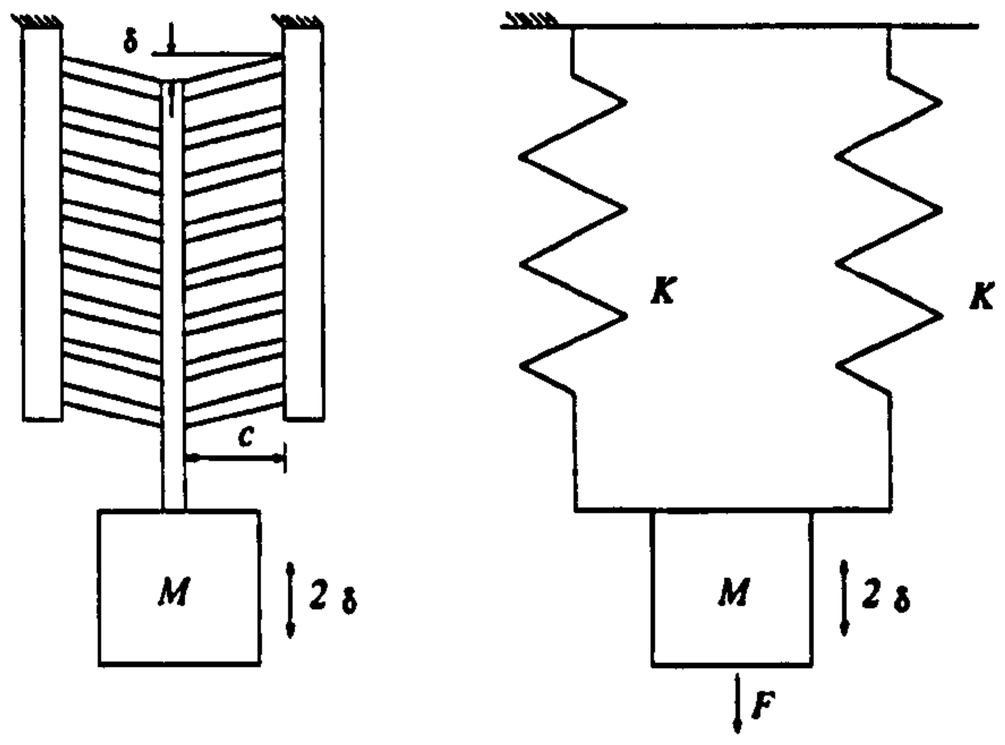

Fig. 4.6 *Schematic representation of honeycomb shear test piece*

For harmonic vibration of M, the frequency is given by

$$f_n = \frac{1}{2\pi} \sqrt{(2K/M)} \qquad (4.2)$$

However, the total stiffness of the springs subjected to a force F is given as

$$2K = \frac{F}{\delta} \tag{4.3}$$

and the shear modulus is given by

$$G = \frac{F}{2A}\ \frac{c}{\delta} \tag{4.4}$$

where A and c are, respectively, the shear area and thickness of each honeycomb slice. Then, the dynamic shear modulus of the honeycomb may be found from **Eqns. (4.2)** to **(4.4)** as

$$G = \frac{2\pi^2 f_n^2 M c}{A} \tag{4.5}$$

4.2.1.2 Steady-state shear vibration damping

The specific damping capacity of the vibrating system is given as

$$\psi = \frac{\Delta U}{U} \tag{4.6}$$

where the damping energy per cycle, ΔU, is found from the measurement of the drive current and the pick-up voltage, as described in *Appendix (A)*. For small damping, the total maximum strain energy, U, may be assumed as equal to the total maximum kinetic energy. The latter is given as

$$K.E. = M\ (\omega_n \delta)^2 \tag{4.7}$$

where ω_n is the angular frequency and δ is the peak displacement amplitude at either end, which is obtained from the frequency of vibration and the induced voltage in the pick-up coil (**Eqn (A.6)**, *Appendix (A)*). In **Eqn. (4.7)**, compared to the total end masses ($2\times M = 2.28$ kg), the mass of the honeycomb has been neglected.

The SDC may be plotted as a function of the maximum shear stress in the honeycomb, and the latter may be obtained from the maximum shear strain as

$$\tau_{mx} = G\ (\delta / c) \tag{4.8}$$

4.2.2 Honeycomb shear tests

A series of shear tests was carried out on aluminium (**Aeroweb Type 3003**) and the polymeric based **Nomex** (**Aeroweb Type A1**) honeycomb samples with different specifications. The latter honeycomb is described by the manufacturer (Ciba-Geigy Information sheet No. ATA 55k) as 'high temperature resistant fibrous aramid' coated with phenolic resin. The tests were carried out in air and at room temperature.

The basic method of manufacture of the honeycomb involves rolling glue lines onto alternate flat sheets which are subsequently stacked, bonded to each other and then expanded to form the honeycomb panels. The cell size is controlled by the distance between the glue lines. Alternatively, the sheets are corrugated to form a series of half-cells, the adhesive is applied at nodes and the sheets are stacked and bonded on the nodes. Due to the geometry of the cells as well as the fact that the glue lines are locations of bonded double-web junctions (also called node or ribbon) which are aligned along one direction of the panel, a degree of orthotropy exists in the honeycomb panel.

The honeycomb density refers to the bulk density of the expanded cells and therefore depends on both the cell size and the degree of expansion. In this work, only the honeycombs which have been nominally expanded to regular hexagonal cells have been considered. As such, the honeycomb density would depend on the cell size only, the latter being defined as the diameter of the inscribed circle of the regular hexagonal cell. For the same cell size, the variation in bulk density indicates a variation in one of, or both, thickness and density of the honeycomb web.

The same designation system used by the manufacturer for the honeycombs is used here. This designation is best described through the use of the following example. The designation: **Aeroweb 2.3,3/8,15 - 3003** refers to, respectively, a particular Aeroweb hexagonal honeycomb of 2.3 lbf/ft^3 bulk density, 3/8 in. cell size, and made from a foil having a thickness of 15×0.0001 in. and being an aluminium alloy of the 3003 type.

The same basic designation system is also used for Nomex honeycombs, although metric units are used here. The Nomex honeycombs are distinguishable from the aluminium ones by the presence of the characters **A1** in their designation as in **Aeroweb A1,50,6** which refers to an Aeroweb A1 type honeycomb (Nomex) with hexagonal cells having a bulk density of 50 kg/m³ and a cell size of 6 mm. It is also noted that, unlike aluminium honeycomb, the thickness of the web is absent from the designation of the Nomex honeycombs, although these are quoted in the manufacturer's brochures.

Preparation of each shear test piece involved cutting four small slices of honeycomb and eight pieces of adhesive film (**Redux 609**) of the same size. These were then assembled onto the Duralumin plates, which had already been degreased with acetone, to form the shear test piece (**Fig. 4.3**). The test piece was placed in the pre-heated press and cured at 120° C temperature and under about 5 kN force for one hour.

To avoid distorting the honeycomb geometry and specially crushing the cells, all the honeycomb samples were cut cell by cell using a pair of scissors. As far as possible, symmetry in each slice was maintained by cutting along the same row of cells. This was easily achievable with the well regulated and more resilient Nomex cells but not always possible with aluminium honeycombs which are very malleable.

Altogether, nine different types of aluminium and Nomex honeycombs were subjected to steady-state shear vibration tests, and the shear modulus and the SDC were computed. In some cases, the degree of orthotropy in the honeycomb was determined by measuring the shear properties across as well as along the ribbon direction. In one case, different thicknesses of the same specimen were subjected to shear tests. The specimens tested were as follows

1 - Aeroweb 2.3,3/8,15 - 3003
2 - Aeroweb 3.4,1/4,15 - 3003
3 - Aeroweb 5.2,1/4,25 - 3003
4 - Aeroweb A1,29,3
5 - Aeroweb A1,48,3
6 - Aeroweb A1,50,6
7 - Aeroweb A1,64,3
8 - Aeroweb A1,64,5
9 - Aeroweb A1,96,3

The tests were carried out in air, and at room temperature. The frequencies for the aluminium honeycombs fell in the range 1000 to 2500 Hz, and for the Nomex honeycomb in the range 700 to 1500 Hz.

For each test, the shear frequency was verified using an accelerometer as described earlier. The test was carried out by noting the pick-up voltage at a number of drive currents, as the latter was increased.

4.2.2.1 Edge effects

So far, the assumption has been made that the honeycomb in the double-lap test piece is subject to shear stresses only. This, however, is not entirely true. As mentioned previously, because of the eccentricity of forces applied to the honeycomb, bending moments will be induced which, because of the symmetry of the test piece, will have zero global effect, but nonetheless tend to distort the honeycomb locally in a non-shear manner. The edge near the central loading point (**Fig. 4.7(a)**) is subjected to tensile stresses, while the edge further from this point is subjected to compressive stresses [Adams and Wake, 1984].

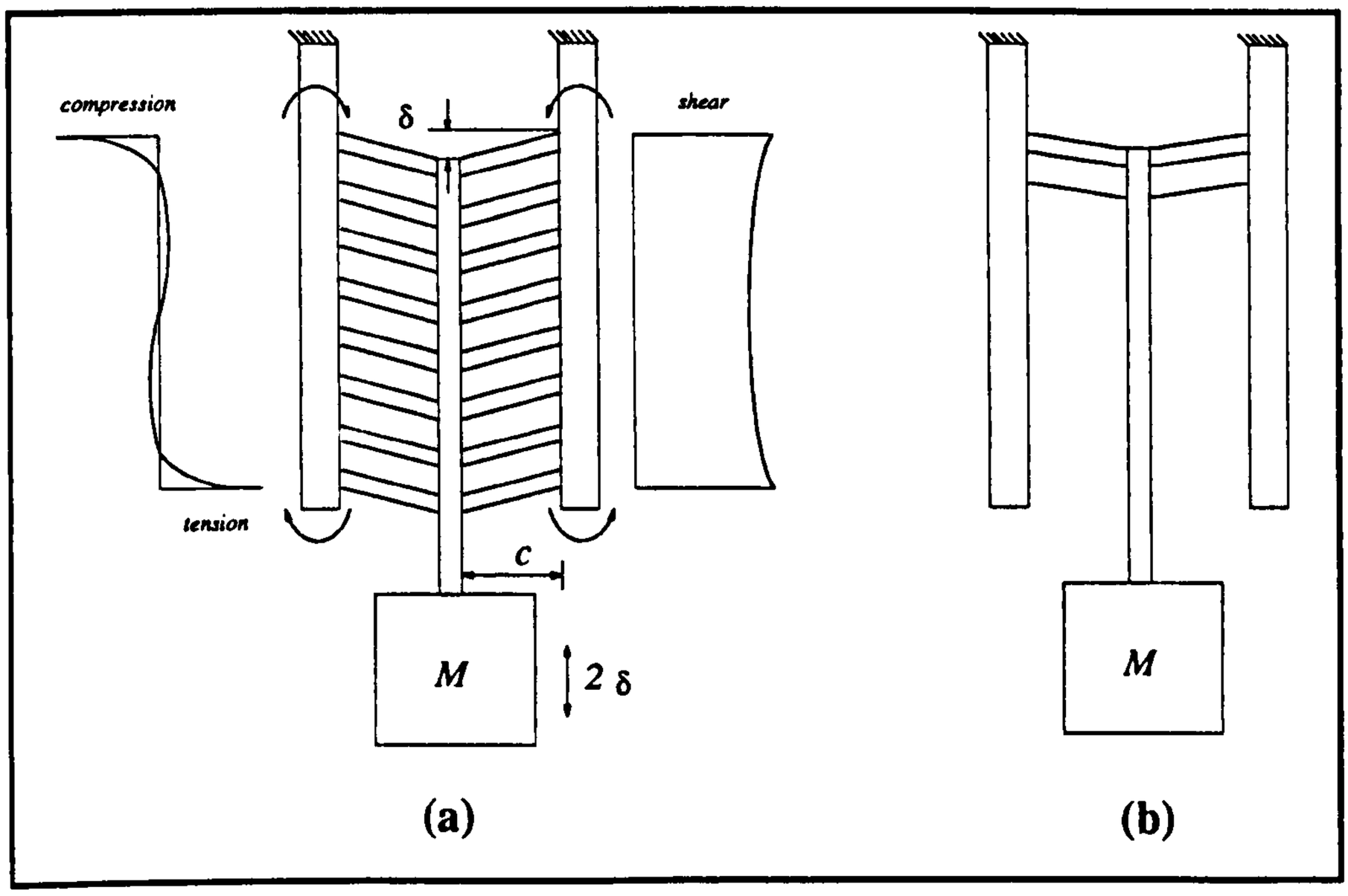

Fig. 4.7 *Schematic honeycomb edge effects*
a) *Bending moments and, transverse and shear stress distribution,* **b)** *Extreme case of edge effects*

Similarly, the magnitude of the stresses developed at the edges will be different from those in the honeycomb slices. In their extensive treatment of the lap joint employed in adhesive testing, Adams and Wake [1984] present results from finite element stress analysis, based on which they conclude that stress concentration at the edge is 'at least 10 times the applied shear stress on the joint'.

Because honeycomb is basically a structure, the stress distribution in honeycomb cells is less uniform than in an otherwise solid material, and the stress concentration is expected to be more severe at and near the edge. Furthermore, the geometry of the cells and whether or not these are complete structures at the edge, will play a significant role in the extent of stress concentrations. These stress concentrations in the honeycomb will generally cause the damping to become increasingly non-linear [Keer and Lazan, 1961].

In an attempt to assess the significance of these 'edge effects' in the double-lap honeycomb shear test piece, a series of tests was carried out on aluminium honeycomb with a cell size of 3/8 in., this being the largest cell size used in a sandwich configuration in the present work. The honeycomb, in the shape of the double-lap joint, was progressively sliced through symmetrically at both ends and along the length of the test piece. For each reduced shear area so obtained, the test piece was subjected to the shear test. The shear modulus and SDC were then calculated and plotted against the normalised shear area (**Fig. 4.8**).

As the figure indicates, with the present total shear area in the double-lap test piece (4×(91mm×62mm)), the edge effects are small in the computation of modulus. For a reduction of up to 60% or so in the shear area, the computed modulus remains independent of the variation in the area, while from about 60% to 80% the increase in the computed shear modulus is relatively slight. This tends to suggest a fairly uniform shear stress distribution over the length, as has been suggested in **Fig. 4.7(a)**. The sudden upsurge of the computed shear modulus for the lowest 'shear' area (about 93% reduction in the original shear area) seems to be due to a sharp increase in the relative stiffness owing to, it is suggested, a change of mode from a predominantly shear deformation for a sufficiently large number of honeycomb cells (**Fig. 4.7(a)**), to a deformation comparable to that caused by the lateral deflection of a fixed-fixed beam (**Fig. 4.7(b)**).

The SDC results, however, indicate that eliminating the non-linear damping is somewhat more difficult. The relatively low rate at which the damping approaches linearity (**Fig. 4.8**) may be explained by the fact that, there will always be stress concentrations in the outer honeycomb webs at the edges regardless of the shear area, especially if these are not parts of a complete cell structure. Nonetheless, the trend of the damping results seems to suggest that, for this particular cell size, the present total shear area of the test piece is the minimum area required in order to make any non-linear damping due to edge effects insignificant. As the largest cell size, together with the highest modulus, present the worst case for edge

effects, it may therefore be safely assumed that the latter is effectively eliminated on both counts of modulus and the SDC in aluminium and Nomex honeycombs with smaller cells.

4.2.2.2 Test results

Results of tests on aluminium and Nomex honeycombs are presented in **Figs. 4.9** to **4.11**, and **4.12** to **4.16** respectively.

The aluminium honeycomb Aeroweb 2.3,3/8,15-3003 (**Fig. 4.9**) is almost exactly the same sample as one tested by James [1962, Table 3, second sample], save for the lower foil thickness of the former (0.0015 and 0.002 in.). His figures for the SDC, after the necessary conversion through **Eqn. (4.1)**, are 1.8% along and 5.6% across the ribbon direction. Compared to 0.7% in both cases as found in the present work, James' figures are considerably higher, especially in the cross-ribbon direction where the above figure for aluminium honeycomb is unrealistic. However, unlike the expanded samples used here, his honeycomb sample was corrugated and this may, at least partially, account for the difference between the two sets of results. James could not find a convincing explanation for the unexpectedly high damping result in the cross-ribbon direction, including possible increased extraneous damping in the apparatus owing to 'more compliant' orientation, and the cause remained 'obscure'.

Tests by Keer and Lazan [1961] on the other hand, showed slightly higher damping along than across the ribbon direction (1.88% and 1.60% SDC respectively). Generally, the aluminium cross-ribbon damping results are somewhat erratic and unpredictable. Both **Fig. 4.9** and particularly **Fig. 4.10** indicate non-linear damping in this direction, possibly due to one or both friction damping caused by imperfect bonding in the nodes and stress concentration owing to misalignment of a number of honeycomb cells. However, as is evident from **Figs. 4.9** and **4.11** there is no or very little difference in the low stress damping when stressing the honeycomb along and across the ribbon direction. All other factors being

the same, it is believed that the significant difference observed in **Fig. 4.10**, and possibly also the difference in the James' results, could well be due to an unsound specimen.

The ribbon-direction modulus of the above named honeycomb is some 30% lower than the figure reported by James (141 and 206 MPa), although this difference should be considered against a 25% lower density. The cross-ribbon modulus is only slightly lower (98 and 103 MPa).

A similar honeycomb to Aw 5.2,1/4,25 (**Fig. 4.11**) was tested by Nordby *et al* [1965, Table 1] through the above mentioned procedure (section **4.1**), and the shear modulus, measured along the ribbon, agrees well with the value found here (281 and 285 MPa respectively), although the latter value is some 35% lower than the manufacturer's quoted figure (440 MPa, Ciba-Geigy Publication No. LGC 35c). This is a considerable difference and cannot be readily accounted for by such factors as, for example, misalignment of the honeycomb cells. It should, however, be pointed out that the manufacturer's figure is the result obtained by a different test-method, namely, the three-point bending test (a full description of this test is given by Teti and Caprino [1989]).

The damping results for different Nomex samples (**Figs. 4.12** to **4.16**) indicate a low amplitude sensitivity of the SDC. In the case of the A1,48,3 Nomex (**Fig. 4.13**) for example, a rise of the SDC of the order of 3% is observed before the latter becomes constant with the amplitude. Whether this low amplitude non-linearity is indeed the damping characteristic of the honeycomb Nomex material, or whether it has been caused by such external factors as the low sensitivity of the pick-up voltmeter at lower frequencies, is difficult to determine with certainty. However, as will be seen later (*Chapter 6*), the practical level of the shear stress in the sandwich honeycomb is well above the limit of non-linearity observed here. For that reason, in using the damping data of the Nomex honeycombs in subsequent computations, the apparent non-linear lower regions of these graphs have been ignored.

The damping results for the Nomex honeycombs (**Figs. 4.12 to 4.17**) further indicate that, similar to aluminium, the orthotropy of the honeycomb structure does not affect damping to any appreciable extent. Moreover, referring to the same results, and in particular to **Figs. 4.15 and 4.17**, it may be concluded that neither the honeycomb density nor the cell size is a determining factor in the damping of the Nomex honeycomb. In short, whatever the specifications, Nomex honeycombs posses a high damping level (about 10% to 12% SDC) and any variation in the damping between different specimens, or due to the orthotropy of the honeycomb, will be relatively marginal.

In **Fig. 4.17** the variation of shear properties with density for the same cell size are shown. The manufacturer's quoted results are also included (Ciba-Geigy Information Sheet No. ATA 55k; the cell size is not specified for the 'Typical' results). As can be seen, evaluation of moduli of the Nomex honeycombs agrees reasonably well with the manufacturer's figures for most parts, the major difference being in the modulus of the 96 kg/m³ Nomex honeycomb which is seen to be some 30% lower (70 and 100 MPa). However, too few experimental results and the scatter observed make it difficult to find with certainty any particular trend from the present results, although it would be safe to assume that, at least initially, the modulus increases linearly with density. More tests are needed for a conclusive verification. Benjamin [1969] quotes static shear modulus versus density test results for glass cloth honeycomb, showing that the modulus could vary by about 20% from an expected linear mean 'depending upon the resin used, the dimensions of the honeycomb, etc'.

4.2.3 Conclusions

The double-lap shear test piece is an effective arrangement for measuring the dynamic properties of honeycomb in shear. Compared to flexural tests, fewer sources of extraneous damping are present in this configuration. Main sources of energy loss are friction at the points of attachment of the end masses to the test piece, and the energy transmission from

the drive unit to the frame. However, these sources of extraneous damping would be of any significance only when testing low damping materials such as aluminium honeycomb.

Preparation of the test piece is a somewhat lengthy and laborious procedure, but the method should ensure minimum extraneous damping. This is testified by measuring a SDC of 0.7% for aluminium honeycomb in shear, by far the lowest figure reported for a comparable sample in the literature.

There is still some room for modification of the test-rig from its present state. In particular, a frame rigid enough to evade the expected frequencies of the honeycomb is warranted. Otherwise, due care should be taken in interpreting the system response to excitation.

The test results clearly show that a sound honeycomb sample experiences linear damping at low stress amplitudes. Furthermore, the orthotropy of both aluminium and Nomex honeycombs is manifested only in the considerable difference in the shear moduli; there is little difference, if any, between the low stress damping of the shear vibration along the two principal directions. Results not conforming to these trends, should be treated as the characteristics of the particular sample under test.

Chapter 5

THE STEADY-STATE FLEXURAL DAMPING TEST

Scope - In this chapter, the centrally driven test-rig, suitable for measuring the SDC of beams in steady-state flexural vibration, is described. Test results are presented showing that in most cases, the extraneous energy losses are well within the tolerances of the results for the materials tested in this work.

Both in-air and *in-vacuo* damping of all-aluminium sandwich beams will also be considered.

5.1 The test-method

The test-method used here is originally due to Adams *et al* [1969]. Later improvements of the apparatus were carried out by Bacon [1973] who gives a full description of the development of the test-rig. However, Bacon's test-rig was inadequate for this work. Having been designed for testing slender composite beams, it was too small and ineffectual for the relatively larger and stiffer sandwich beams. Consequently, based on the original design, a larger apparatus, incorporating a more powerful drive system, had to be utilised.

The basic principles of the test are given below. The theory behind the test is given in *Appendix (A)*. The computation of the SDC for the slender beams tested here is based on **Eqn. (3.41).**

Basically, the test involves suspending a uniform beam horizontally at its nodal points so that free-free boundary conditions are achieved at the beam ends. Then, the beam is excited at one of its flexural natural frequencies (usually the fundamental frequency) and the input energy per cycle and the lateral displacement amplitude of the steady-state vibration measured.

The means of excitation and displacement measurement are by two flat coils of wire, the planes of which are mutually perpendicular (**Fig. 5.1(a)**). The coil assembly incorporates a clamping arrangement and is secured at the mid-span of the beam with the coils positioned on opposite faces. Each coil can move freely in the gap of a U-magnet cutting the magnetic flux at right angles. The gaps are deliberately narrowed in order to intensify the flux and to keep the lines of flux straight, while the mutually perpendicular arrangement of the two coils is intended to minimise, if not quite eliminate, the interference of the drive magnetic flux with the pick-up coil (the pick-up flux from a relatively small permanent U-magnet, is too weak to have had any detectable effect on the drive coil).

In constructing the coil assembly, consideration should be given to the lightness and to the choice of material which should be ferrous-free. Aluminium adequately satisfies both requirements and was, therefore, used for the coil assembly. Excess material was removed by drilling holes in the clamping beams and the coil yoke, while maintaining symmetry **(Fig. 5.1(a))**.

In the test set-up used (**Fig. 5.1(b)**), the initial steady-state sine-wave is supplied by a signal generator which also provides the means to adjust and read, digitally, the frequency to within one millionth of a Hertz. The signal is amplified to the required level and is fed to the drive coil which interacts with the magnetic flux of the drive magnet to induce a magnetic force proportional to the drive current. This causes the beam to vibrate at the frequency of the initial signal. At the same time, the cutting by the pick-up coil of the magnetic flux of the pick-up magnet will induce a voltage across this coil which is proportional to the velocity of vibration. A digital ammeter in the drive circuit is used to read the current supplied to the drive coil and a digital voltmeter is used to read the voltage across the pick-up coil. Both drive and pick-up signals are monitored on the oscilloscope, the latter signal after being conditioned through the signal conditioner.

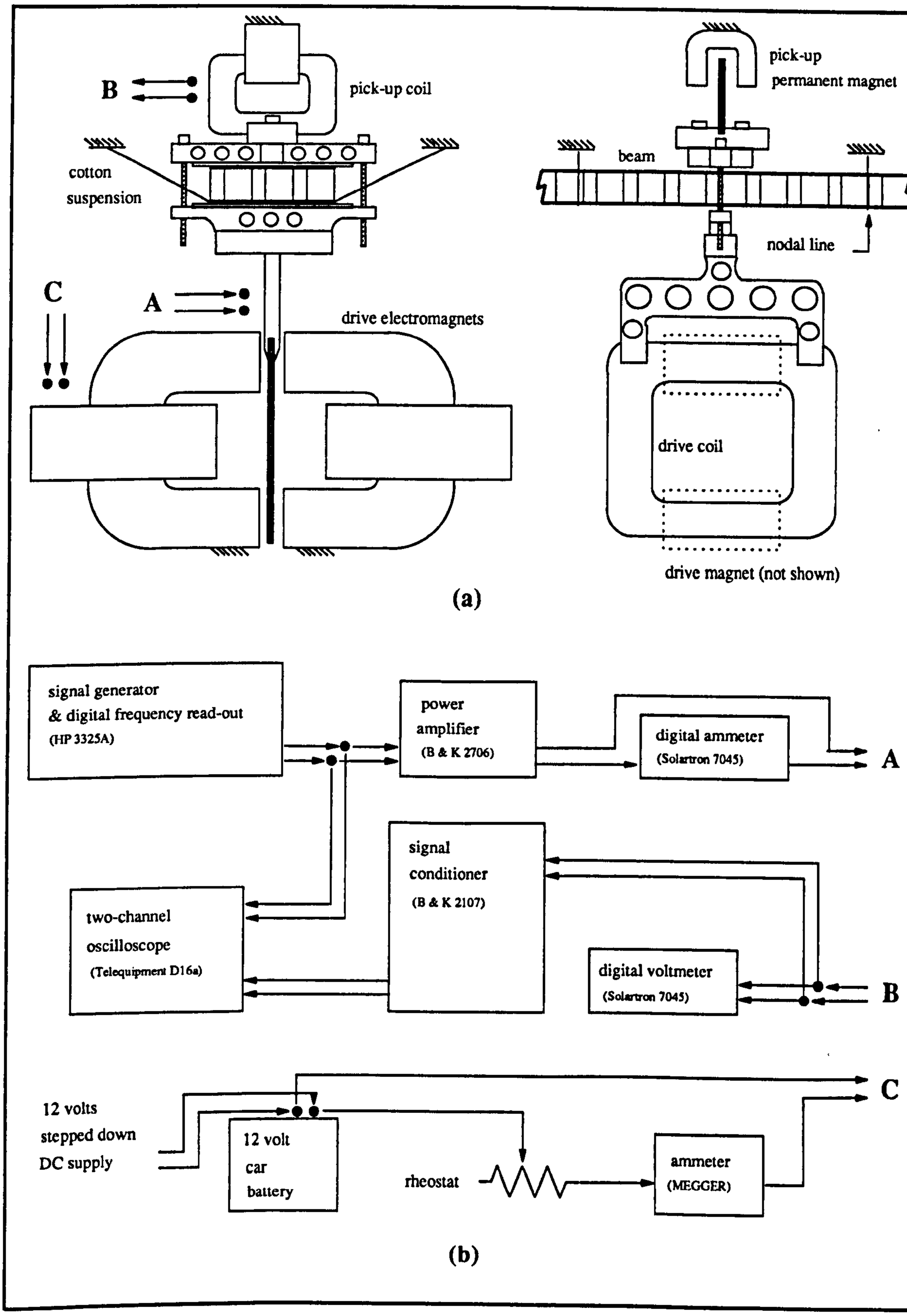

Fig. 5.1 *Flexural test-rig*

a) *centrally-loaded coil,* **b)** *drive, pick-up & electromagnet circuitary*

An electromagnet, capable of taking a current of up to 8 A, was used in the drive system. A 3 A current, however, was found to be adequate which, with a maximum allowable rms drive current of 1.5 A, provides a cyclic force of about 0.9 N amplitude (see *Appendix (A)*). The D.C. current supplied to the electromagnet had to be kept constant during the test period, and this was achieved by connecting a car battery across the stepped-down D.C. supply, with the battery in effect acting as an electric buffer for any fluctuation in the current. A rheostat in series with an ammeter were used to adjust and monitor the current. The drive and pick-up coil/magnet pair had to be calibrated and re-calibrated from time to time. The details of the calibration method are given in *Appendix (A)*.

Measuring the current input to the drive coil will provide the means to compute the energy needed to maintain the vibration at a steady-state and will, therefore, give a measure of the energy dissipation. At the same time, by measuring the induced voltage across the pick-up coil, the displacement amplitude of vibration at the centre of the beam may be computed. When the displacement amplitude is known, the strain energy of the beam or the kinetic energy of the vibrating system can then be computed.

5.2 Extraneous damping

Provided it can be shown that the energy dissipation mentioned above is limited to the specimen, then this energy would represent the damping energy of the specimen, or in a more general term, the 'material damping'. Otherwise, the experimenter should verify that the extraneous damping energies are sufficiently small not to impair the measurement of the overall damping of the specimen.

In practice, losses occur due to interaction between the material under test and its environment. Generalisations of the chief sources of extraneous damping have been made [Lazan, 1960] as structural (interfaces with the vibrating system), hydro-mechanical (e.g. air damping) and electro-mechanical (eddy currents and magnetic hysteresis).

All the flexural tests in this work were carried out using the free-free resonant test method. With the free-free end conditions, the extraneous damping introduced due to an otherwise clamped specimen will be avoided.

Air damping is caused by the cyclic flow of air particles due to lateral pressure difference induced by the vibrating system. As such, air damping would be expected to be a function of the dimensions of the vibrating system, frequency and amplitude of vibration as well as the viscosity and density of the air. Bacon [1973] distinguished the lower, amplitude independent, and upper regions of the SDC versus Amplitude graph as 'viscous' and 'inertia' effects respectively, associated with lower and higher Reynolds numbers. His attempts, however, for predicting the air damping proved futile, leading him to the conclusion that 'the only satisfactory way' would be to test *in-vacuo*.

At low displacement amplitudes, air damping remains constant with amplitude. Furthermore, air damping is known to be more amplitude dependent in the clamped-free than free-free vibrations [Soovere and Drake, 1985]. Hence, strictly speaking, if it is intended to measure the damping as, for example, a means of material assessment, then the material should be tested in a vacuum. Otherwise, the beam should be tested in the free-free condition and only the test-results at the lower amplitudes should be considered. No such general statements, however, may be made as regards to the frequency of vibration and the relative dimensions of the specimen since, all other factors being the same, these only vary in inverse proportion to one another.

Another source of energy loss is the friction caused between the specimen and the points of attachment of the coil assembly to the beam. The beam is secured between two thin silver steel rods cemented in V-grooves which are cut on the surfaces of the clamping beams, the latter forming an integral part of the coil retaining yoke (**Fig. 5.1(a)**). At first, it would seem best to secure the coil assembly on two points across the beam and on the neutral axis where no straining occurs. However, any gain in so doing should be weighed against the practical

difficulties in maintaining the stability of the coil assembly during the vibration and on the method of point-attachment if a new source of friction damping is to be avoided. The clamping arrangement was consequently used.

The suspension mechanism brings about another source of energy loss which is more difficult to resolve. The beam rests on its lower face at two nodal points on two pieces of cotton string which are attached to the supporting structure. Here, the energy losses are caused in mainly two ways, one friction between the beam and the supporting string in much the same way as the clamping arrangement mentioned above, and the other by vibration transmission via the suspension to the supporting structure. Again, an effective remedy to reduce losses in the suspension mechanism would seem to be to position the supports on the neutral axis of the beam, but, as mentioned previously, this method would impose practical difficulties. The vibration of the suspension strings, however, cannot be eliminated regardless of where the supports are located, because the nodal cross-sections have a longitudinal vibration.

5.2.1 Assessment of extraneous damping

Before carrying out the flexural tests, it was necessary to ensure that the contribution of extraneous damping to the overall damping was insignificant. To this end, tests were carried out on slender Duralumin beams. Aluminium is known to have a very low damping level; figures as low as 0.002% for the *in-vacuo* SDC of Duralumin in torsion have been reported [Cottell *et al*, 1948]. Duralumin has been frequently used as a reference material in the assessment of background damping [Adams *et al*, 1969; Bacon, 1973; Adams and Bacon, 1973-a; Guild and Adams, 1981 *etc.*], where the material damping of the beam, as compared to the background damping, has been assumed to be negligible. In the ensuing discussions, this assumption has been maintained. The frequencies of tests on Duralumin beams fell in the range 70 to 80 Hz.

5.2.1.1 Air damping

Air damping may be accounted for by testing in a partial vacuum. A specially designed vacuum chamber, originally due to Bacon [1973], was available for this purpose. The *in-vacuo* tests were carried out under the minimum air pressure which could be achieved, and this was recorded to be about 1 kPa or 1% of the atmospheric pressure. This is believed to be a good enough vacuum for effectively removing air damping.

In Fig. 5.2, the results of the in-air and *in-vacuo* tests on the same Duralumin beam are shown. From this figure it is noted that the *in-vacuo* damping remains almost constant at about 0.15%, a figure which agrees with previous results [Bacon, 1973, Fig. 8]. The in-air results indicate the initial invariability of the SDC with amplitude, and the increase of the SDC at higher amplitudes, attributed to air damping, is seen to be linear. Extrapolation of the two curves to zero displacement amplitude suggests a difference of about 0.04% SDC between the Duralumin beam in-air and *in-vacuo* . This is believed to be partly due to aerodynamic losses but mainly due to the damping caused on the beam surface under hydrostatic stresses. For this particular test, therefore, this figure represents low amplitude air damping. Generalisation to other materials, however, is not possible since the low amplitude air damping would depend on the material under test.

Air damping is proportional to the size of the vibrating system. The new and larger coil assembly was compared with Bacon's coil as regards to air damping. The results of the tests on the same Duralumin beam are presented in Fig. 5.3. From the in-air results in this figure, it is noted that using a larger coil would indicate a larger SDC than a smaller coil, significantly more so at higher amplitudes. At lower amplitudes, however, the difference is within 0.02% SDC, a portion of which (about 0.01%) is believed to be due to a higher friction damping inherent in the larger coil, as indicated by the *in-vacuo* results.

5.2.1.2 Friction damping

Compared with the quoted figure of 0.002%-0.02% for Duralumin [Cottell *et al*, 1948], a SDC of 0.15%, as indicated by the *in-vacuo* results of **Fig. 5.2**, suggests that the major proportion of the in-air damping at low amplitude is due to the friction caused at the clamping lines and to the suspension mechanism. Induction of eddy currents in the coil assembly owing to radiation from the coils is possibly another contributory factor [Bacon, 1973], although compared to the two former sources, these are believed to be of little effect.

For stability reasons, the coil assembly originally incorporated a 3-line clamping arrangement whereby the beam could be clamped between two silver steel rods on the upper surface and one rod, positioned between the two upper rods, on the lower surface. This was modified to a 2-line clamping with one upper and one lower rod positioned immediately opposite each other. Careful and even tightening of the coil assembly to the beam proved that the stability was not compromised in the latter arrangement. In **Fig. 5.4** the in-air and *in-vacuo* results of the two arrangements are compared. This figure clearly shows the increase in the SDC due to the friction caused at the extra clamping line. The results indicate that, at lower amplitudes, the difference in damping of the 2 and 3-line clamping is almost the same (a SDC of about 0.02%) for the in-air and *in-vacuo* tests, although at about a displacement amplitude of 0.35 mm an increase in both cases occurs, but remains constant for higher amplitudes. The constant difference in damping due to the extra clamping line is in support of the proposition that friction damping is independent of sliding velocity and depends only on the number of friction points [Soovere and Drake, 1985].

The losses due to the clamping of the coil to the specimen may be accounted for by using the Guild and Adams [1981] test-method. In this arrangement, two small U-magnets are bonded to the beam at either end and are positioned in suspension on top of two small coils which act as the drive and the pick-up coils. Hence, the friction damping which is otherwise encountered in the clamping of the coil to the beam will be avoided, although some energy

losses may occur at the points of attachment of the magnets to the beam due to the straining of the adhesive layer. However, being located at the beam ends, strains are minimal, and energy losses can be reduced further by using the least amount of adhesive necessary.

Using the end driven technique, the *in-vacuo* SDC of the Duralumin beam was found by the free-decay method. Free-decay tests were also carried out on the centrally driven beam *in-vacuo*. In each case, the test was repeated three times and, using the error criterion analogous to **Eqn. (3.43)**, it was found that within a tolerance of ±0.01% a good consistency existed in each set of results. The SDC of the centrally driven beam was found to be 0.135% (*cf.* 0.15% found in steady-state) while for the end driven beam it was recorded as 0.053%. A major proportion of the latter figure should, therefore, represent a measure of the damping due to the suspension as well as any energy losses at the points of adhesion of the end magnets to the beam. This figure agrees with a value of 0.05% suggested by Adams *et al* [1969] although they used foam knife edges for supporting the beam, a method which, when compared to cotton suspension, is known to impart more damping on the system [James, 1962; Bacon, 1973]. The difference between the results obtained using the centrally and end driven methods, amounting to a SDC of about 0.08%, is believed to indicate the order of the friction damping at the clamping lines using the centrally driven method.

5.3 Damping of aluminium sandwich beams

At this point, it is appropriate to consider the damping of all-aluminium sandwich beams which exhibit a low level of damping. In so doing, the application of Timoshenko's modified equations for steady-state damping measurement will also be considered.

Three thicknesses of pre-fabricated all-aluminium sandwich beams (Ciba-Geigy's Aerolam M-board) were subjected to both in-air and *in-vacuo* steady-state damping tests, using the centrally driven arrangement. The damping of the sandwich with respect to the orthotropic

properties of the core were also considered. The results are presented in **Figs. 5.5** to **5.7.** The frequencies of tests on sandwich beams fell in the range 400 to 1200 Hz.

Also included in these figures are the free-decay (FD) results, obtained from the decay of the lowest displacement amplitude of the steady-state tests. The free-decay results are the average of results of three tests, although for the most part they were noted to be fairly consistent.

The beams, 2SB1,2,4, were all of dimensions 400 mm length × 40 mm width, and 0.57 mm skin thickness, as previously tabulated in **Table (3.3)**; the core was Aeroweb 5.2,1/4,25-3003, the dynamic shear properties of which were already presented in **Fig. 4.11.**

Computation of the SDC in steady-state flexural vibration was based on **Eqn. (3.41)**, and the computation of the maximum stress in the skins was based on **Eqn. (3.28)**. As mentioned previously (section **3.4**), no raw material was available for the skins and no prediction of the sandwich damping could be made from the damping properties of the constituent parts.

In **Fig. 5.5**, the damping results of the 1/2 in. beam are shown. The shear correction factor, k, was found so that the test frequency was accurately predicted (within ±0.5%), as advocated previously (**3.3.4**). Also included in this figure are the results for a unit factor, as well as for a factor tending to infinity (Bernoulli-Euler beam).

The in-air results (**Fig. 5.5**) generally show the trend observed earlier for the Duralumin beam, *i.e.*, a constant initial damping with respect to the stress amplitude, followed by an increase in damping. However, unlike the Duralumin beam (**Fig. 5.2**), the *in-vacuo* damping results show an increase with stress amplitude, which can be seen to happen even at comparable stress levels (*cf.* **Figs. 5.2, 5.6** and **5.7**). For the thicker beams (**Figs. 5.6** and **5.7**), an unexpected rapid change is noticed in the SDC of the low stress region of the *in-vacuo* tests. This apparent upsurge of the SDC cannot be explained, although it is also noted that the

free-decay results are generally higher than is indicated by steady-state results at these low stress regions.

The *in-vacuo* results in **Fig. 5.5** indicate a low stress damping of aluminium sandwich of 0.25%. Assuming the extraneous dampings are of about 0.15%, the *in-vacuo* SDC of the aluminium sandwich will be roughly of the order of 0.1%.

The SDC was read off at 1 MPa skin maximum stress from **Figs. 5.5** to **5.7**, and was plotted against the core thickness in **Fig. 5.8**. From this latter figure, it is clear that at low level stress, both in-air and *in-vacuo* SDC of the beam increases with the core thickness. The similarity of the trends in the in-air and *in-vacuo* results tends to rule out the influence of aerodynamic damping, which is only to be expected since these are negligible at low amplitudes. Moreover, since at the same skin stress, the core shear stress subsides with the increase in the core thickness, the possibility of the influence of any non-linear damping in the core on the observed increase in the SDC also seems to be an unlikely cause.

In fact, the increase in the SDC with the core thickness follows the mechanism by which the sandwich constituent parts contribute to the overall damping. Both the bending and shearing energies increase with the sandwich thickness. However, as is shown in **Fig. 5.8**, the rate of increase of the shearing energy (U_s) is more than that of the bending energy (U_b), which means that the skin contribution to damping falls and that of the core rises with the core thickness (**Eqns. (3.23)**). Since the strain energy in bending is the dominant of the two, this in turn implies that the rise in the core contribution to the overall damping is proportionally more than the fall in the skin contribution, resulting in a net gain in overall damping. This process will be considered again in the next chapter (section **6.7.2.2**), with reference to actual skin and core damping contribution.

In measuring the damping of the sandwich by the forced resonance method described above, the main result of not allowing for shearing of the core (Bernoulli-Euler beam) is to not

account for strain energy in shearing of the core. Moreover, the computed strain energy in bending of the skin is also overestimated. In Fig. 5.9, the bending and shearing energies of the X-oriented 1/2 in. thick sandwich beam have been plotted against the central displacement amplitude. The bending energy of the beam obtained by the elementary (Bernoulli-Euller) analysis is also included in this figure. When shear is ignored, the elementary theory attributes all the central deflection to the direct strain in the skin and therefore, a rise in the strain energy of bending compared to the same energy in the sandwich will result. As the figure shows, this theory increasingly overrates the total energy of the beam with amplitude and therefore, as is indicated in Fig. 5.5, underrates the damping. However, provided the core strain energy is substantially lower than that of the skin, the difference in measured damping at low amplitudes will be relatively small. For the same reason, any correction for shear, will also have marginal effect on the measured damping (Fig. 5.5).

Generally, good agreement is seen to exist between the free-decay damping results and those measured in the steady-state, the only exceptions being the *in-vacuo* results of the 1 and 2 in. thick beams (Figs. 5.6 and 5.7), as mentioned previously.

The cross-ribbon (Y) damping results also follow the trend shown by the results in the ribbon (X) direction, although as observed in the double-lap shear tests, they are generally slightly higher (Fig. 5.8).

5.4 Conclusions

The centrally driven system described above offers an adequate method for determining the SDC in free-free steady-state vibration. Compared to the end driven method, the system is more stable, the loading points are better defined, and the rotary inertia is limited to the specimen, making the steady-state damping analysis and tests that much more reliable. One

drawback, inevitably, is the fact that it involves more extraneous damping, roughly by a factor of 3 to 1.

At low amplitudes, friction-damping is the major contributor to the overall extraneous damping, surpassing the air damping by a factor of about 4 to 1. Nonetheless, the overall extraneous damping of the centrally driven system used in this work, is within a SDC of 0.2%, a figure which should be taken into account when measuring the properties of lightly damped materials, such as unidirectional composites or aluminium sandwich beams, but is low enough to be discarded for most other cases.

In the absence of air damping, the extraneous damping in the centrally driven system amounts to a maximum SDC of about 0.15%. Roughly 2/3 of this figure results from the friction at the clamping points where the coil assembly is secured to the mid-span of the beam. The remaining 1/3 may be attributed to friction and the vibration transmission in the suspension arrangement.

Testing all-aluminium sandwich beams, the steady-state damping results were found to be in good agreement with those obtained by the free-decay of the resonant amplitude. Depending on the sandwich thickness, the *in-vacuo* damping of all-aluminium sandwich beams was found to be in the range of 0.25% to 0.55% SDC, including the extraneous damping. Due to the fact that strain energy in bending of the sandwich skin was the dominant contributor to the total strain energy of the beam, no appreciable difference in damping measurement resulted from considering a shear correction factor, especially at low amplitudes of vibration.

Chapter 6

DAMPING OF COMPOSITE/HONEYCOMB SANDWICH BEAMS

Scope - In this chapter, first, utilising the basic relations of unidirectional composites and the Adams-Bacon damping criteria, equations are derived for prediction of moduli and damping of the sandwich skins from constitutive data.

Then, using the above results and the results obtained in *Chapter 4* for the dynamic shear properties of the honeycomb core, the equations developed in *Chapter 3* are utilised for computation of damping in sandwich beams, and the proportion of the skin and core contribution.

In each case, the predicted results are verified experimentally. Particular attention will be paid to the variation of damping with stress in the laminated composites with different orientations.

6.1 Constitutive equations of unidirectional composites

The three-dimensional stress-strain relations in the fibre co-ordinate system (**Fig. 6.1**) of a transversely isotropic unidirectional lamina are given as

$$\begin{Bmatrix} \varepsilon_{xx} \\ \varepsilon_{yy} \\ \varepsilon_{zz} \\ \varepsilon_{yz} \\ \varepsilon_{xz} \\ \varepsilon_{xy} \end{Bmatrix} = \begin{bmatrix} 1/E_x & -\upsilon_{xy}/E_x & -\upsilon_{xy}/E_x & 0 & 0 & 0 \\ -\upsilon_{yx}/E_y & 1/E_y & -\upsilon_{yz}/E_y & 0 & 0 & 0 \\ -\upsilon_{zx}/E_z & -\upsilon_{zy}/E_z & 1/E_z & 0 & 0 & 0 \\ 0 & 0 & 0 & 1/G_{yz} & 0 & 0 \\ 0 & 0 & 0 & 0 & 1/G_{xz} & 0 \\ 0 & 0 & 0 & 0 & 0 & 1/G_{xy} \end{bmatrix} \begin{Bmatrix} \sigma_{xx} \\ \sigma_{yy} \\ \sigma_{zz} \\ \sigma_{yz} \\ \sigma_{xz} \\ \sigma_{xy} \end{Bmatrix} \tag{6.1}$$

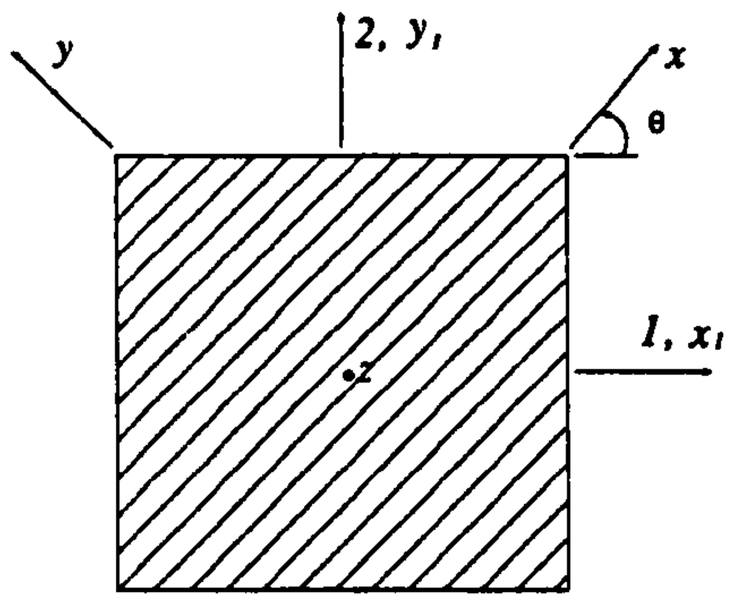

Fig. 6.1 *Coordinate system of unidirectional lamina*

where from the material symmetry

$$E_y=E_z\ ,\ \upsilon_{yx}/E_y = \upsilon_{xy}/E_y = \upsilon_{zx}/E_z\ ,\ \upsilon_{yz}/E_y = \upsilon_{zy}/E_z$$

The elastic properties in **Eqn. (6.1)** refer to those obtained by uniaxial tests on a typical unidirectional laminate, *viz*

$$E_x = E_l\ ,\ E_y = E_t\ ,\ G_{xy} = G_{lt}\ ,\ \upsilon_{xy} = \upsilon_{lt}$$

where suffixes l and t refer to the directions along and transverse to the fibre respectively, G_{lt} is the longitudinal shear modulus, υ_{lt} is the major Poisson's ratio and G_{yz} and G_{zx} are interlaminar shear moduli.

In practical applications, laminae are sufficiently thin to assume that a state of plane stress within the lamina prevails. In this case $\sigma_{zz} = \sigma_{yz} = \sigma_{zx} = \varepsilon_{yz} = \varepsilon_{zx} = 0$. Strict application of the plane stress criterion, however, cannot account for significant interlaminar shearing which does occur in flexure of thick laminates. For that reason, formulations have been developed in which the transverse shears, ε_{yz} and ε_{zx} , are retained in **Eqn. (6.1)** to account for interlaminar shears, while keeping with the assumption that the state of stress within the lamina remains that of plane stress [Pagano, 1970; Whitney and Pagano, 1970; Chow, 1971; Kulkarni and Pagano, 1972; Whitney, 1972, 73, 87 *etc.*]. These formulations, generally referred to as the 'shear deformation theory', are an extension of Mindlin's theory for homogeneous plates and as such are based on the assumption of a state of plane strain for

the laminate. However, as pointed out by Whitney [1987], the state of the plane stress within a lamina leads to the implication of the stress discontinuity at the ply interface, warranting further modifications for a more reasonable shear distribution. Similar formulations have been used, with reasonable success, as the basis for finite element analysis of modal vibration of thick isotropic plates [Cawley and Adams, 1978, 79] and laminated composites [Lin *et al*, 1984]. Whitney [1987] shows that for a symmetric laminated beam, the shear deformation theory leads to the Timoshenko beam equations. His application of the theory to a soft core sandwich beam, however, involves no shear correction factor.

The approach in this work was to treat the skins as thin and homogeneous materials undergoing uniaxial tension/compression about the sandwich mid-plane. Timoshenko beam equations, adopted through the usual simplifying assumptions could then be used to determine the bending/shearing energy ratio and damping in a sandwich, as advocated previously (*Chapter 3*). Both assumptions of thin as well as homogeneous skins are justifiable for relatively high ratios of skin/core thickness [Whitney, 1987]. The minimum skin/core thickness ratio used in this work was of the order 1:6; for the majority of the beams, however, this ratio was of the order 1:12.

For the sandwich skins, therefore, a state of plane stress is assumed. In this case, **Eqn. (6.1)** reduces to

$$\begin{Bmatrix} \varepsilon_{xx} \\ \varepsilon_{yy} \\ \varepsilon_{xy} \end{Bmatrix} = \begin{bmatrix} 1/E_x & -\upsilon_{xy}/E_x & 0 \\ -\upsilon_{yx}/E_x & 1/E_y & 0 \\ 0 & 0 & 1/G_{xy} \end{bmatrix} \begin{Bmatrix} \sigma_{xx} \\ \sigma_{yy} \\ \sigma_{xy} \end{Bmatrix} \qquad (6.2)$$

or

$$\{ \varepsilon_{x,y} \} = [C_{x,y}] \{ \sigma_{x,y} \} \qquad (6.3)$$

The suffix x,y here is intended to indicate reference to the fibre coordinates system. In this equation, $\varepsilon_{x,y}$ and $\sigma_{x,y}$ are on-axis strain and stress, and $C_{x,y}$ is the on-axis compliance matrix. Equation (6.2) is applicable to an orthotropic lamina under plane stress conditions, and as can

be seen, to completely characterise such a lamina four independent elastic properties are required.

Equation (6.3) may be written as

$$\{ \sigma_{x,y} \} = [Q_{x,y}] \{ \varepsilon_{x,y} \} \tag{6.4}$$

where

$$[Q_{x,y}] = [C_{x,y}]^{-1} = \begin{bmatrix} Q_{xx} & Q_{xy} & 0 \\ Q_{xy} & Q_{yy} & 0 \\ 0 & 0 & Q_{ss} \end{bmatrix} \tag{6.5}$$

and

$$Q_{xx} = \frac{E^2_x}{E_x - \upsilon^2_{xy} E_y}, \quad Q_{yy} = \frac{E_x E_y}{E_x - \upsilon^2_{xy} E_y}, \quad Q_{xy} = \frac{\upsilon_{xy} E_x E_y}{E_x - \upsilon^2_{xy} E_y}, \quad Q_{ss} = G_{xy} \tag{6.6}$$

Transformation of stress from the fibre to the lamina coordinate system is carried out through the transformation matrix $[T]_\sigma$

$$\{\sigma_i\} = [T_{ij}]_\sigma \{\sigma_{x,y}\} \qquad i,j = 1,2,6 \tag{6.7}$$

Similarly

$$\{\varepsilon_i\} = [T_{ij}]_\varepsilon \{\varepsilon_{x,y}\} \qquad i,j = 1,2,6 \tag{6.8}$$

where $i = 1, 2, 4, 5, 6$ in the laminate coordinate system are analogous to xx, yy, yz, xz, xy in the fibre coordinate system. Equations (6.4), (6.7) and (6.8) will give

$$\{\sigma_i\} = [T_{ij}]_\sigma [Q_{x,y}] [T_{ij}]^{-1}_\varepsilon \{\varepsilon_j\} \qquad i,j = 1,2,6$$

or

$$\{ \sigma_i \} = [Q_{ij}] \{ \varepsilon_j \} \qquad i,j = 1,2,6 \tag{6.9}$$

where

$$[Q_{ij}] = [T_{ij}]_\sigma [Q_{x,y}] [T_{ij}]^{-1}_\varepsilon \qquad i,j = 1,2,6 \tag{6.10}$$

and

$$[T]_\sigma = \begin{bmatrix} m^2 & n^2 & -2mn \\ n^2 & m^2 & 2mn \\ mn & -mn & m^2 - n^2 \end{bmatrix} \tag{6.11}$$

where $m = \cos\theta$, $n = \sin\theta$.

In general $[T]_\sigma \neq [T]_\varepsilon$ due to the use of engineering rather than tensorial shear strains. The matrix $[T]_\varepsilon$ is given by $[T]_\sigma$ when the elements *13* and *23* in the latter are divided by two and the elements *31* and *32* multiplied by two.

The components of $[Q_{ij}]$ are given as

$$[Q_{ij}] = \begin{bmatrix} Q_{11} & Q_{12} & Q_{16} \\ Q_{12} & Q_{22} & Q_{26} \\ Q_{16} & Q_{26} & Q_{66} \end{bmatrix} \tag{6.12}$$

where from **Eqn. (6.10)**

$$\begin{aligned}
Q_{11} &= m^4 Q_{xx} + n^4 Q_{yy} + 2 m^2 n^2 (Q_{xy} + 2 Q_{ss}) \\
Q_{12} &= m^2 n^2 (Q_{xx} + Q_{yy} - 4 Q_{ss}) + (m^4 + n^4) Q_{xy} \\
Q_{16} &= m n [m^2 Q_{xx} - n^2 Q_{yy} - (m^2 - n^2)(Q_{xy} + 2 Q_{ss})] \\
Q_{22} &= n^4 Q_{xx} + m^4 Q_{yy} + 2 m^2 n^2 (Q_{xy} + 2 Q_{ss}) \\
Q_{26} &= m n [n^2 Q_{xx} - m^2 Q_{yy} + (m^2 - n^2)(Q_{xy} + 2 Q_{ss})] \\
Q_{66} &= m^2 n^2 (Q_{xx} + Q_{yy} - 2 Q_{xy}) + (m^2 - n^2)^2 Q_{ss}
\end{aligned} \tag{6.13}$$

In **Eqn. (6.9)**, $[Q_{ij}]$ for $i, j = 1, 2, 6$ is referred to as the off-axis reduced plane-stress stiffness matrix of the lamina.

6.2 Flexure of a thin laminate

From the usual assumption of plane stress conditions for a thin composite plate, it follows that the normals to the undeformed planes in the plate would remain normal and undeformed in the deformed planes with the implication that the in-plane strains in the plate

are linear functions of thickness. Then, the following strain-displacement relations apply to the composite plate

$$\begin{bmatrix} \varepsilon_1 \\ \varepsilon_2 \\ \varepsilon_6 \end{bmatrix} = \begin{bmatrix} \partial^2 W/\partial x_1^2 \, z \\ \partial^2 W/\partial y_1^2 \, z \\ 2\partial^2 W/\partial x_1 \partial y_1 \, z \end{bmatrix} = \begin{bmatrix} \chi_1 \, z \\ \chi_2 \, z \\ \chi_6 \, z \end{bmatrix} \tag{6.14}$$

where W is the lateral displacement and χ_1 , χ_2 and χ_6 are curvatures.

The constitutive equations for general loading of a laminated plate are given in terms of stress and moment resultants per unit length, N_i and M_i , at the mid-plane

$$\begin{bmatrix} N_i \\ M_i \end{bmatrix} = \begin{bmatrix} A_{ij} & B_{ij} \\ B_{ij} & D_{ij} \end{bmatrix} \begin{bmatrix} \varepsilon^0_j \\ \chi_j \end{bmatrix} \qquad i,j = 1,2,6 \tag{6.15}$$

where ε^0_j are mid-plane strains, and

$$(A_{ij}\,,\ B_{ij}\,,\ D_{ij}) = \int_{-h/2}^{h/2} Q^k_{ij} \ \ (1, z, z^2)\, dz \qquad i,j = 1,2,6 \tag{6.16}$$

in which Q^k_{ij} refers to the reduced stiffness matrix of the *k'th* layer and h is the thickness of the plate. The matrices A_{ij} , B_{ij} and D_{ij} are referred to as the in-plane modulus, bending-stretching coupling modulus and the flexural modulus respectively.

In the absence of in-plane forces, **Eqn. (6.15)** is reduced to

$$M_i = B_{ij} \ \varepsilon^0_j + D_{ij} \ \chi_j \qquad i,j = 1,2,6 \tag{6.17}$$

For symmetric laminates, the bending-stretching coupling effect, which mutually induces in-plane stresses and moments, is removed and **Eqn. (6.17)** is reduced to

$$M_i = D_{ij} \ \chi_j \qquad i,j = 1,2,6 \tag{6.18}$$

The *k'th* layer stiffness matrix, Q^k_{ij} , is a function of both material properties and ply orientation. The flexural damping of special cases where either material properties or orientation remain constant across the section, and therefore may be factored out of the integral in **Eqn. (6.16)**, are discussed in [Ni *et al*, 1984] and [Ni and Adams, 1984] respectively.

The flexural modulus, D_{ij} , is given by **Eqn. (6.16)**. In this equation, the reduced stiffness matrix, Q_{ij} , is independent of thickness within the *k'th* lamina. The equation, therefore, may be written as

$$D_{ij} = \int_{-(N/2)}^{(N/2)} Q^k_{ij} \; z^2 \; dz$$

$$= 2 \sum_{k=1}^{N/2} Q^k_{ij} \int_{h_{(k-1)}}^{h_{(k)}} z^2 \; dz$$

$$= \frac{2}{3} \sum_{k=1}^{N/2} Q^k_{ij} \left(h_{(k)}^3 - h_{(k-1)}^3 \right) \qquad i,j = 1,2,6$$

where N is the total number of layers and $h_{(k)}$, $h_{(k-1)}$ are the upper and lower coordinates of the *k'th* layer. For the case where the layers are of the same thickness, h_0 , this equation may be written as

$$D_{ij} = \frac{2h_0^3}{3} \sum_{k=1}^{N/2} Q^k_{ij} \left(k^3 - (k-1)^3 \right) \qquad i,j = 1,2,6$$

$$\therefore \qquad D_{ij} = \frac{h^3}{12} \frac{8}{N^3} \sum_{k=1}^{N/2} Q^k_{ij} \left(k^3 - (k-1)^3 \right) \quad i,j = 1,2,6 \qquad \textbf{(6.19)}$$

Normalised flexural modulus is defined as

$$D^*_{ij} = \frac{D_{ij}}{(h^3 / 12)} = \frac{D_{ij}}{h^*}$$

$$\therefore \qquad D^*_{ij} = \frac{8}{N^3} \sum_{k=1}^{N/2} Q^k_{ij} \left(k^3 - (k-1)^3 \right) \quad i,j = 1,2,6 \qquad \textbf{(6.20)}$$

And, therefore, the normalised flexural compliance is given as

$$C^*_{ij} = \frac{1}{D^*_{ij}} = C_{ij} h^* \qquad i,j = 1,2,6 \qquad \textbf{(6.21)}$$

6.3 Effective Young's modulus of laminated beams in flexure

The curvatures are given by **Eqn. (6.18)** as

$$\{ \chi_i \} = [D_{ij}]^{-1} \{ M_j \} = [C_{ij}] \{ M_j \} \qquad i,j = 1,2,6 \qquad \textbf{(6.22)}$$

If a beam is subjected to the bending moment M_1 only, the deformation is referred to as 'free flexure'. In this case, if the assumption is made that application of the bending moment M_1 involves only one curvature along the '1' direction, χ_1 , then, **Eqn. (6.22)** is reduced to

$$\chi_1 = C_{11} M_1 \tag{6.23}$$

The analogous curvature for a homogeneous isotropic beam is given by

$$\chi_1 = \frac{M_1}{E I} \tag{6.24}$$

where in accordance with the definitions in **Eqn. (6.15)**, M_1 and I are moment and moment of inertia per unit width of the beam. Then, the effective Young's modulus in free flexure, E_{ff} , is defined as that of a laminated beam equivalent to a homogeneous isotropic beam; and is obtained by equating **Eqns. (6.23)** and **(6.24)**

$$E_{ff} = E = \frac{1}{C_{11} h^*} = \frac{1}{C^*_{11}} \tag{6.25}$$

In 'pure flexure', any twisting curvature, χ_6 , resulting from the application of the moment M_1 is constrained to zero by the application of the twisting moment M_6 . In this case, **Eqn. (6.22)** gives

$$M_6 = \frac{-C_{16}}{C_{66}} M_1$$

and, therefore, the effective Young's modulus in pure flexure, E_{pf} , is given by

$$E_{pf} = \frac{C^*_{66}}{C^*_{11} C^*_{66} - C^{*2}_{16}} \tag{6.26}$$

The case of free flexure is applicable to the free-free flexural vibration tests in this work and will be used for the prediction of the effective Young's modulus.

6.4 Damping prediction of laminated beams

Experiments of Adams and Bacon [1973-c], Ni and Adams [1984], Ni *et al* [1984], Lin *et al* [1984] and Wren and Kinra [1989-b] have shown that damping properties of unidirectional fibrous composites can be predicted with a good degree of accuracy using the Adams-Bacon damping criteria. Adams and Bacon [1973-c] postulated that the energy dissipation in a thin

unidirectional lamina is the sum of separable energy dissipations due to σ_x , σ_y and σ_{xy}[1]. Then, the specific damping capacity of a laminated composite may simply be written as

$$\psi = \psi(x, y, xy) = \frac{\Delta U_x}{U} + \frac{\Delta U_y}{U} + \frac{\Delta U_{xy}}{U} \qquad (6.27)$$

By definition, the energy dissipation due to σ_x is given by

$$\Delta U_x = \frac{1}{2} \int_v \psi_l \, \varepsilon_x \, \sigma_x \, dv \qquad (6.28)$$

Substituting for σ_x and ε_x from (6.7) and (6.8) gives

$$\Delta U_x = \frac{1}{2} \int_v \psi_l \, \{ [T_{ij}]_t^{-1} \{ \varepsilon_j \} \} \{ m^2 \{ \sigma_1 \} \} \, dv \qquad i = 1, j = 1, 2, 6$$

noting that for free flexure of the beam, $\sigma_2 = \sigma_6 = 0$. Substitution for σ_1 from (6.9) gives

$$\Delta U_x = \frac{1}{2} \int_v \psi_l \, \{ [T_{ij}]_t^{-1} \{ \varepsilon_j \} \} \{ m^2 [Q_{ij}]^k \{ \varepsilon_j \} \} \, dv \qquad i = 1, j = 1, 2, 6$$

Substituting for ε_j from (6.14) gives

$$\Delta U_x = \frac{1}{2} \int_v \psi_l \, \{ [T_{ij}]_t^{-1} \{ \chi_j \} z \} \{ m^2 [Q_{ij}]^k \{ \chi_j \} z \} \, dv \qquad i = 1, j = 1, 2, 6$$

Substituting for χ_j from (6.22) gives

$$\Delta U_x = \frac{1}{2} \int_v \psi_l \, [T_{ij}]_t^{-1} [C_{ij}] M_1 [Q_{ij}]^k [C_{ij}] M_1 m^2 z^2 \, dv \qquad i = 1, j = 1, 2, 6$$

Then, for a beam of unit width, the energy dissipation becomes

$$\Delta U_x = 2 \int_0^{L/2} M_1^2 \, dx \int_0^{h/2} \psi_l \, [T_{ij}]_t^{-1} [C_{ij}] [Q_{ij}]^k [C_{ij}] m^2 z^2 \, dz \qquad i = 1, j = 1, 2, 6$$

Strain energy stored in the beam under the bending moment resultant, M_1 , is given by

$$U = \int_0^{L/2} M_1 \chi_1 \, dx$$

---

1 Analogous suggestions have been postulated with reasonable success, for example, regarding the strain energy of natural rubber as a separable function of the extension ratios (author's M.Sc. thesis).

Substituting for χ_1 from (6.23) gives

$$U = C_{11} \int_0^{L/2} M_1^2 \, dx \qquad (6.29)$$

The specific damping capacity due to σ_x is, therefore, given by

$$\psi_x = \frac{2}{C_{11}} \int_0^{h/2} \psi_l \, [T_{ij}]_\varepsilon^{-1} \, [C_{ij}] \, [Q_{ij}]^k \, [C_{ij}] \, m^2 z^2 \, dz \qquad i = 1, j = 1, 2, 6$$

Assuming that the linear damping mechanism holds, that is that the amplitude of vibration is sufficiently low to make the specific damping capacity independent of the stress amplitude, then this equation may be written as

$$\psi_x = \frac{2\psi_l}{C_{11}} \int_0^{h/2} [T_{ij}]_\varepsilon^{-1} \, [C_{ij}] \, [Q_{ij}]^k \, [C_{ij}] \, m^2 z^2 \, dz \qquad i = 1, j = 1, 2, 6$$

The orientations m , n and the stiffness matrix Q_{ij} are independent of thickness within the *k'th* lamina. Then following the same arguments in deriving **Eqn. (6.20)**, the above equation reduces to

$$\psi_x = \frac{h^3}{12 C_{11}} \frac{8\psi_l}{N^3} \sum_{k=1}^{N/2} [T_{ij}]_\varepsilon^{-1} \, [C_{ij}] \, [Q_{ij}]^k \, [C_{ij}] \, m^2 \, (k^3 - (k-1)^3) \qquad i = 1, j = 1, 2, 6$$

Using the normalised flexural compliance, as defined in **Eqn. (6.21)**, this equation is simplified further to

$$\psi_x = \frac{1}{C^*_{11}} \frac{8\psi_l}{N^3} \sum_{k=1}^{N/2} [T_{ij}]_\varepsilon^{-1} \, [C^*_{ij}] \, [Q_{ij}]^k \, [C^*_{ij}] \, m^2 \, (k^3 - (k-1)^3) \qquad i = 1, j = 1, 2, 6$$

or

$$\psi_x = \frac{8\psi_l}{C^*_{11} N^3} \sum_{k=1}^{N/2} m^2 \, (m^2 C^*_{11} + n^2 C^*_{12} + mn C^*_{16}) \, (C^*_{11} Q^k_{11} + C^*_{12} Q^k_{12} + C^*_{16} Q^k_{16}) \, (k^3 - (k-1)^3)$$

(6.30)

Similarly, it can be shown that

$$\psi_y = \frac{8\psi_l}{C^*_{11}N^3} \sum_{k=1}^{N/2} n^2 (n^2 C^*_{11} + m^2 C^*_{12} + mn C^*_{16}) (C^*_{11} Q^k_{11} + C^*_{12} Q^k_{12} + C^*_{16} Q^k_{12}) (k^3 - (k-1)^3) \qquad (6.31)$$

and that

$$\psi_{xy} = \frac{8\psi_{lt}}{C^*_{11}N^3} \sum_{k=1}^{N/2} mn (2mn C^*_{11} - 2mn C^*_{12} - (m^2 - n^2) C^*_{16}) (C^*_{11} Q^k_{11} + C^*_{12} Q^k_{12} + C^*_{16} Q^k_{12}) \times (k^3 - (k-1)^3) \qquad (6.32)$$

6.5 Computer implementation

The above analyses were put into computer code using *FORTRAN77*. The necessary data for running this program includes the modulus and SDC of the 0° and 90° orientations in flexural mode, modulus and SDC of the longitudinal shear mode and the major Poisson's ratio. Once these data are supplied, the program can compute the effective Young's modulus and SDC in flexure of a beam having mid-plane symmetry of orientation. Although the need did not arise in this work, the program can be easily modified to account for beams having material symmetry across the section so that it can be run for beams consisting of different composites.

Similar to the computer programs mentioned previously (section **3.3.6**), this program, *PREDAMP.FOR*, can provide the user with a file containing a detailed description of a data file, again avoiding the need for a separate user-guide. A desk-top computer can be conveniently used to run the program.

6.6 Experimental procedure

Combinations of three different unidirectional composites and three different honeycombs were used for the fabrication of the sandwich beams. In all cases, both skins consisted of eight plies of the same unidirectional composite material. The skins were of identical orientations and the sandwich was of mid-plane symmetry. In addition to the orthotropic 0°/90° skins (0° along the beam), for which $D^*_{16}=0$, two systems of anisotropic skins ($D^*_{16}\neq 0$), namely the 'off-axis' (all layers at θ) and the symmetric 'angle-ply' (layers at -θ, θ, -θ, θ, θ, -θ, θ, -θ), were considered. For either system and each particular skin/core material combination, a series of sandwich beams was fabricated for increments of 15° of fibre orientation covering the 0° to 90° range. Experimental and theoretical results were obtained for both the beams (sandwich skins) and the sandwich beams regarding the variation of modulus and the SDC with respect to orientation.

In all cases, the sandwich cores were aligned along the ribbon direction.

6.6.1 Preparation of the sandwich skins

All the sandwich skins were moulded from the pre-preg sheets using a hot press. To make sure of accurate orientation, the pre-preg sheet was pinned down on a board and the plates were marked on the pre-preg prior to cutting out the ply with a sharp scalpel. The plies, cut slightly over the size of the mould, were then stacked and trimmed along the edges to the same size as the mould. This step was necessary since in stacking the plies it is not always possible to make the edges coincide, and once the plies are in contact it is difficult to separate them without disturbing the fibres. The backing sheets at the outer surfaces were not removed until the moulding stage for protection.

In compression moulding of composites, flushing of some resin through the mould openings is not only inevitable but also desirable since this helps the flow of the resin through the fibres thereby filling voids and expelling air and gases from the moulding. Excess flushing,

on the other hand, might lead to areas of 'resin starvation' and possible debonding of fibres. With this in mind, it was decided to set the height of the mould cavity to the nominal thickness of the laminate. Shims, inserted between the top mould surface and its backing plate, were used for this purpose. The amount of flushing varied for different mouldings. In some cases, these were carefully removed from the mould and the moulding and weighed. The weight of the excess resin was found to be generally below 1% of the weight of the moulding.

Prior to each moulding operation, the mould was cleaned and degreased with acetone. It was then heated to 60° C and the release agent (Frekote 700-NC) was sprayed onto the surfaces of the pre-heated mould. The mould was re-heated, this time to 120° C, and the laminate was carefully placed on the bottom surface and the top plate was lowered into the mould. The mould walls were then tightened up and the mould was placed in the hot press. In closing the press platens onto the mould, it is important to apply the pressure as gently as possible in order to minimise fibre misalignment caused by otherwise too violent a resin flow around the fibres. The press used lacked the facility for setting the closing rate, but this could be controlled manually by throttling the flow valve.

The manufacturer's curing specifications were used in moulding of the plates, and these are listed in section **6.6.1.1.**

For the off-axis beams, unidirectional square plates (300 mm × 300 mm) were first moulded and the beams with the different orientations marked on the plates. Two plates were then stacked together and cut through giving pairs of beams with identical size and orientation. Smaller, rectangular plates (300 mm × 70 mm) were moulded for angle-ply orientations. Each plate was subsequently cut into halves along its length for the two sandwich skins. A milling machine with a diamond-wheel cutter was used for cutting the beams. Using this cutter results in very smooth edges. To avoid any edge-effects, a width of about 2 mm of all the edges of the moulding were also removed.

6.6.1.1 Pre-preg and moulding specifications

Three different unidirectional composites were used. These were

1 - DLS-280
2 - Fibredux 913G-E-5-30
3 - Fibredux 913C-TS-5-40

The first two are glass fibre reinforced plastic (GFRP) composites and the third is carbon fibre reinforced plastic (CFRP) composite. The **Fibredux 913** refers to the resin used in the pre-preg and is specified by the manufacturer (Ciba-Geigy Information Sheet No. FTA.46e) as a modified epoxy resin for use at a working temperature in the range -55 to +130° C. The designation **G-E-5-30** in the second composite refers to, respectively, the fibre type as Glass fibre of type E, with a cured pre-preg thickness of 5×0.001 in. and, finally, the resin content of the pre-preg as 30% by weight (equivalent to 54% of fibre by volume - personal communication with the manufacturer). Similarly, the designation **C-TS-5-40** in the third composite refers to Carbon fibre of 'high tensile strength, with a cured pre-preg thickness of 5×0.001 in. and a resin weight fraction of 40% (equivalent to 54% of fibre by volume).

The following moulding specifications, recommended by the manufacturer (personal communication), were used.

DLS-280	cured at 90° C for 1/2 hr. and at 120° C for 1 hr.
Fibredux 913G-E-5-30	cured at 120° C for 1 hr.
Fibredux 913C-TS-5-40	cured at 120° C for 1 hr.

All the plates were moulded under a nominal pressure of 600 kPa on the mould backing plate. At the end of the curing cycle, the mould was removed from the press and allowed to cool at room temperature. Close inspection of the mouldings revealed that, in most cases, these were of reasonably good finish, although a few visible surface imperfections proved to be unavoidable.

6.6.2 Preparation of the sandwich beams

Three different honeycombs were used for the fabrication of the sandwich beams (**Table (6.2)**). The honeycomb was cut from stock using the same method described previously (section **4.2.2**).

The adhesive film used for the fabrication of the sandwich beams was Redux 609, specified by the manufacturer (Ciba-Geigy Instruction Sheet No. RTC. 101d) as a high strength epoxy adhesive incorporating a cotton scrim for easy handling. The adhesive film is said to possess a good filleting property to be particularly suitable for honeycomb sandwich construction.

Having degreased the composite skins, the adhesive film, previously cut to size, was peeled off the backing sheets and placed on the skin. The skins were then carefully assembled onto the honeycomb core, applying a slight pressure to make the sandwich hold together. The beams were then placed side by side between two aluminium plates for uniform pressure and for protection of the outer surfaces. The assembly was then placed in the heated press. The manufacturer's curing specifications for Redux 609 were followed, namely at 120° C for one hour. A nominal pressure of 100 kPa on the sandwich skins was used. At the end of the cure cycle, the beams were removed from the press and let to cool at room temperature. Excess adhesive on the edges was carefully scraped off using a sharp scalpel.

6.7 Test procedure and results

The tests were carried out in two stages. First, having prepared the sandwich skins, dynamic flexural tests were carried out on one of each pair of the skins. Having obtained the necessary data for the skins, the latter were subsequently used to construct the sandwich beams. Dynamic flexural tests were then carried out on the sandwich beams.

The tests basically involved determination of modulus and the SDC in the first flexural mode. All the tests were carried out in the steady-state vibration using the centrally mounted coils, in air and at room temperature (19° to 22° C). For each test piece, the SDC results were obtained for increments of the maximum bending stress of the composite (skins).

Computation of the effective dynamic Young's modulus of the skins bending about their own neutral axis was based on **Eqn. (3.8)** after reduction to the elementary theory (section **3.3.3**), while the computation of the effective dynamic Young's modulus of the skins of the fabricated sandwich bending about the sandwich mid-plane was based on **Eqn. (3.31)**. The two moduli are referred to as the 'skin modulus' and the 'sandwich modulus' respectively.

Computation of the SDC of the skins in steady-state flexural vibration was based on **Eqn. (3.41)**, and that for the sandwich on **Eqn. (3.40)**.

Computation of the maximum stress in the skin on its own and in the sandwich was based on **Eqn. (3.28)**, in the first case after reduction to the elementary theory. Computation of the shearing stress in the core was based on **Eqn. (3.29)**.

Regarding the sandwich skins, prediction of the modulus and the SDC at different orientations was based on **Eqns. (6.25)** and **(6.27)** respectively, utilising the constituent data obtained from tests on narrow beams (**Table (6.1)**). Prediction of the sandwich beam damping was based on **Eqn. (3.39)**, utilising the predicted properties of the skins, and the honeycomb shear results obtained in *Chapter 4* (**Table (6.2)**).

A detailed account of these computations, together with estimation of experimental error, is presented in *Appendix (D)* with reference to a typical result.

6.7.1 Sandwich skins

Before fabricating the sandwich beams, steady-state flexural tests were carried out on the composite beams subsequently used as the sandwich skins. However, in the case of the off-axis beams, owing to the relatively large mass of the central coils, achieving resonance, specially for orientations higher than 45°, proved to be difficult. In the off-axis case, therefore, tests had to be carried out on smaller beams (nominally 200×12×1 (mm)), using the small central coils.

The skin dimensions were nominally 250×35×1 (mm). The beams used in the flexural tests were, therefore, of a sufficiently high length/thickness aspect ratio (at least 200) for the application of the elementary theory with good accuracy. This was verified in the case of one beam (0° 913C, 252×36×1.1 (mm) at 103 Hz) which was treated as a Timoshenko type, with an assumed shear correction factor of 0.82. The shear modulus in flexure of a laminated Timoshenko beam is given by G_{xz} [Ritchie *et al*, 1975] and this was measured from a torsion test (*Appendix (B)*) on the 90° beam. The improved theory showed an increase of 0.12% in modulus (113.86 and 113.72 GPa) and a reduction of 0.06% in the SDC (0.8488% and 0.8493%). Subsequently, the beams were treated as Bernoulli-Euler type, and the experimental values of the modulus and the SDC were obtained for all orientations.

For each composite type, longitudinal shear tests were also carried out and the modulus and the SDC in this mode were obtained. The longitudinal shear tests are discussed in *Appendix (B)*.

In **Table (6.1)**, the flexural and longitudinal shear data needed for the prediction of the modulus and the SDC of the composite sandwich skins tested in this work are listed. The flexural data represent results of tests on the beams of nominal dimensions 200×12×1 (mm).

Table (6.1) *Constitutive data of sandwich skins*

composite	V_f (%)	E_l (GPa)	E_t (GPa)	ψ_l (%)	ψ_t (%)	G_{lt} (GPa)	ψ_{lt} (%)	υ_{lt}
DLS-280	52	47.4	10.7	1.17	7.8	5.9	7.80	0.290
Fibredux 913C	54	112.5	8.4	0.74	7.3	4.8	6.60	0.301
Fibredux 913G	54	41.5	12.5	1.61	6.7	5.0	7.30	0.286

The SDC values ψ_l , ψ_t and ψ_{lt} were measured at the lowest stress amplitude attainable, where a stress independent SDC was assumed. This point will be discussed later (**6.7.1.2**) with reference to experimental results.

The major Poisson's ratio, υ_{lt} , was measured using strain gauges (TML, type : FLA-3-11). A strip of material of 0° fibre orientation, 1 mm thick, 15 mm wide and of about 180 mm gauge length was used as the test piece. To avoid damaging the test piece in the grips, and also for a more uniform distribution of load, each end of the test piece was bonded between two rectangular metal pieces. Gauges were used on both faces of the test piece to account for any possible bending effects. Two strain gauges, connected in series and forming one arm of the bridge, were bonded on opposite faces of the test piece in the longitudinal direction. A second pair of gauges, connected in series and forming the second arm of the bridge, were similarly bonded in the transverse direction. The test piece was then subjected to a number of tensile loads, in the range 0 to 10 kN, and the longitudinal and transverse displacements were recorded.

6.7.1.1 Modulus

Prediction of the moduli follows from the application of the basic laminated plate theory reduced to the one dimensional case (**Eqn. (6.25)**). The experimental points and the predictions are presented in **Figs. 6.2** to **6.6**. As mentioned previously (**6.7.1**), because of

practical difficulties, narrow beams had to be used for tests on the off-axis series, and the predictions for these beams are based on results obtained from tests on narrow beams (nominal dimensions 200×12×1 (mm)). The predictions for the angle-ply beams are based on results obtained from tests on actual sandwich skins (nominal dimensions 250×35×1 (mm)).

Results generally show excellent prediction of the experimental moduli for the off-axis beams, while in the case of the angle-ply beams discrepancies exist. Subsequently, tests were also carried out on a series of angle-ply narrow beams (nominal dimensions 200×12×1 (mm)) and, as can be seen (**Figs. 6.3** and **6.5**), the results of the tests on the narrow beams fall close to the predicted points.

Clearly then, the source of the discrepancy should be sought in the dimensions of the sandwich skins. These were nominally 250×35×1 (mm), where the length was limited to the mould size and the minimum width was limited to a size which could accommodate a reasonable number of honeycomb cells in order to avoid edge effects. On the other hand, it was felt that tests should be carried out on the actual skins in order to have as few variables as possible.

Adams and Bacon [1973-c] investigated the variation of the flexural modulus of orthotropic angle-ply beams with respect to orientation. Their angle-ply beams consisted of a total of 5 $\pm\theta$ ply pairs which were repeated through the thickness. With no mid-plane symmetry, this type of laminate is referred to as the antisymmetric (or quasi-symmetric) angle-ply laminate. Their tests on both narrow (0.5 in.) and wide (1 in.) beams, all of 10 in. length, showed 'no significant effect' in the SDC or the modulus due to the beam width. Experiments of Wren and Kinra [1989-b] on symmetric graphite/aluminium angle-ply beams also showed close prediction of the experimental results. Their beams had length/width aspect ratios ranging from 10 to 20.

The basic difference between the anisotropic and orthotropic laminates lies in the presence or otherwise of the shear and normal couplings. For an antisymmetric angle-ply laminate, the bending-twisting couplings (D_{16} and D_{26}) are eliminated but the bending-stretching couplings (B_{16} and B_{26}) are mutually induced. A complete reversal of this process occurs for the symmetric laminates (this, in fact, can be shown to follow from **Eqn. (6.16)** where for a symmetric laminate $Q^k_{ij}(z) = Q^k_{ij}(-z)$ while for an antisymmetric laminate $Q^k_{ij}(z) = -Q^k_{ij}(-z)$; and it can further be shown that both these effects tend to diminish as the number of plies is increased resulting in a 'quasi-homogeneous' material).

Hence, for the 0° and 90° beams, from the data of which the predictions are made, and for the antisymmetric angle-ply beams, any deviation from the definition of a beam will be confined to the curvature χ_2, due to the Poisson's coupling D_{12} (**Eqn. (6.22)**), while for the symmetric angle-plies the curvature χ_6, due to the shear coupling D_{16}, also comes into effect. The Poisson's coupling, however, tends to diminish rapidly with decreasing aspect ratio, while the shear coupling becomes negligible only for high aspect ratios [Whitney and Dauksys, 1970; Whitney, 1987]. This process, on the one hand, explains the close predictions of Adams and Bacon [1973-c] for both widths of the beam, and on the other, the close predictions of the narrow beams results in the present work as well those of Wren and Kinra [1989-b]. It further explains the more pronounced deviations observed for the low angle wide beams (15° to 45°, **Figs. 6.3** and **6.5**) where the shear effect is more severe. The Poisson's effect is noticed in the 0° and 90° beam results on **Fig. 6.3**, and more clearly on **Fig. 6.5**, where the moduli of the narrow beams fall below the apparent moduli of the wider sandwich skins. Even closer predictions of the results of the angle-ply narrow beams are obtained if the predictions are derived from the 0° and 90° data of the narrow beams (these predictions are not included on the figures).

The effect of the shear coupling D_{16} on the off-axis beams is even larger than the angle-ply beams. Close inspection of the off-axis results reveals some deviation in the shear sensitive

regions even for the narrow beams (**Figs. 6.4** and **6.6**). Compared with the angle-ply beams, the sharp fall of the modulus of the off-axis beams with increasing θ is due to the lack of constraints which adjacent layers impose on one another, allowing the plies to deform independently.

6.7.1.2 The specific damping capacity

In supporting the beams on the cotton strings, one rule was followed, and that was supporting the beam where the least amount of vibration was transmitted to the supporting structure. At the same time, it was verified that this position also coincided with the peak displacement amplitude, as indicated by the pick-up voltage. In all cases of the angle-ply beams, the nodal lines were lateral to the beam, and the optimum locations for supports coincided with the nodal lines; the latter being determined by sensing the vibration (the customary use of sand or powder for nodal location was not always possible owing to relatively low frequencies). In the case of the off-axis beams, the nodal lines were at an angle to the transverse direction of the beam, being at a maximum of about 50° for the 15° beam and gradually tending to 0° for the 90° beam. However, supporting the beam on the nodal lines did not necessarily lead to the least amount of vibration transmission, possibly due to a more complex nature of behaviour of the nodal lines than conceived. In fact, in a few cases where the nodal lines were at a large angle to the lateral direction (15° and 30° beams), it was found that maintaining the nodal supports lateral to the beam led to less damping (higher pick-up voltage) than otherwise supporting the beam on the nodal lines.

Both the symmetric angle-ply and the off-axis beams are subject to the bending-twisting effect. Using a stroboscope, the motion of the centrally driven 30° off-axis as well as that of the 45° angle-ply wide beams was studied. In each case, the stroboscope was tuned to a small frequency difference thus showing the beam movement in slow motion. The beam end was then viewed against a horizontal datum line. Up to a maximum peak-to-peak displacement amplitude of approximately 10 mm at the end of the beam, no twisting could

be detected in either case. Given that the damping test displacement amplitudes are well below this figure (3 mm at most), and that the Young's moduli are well above the shear modulus, the effect on the strain energy due to any twisting of the beam is believed to be negligible. Pagano and Halpin [1968] showed that the twisting of the beam end had little effect on the normal strain field.

The SDC results for various stress amplitudes are presented in **Figs. 6.7** to **6.11**. Comparisons of the experimental SDC results at the lowest stress amplitude and the predicted results are presented in **Figs. 6.12** to **6.16**.

Ideally, the SDC values used for the predictions should be measured at the same stress level and, similarly, comparison should be made with those experimental points which are at the same stress level. However, because of the low sensitivity of the voltmeter at low pick-up voltages, there was a limit to the lowest displacement amplitude which could be attained. Consequently, depending on the modulus of each beam, the initial SDC results fell at different stress levels (**Figs. 6.7** to **6.11**). Nonetheless, referring to the results, it can be seen that in most cases the lowest amplitude falls within a stress level not more than 1 MPa and, since those results which do not fall into this range (0° and 15°) are the ones which show most stress independence, it may therefore be safely said that the SDC results represent damping at a stress amplitude not more than 1 MPa. Moreover, in most cases the assumption of stress independence at low stress amplitude seems to hold, although in some cases closer examination of the SDC at low stress amplitudes is needed. For example, an initial apparent sensitivity of the SDC is observed in a number of the higher angle beams (75° and 90° beams in the DLS series (**Fig. 6.7**), 75° in the off-axis 913C series (**Fig. 6.9**), 45° to 90° in the angle-ply 913G series (**Fig. 6.10**)), but as can be seen, this effect is not universal. Similar low stress sensitivity of the damping values was also observed in some of the damping tests on the honeycomb cores (**Figs. 4.13** to **4.16**).

Several trends can be seen in the results. In all cases, the low level damping, which is observed in the low-angle beams (0° and 15°), is seen to be relatively stress independent over the whole stress range. In these cases, the fibre properties are dominant and the composite approaches a Hookean elastic material. The low angle beams show the closest resemblance to linear damping where the hysteresis loop is elliptical and the energy dissipation is proportional to the square of the stress amplitude. For the higher angle beams, the stress sensitivity of the SDC seems to be a function of fibre/resin interaction. For example, in the case of the angle-ply 913C series (**Fig. 6.8**), the onset of non-linear damping for the high-angle beams (30° to 90°) can be seen to be about 1 MPa, while a change of fibre from carbon to glass (**Fig. 6.10**) results in a substantially reduced non-linearity of the SDC for up to the test range of 4 MPa. A similar low sensitive SDC is noticed in the second glass fibre composite (DLS, **Fig. 6.7**). Bacon [1973] reports non-linearity in the SDC of the HM-S/DX209 (CFRP) angle-ply beams, although no results are given indicating the extent or the onset of non-linear damping. He associates the phenomenon with 'a more complex state of stress than predicted by plate theory'.

Non-linear damping is generally attributed to a plastic-type deformation which most materials experience beyond certain critical stress limits [Lazan, 1960, 68]. With fibre reinforced composites having a polymeric matrix, the non-linear behaviour becomes even more significant, particularly in the transverse direction and in shear where the resin undergoes a considerable amount of straining.

Poor material integrity also causes non-linear damping. Defects in the micro structure, such as voids, crazing, impurities and 'frozen-in' stresses in the resin, and imperfect resin/fibre bonding or delamination in the composite are locations of stress concentration and/or friction, both of which tend to increase the damping energy in a proportion exceeding the second power of the stress amplitude. Hence, Bacon [1973, p. 39] would be correct in suggesting that linear damping indicates a modulus which is invariant of amplitude, but his

assertion that, similar to certain cast irons, non-linear damping in composites is necessarily indicative of a decreasing modulus is not entirely true. Damping is more sensitive to the composite material integrity than is the modulus.

Rate-dependent damping as a contributory factor to non-linear damping cannot be ruled out, given that increasing the displacement amplitude increases the strain rate even at a constant frequency. The rate-dependent damping mechanism is manifestly observed in viscoelastic materials where the material shows a time/temperature dependent response to the applied load due to the inertia of the molecular chains in coiling/uncoiling and the intermolecular movements. The viscoelastic damping is known to peak at the 'glass transition temperature', marking a transition from the 'rubbery' (higher temperatures/lower frequencies) response to the applied load to a 'glassy' (lower temperatures/higher frequencies) response. The viscoelastic phenomenon is not strong in thermosets, and the degree of the viscoelastic response depends on such factors as the degree of cross-linking and on the fibre contribution in load bearing in the fibrous composites. Increasing the frequency by a combination of shortening the beam length in the first flexural mode as well as testing in the second mode, Bacon [1973] found 'some' frequency dependence in the steady-state damping of the F/MNA epoxy resin even at room temperature (an increase in the SDC from 3% at 250 Hz to 5.7% at 2200 Hz). In interpreting these results, it should be borne in mind that he used the elementary (Bernoulli-Euler) theory which tends to give lower modulus/higher SDC with increase in frequency. Soovere [1985], however, recorded a 'constant' variation of damping with frequency in the (1,1) mode for both composite as well as aluminium honeycomb panels.

Generally, good correlation exists over the whole range of θ between the experimental and the predicted damping results (**Figs. 6.13 to 6.16**); an exception is the results of the off-axis DLS beams (**Fig. 6.12**) which will be discussed later.

The results generally show that the longitudinal component of the SDC is the sole contributor in the 0° beams, and the major contributor in the 15° angle-ply beams. Its contribution at higher angle beams becomes insignificant, although it falls more gradually in the angle-plies than the off-axis beams.

The shear component of the SDC peaks at 30° in the off-axis beams (**Figs. 6.12, 6.14** and **6.16**) and at 45° in the angle-plies (**Figs. 6.13** and **6.15**). Peaking of the shear component at 45° is analogous to the shear distribution in an isotropic material, indicating the more uniform nature of the shear constraint with respect to the angle of ply in the angle-ply laminates. In the off-axis beams, the shear component is the dominant contributor in the 15° to 45° range, while with the angle-plies it is the major contributor only in the 30° and 45° beams.

The transverse component of the SDC rises with the angle of orientation, but more gradually so in the angle-ply beams. It becomes the major contributor in the 60° and 75° beams and the sole contributor in the 90° beams.

As expected, comparison of the overall damping results in the off-axis and angle-ply beams shows a reversal of the process observed with the moduli. Here, a rapid increase in the SDC of the off-axis beams occurs with increasing angle of orientation, and a more gradual rise is seen in the angle-ply beams.

Naturally, the degree of the contribution of each component to the overall damping at any angle would depend on the proportion of the longitudinal, transverse and longitudinal shear damping of the particular composite. Hence, the peaks in the overall damping reported, for example, by Adams and Bacon [1973-c] (at 30° for the off-axis, and at 45° for the angle-ply beams of the HM-S/DX209 (CFRP) composite), are absent in the present results, since they used a longitudinal-shear SDC of some 10%, compared to a value of 6.6% found for the CFRP tested in this work.

The test results for the SDC of the angle-ply narrow beams (200×12×1 (mm)) are also included on **Figs. 6.13** and **6.15**. Generally, the beam width does not seem to have affected the damping results to any appreciable extent. With the 913G narrow beams (**Fig. 6.15**), the computed SDC is of a lower value than that of the wider sandwich skins for the 0° and 15° orientations, and slightly higher for higher orientations. The same trend is observed for the 913C beams (**Fig. 6.13**) for the 0° and 15° orientations, although even less deviation exists here, and for the higher orientations the results are more scattered than the 913G, but still no significant difference exists between the two results. It is unlikely that the increase in the SDC of the 0° and 15° wide beams is due to the increase in the air damping at higher frequencies since, comparing the 913C and the 913G results (**Figs. 6.13** and **6.15**), higher frequencies of the latter have not led to lower deviations.

In contrast to the 913 composites, large deviations exist between the experimental and the predicted SDC of the DLS composite (**Fig. 6.12**). This is almost certainly due to the problems experienced in moulding this pre-preg. Being dry, and possibly out of shelf life, it was found necessary to wet the surface of the layer (with acetone) when stacking the plies. As a consequence of wetting the layers, if not because of an already degraded resin, the mouldings were found to contain voids, as indicated by opacity. The moduli, however, do not seem to have suffered (**Fig. 6.2**), indicating that there was no serious delamination. Furthermore, and somewhat unexpectedly, no undue non-linearity is observed in the SDC results (**Fig. 6.7**). Comparison of the experimental and the predicted results (**Fig. 6.12**) seems to suggest overestimation of the longitudinal shear and, possibly also, the transverse damping used for the predictions. Only a limited amount of this pre-preg was available, and no attempt could be made to produce improved mouldings. The material, nonetheless, was used for fabrication of some of the sandwich beams and the results are included here.

6.7.2 Sandwich beams

Similar to the sandwich skins, steady-state flexural tests were carried out on the fabricated sandwich beams. The SDC of the sandwich beams were computed for increments of the maximum direct stress in the skins.

In **Table (6.2)**, the sandwich beams tested in this work, together with the core dynamic shear properties, are listed (The skin properties were listed previously in **Table (6.1)**).

Table (6.2) *Composite sandwich beams and core specifications*

skin		core			
material	orientation	material	c (mm)	G (MPa)	ψ (%)
DLS-280	off-axis	A1,50,6 (Nmx)	12.75	48.0	10.4
Fibredux 913C	off-axis	A1,50,6 (Nmx)	12.75	48.0	10.4
Fibredux 913C	angle-ply	A1,50,6 (Nmx)	12.75	48.0	10.4
Fibredux 913C	angle-ply	5.2,1/4,25 (Alum)	12.70	284.0	0.75
Fibredux 913G	angle-ply	A1,64,5 (Nmx)	6.90	56.9	10.6

6.7.2.1 The factor *k*

From the works on the shear correction factor for solid laminated beams and plates (section 2.1.1), the work by Chow [1971] on the subject seems to have drawn particular attention. Using a strain energy method and treating the case of static flexural loading of symmetric laminated beams, he derived expressions showing that the value of k 'depends heavily on the material constants' and ply orientations. For homogeneous anisotropic materials, his results reduced to the earlier results of Reissner [1945] for homogeneous isotropic materials and a value of $5/6$ for k . Suggestions were also made to the effect that, for low frequency dynamic loading of the beam, k could be ignored (*i.e.* $k=1$), and that for high frequencies, k was

'usually of order unity'. Kulkarni and Pagano [1972] suggested the values of *2/3* and *5/6*, depending on the mode of vibration. They too, confirmed that k was a function of fibre orientation, though apparently not dependent on the number of layers.

Bert *et al* [1967] found that for a sandwich beam with a sufficiently stiff core, such as aluminium, the damping was relatively insensitive to the value of the factor k, while for a more flexible core, such as fibre-glass honeycomb, the experimental results for frequency, nodal location and damping did not 'clearly distinguish' any one value of k - obtained according to four different theories and in the range of 0.706 to 1.94 - as being superior.

As mentioned previously (**3.3.4**), an empirical approach to the determination of the factor k has been made in the present work, *i.e.*, that its value be such that the test frequency is accurately predicted. The three basic conclusions made regarding the shear factor of all-aluminium sandwich beams, are reiterated here. These were that a) it is a linear function of the relative thickness of the skin and of the core, b) its value is more than unity and c) it is basically frequency independent.

Through similar frequency tests, the feasibility of establishing any relationship which might exist between the factor k and laminated sandwich parameters were examined. A plot such as in **Fig. 3.20**, for example, would change the status of the factor k from a purely empirical to a semi-empirical quantity, such that for the given parameters, its value could be estimated. Initially, frequency tests were conducted on two 0° composite sandwich beams used for the damping tests, and the results are presented in **Figs. 6.17** and **6.18** (for more clarity of the improved predictions, the full extent of the elementary predictions is not shown). As before, the theoretical results are based on a k factor which would accurately predict the last frequency attainable (within ±0.5%). Figure **6.17** shows frequency test results for the 0° beam with the same aluminium honeycomb specifications used in the 2SB1-X (Aerolam M-Board) sample (**Fig. 3.15**). Compared to the latter, what is immediately apparent here is the relatively large increase in the overestimations of the elementary theory, even for the

fundamental frequency, which is basically due to some 60% increase in the skin modulus (70 and 113 GPa) although, as before, the accuracy of the predictions of the improved theory are maintained over the whole frequency range. When the aluminium honeycomb of the 0° beam is replaced by Nomex (**Fig. 6.18**), a reduction of some 490% in the core modulus (285 and 48 GPa) brings about an even sharper increase in the overrating of the elementary theory and, more to the point, a distinct deviation in the improved theory results. This deviation (also visible on a reduced scale in the 913C/aluminium beam, **Fig. 6.17**), seems to be primarily due to a frequency dependence of the Nomex honeycomb modulus, and can be attributed to a viscoelastic characteristic of the material where the measured properties are not constant but functions of the test conditions, namely frequency and temperature.

Clearly then, no single value of k could be expected to fit the experimental points over the whole frequency range, unless the frequency dependence of the moduli is taken into account.

On the other hand, shear correction for all orientations in a series of beams is not always possible. The sensitivity of the sandwich frequencies to the factor k much depends on the relative stiffness of the skin and the core. Increasing the factor k , for example, is tantamount to increasing the core stiffness and therefore to sustaining a higher portion of a given lateral deflection to direct strains in the skins. As a consequence, the extent of the sensitivity of the frequency to the factor k would depend on the skin stiffness. The stiffer the skin, the more sensitive the frequencies become to k. This is the case with the lower angle beams (0° to 30°) where only a small adjustment of the shear factor is needed to arrive at the exact test frequency. Conversely, the change in the factor k is of little consequence to the frequencies of the 90° beam. In this case, larger changes of k are needed to predict the exact frequency. Further complications arise from the fact that the moduli of the higher angle beams tend to become more frequency dependent with the result that the test frequencies are generally

higher than the predicted frequencies, thus impeding shear correction for higher angle beams.

Subsequently, for each series of the beams, the factor k was chosen such that the damping test frequency of the 0° beam was predicted, and this value was maintained for the rest of the beams in the series.

The effect of a shear correction on the damping mechanisms is considered in **Fig. 6.19.** As can be seen, the influence of a shear correction is more pronounced in the bending/shearing damping ratio than in overall damping, specially for the skins of lower moduli. The figure can also be interpreted as showing the result of stiffening the core, which tends to have little effect on a sandwich of highly stiff skin but, as expected, for skins of lower stiffness, it would lead to a higher skin/core damping ratio.

In **Figs. 6.20** to **6.24**, the results of the sandwich moduli are presented. In these figures, the 'skin modulus' refers to the sandwich skin modulus as obtained from the frequencies of the narrow beams, while the 'sandwich modulus' refers to the apparent modulus of the sandwich skin computed from the sandwich frequency. The considerable discrepancy which could result from the assumption of unit correction factor is clearly evident from these results. In **Fig. 6.20**, for example, for the unidirectional skin (0°) of the DLS series, a 28% overrating of the sandwich modulus results by not allowing for shear correction, and a similar order of discrepancy is maintained over the whole orientation range to the 90° beam where a 27% overrating occurs. For the latter beam, the shear correction reduces the deviation of the sandwich modulus from the skin modulus to +11%, although, as mentioned previously, the fact that the two moduli have been measured at different frequencies (510 and 38 Hz respectively) is a possible contributory cause of the deviation. The second GFRP series (913G, **Fig. 6.24**) also shows a similar order of overrating of the sandwich modulus (25% for the 0° beam). In **Figs. 6.21** and **6.22**, the results of the same angle-ply sandwich beams but with different cores are presented. For the beams with aluminium core, larger deviations are

noticed between the skin modulus and the sandwich modulus (*cf.* the 30° and 45° beams on the figures), most likely due to a stiffening effect arising from the flexure of an anisotropic skin constrained by a higher modulus core (aluminium). The discrepancies between the skin and the sandwich modulus result in corresponding discrepancies in the measured and predicted damping results, as will be discussed later.

However, testing on all-aluminium sandwich beams, James [1962] found overrating of the experimental frequencies (underrating of modulus) by the predictions of the order of 17%. He attributed the discrepancy partly to an overrating of the honeycomb shear modulus, owing to the use of 'heavy adhesive layer' in his shear test on the honeycomb. It is more likely that, the overestimates were due to his use of a theory which was basically of the Bernoulli-Euler type.

6.7.2.2 The specific damping capacity

Steady-state damping tests on the sandwich beams were carried out twice, with an interval of eight weeks in between. In all cases, the earlier results were reproduced, although slightly lower values were obtained in the second series of tests, almost certainly due to a drop in the temperature.

The free-decay tests were also carried out, and the results are included. It should be pointed out that in some cases, the free-decay results were rather erratic. Tests on the same sample gave results which could be different by as much as 1.5% in the SDC between two tests, or the SDC at two different amplitudes for the same specimen. The signal was found to degenerate for the lower amplitudes of the sandwich beam, mainly due to coupled modes. The free-decay results reported here are those obtained from the decay of the highest displacement amplitude of the steady-state tests. All the free-decay results were obtained from the average of the results of three tests.

The SDC results for increments of the skin stress amplitude are given in **Figs. 6.25** to **6.29.** Comparisons of the steady-state SDC results at the lowest stress amplitude and the predicted results, as functions of the sandwich skin fibre orientation, are presented in **Figs. 6.31** to **6.35.**

The maximum skin stress which could be achieved depended on the stiffness of the particular sandwich, and was limited to the maximum current which could be safely fed to the drive coil (not more than 2 A). Hence, as can be seen, the stress in the sandwich skins falls well below the corresponding stress obtained when testing the skins on their own, and in almost all cases is within the limit of linear damping observed for the skins.

For the 913C/Nomex samples, non-linear damping is observed in the shear sensitive skins for both off-axis and angle-ply orientations (15° to 60° beams, **Figs. 6.27** and **6.28**). However, no such trend is observed when the Nomex core is replaced by aluminium (*cf.* **Figs. 6.26** and **6.27**). This is almost certainly due to the bending-twisting effect imposed by the skins on the core, which causes non-linear damping in the Nomex core, but has little effect on the aluminium core owing to the low damping properties of aluminium. The same trend, but on a reduced scale, is observed in the DLS/Nomex (**Fig. 6.25**) beams. The reason for the reduced non-linear damping in this case should be sought in the skin properties. For the same core thickness, and at the same lateral displacement amplitude, the bending-twisting deformation is larger in the 913C skins than in the DLS, because of the substantially higher moduli of the 913C skins. The shear coupling, D_{16} , becomes more severe in the sandwich [Lantz, 1969; Whitney and Dauksys, 1970], because of the weighting factor introduced by the core (*cf.* **Eqn. (6.20)**). Hence, only slight non-linear damping is observed in the 913G/Nomex samples (**Fig. 6.29**) compared to the DLS/Nomex (**Fig. 6.25**), because of the (slightly) lower skin moduli and the thinner core of the former.

It is noted that, apart from the anisotropic cases mentioned above, the SDC results for the sandwich do not violate the results obtained earlier for the constituent parts. Linear damping in the sandwich is maintained within the limits of linear damping of the skins. For the

angle-ply 913C/aluminium series, the results of the SDC versus core shear stress amplitude are also included (**Fig. 6.30**). Although core shear stresses were found to exceed the maximum shear stress when testing the cores on their own (e.g. compare **Figs. 6.30** and **4.11**), the indications are that the shear stresses in the cores are within the linear damping range.

The variation of damping with stress in the 0° DLS beam (**Fig. 6.25**) seems to be an exception. The results show an unexpected non-linear damping, compared to, say, the 15° beam. Although the cause is difficult to pin-point, partial debonding of the skin due to the lack of adhesive was possible, given that the adhesive layer was not uniform and there were locations of thinning of the adhesive. The moduli results (**Fig. 6.20**) do not seem to contradict the postulation. If there is a partial debonding of the 0° sandwich skin, a drop in the measured modulus of the sandwich, and consequently a higher value of k , should result, hence underestimating the sandwich modulus of the immediately higher angle beam, *i.e.* the 15° beam, which is seen to be the case.

The SDC results as functions of the skin orientation are given in **Figs. 6.31** to **6.35**. Although, as expected, the results are more scattered and somewhat less consistent than those obtained for the sandwich skins, closer examination will show that for most parts, the predicted results faithfully follow the earlier results concerning the damping and modulus of the skin.

For example, a general overestimate of the predicted SDC results in the DLS series is seen to be confined to this series. In almost all other cases, the theoretical results underestimate the experimental ones. Since the moduli results in the DLS series (**Fig. 6.20**) are fairly close, the overrating of the damping by the predictions seem to be mainly due to the overrating of the constituent damping data used for the predictions; as suggested previously (section **6.7.1.2**).

The general underrating of the experimental damping by the predictions have been caused mainly by the energy dissipations which have not been accounted for, namely, the bending-twisting effect and the adhesive layer.

The geometry of the adhesive layer in the honeycomb sandwich is too complex for an assessment of stress distribution, even if a uniform distribution of adhesive is assumed. However, owing to the open-ended honeycomb, it is for most parts an unrestrained layer and as such is not expected to experience an otherwise substantial shearing. More likely, it basically follows the flexure mode of the skin, and if warranted, its strain energy may be approximated on that basis. However, in practical applications of the sandwich where the skin is highly stiff, the strain energy due to the adhesive layer becomes negligible. Then, provided the core is damped (e.g. Nomex core), the damping contribution due to the adhesive also becomes negligible. This point will be discussed further.

To this should be added the complications brought about by the twisting phenomenon, believed to be clearly manifested in the angle-ply 913C/aluminium series (**Fig. 6.32**). The influence of the aluminium core damping due to the bending-twisting effect on the overall damping is unlikely to be significant. Then, assuming the free-decay results represent actual damping, the underestimates in the 15° to 45° range in the computed steady-state results can be attributed to mainly the bending-twisting of the skin and adhesive layer which, as expected, peaks at 45°. The underestimation of the experimental results by the prediction is, at least in part, due to the additional damping introduced by the adhesive layer. This point will be discussed further.

The process mentioned earlier for the all-aluminium sandwich beams (section **5.3**), by which the SDC increases with the core thickness, is graphically illustrated here. Comparing **Figs. 6.31** and **6.35**, where skin and core properties are (roughly) compatible and the predominant factor is the difference in the core depth (12.75 mm and 6.90 mm respectively (**Table (6.2)**), the sharp fall of the core contribution to the overall damping in the thinner beams (**Fig. 6.35**)

is seen to be accompanied by only a modest increase in the skin contribution. As a result, a similar sharp fall of the overall damping is noticed in the lower region (low angle beams) where core damping dominates, while the increase in the overall damping in the skin-dominant region is relatively slight. Moreover, it is seen that as the core depth is increased (**Figs. 6.35** and **6.31** respectively), the point where the core contribution predominates extends further such that, for a sufficiently deep core, the latter could become the principal contributor to the overall damping for any skin orientation or modulus.

The influence of the adhesive layer on the overall damping is well illustrated in the shallow beam results (**Fig. 6.35**). Here, since the skin becomes the principal contributor in the higher angle beams, and also any discrepancies due to the shear coupling are greatly reduced, the relatively large underestimating of the tests results by the predictions at higher angle beams can be more assuredly attributed to, mainly, the damping due to flexure of the adhesive layer. It is notable that, for the same reason, the computed SDC results (steady-state) generally overestimate the results obtained by free-decay since, in the former, the increase in the strain energy due to the flexure of the adhesive layer is not accounted for. It will be appreciated that, as the angle of fibre orientation is increased, the beam modulus approaches that of the adhesive layer; for the 90° beam, the two are roughly compatible. Furthermore, it is noted that since in the lower angle beams the core damping dominates, the discrepancies due to the flexural damping of the adhesive layer are minimised and, consequently, all the results can be seen to fall very close together.

In fact, referring to the results, the above arguments are seen to hold for all the samples. That is, where the discrepancies due to the anisotropy of the skin are absent, and the adhesive damping is marginal, the steady-state, free-decay and the predicted results fall very close together. This can be observed from the 0° and 90° beam results in **Figs. 6.31** and **6.33**, the 90° result in **Fig. 6.32**, and the 0° results in **Fig. 6.35**. It could similarly be argued that, with orthotropic skins, the discrepancies are most likely due to the adhesive layer. This can be

seen to be the case in the 0° 913C/aluminium beam (**Fig. 6.32**) and the 90° 913G/Nomex (**Fig. 6.35**), where the experimental results are underestimated by the predictions. In the first case, the discrepancy is due to low damping of the aluminium core, making the skin damping dominant at all orientations. As a result, the energy dissipation in the 0° beam will be mainly due to the flexure of the adhesive layer, and possibly also some air-damping. In the second case, the discrepancy was already mentioned to have been caused by the relative shallowness of the sandwich, making the damping due to the adhesive layer more pronounced at higher orientations.

Comparing the angle-ply and the off-axis results (**Figs. 6.33 and 6.34**), as expected, the trend observed earlier in the variation of damping with orientation is seen to recur, that is, a sharp rise in the damping due to the skin with fibre orientation in the off-axis series, followed by an almost constant damping with orientation, as opposed to a more gradual rise with the angle-plies. The fact that the fall in the core damping with fibre orientation follows the same pattern as the rise in the skin damping arises from **Eqn. (3.42)**, where the strain energy due to bending of the skin, U_b , is the dominant contributor to the total strain energy.

Comparing the sandwich beam results with those obtained earlier for the sandwich skins, the relatively larger discrepancies are not entirely unexpected, bearing in mind, in addition to the discrepancies caused by the above mentioned factors, also the following

a) here, a compound structure is involved, with more variables, analysis and simplifying assumptions;

b) within the laboratory environment, the consistency of material (adhesive layer, honeycomb core) for all the samples cannot be ensured;

c) the method of manufacture is entirely different; the sandwich beams are individually assembled by hand and any off-set of the skins or misalignment of the core *etc.* is not always obvious;

d) some additional assumptions have been implied; for example it has been assumed that both modulus and damping are independent of frequency (and temperature) within the test range, and that no post curing of the sandwich skin, or core, has occurred.

In most cases, the steady-state and the free-decay results are seen to be reasonably close. The maximum error, with reference to the free-decay results, was found to be -20%, in the 15° 913C/aluminium beam results (**Fig. 6.32**). Given the factors mentioned above, and in particular the complexities brought about by the shear coupling effect and the adhesive layer, these results seem to verify the adequacy of the Timoshenko beam equations in measuring the steady-state damping, and justify the simplifying assumptions made in adopting these equations for a sandwich beam.

It will be noted that, unlike the simple beams, sandwich damping properties will be necessarily a function of beam length, end conditions or any load supported by the beam, since such factors have an influence on the relative bending/shearing the beam undergoes. The point is illustrated in the theoretical variation of the SDC with the mode number, and the core depth/length ratio presented in **Figs. 6.36** and **6.37** respectively. As expected, the

graphs follow a similar trend which covers a range between two extremes. On one extreme, a sufficiently long sandwich beam would experience little shearing and the energy dissipation is almost entirely through bending of the skins. The beam would be in effect a Bernoulli-Euler type. On the other extreme, the beam experiences a thickness-shear type mode of deformation. Theoretically, depending on the beam length, the damping of the sandwich could be almost entirely due to either the core or the skin. This concept is of great significance in the overall damping of the sandwich if unlike, for example, all-aluminium sandwich, the two constituent dampings are not compatible.

The effect of a load on damping contribution of the constituent parts is shown in **Fig. 6.37.** Evidently, for the free-free beam, the contribution of the skin to the total damping drops when the beam is loaded in the mid-span, although the mutual increase in the core damping would more than compensate for the decrease. This follows from consideration of the mode shape, together with **Eqn. (3.42).** The load on the beam moves the nodal lines closer to the mid-span. This has the effect of increasing the strain energy of shearing in the core and a mutual, proportionately higher, reduction in the strain energy of bending of the skins.

6.8 Conclusions

The tests showed that, using basic plane-stress relations for laminated composites and the Adams-Bacon damping criterion, the moduli and the SDC of both symmetric angle-ply and off-axis beams at any orientation can be predicted with fairly good accuracy. However, the bending-twisting could result in serious overestimates of the measured effective Young's moduli in flexure, although its effect on the measured SDC was found to be not as severe. The absence of bending-stretching coupling has made the symmetric angle-ply laminated plates of particular interest on two accounts. First, these are less prone to warping caused by thermal contraction, and second they are more amenable to closed form mathematical analysis. However, anisotropy could cause serious discrepancies between the measured and predicted effective flexural moduli of the beams, unless these are of sufficiently large aspect

ratios to make the deformations not accounted for in the simple bending of beams insignificant.

A variety of composites, orientations and honeycombs was used in the construction of the sandwich beams, to allow a broader assessment of the damping mechanisms in the sandwich. Generally, the results showed a high degree of inter-dependence between the skin and the core in either one's capacity in contributing to the overall damping of the sandwich.

It was shown that the Timoshenko beam equations were adequately capable of accounting for energy mechanisms of simple bending/shearing in a shear soft beam. These equations were used for the steady-state measurement of the SDC in a sandwich beam, and for determining the bending/shearing proportion to the overall damping. It was suggested that the shear factor be found empirically for the particular damping test, and it was concluded that the shear correction is of more significance to the bending/shearing damping ratio than to the overall damping.

The theoretical results were found to follow the free-decay results with reasonable accuracy. In most cases where discrepancies occurred, these were found to correlate with the energy dissipations not accounted for in the theory, namely, 1) the bending-twisting inherent in the anisotropic composite skin, which is more severe than when testing the skins on their own owing to the weighting factor introduced by the sandwich core, and 2) the adhesive layer. The latter, however, would be of little significance in most practical constructions of the polymer based honeycomb sandwich, where the skin stiffness is sufficiently high to allow the core damping to predominate.

Chapter 7

GENERAL CONCLUSIONS

Relevant conclusions have been drawn at the end of each chapter. Here, general conclusions which can be made collectively from different aspects of the work will be outlined.

The modified Timoshenko beam equations may be used with confidence for measuring the flexural damping of shear-flexible symmetric, honeycomb sandwich beams in steady-state vibration. Excellent repeatability of the damping results can be expected. The same equations can be utilised for predicting the skin/core contribution to the overall damping. However, discrepancies will inevitably arise if the beam vibration is not exclusive to the simple bending/shearing of the skin/core components.

In adapting these equations for a sandwich configuration, certain assumptions are made which cannot be fully verified. The problem becomes more complicated with the presence of the as-yet ill-defined shear correction factor, k, associated with these equations. Nonetheless, it was shown in the case of solid beams, with or without a shear correction, that these equations are well capable of predicting the frequencies with good accuracy even in the high frequency domain; also, for the all-aluminium sandwich beams, a linear relationship exists between the optimum value of k and the skin/core thickness ratio. For the all-composite sandwich, a frequency-dependent modulus was noticed with the result that no single value of k could be expected to fit all the experimental values. The shear correction was found to be of less influence on the overall damping of the sandwich than it was on the skin/core contribution to damping. An empirical approach for the determination of the factor k was suggested.

It was further shown that it is possible to predict, with a good degree of accuracy, the modulus and the specific damping capacity of laminated composite beams having an anisotropic flexural modulus. The effective flexural modulus was found to be more sensitive to the plan aspect ratio than the orthotropic modulus as reported in the literature. The discrepancies in the damping results due to anisotropy were found to be only noticeable when the beams were used as skins in a sandwich configuration.

The sandwich damping results were generally found to follow the expected trend, and a correlation was found to exist between the degree of the discrepancies and the skin anisotropy and/or the energy dissipation in the adhesive layer.

Regarding the skin orientation, two sandwich beams of the same dimensions and fabricated from the same composite skin and damped honeycomb core materials, might show the same order of vibration damping, yet the mechanism of damping in each, could be entirely different. In a beam with 0° skins, for example, the core is the principal contributor to damping while, in a 90° beam the skin becomes the principal contributor. The end conditions, any loads supported by the beam, and the beam dimensions would all influence the proportion of the contribution of the skin and of the core, and hence, the overall damping of the beam.

A test method was developed for measuring the modulus, as well as the specific damping capacity of honeycomb in steady-state shear vibration. Though somewhat laborious to produce, the double-lap test piece was found to give by far the lowest relevant SDC reported in the literature.

Suggestions for further work

Some aspects of the present work are believed to merit further investigation. These are

1) The establishment of any possible relationship between the shear factor and the relevant parameters (core thickness, fibre orientation *etc.*) of the composite/honeycomb beam

2) Only the first mode of vibration was considered in this work. Of particular relevance to the present work is the prediction and measurement of sandwich damping in higher modes of vibration, where the specimen is subjected to intensified shear deformation. In both of the above cases, any frequency dependence of modulus should be accounted for

3) Only free-free end conditions were considered. Similar investigation of sandwich damping with respect to other end conditions (clamped-clamped, clamped-free) is also warranted

4) In the range between the orthotropic 0° and 90° orientations, only anisotropic orientations (symmetric angle-ply) were considered. It would be of interest to see if, as expected, using orthotropic orientations (*e.g.* anti-symmetric angle-ply laminate) reduces the discrepancies in the damping of the sandwich.

Closed form analyses have been used in this work. The disadvantage here is the limitation of a closed form analysis to model accurately the actual deformation. More accurate modelling should be possible using such numerical methods as the Finite Elements Analysis. Indeed, some work was carried out to modify an existing Finite Element program (*LIN.FOR*, Lin *et al* [1984]) for a composite/honeycomb sandwich configuration using the shear deformation theory [Whitney, 1987]. Although implemented, the program (*PLATE.FOR*) remains to be tested on its own ('debugged'), and to be verified experimentally.

Appendix (A)

ANALYSIS OF THE FLEXURAL TEST-RIG

A.1 Determination of the specific damping capacity

The specific damping capacity, SDC, is defined as

$$\Psi = \frac{\Delta U}{U} \tag{A.1}$$

where ΔU is the energy dissipated per cycle, and U is the maximum strain energy.

With an applied cyclic force, F, maintaining the vibration in a steady-state, the energy dissipation per cycle is given by

$$\Delta U = \oint F\, dw$$

where

$$F = F_m \cos(\omega t)$$

For relatively low damping, at resonance the response lags the applied force by $\pi/2$ to a close approximation. Then

$$W = W_m \sin(\omega t)$$

and

$$\Delta U = \pi F_m W_m \tag{A.2}$$

where F_m and W_m are maximum force and the corresponding displacement amplitude respectively.

The quantities F_m and W_m are found by measuring the current flowing through the drive coil and the voltage induced across the pick-up coil respectively, as follows

The maximum induced force on a total length, L_d, of the drive coil subjected at right angles to the lines of flux of intensity B_d of the drive magnet is given by

$$F_m = I_{peak} L_d B_d$$

where I_{peak} is the peak current in the drive coil. Provided I_{peak} remains the only variable in a damping test, then this equation may be written as

$$F_m = I_{peak} \Gamma_d \tag{A.3}$$

where the constant Γ_d is termed the 'drive sensitivity'.

Similarly, the maximum induced voltage across a total length, L_p, of the pick-up coil cutting at right angles the lines of flux of intensity B_p of the pick-up magnet is given by

$$V_{peak} = v_m L_p B_p$$

which may be written in terms of the 'pick-up sensitivity', Γ_p, as

$$V_{peak} = v_m \Gamma_p \tag{A.4}$$

where v_m is the maximum velocity of the pick-up coil and is given by

$$v_m = \omega W_m \tag{A.5}$$

Then
$$W_m = \frac{V_{peak}}{\Gamma_p} \frac{1}{\omega_n} \tag{A.6}$$

Equations (A.1), (A.2), (A.3) and (A.6) will now give

$$\Psi = \frac{1}{U} \left(\frac{\Gamma_d}{\Gamma_p} \frac{I_{rms} V_{rms}}{f_n} \right) \tag{A.7}$$

The computation of the maximum strain energy, U, of a free-free beam carrying a central mass, M_c, in the first mode of flexural vibration of lateral displacement amplitude W_m has been covered previously (*Chapter 3*).

A.2 Calibration of the drive and pick-up coil/magnet sets

One way of finding the sensitivities Γ_d and Γ_p is to treat both the drive and pick-up sets as pick-up. This may be conveniently achieved by using the flexural test set-up itself. In this case, the coil assembly, mounted on the mid-span of a low damping beam (e.g. Duralumin), is tuned to an appropriate frequency and a number of V_{peak} Vs W_m points are measured for each coil/magnet set while employing the second coil/magnet set as the drive unit. The displacement amplitude, W_m , may be measured by an optical image shearing device, as was done in this work using 'WISE', or any other appropriate method. Then, in each case, the quantity Γ_p may be found according to **Eqn. (A.4)**. The unit of Γ_p so found will be V.s/m which is applicable to the pick-up set. For the drive set, however, the sensitivity Γ_d is of the unit N/A according to **Eqn. (A.3)**. It is easily verified that since

Watt = Newton . meter / second = Volt . Amp

Then 1 (V.s/m) = 1 (N/A)

The sensitivities might change over a period of time and it would be sensible to check these regularly. The changes in the sensitivities may be due to any change in the gap size of the drive electromagnet, possible short circuit of one or more loops in the coils, room temperature *etc.* In most cases, however, it was found that the variation in the sensitivities was small (less than 1%).

Calibration graphs are presented in **Figs. A.1** to **A.3**. The solid lines join the first and last points in the range. Figures **A.1** and **A.2** indicate the sensitivities of both drive and pick-up units remain constant over the whole range of displacement amplitude. Figure **A.3** shows the calibration of the drive sensitivity over a range of the electromagnet current. As can be seen, up to a current of 5 A the sensitivity is linear and, if need be, may be read off directly from this graph with reasonable accuracy.

Appendix (B)

THE LONGITUDINAL SHEAR TESTS

Fox [1972] and Flitcroft [1976] used test rigs which were based on the torsion pendulum arrangement for measuring the dynamic properties in torsion. Both apparatuses used two sets of coil/magnet for the drive and pick-up systems.

Investigating the dynamic properties of cast iron for up to and beyond fatigue endurance limit, Fox developed an apparatus capable of producing relatively large torques. As such, this apparatus consisted of a heavy metal frame on which large drive and pick-up magnets were fixed, while the drive and pick-up coils were fixed at either ends of a symmetrical inertia bar. The specimen was clamped at one end to the frame and at the other to the inertia bar. A Duralumin 'dummy specimen' was similarly clamped to the inertia bar at one end and to the frame at the other end, thereby establishing clamped-clamped end conditions. The dummy specimen had been incorporated in the system in order to constrain flexural/torsional coupling, and also to have a degree of control over the resonance frequency by using dummies with different dimensions.

Flitcroft, investigating the dynamic torsional properties of fibrous composites, found Fox's apparatus to be inadequate for this purpose. This was because the dummy specimen dominated the stiffness of the system and hence the calculation of the stiffness of the test specimen would involve small differences between large numbers. Removing the dummy specimen, however, would bring about adverse affects on two accounts. First, flexure of the specimen tended to occur due to the imbalance of the inertia bar, although he found that dynamic balancing of the inertia bar 'eliminated' this problem; and second, the system was of too large an inertia for testing of composites at an appropriate frequency. He developed a similar apparatus with the necessary modifications which included removing the dummy

specimen and replacing the inertia bar with a cylindrical coil arrangement incorporating the drive and pick-up coils thereby reducing inertia as well as enhancing dynamic balance.

Both these rigs were available for the present work, but were found to be of too high an inertia for the stiffness of the test piece. They are also rather tedious to set up due to the lack of adequate access and the hindrance caused by the presence of various fly wires.

Consequently, a new and simple rearrangement was utilised. The test-rig used is basically a scaled down version of Fox's rig but in a clamped-free formation, that is, without a dummy specimen. With a relatively small inertia bar, higher frequencies, more compatible with the tests in this work, can be attained. It has the added advantage that, unlike the previous rigs, no fly wires are involved, although any gain in reducing extraneous damping would be of significance only for low damping materials. Moreover, as pointed out by Willway and White [1988], with the clamped-clamped formation direct strains are induced which cannot be neglected for higher amplitudes.

The rig was originally intended for testing the less stiff flat specimens at adequate frequencies (not below 30 Hz), but it also proved to be suitable for testing standard circular section specimens, although a heavier inertia bar had to be used in this case.

The test-rig consists of a relatively small symmetric inertia bar which carries two pairs of small permanent magnets (**Fig. B.1(a)**). The inertia bar is fixed to one end of the specimen, and the latter is firmly clamped at the other end to a concrete block. Two corresponding pairs of coils, each pair in series and each pair positioned diagonally on an aluminium frame (**Fig. B.1(b)**), provide the drive and pick-up coils.

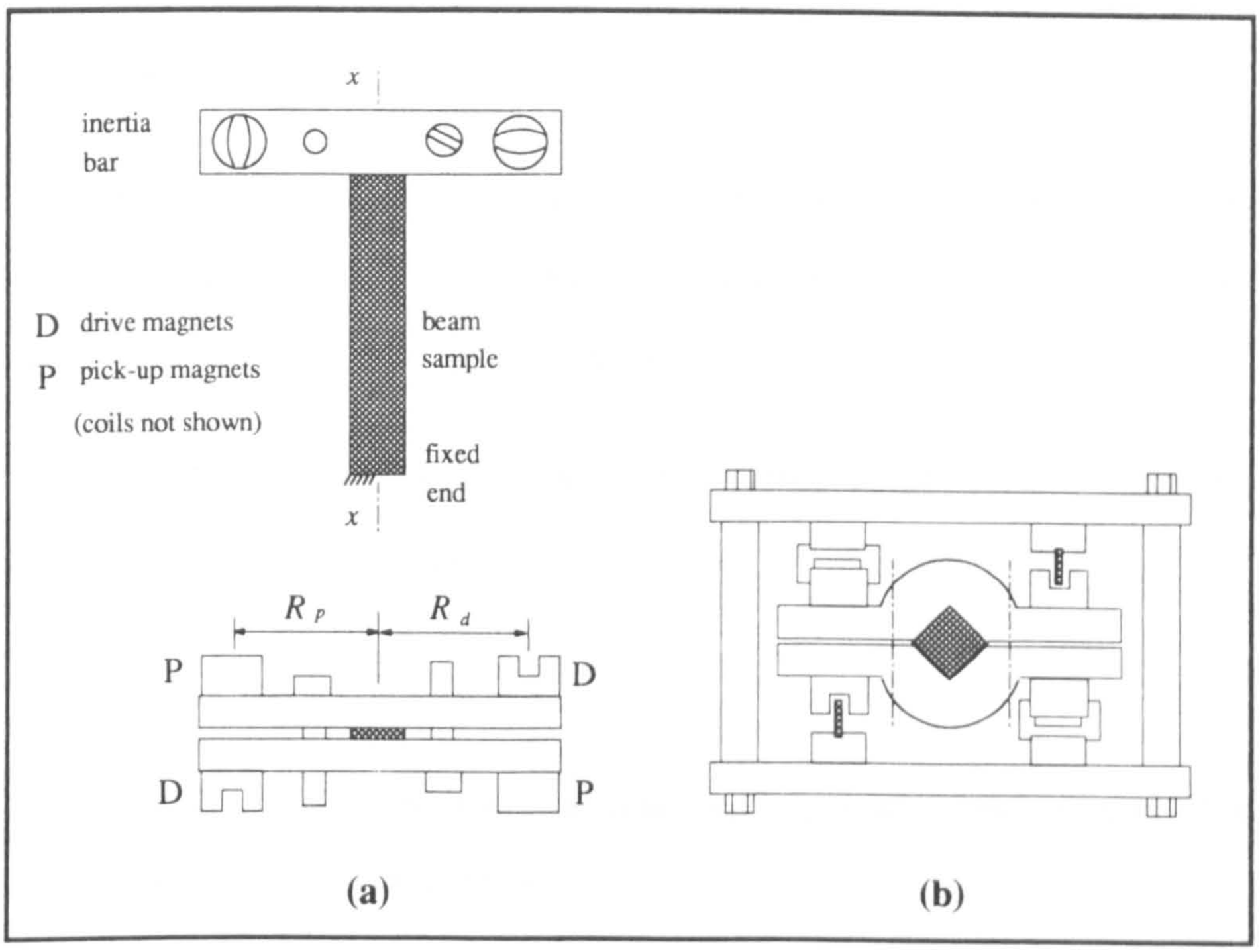

Fig. B.1 *Longitudinal shear test-rig*

The instrumentation and the test procedure are similar to those in the flexural tests. With a current flowing through the drive coils forces are induced which can be made of opposite directions by ensuring that the position of one drive magnet poles relative to the current flow is opposite to that of the poles of the second drive magnet. Then, provided the inertia bar is dynamically balanced and that the two drive coils are of the same sensitivity, a pure couple should result.

In the case of the Fibredux 913C and 913G composites, circular section samples were machined from the square section mouldings prepared by stacking strips of the unidirectional pre-preg. In the case of DLS-280, the same moulded material which was used for flexural tests was also used for longitudinal shear test [1]. Hence, in this latter case, the

---

[1] This was due to the lack of material for this particular composite.

specimen was in the shape of rectangular flat strip which was cut from the moulded unidirectional plate.

The circular section test pieces were of standard dimensions (nominally 10 mm diameter and 140 mm gauge length) with square ends. For these test pieces, a heavier inertia bar, incorporating two V-clamps (**Fig. B.1(b)**), was used.

The arrangement, therefore, imposes a single DOF system of torsional vibration on the test piece, the frequency of which is given by

$$f_n = \frac{1}{2\pi} \sqrt{(K/J_{bar})} \qquad \textbf{(B.1)}$$

where K is the torsional stiffness of the specimen and J_{bar} is the mass moment of inertia of the inertia bar about the x axis (**Fig. B.1(a)**).

The moment of inertia of the inertia bar was obtained by comparing its period of oscillation with that of a uniform disc whose moment of inertia, J_{disc} , could be readily calculated. The inertia bar and the disc were in turn suspended from the same length of wire and, following a small initial twist, the period of oscillation in each case was measured. Applying **Eqn. (B.1)** to each case and equating the stiffness yields

$$J_{bar} = \left(\frac{\tau_{bar}}{\tau_{disc}}\right)^2 J_{disc} \qquad \textbf{(B.2)}$$

B.1 Analysis of the circular section test piece

B.1.1 Shear modulus

The angle of twist resulting from the application of torque T over a uniform length L of the specimen is given by

$$\theta = \frac{TL}{GJ} \qquad \textbf{(B.3)}$$

where G is the shear modulus and J is the polar second moment of area of the specimen.

By definition, the torsional stiffness is given as

$$K = \frac{T}{\theta} \tag{B.4}$$

Then, **Eqns. (B.1), (B.3)** and **(B.4)** will give the shear modulus as

$$G = \frac{128 \pi f_n^2 J_{bar} L}{d^4} \tag{B.5}$$

where d is the diameter of the specimen.

B.1.2 Steady-state vibration damping

By analogous arguments in deriving **Eqn. (A.2)** in *Appendix (A)*, the energy dissipation per cycle of the longitudinal shear vibration is shown to be given by

$$\Delta U = \pi T_m \theta_m \tag{B.6}$$

where T_m and θ_m are the peak values of the torque and the corresponding angle of twist respectively. These are given by

$$T_m = \sqrt{2}\, I_{rms}\, \Gamma_d\, R_d \tag{B.7}$$

$$\theta_m = \frac{\sqrt{2}\, V_{rms}}{2\pi\, \Gamma_p\, R_p\, f_n} \tag{B.8}$$

where I_{rms} and V_{rms} are the current through the drive coil and voltage across the pick-up coil, R_d and R_p are the mean radii of the drive and pick-up coils from the axis of rotation (**Fig. B.1**), and Γ_d and Γ_p are the total sensitivities of the drive and pick-up coil pair respectively. It will be noted that in order to avoid imposing any flexural deformation on the specimen a pure couple should be applied, and ideally this is achieved by ensuring that the two drive coil/magnet pairs have the same sensitivity. However, manipulating the sensitivities of the ready made coils is not without difficulty, and a compromise should be made as regards to the closeness of the sensitivities. The drive units used here were of sensitivities 0.070 and 0.074 N/A, believed to be sufficiently close to make any flexural deformation negligible.

Assuming a uniform distribution of stress in the material, the maximum strain energy in torsion is given by

$$U = \frac{1}{4} G \gamma_m^2 v$$

where γ_m is the maximum shear strain and v is the volume of the working length of the material.

Since

$$\gamma_m = \frac{d}{2L} \theta_m$$

therefore

$$U = \frac{\pi G d^4 \theta_m^2}{64 L} \quad \textbf{(B.9)}$$

Then, by the definition of the SDC as $\psi = \Delta U/U$, the latter is given by **Eqns. (B.5)** to **(B.9)** as

$$\psi = \frac{I_{rms} \Gamma_d \Gamma_p R_d R_p}{J_{bar} V_{rms} f_n} \quad \textbf{(B.10)}$$

Also, the maximum shear stress is found as

$$\tau_m = \frac{\sqrt{2} G d V_{rms}}{4\pi L \Gamma_p R_p f_n} \quad \textbf{(B.11)}$$

B.2 Analysis of the rectangular section test piece

B.2.1 Shear modulus

Exact solutions are obtained in torsion of circular shafts by assuming, to a good approximation, that the plane cross sections remain plane. This assumption, however, does not hold for prismatic bars [Timoshenko and Goodier, 1951]. The usual solution to this problem has been through the membrane analogy in which the outline of the cross section is treated as a membrane subjected to tension and lateral pressure.

Utilising the membrane analogy, the torque on a rectangular section uniform beam can be shown to be given by [Timoshenko and Goodier, 1951]

$$T = k_1 G \frac{\theta}{L} w h^3 \qquad \textbf{(B.12)}$$

where w and h are the width and depth of the bar respectively, and k_1 is a numerical factor the value of which will depend on the ratio w/h. The factor k_1 is given as

$$k_1 = \frac{1}{3} \left(1 - \frac{192}{\pi^5} \frac{h}{w} \sum_{n=1,3,5...}^{\infty} \frac{1}{n^5} \tanh(n\pi b/2d)\right) \qquad \textbf{(B.13)}$$

Then, **Eqns. (B.1), (B.3)** and **(B.12)** give the longitudinal shear modulus as

$$G = \frac{4 \pi^2 f_n^2 J_{bar}}{k_1 w h^3} \qquad \textbf{(B.14)}$$

The maximum shear stress is given by

$$\tau_m = k G \frac{\theta_m}{L} h \qquad \textbf{(B.15)}$$

where similar to k_1, k is a numerical factor depending on the ratio w/h. The factor k is given as

$$k = \left(1 - \frac{8}{\pi^2} \sum_{n=1,3,5,...}^{\infty} \frac{1}{n^2 \cosh(n\pi b/2d)}\right) \qquad \textbf{(B.16)}$$

Substituting for θ_m from **(B.8)** in **(B.15)** will give

$$\tau_m = \frac{\sqrt{2}\, k G V_{rms}}{2\pi L \Gamma_p R_p f_n} \qquad \textbf{(B.17)}$$

B.2.2 Steady-state vibration damping

The maximum strain energy in torsion of a narrow rectangular bar of width w and depth h is given by [Timoshenko and Goodier, 1951]

$$U = \frac{1}{2} k_1 G \frac{\theta^2_m}{L} w h^3 \qquad \textbf{(B.18)}$$

Then, **Eqns. (B.6), (B.7), (B.8), (B.14)** and **(B.18)** will now give the SDC as

$$\psi = \frac{I_{rms}\,\Gamma_d\,\Gamma_p\,R_d\,R_p}{J_{bar}\,V_{rms}\,f_n} \qquad \textbf{(B.19)}$$

As expected, this expression is seen to be identical with the one obtained for a circular section sample.

B.2.3 Experimental verification

Walton [1973] found that for both round and rectangular section beams, a decrease in the cross sectional area resulted in a small but detectable decrease in the measured shear modulus, and the decrease was, therefore, accompanied with an increase in the measured SDC of the material.

The theoretical values for longitudinal shear modulus and damping, as given by **Eqns. (B.14)** and **(B.19)**, were verified experimentally. For shear modulus, a torsion test was carried out on a rectangular section aluminium beam and the shear modulus was computed using **Eqns. (B.14)**. The modulus so found was then compared with the expected shear modulus of aluminium.

The following data for the shear modulus test was recorded

L	=	107	mm
w	=	12.74	mm
h	=	3.38	mm
J_{bar}	=	3.22×10^{-5}	kg m²
f_n	=	60.8	Hz

A digital computer can be conveniently programmed to compute the factors k_1 and k according to **Eqns. (B.13)** and **(B.16)**. The series converge fast and these factors can be found very accurately for any given value of w/h. For the aluminium test piece, $w/h = 3.77$ for

which it was found that $k_1 = 0.2776$. Equation (B.14) will now give

$$G = 25.8 \text{ GPa}$$

The Young's modulus was measured dynamically, and was found to be

$$E = 69.52 \text{ GPa}$$

Taking the Poisson's ratio, υ, for the aluminium sample as 0.35, then the static value of G is given as

$$G = \frac{E}{2(1+\upsilon)} = 25.75 \text{ GPa}$$

This value is almost identical with the value computed using Eqn (B.14).

The SDC as given by Eqn. (B.16) was checked by simply comparing the result with the one obtained by free-decay method. The following data were recorded for the longitudinal shear damping test on the GFRP (DLS-280) specimen at the lowest displacement amplitude.

w	=	13.7	mm
h	=	1.60	mm
I_{rms}	=	21	mA
V_{rms}	=	1.79	mV
Γ_d	=	0.144	N/A
Γ_p	=	0.081	mV.s/mm
R_d	=	$R_p = 25.5$	mm
f_n	=	35.2	Hz

The coil sensitivities had been found individually for each coil using the same procedure as described for flexural test-rig (*Appendix (A)*).

For the ratio $w/h = 8.562$, $k_1 = 0.3088$ and $k = 1.0$. Equations (B.17) and (B.19) will now give

at $\tau_m = 0.81$ MPa

$\psi = 7.85\%$

The average of three free-decay test results (7.45, 7.57 and 7.52%) for this sample was found to be

$$\psi = 7.51\%$$

The computed result is 4.5% higher than the free-decay value of the SDC. This is a fair agreement between the two results.

The results of the steady-state tests on the three sample are presented in **Figs. B.2** and **B.3**. These results indicate that, within the range tested, the stress dependency of the SDC is only marginal.

Adams *et al* [1969] found that the longitudinal shear damping of the CFRP was both stress and (slightly) stress-history dependent, but for GFRP it was found to be generally stress independent. Experiments of Willway and White [1988] also showed stress dependent damping in resin and CFRP rods, under both clamped-clamped and clamped-free conditions.

Appendix (C)

ANALYSIS OF A SYMMETRICALLY END-LOADED TIMOSHENKO BEAM

Scope - In this appendix, the uncoupled Timoshenko beam equations are first derived, and are subsequently applied to a symmetrically end loaded beam.

C.1 Timoshenko's uncoupled equations

Applying Newton's second law of motion to an element of a uniform beam (**Fig. C.1**) subjected to lateral vibration will give [Timoshenko, 1955]

$$\frac{\partial Q}{\partial x}\, dx = (\rho A\, dx)\, \frac{\partial^2 w}{\partial t^2} \qquad \text{(C.1)}$$

$$-\frac{\partial M}{\partial x}\, dx + Q\, dx = (\rho I\, dx)\, \frac{\partial^2 \phi}{\partial t^2} \qquad \text{(C.2)}$$

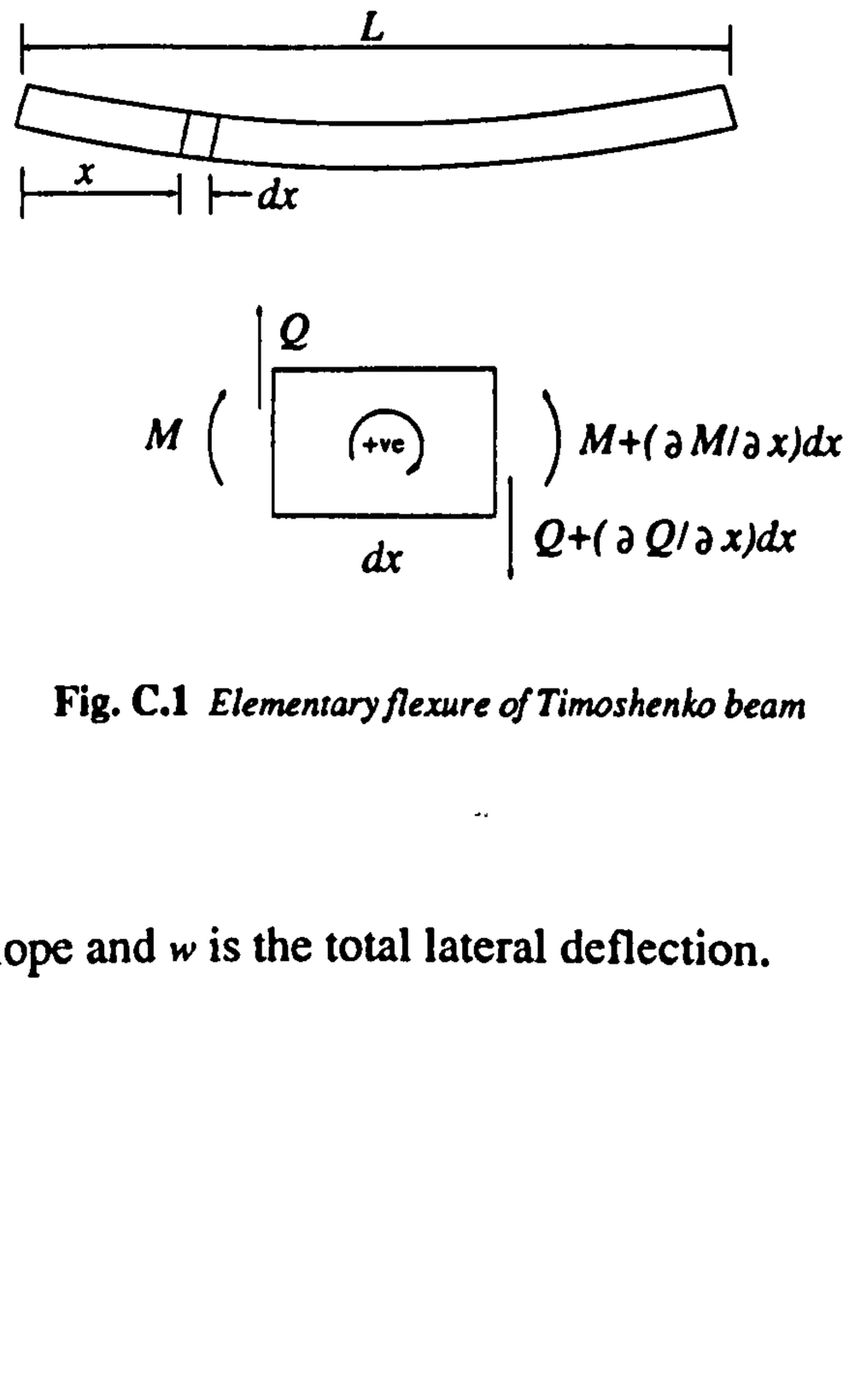

Fig. C.1 *Elementary flexure of Timoshenko beam*

where ϕ is the bending slope and w is the total lateral deflection.

Now,

$$M = -EI\frac{\partial\phi}{\partial x} \tag{C.3}$$

and

$$Q = kAG\gamma$$

$$= kAG\left(\frac{\partial w}{\partial x} - \phi\right) \tag{C.4}$$

Then, substituting for M and Q in **Eqns. (C.1)** and **(C.2)** will give

$$EI\frac{\partial^2\phi}{\partial x^2} + k\left(\frac{\partial w}{\partial x} - \phi\right)AG - \rho I\frac{\partial^2\phi}{\partial t^2} = 0 \tag{C.5}$$

$$\rho A\frac{\partial^2 w}{\partial t^2} - k\left(\frac{\partial^2 w}{\partial x^2} - \frac{\partial\phi}{\partial x}\right)AG = 0 \tag{C.6}$$

Solving **Eqn. (C.6)** for ϕ gives

$$\phi = \int\left(\frac{\partial^2 w}{\partial x^2} - \frac{\rho}{kG}\frac{\partial^2 w}{\partial t^2}\right)dx$$

$$= \frac{\partial w}{\partial x} - \int\frac{\rho}{kG}\frac{\partial^2 w}{\partial t^2}\,dx + Const.$$

Substituting for ϕ in **Eqn. (C.5)** gives

$$EI\left(\frac{\partial^3 w}{\partial x^3} - \int\frac{\rho}{kG}\frac{\partial^4 w}{\partial x^2\,\partial t^2}\,dx\right) + kAG\int\frac{\rho}{kG}\frac{\partial^2 w}{\partial t^2}\,dx -$$

$$\rho I\left(\frac{\partial^3 w}{\partial x\,\partial t^2} - \int\frac{\rho}{kG}\frac{\partial^4 w}{\partial t^4}\,dx\right) + Const. = 0$$

Differentiating w. r. t. x gives

$$EI\frac{\partial^4 w}{\partial x^4} + \rho A\frac{\partial^2 w}{\partial t^2} - \left(\rho I + \frac{E\rho I}{kG}\right)\frac{\partial^4 w}{\partial x^2\partial t^2} + \frac{\rho^2 I}{kG}\frac{\partial^4 w}{\partial t^4} = 0 \tag{C.7}$$

Similarly, from **Eqn. (C.5)**

$$w = \int\left(\phi - \frac{EI}{kAG}\frac{\partial^2\phi}{\partial x^2} + \frac{\rho I}{kAG}\frac{\partial^2\phi}{\partial t^2}\right)dx$$

Substituting for w in **Eqn. (C.6)** gives

$$\rho A \int \left(\frac{\partial^2 \phi}{\partial t^2} - \frac{EI}{kAG} \frac{\partial^4 \phi}{\partial x^2 \partial t^2} + \frac{\rho I}{kAG} \frac{\partial^2 \phi}{\partial t^2} \right) dx - kAG \left[\int \left(\frac{\partial^2 \phi}{\partial x^2} - \frac{EI}{kAG} \frac{\partial^4 \phi}{\partial x^4} + \frac{\rho I}{kAG} \frac{\partial^4 w}{\partial x^2 \partial t^2} \right) dx - \frac{\partial \phi}{\partial x} \right] + Const. = 0$$

Differentiating w. r. t. x gives

$$EI \frac{\partial^4 \phi}{\partial x^4} + \rho A \frac{\partial^2 \phi}{\partial t^2} - \left(\rho I + \frac{E \rho I}{kG} \right) \frac{\partial^4 \phi}{\partial x^2 \partial t^2} + \frac{\rho^2 I}{kG} \frac{\partial^4 \phi}{\partial t^4} = 0 \qquad \textbf{(C.8)}$$

Equations **(C.7)** and **(C.8)** are Timoshenko's uncoupled differential equations of lateral vibration corresponding to **Eqns. (3.4.a)** and **(3.4.b).**

C.2 End loaded beam

Consider a Timoshenko beam symmetrically loaded with equal symmetric masses at either ends **(Fig. C.2)** and vibrating in a normal mode.

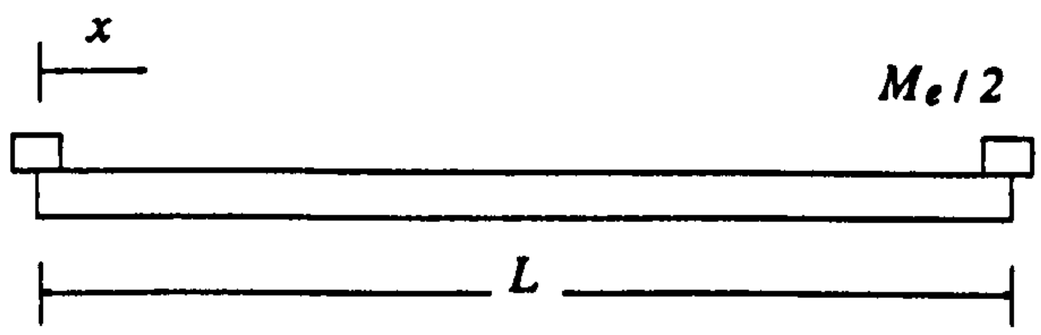

Fig. C.2 *Symmetrically end loaded beam*

Provided the end masses do not hinder rotation of the beam end, then the beam may be considered as being free-free and will be subjected to the following conditions

i) at $x = 0$, $EI \frac{\partial \Phi}{\partial x} + J \omega^2 \frac{\partial W}{\partial x} = 0$ **(C.9.a)**

(bending moment due to rotary inertia, J, of end mass)

ii) at $x = 0$, $kAG \left(\frac{\partial W}{\partial x} - \Phi \right) + \frac{M_e}{2} \omega^2 W = 0$ **(C.9.b)**

(shear force due to acceleration of end mass)

For symmetric modes, the following conditions apply

$$\text{iii)} \quad \text{at} \quad x = \frac{L}{2}, \quad \Phi = 0 \qquad \text{(zero bending slope)} \qquad \textbf{(C.9.c)}$$

$$\text{iv)} \quad \text{at} \quad x = \frac{L}{2}, \quad kAG\left(\frac{\partial W}{\partial x} - \Phi\right) = 0 \qquad \text{(zero shearing force)}$$

$$\text{so,} \quad \frac{\partial W}{\partial x} = 0 \qquad \textbf{(C.9.d)}$$

For anti-symmetric modes, the following conditions apply

$$\text{iii)} \quad \text{at} \quad x = \frac{L}{2}, \quad W = 0 \qquad \text{(zero lateral displacement)} \qquad \textbf{(C.9.e)}$$

$$\text{iv)} \quad \text{at} \quad x = \frac{L}{2}, \quad \frac{\partial \Phi}{\partial x} = 0 \qquad \text{(zero bending slope)} \qquad \textbf{(C.9.f)}$$

C.2.a Symmetric modes

Equations **(C.9.a,b,c,d)** will respectively lead to the following equations

$$(C_1(\alpha^2+s^2) - C_3(\beta^2-s^2))\, mL^2 + (C_2\alpha + C_4\beta)\, Jb = 0 \qquad \textbf{(C.10.a)}$$

$$-2m(C_2\beta - C_4\alpha) + M_e\, b\,(C_1 + C_3)\,\alpha\beta = 0 \qquad \textbf{(C.10.b)}$$

$$\beta(\alpha^2+s^2)(C_1\, sinh(H) + C_2\, cosh(H)) - \alpha(\beta^2-s^2)(C_3\, sin(T) - C_4\, cos(T)) = 0 \qquad \textbf{(C.10.c)}$$

$$C_1\,\alpha\, sinh(H) + C_2\,\alpha\, cosh(H) - C_3\,\beta\, sin(T) + C_4\,\beta\, cos(T) = 0 \qquad \textbf{(C.10.d)}$$

where

$$H = b\alpha/2 \qquad ; \qquad T = b\beta/2$$

By setting the determinant of the matrix of coefficients to zero, the following frequency equation for the symmetric modes of the end loaded Timoshenko beam is obtained

$$\frac{(\beta^2-s^2)\, mL^2 - \beta\, tan(T)\, Jb}{(\alpha^2+s^2)\, mL^2 - \alpha\, tanh(H)\, Jb} + \frac{\alpha\beta\, M_e\, b + 2\alpha m\, tan(T)}{\alpha\beta\, M_e\, b + 2\beta m\, tanh(H)} = 0 \qquad \textbf{(C.11)}$$

From **Eqns. (C.10)**, the constants C_1 , C_2 , C_4 may be found in terms of C_3 , giving the total lateral deflection, W, as

$$W = P\, C_3\, cosh(b\alpha\zeta) - P\, C_3\, tanh(H)\, sinh(b\alpha\zeta) + C_3\, cos(b\beta\zeta) + C_3\, tan(T)\, sin(b\beta\zeta) \qquad \textbf{(C.12)}$$

where

$$P = -\frac{\alpha}{\beta}\frac{\beta M_e b + 2m\tan(T)}{\alpha M_e b + 2m\tanh(H)} \tag{C.13}$$

C.2.b Anti-symmetric modes

Equations (C.9.e,f) will respectively lead to the following equations

$$C_1\cosh(H) + C_2\sinh(H) + C_3\cos(T) + C_4\sin(T) = 0 \tag{C.14.a}$$

$$(\alpha^2+s^2)(C_1\cosh(b\alpha\zeta) + C_2\sinh(b\alpha\zeta)) - (\beta^2-s^2)(C_3\cos(b\beta\zeta) + C_4\sin(b\beta\zeta)) = 0 \tag{C.14.b}$$

By setting to zero the determinant of the matrix of coefficients in Eqns. (C.9.a,b) and (C.14), the following frequency equation for the anti-symmetric modes of the end loaded Timoshenko beam is obtained

$$\frac{(\beta^2-s^2)mL^2 + \beta\cot(T)Jb}{(\alpha^2+s^2)mL^2 - \alpha\coth(H)Jb} + \frac{\alpha\beta M_e b - 2\alpha m\cot(T)}{\alpha\beta M_e b + 2\beta m\coth(H)} = 0 \tag{C.15}$$

The constants C_1, C_2, C_4 are found in terms of C_3 using Eqns. (C.9.a,b) and (C.14). The total deflection, W, is then given as

$$W = C_3 P\cosh(b\alpha\zeta) - C_3 P\coth(H)\sinh(b\alpha\zeta) + C_3\cos(b\beta\zeta) - C_3\cot(T)\sin(b\beta\zeta) \tag{C.16}$$

where

$$P = -\frac{\alpha}{\beta}\frac{\beta M_e b - 2m\cot(T)}{\alpha M_e b + 2m\coth(H)} \tag{C.17}$$

C.2.1 Strain energy

Strain energy of an end loaded Timoshenko beam is given by Eqn. (3.20), for which, similar to the centrally loaded case (*Chapter 3*), it will be convenient to rewrite Eqns. (3.14) in the form of Eqns. (3.21).

The coefficients of **Eqns. (3.21)** for symmetric modes of an end loaded Timoshenko beam are found as follows

In Eqn. (3.21.a)

$$A = P C_3 \quad ; \quad B = -\tanh(H)\, P C_3$$
$$C = C_3 \quad ; \quad D = \tan(T)\, C_3 \quad , \qquad \textbf{(C.18.a)}$$

in Eqn. (3.21.b)

$$A = -\alpha \tanh(H)\, P C_3 \quad ; \quad B = \alpha P C_3$$
$$C = \beta \tan(T)\, C_3 \quad ; \quad D = -\beta C_3 \quad , \qquad \textbf{(C.18.b)}$$

in Eqn. (3.21.c)

$$A = -\frac{\alpha^2+s^2}{\alpha} \tanh(H)\, P C_3 \quad ; \quad B = \frac{\alpha^2+s^2}{\alpha} P C_3$$
$$C = \frac{\beta^2-s^2}{\beta} \tan(T)\, C_3 \quad ; \quad D = -\frac{\beta^2-s^2}{\beta} C_3 \quad , \qquad \textbf{(C.18.c)}$$

and in Eqn. (3.21.d)

$$A = (\alpha^2+s^2)\, P C_3 \quad ; \quad B = -(\alpha^2+s^2) \tanh(H)\, P C_3$$
$$C = -(\beta^2-s^2)\, C_3 \quad ; \quad D = -(\beta^2-s^2) \tan(T)\, C_3 \qquad \textbf{(C.18.d)}$$

The coefficients of **Eqns. (3.21)** for anti-symmetric modes of an end loaded Timoshenko beam are found as follows

In Eqn. (3.21.a)

$$A = P C_3 \quad ; \quad B = -\coth(H)\, P C_3$$
$$C = C_3 \quad ; \quad D = -\cot(T)\, C_3 \quad , \qquad \textbf{(C.19.a)}$$

in Eqn. (3.21.b)

$$A = -\alpha\, coth(H)\, P\, C_3 \quad ; \quad B = \alpha\, P\, C_3$$

$$C = -\beta\, cot(T)\, C_3 \quad ; \quad D = -\beta\, C_3 \quad , \qquad \textbf{(C.19.b)}$$

in Eqn. (3.21.c)

$$A = -\frac{\alpha^2+s^2}{\alpha}\, coth(H)\, P\, C_3 \quad ; \quad B = \frac{\alpha^2+s^2}{\alpha}\, P\, C_3$$

$$C = -\frac{\beta^2-s^2}{\beta}\, cot(T)\, C_3 \quad ; \quad D = -\frac{\beta^2-s^2}{\beta}\, C_3 \quad , \qquad \textbf{(C.19.c)}$$

and in Eqn. (3.21.d)

$$A = (\alpha^2+s^2)\, P\, C_3 \quad ; \quad B = -(\alpha^2+s2)\, coth(H)\, P\, C_3$$

$$C = -(\beta^2-s^2)\, C_3 \quad ; \quad D = (\beta^2-s^2)\, cot(T)\, C_3 \qquad \textbf{(C.19.d)}$$

Strain energy of bending is now given by **Eqn. (3.24)** in which A, B, C and D are given by **Eqns. (C.18.d)/(C.19.d)** for symmetric/anti-symmetric modes of an end loaded Timoshenko beam.

Similarly, strain energy of shearing of an end loaded Timoshenko beam is given by **Eqn. (3.26)**, in which

$$A_{12}\,,\ B_{12}\,,\ C_{12}\,,\ D_{12} = A_1 - A_2\,,\ B_1 - B_2\,,\ C_1 - C_2\,,\ D_1 - D_2$$

where

$$A_1\,,\ B_1\,,\ C_1\,,\ D_1 = A\,,\ B\,,\ C\,,\ D$$

as given by **Eqns. (C.18.b)/(C.19.b)** for symmetric/anti-symmetric modes; and

$$A_2\,,\ B_2\,,\ C_2\,,\ D_2 = A\,,\ B\,,\ C\,,\ D$$

as given by **Eqns. (C.18.c)/(C.19.c)** for symmetric/anti-symmetric modes.

C.2.2 Bending and shearing stresses

For the first mode of flexural vibration of an end loaded beam, the maximum bending stress is obtained from **Eqns. (3.27)** and **(3.28)**, where $\partial\Phi/\partial x$ is given by **Eqn. (3.21.d)** in which the constants A, B, C and D are given by **Eqns. (C.18.d)**.

Similarly, the shearing stress is given by **Eqn. (3.29)**, where $\partial W/\partial x$ is given by **Eqn. (3.21.b)**, in which the constants A, B, C and D are given by **Eqns. (C.18.b)**; and Φ is given by **Eqn. (3.21.c)**, in which the constants A, B, C and D are given by **Eqns. (C.18.c)**.

C.2.3 Bernoulli-Euler simplification

Simplification of the end loaded Timoshenko equations to the Bernoulli-Euler equations (section 3.3.3) will establish the following relationship between the quantity b in the present work and Φ in [Guild and Adams, 1980]

$$\sqrt{b} \quad = \quad \Phi \qquad \textbf{(C.20)}$$

Once relevant substitutions are made, **Eqns. (C.11)** and **(C.12)** will be identical to **Eqns. (10)** and **(11)** in [Guild and Adams, 1980]. The total strain energy in **Eqn. (3.20)** will now reduce to the strain energy due to bending, U_b , and the latter will reduce to the corresponding **Eqn. (14)** in [Guild and Adams, 1980].

Appendix (D)

AN EXAMPLE OF THE COMPUTATION OF THE RESULTS AND ESTIMATION OF EXPERIMENTAL ERROR

Scope - In this appendix, a detailed account of different stages of computations involved in the determination of both theoretical and experimental results for a typical sandwich beam is presented. The results under consideration are the modulus and the SDC of the angle-ply 913C/Nomex sandwich beam at 15° orientation (**Fig. 6.33**). All the predictions regarding the sandwich skins are based on the constituent data obtained from tests on narrow beams.

Also included in this appendix is an estimation of the experimental error for this particular beam.

D.1 Sandwich skin

D.1.1 Prediction of modulus and the SDC of the sandwich skin

In order to predict the modulus and SDC of the above sandwich skin, the longitudinal, transverse and longitudinal shear properties (modulus and SDC) of the unidirectional composite will be needed. The first two sets of data are obtained from flexural tests on the 0° and 90° beams using the centrally driven flexural test-rig, while the longitudinal shear properties are obtained from the longitudinal shear test.

The following data were recorded for the flexural test on the 0° beam

Test piece specifications

m	=	3.8	g
L	=	200	mm
w	=	12.8	mm
h	=	1.00	mm

Test parameters (small coils)

M_c	=	45.2	g
Γ_d	=	0.514	N/A
Γ_p	=	0.784	V.s/m

Test readings in the first flexural mode at the lowest amplitude

f_n	=	144.1	Hz
I_{rms}	=	10	mA
V_{rms}	=	3.82	mV

Using the above data in the program *BEAM4.FOR* gives the following results

modulus	=	112.5	GPa	(D.1)
maximum bending stress	=	4.93	MPa	
SDC	=	0.74%		(D.2)

The following data were recorded for the flexural test on the 90° beam

Test piece specifications

m	=	4.2	g
L	=	202	mm
w	=	12.5	mm
h	=	1.12	mm

Test parameters

same as for 0°

Test readings in the first flexural mode at the lowest amplitude

f_n	=	43.3	Hz
I_{rms}	=	20	mA
V_{rms}	=	2.82	mV

Using the above data in the program *BEAM4.FOR* gives the following results

modulus	=	8.4	GPa	**(D.3)**
maximum bending stress	=	0.9	MPa	
SDC	=	7.3%		**(D.4)**

The following data were recorded for the longitudinal shear test on a unidirectional cylindrical sample of the 913C composite.

Test piece specifications

L	=	141.5	mm
d	=	9.94	mm

Test parameters

J_{bar}	=	5.52×10^{-5}	kg m²
R_d	=	26.0	mm
R_p	=	26.0	mm
Γ_d	=	0.144	N/A
Γ_p	=	0.081	V.s/m

Test readings at the lowest angular amplitude

f_n	=	122.2	Hz
I_{rms}	=	40	mA
V_{rms}	=	0.81	mV

Using the above data, first the shear modulus was obtained from **Eqn. (B.5)** (*Appendix (B)*). Then, the SDC and the corresponding maximum shear stress were computed from **Eqns. (B.10)** and **(B.11)** respectively. The following results were obtained

shear modulus	=	4.8	GPa	**(D.5)**
maximum shear stress	=	0.104	MPa	
SDC	=	6.6%		**(D.6)**

The data given by **(D.1)** to **(D.6)** constitute the necessary data for the prediction of the modulus and the SDC of the 15° angle-ply laminate. These data, together with the major Poisson's ratio found for the material, are summarised below

ψ_l	=	0.74%
ψ_t	=	7.3%
ψ_{lt}	=	6.6%
E_l	=	112.5 GPa
E_t	=	8.4 GPa
G_{lt}	=	4.8 GPa
υ_{lt}	=	0.30
laminate		$(-15, 15, -15, 15)_s$

Using these data in the program *PREDAMP.FOR* gives the following predictions for the 15° angle-ply laminate

modulus	=	86.3 GPa	**(D.7)**
ψ_l	=	0.62%	
ψ_t	=	0.05%	
ψ_{lt}	=	1.04%	
SDC	=	1.71%	**(D.8)**

D.1.2 Measurement of modulus and the SDC of the sandwich skin

The following data were recorded for the flexural test on the 15° beam

Test piece specifications

			Measured to within		Error
m	=	3.8 g	0.01	g	±0.26%
L	=	200 mm	0.5	mm	±0.25%
w	=	12.0 mm	0.05	mm	±0.42%
h	=	1.05 mm	0.005	mm	±0.48%

Test parameters (same as for 0°)

			Measured to within		Error
M_c	=	45.2 g	0.05	g	±0.11%
Γ_d	=	0.514 N/A	-		±2% (estimated)
Γ_p	=	0.784 V.s/m	-		±2% (estimated)

Test readings in the first flexural mode at the lowest amplitude

f_n	=	132.8 Hz	0.1	Hz	±0.08%
I_{rms}	=	10 mA	0.1	mA	±1.00%
V_{rms}	=	1.81 mV	0.05	mV	±2.76%

Using the above data in the program *BEAM4.FOR* gives the following results

modulus	=	88.0	GPa	**(D.9)**
maximum bending stress	=	2.1	MPa	
overall SDC	=	1.70%		**(D.10)**

The theoretical and experimental values of the modulus, given by **(D.7)** and **(D.9)** respectively, are compared on **Fig. 6.3** (for the 15° orientation). The SDC versus stress amplitude can be found in **Fig. 6.8**, while the theoretical and experimental values of the SDC, given by **(D.8)** and **(D.10)**, as well as the theoretical damping components ψ_t, ψ_t and ψ_{tt}, are given in **Fig. 6.13**, although as mentioned in the text (section **6.7.1.1**), the predictions on these figures are based on the data of the wide beams which give slightly different values of 87.3 GPa for modulus and 1.80% for the overall SDC.

Estimation of experimental error

The modulus is found from **Eqn. (3.8)** in which b is found iteratively to within 10^{-9} from the frequency equation **(3.17)**. After reduction to the elementary theory, this latter equation will be a function of M_c/m. Then, neglecting the error in computations, b is found to within

$$\pm [(m\%)^2 + (M_c\%)^2]^{1/2} = \pm [(0.26)^2 + (0.11)^2]^{1/2} = \pm 0.28\%$$

The modulus is, therefore, accurate to within

$$\pm [2^2(b\%)^2 + (m\%)^2 + 3^2(L\%)^2 + 2^2(f\%)^2 + (w\%)^2 + 3^2(h\%)^2]^{1/2} =$$

$$\pm [2^2(0.28)^2 + (0.26)^2 + 3^2(0.25)^2 + 2^2(0.08)^2 + (0.42)^2 +$$

$$3^2(0.48)^2]^{1/2} = \pm 1.79\%$$

The maximum bending stress is found from **Eqns. (3.27)** and **(3.28)**. The quantity $\partial\phi/\partial x$ is given by **Eqn. (3.21.d)** which after reduction to the elementary theory will be a function of b, L^2, and W_m . The displacement amplitude, W_m , is given by **Eqn. (A.6)** and is, therefore accurate to within

$$\pm [(V_{ms}\%)^2 + (\Gamma_p\%)^2 + (f\%)^2]^{1/2} = \pm [(2.76)^2 + (2)^2 + (0.08)^2]^{1/2}$$

$$= \pm 3.41\%$$

Then, $\partial\phi/\partial x$ is accurate to within

$$\pm [(b\%)^2 + 2^2(L\%)^2 + (W_m\%)^2]^{1/2} = \pm [(0.28)^2 + 2^2(0.25)^2 + (3.41)^2]^{1/2}$$

$$= \pm 3.46\%$$

The maximum bending stress is, therefore, accurate to within

$$\pm [(E\%)^2 + (\partial\phi/\partial x\%)^2 + (w\%)^2 + 2^2(h\%)^2]^{1/2} = \pm [(1.79)^2 + (3.46)^2$$

$$+ (0.42)^2 + 2^2(0.48)^2]^{1/2} = \pm 4.03\%$$

The SDC is found from **Eqn. (3.41)** in which U_s is given by **Eqn. (3.24)**. After reduction to the elementary theory, this latter equation will be a function of E, I, b^2/L^3 and W_m^2 . From **Eqn. (A.2)**, ΔU is a function of F_m and W_m . The SDC is, therefore, accurate to within

$$\pm [(E\%)^2 + (w\%)^2 + 3^2(h\%)^2 + 2^2(b\%)^2 + 3^2(L\%)^2 + (\Gamma_d\%)^2 + (I_{ms}\%)^2 +$$

$$(W_m\%)^2]^{1/2} =$$

$$\pm [(1.79)^2 + (0.42)^2 + 3^2(0.48)^2 + 2^2(0.28)^2 + 3^2(0.25)^2 + (2)^2 +$$

$$(1.00)^2 + (3.41)^2]^{1/2} = \pm 4.79\%$$

D.2 Sandwich core

The following data were recorded for the shear test on the honeycomb core used for the 15° angle-ply sandwich beam (Aeroweb A1,50,6; **Fig. 4.14**) along the ribbon direction

Test piece specifications

			Measured to within		Error
A	=	63 mm × 97 mm	1×1.5	mm	± (1.6% × 1.5%)
c	=	12.75 mm	0.1	mm	± 0.78%

Test parameters

			Measured to within		Error
M	=	1142 g	1	g	± 0.08%
Γ_d	=	1.185 N/A	-		± 2% (estimated)
Γ_p	=	1.352 V.s/m	-		± 2% (estimated)

Test readings at the lowest amplitude

f_n	=	1010	Hz	0.5	± 0.05%
I_{rms}	=	51	mA	0.1	± 0.20%
V_{rms}	=	0.34	mV	0.02	± 5.88%

Using the above data, first the shear modulus was obtained from **Eqn. (4.5)**, and then the maximum shear stress and SDC were computed using **Eqns. (4.6)** to **(4.8)**, in which ΔU and δ were found using **Eqns. (A.2)**, **(A.3)** and **(A.6)**. These were found to be

shear modulus	=	48.0	MPa	**(D.11)**
maximum shear stress	=	211	Pa	
SDC	=	10.4%		**(D.12)**

as indicated on **Fig. 4.14.**

Estimation of experimental error

The core modulus is given by **Eqn. (4.5)** and is, therefore, accurate to within

$$\pm [2^2(f\%)^2 + (M\%)^2 + (c\%)^2 + (A\%)^2]^{1/2} =$$

$$\pm [2^2(0.05)^2 + (0.08)^2 + (0.78)^2 + (1.60)^2 + (1.50)^2]^{1/2} = \pm 2.33\%$$

The maximum shear stress is given by **Eqns. (4.8)** and **(A.6)**, and is, therefore, accurate to within

$$\pm [(G\%)^2 + (V_{rms}\%)^2 + (\Gamma_p\%)^2 + (f\%)^2 + (c\%)^2]^{1/2} =$$

$$\pm [(2.33)^2 + (5.88)^2 + (2)^2 + (0.05)^2 + (0.78)^2]^{1/2} = \pm 6.68\%$$

The SDC is given by **Eqns. (4.6)**, **(4.7)** and **(A.2)**, and is, therefore, accurate to within

$$\pm [(I_{rms}\%)^2 + (V_{rms}\%)^2 + (\Gamma_d\%)^2 + (\Gamma_p\%)^2 + (M\%)^2 + (f\%)^2]^{1/2} =$$

$$\pm [(0.20)^2 + (5.88)^2 + (2)^2 + (2)^2 + (0.08)^2 + (0.05)^2]^{1/2} = \pm 6.53\%$$

D.3 Sandwich beam

First, the empirical value of the shear correction factor, k , corresponding to the prediction of the exact frequency of the centrally driven 0° sandwich beam, was obtained. For the frequency test on this beam the following data were recorded

Test piece specifications

			Measured to within		Error
m	=	48.3 g	0.2	g	±0.41%
L	=	248.0 mm	0.5	mm	±0.20%
w	=	41.3 mm	0.1	mm	±0.24%
t	=	1.15 mm	0.005	mm	±0.43%
c	=	12.75 mm	0.1	mm	±0.78%
E_f	=	112.5	GPa		(from **D1**)
G_c	=	48.0	MPa		(from **D11**)

Test parameters (large coils)

M_c = 132.5 g

Using these data, the value of k which would predict the first natural frequency of 838 Hz was found to be 1.24.

The following data were recorded for the flexural damping test on the 15° sandwich beam

Test piece specifications

			Measured to within		Error
m	=	42.0 g	0.2	g	± 0.48%
L	=	251.0 mm	0.5	mm	± 0.20%
w	=	36.3 mm	0.1	mm	± 0.28%
t	=	1.12 mm	0.005	mm	± 0.45%
c	=	12.75 mm	0.1	mm	± 0.78%
E_s	=	88.0 GPa			(from (D.9))
G_c	=	48.0 MPa			(from (D.12))
k	=	1.24			

Test parameters (large coils)

			Measured to within		Error
M_c	=	132.5 g	0.5	g	± 0.38%
Γ_d	=	0.585 N/A	-		± 2% (estimated)
Γ_p	=	0.685 V.s/m	-		± 2% (estimated)

Test readings at the lowest amplitude

			Measured to within		Error
f_n	=	833 Hz	0.5	Hz	± 0.06%
I_{rms}	=	101 mA	0.5	mA	± 0.50%
V_{rms}	=	0.8 mV	0.02	mV	± 2.50%

Using the above data in the program *BEAM4.FOR* gives the following results

sandwich skin modulus	=	93.4	GPa	**(D.13)**
maximum bending stress in the skin	=	91	kPa	
shearing stress in the core	=	0.26	kPa	
sandwich SDC	=	8.44%		**(D.14)**

The skin modulus and the sandwich skin modulus, given by **(D.9)** and **(D.13)** respectively, are compared on **Fig. 6.22** for the 15° orientation.

The following data are needed to predict the SDC of the sandwich beam

ψ_f	=	1.7%	(from **(D.8)**)
ψ_c	=	10.4%	(from **(D.12)**)

These data, together with the test piece specifications (above) in which the experimental value of E_f is replaced by the predicted value (86.3 GPa, from **(D.7)**), constitute the necessary data for prediction of the SDC of the 15° sandwich beam. The program *BEAM4.FOR* gives the following results

SDC due to skin	=	0.3%	**(D.15)**
SDC due to core	=	7.7%	**(D.16)**
total sandwich SDC	=	8.0%	**(D.17)**

The experimental and theoretical values of the SDC of the sandwich, given by **(D.14)** and **(D.17)** respectively, as well as the proportion of the contribution of the skin and the core to the overall SDC, given by **(D.15)** and **(D.16)**, are presented in **Fig. 6.33** for the 15° orientation.

Estimation of experimental error

The sandwich modulus (for $k=1$) is found from the sandwich frequency according to **Eqn. (3.8)**. The frequency number, b, in this equation is found iteratively from the frequency equation **(3.17)**. This latter equation is a function of α^2 , β^2 , s^2 , m and M_c . Ignoring the rotary inertia parameter r, α and β are given by **Eqn. (3.12)** as functions of s. From **Eqns. (3.8)** and **(3.10)**, s^2 is found to within

$$\pm [(m\%)^2 + (w\%)^2 + (t\%)^2 + (L\%)^2 + 2^2(f\%)^2 + (G\%)^2]^{1/2} =$$

$$\pm [(0.48)^2 + (0.28)^2 + (0.45)^2 + (0.2)^2 + 2^2(0.06)^2 + (2.33)^2]^{1/2} = \pm 2.45\%$$

Therefore, b is found to within

$$\pm [(\alpha\%)^2 + (m\%)^2 + (M_c\%)^2]^{1/2} =$$

$$\pm [(2.45)^2 + (0.48)^2 + (0.38)^2]^{1/2} = \pm 2.52\%$$

The modulus is, therefore, found approximately to within

$$\pm [2^2(b\%)^2 + (m\%)^2 + (w\%)^2 + 3^2(t\%)^2 + 4^2(L\%)^2 + 2^2(f\%)^2 + 3^2(c\%)]^{1/2} =$$

$$\pm [2^2(2.52)^2 + (0.48)^2 + (0.28)^2 + 3^2(0.45)^2 + 4^2(0.20)^2 + 2^2(0.06)^2 +$$

$$3^2(0.78)^2]^{1/2} = \pm 5.53\%$$

The SDC is found from **Eqn. (3.40)**, in which ΔU is given by **Eqn. (A.2)** and, U_r and U_s are given by **Eqns. (3.24)** and **(3.26)** respectively. Ignoring the rotary inertia parameter, the SDC is found approximately to within

$$\pm [(E\%)^2 + (I_s\%)^2 + 4^2(b\%)^2 + 3^2(L\%)^2 + 2^2(s\%)^2 + (G\%)^2 + (V_{rms}\%) +$$

$$(\Gamma_p\%)^2 + (I_{rms}\%)^2 + (\Gamma_p\%)^2 + (f\%)^2]^{1/2} =$$

$$\pm [(1.79)^2 + (0.28)^2 + 3^2(0.45)^2 + 3^2(0.78)^2 + 4^2(2.52)^2 + 3^2(0.20)^2 +$$

$$2^2(2.45)^2 + (2.33)^2 + (2.50)^2 + (2)^2 + (0.50)^2 + (2)^2 + (0.06)^2 = \pm 12.51\%$$

References

N.B. - The references are listed in the alphabetical order of authors' names. Works by the same author(s), are listed according to the year of publication; for the same author(s) and year of publication, the works are referenced as -a, -b *etc.* which appear with the year of publication.

ADAMS R.D., *The Damping Characteristics of Certain Steels, Cast Irons and Other Metals*, Ph.D. Thesis, Cambridge University, (1967)

ADAMS R. D., BACON D. G. C., *Measurement of the Flexural Damping and Young's Modulus of Metals and Reinforced Plastics*, J. Physics, D: Applied Physics, 6, 27-41, (1973-a)

ADAMS R. D., BACON D. G. C., *The Dynamic Properties of Unidirectional Fibre Reinforced Composites in Flexure and Torsion*, J. Composite Materials, 7, 53-67, (1973-b)

ADAMS R. D., BACON D. G. C., *Effect of Fibre Orientation and Laminate Geometry on the Dynamic Properties of CFRP*, J. Composite Materials, 7, 402-428, (1973-c)

ADAMS R. D., CAWLEY P., *Vibration Techniques in Nondestructive Testing*, Nondestructive Testing, 8, 303-360, (1985)

ADAMS R.D., FOX M.A.O., FLOOD R.J.L., FRIEND R.J., HEWITT R.L., *The Dynamic Properties of Unidirectional Carbon and Glass Fibre Reinforced Plastics in Torsion and Flexure*, J. Composite Materials, 3, 594-603, (1969)

ADAMS R.D., WAKE W. C., *Structural Adhesive Joints in Engineering*, Elsevier Applied Science Publishers, London, (1984)

AGBASIERE J. A., GROOTENHUIS P., *Flexural Vibration of Symmetrical Multi-Layer Beams With Viscoelastic Damping*, J. Mechanical Engineering Science, 10 (3), (1968)

ANDERSON R. A., *Flexural Vibration in Uniform Beams According to the Timoshenko Theory*, J. Applied Mechanics, Trans. ASME, 75, 504-510, (1953)

BACON D. G. C., *The Dynamic Properties of Carbon and Glass Fibre Reinforced Plastic*, Ph.D. Thesis, Dept. Mech. Eng., University of Bristol, (1973)

BENJAMIN B. S., *Structural Design with Plastics*, Polymer Science and Engineering Series, Van Nostrand Company, London, (1969)

BERT C. W., WILKINS D. J., CRISMAN W. C., *Damping in Sandwich Beams With Shear Flexible Cores,* J. Engineering for Industry, Trans. ASME, 89B (4), 662-670, (1967)

CAWLEY P., ADAMS R. D., *The Predicted and Experimental Natural Modes of Free-Free CFRP Plates,* J. Composite Materials, 12, 336-347, (1978)

CAWLEY P., ADAMS R. D., *The Location of Defects in Structures from Measurements of Natural Frequencies,* J. Strain Analysis, 14 (2),49-57, (1979)

CHOW T. S., *On the Propagation of Flexural Waves in an Orthotropic Laminated Plate and Its Response to an Impulsive Load,* J. Composite Materials, 5, 306-319, (1971)

COTTELL G.A., ENTWISTLE K.M., THOMPSON F.C., *The Measurement of Damping Capacity of Metals in Torsional Vibration,* J. Inst. of Metals, 74, 373-424, (1948)

COWPER G. W., *The Shear Coefficient in Timoshenko's Beam Theory,* J. Applied Mechanics, Trans. ASME, 33 (E), 335-340, (1966)

DENGLER M. A., GOLAND M., *Transverse Impact of Long Beams, including Rotatory Inertia and Shear Effects,* Proc. 1st U.S. Natl. Cong. on Appld. Mechs., ASME, 179-186, (1951)

DiTARANTO R. A., *Theory of Vibratory Bending for Elastic and Viscoelastic Layered Finite-Length Beams,* J. Applied Mechanics, Trans. ASME, 87 (E), 881-886, (1965)

DiTARANTO R. A., BLASINGAME W., *Composite Damping of Vibrating Sandwich Beams,* J. Engineering for Industry, Trans. ASME, 89 (B), 633-638, (1967)

DONNELL L. H., *Beams, Plates, and Shells,* McGraw-Hill Book Company, London, (1976)

DREW R.C., WHITE R.G., *An Experimental Investigation into Damage Propagation and its Effects Upon Dynamic Properties in CFRP Composite Material,* Composite Structures 4, 2, Elsevier Applied Science , London, 2.45-2.56, (1987)

FLITCROFT J. E., *The Non-Destructive Testing of Glass and Carbon Fibre Reinforced Plastics,* Ph.D. Thesis, Dept. Mech. Eng., University of Bristol, (1976)

FOX M. A. O., *The Damping and Dynamic Elastic Properties of Cast Iron,* Ph.D. Thesis, Dept. Mech. Eng., University of Bristol, (1972)

GOODMAN L. E., *Discussion of paper [ANDERSON R. A., 1953],* J. Applied Mechanics, Trans. ASME, 76, 202-204, (1954)

GOODMAN L. E., SUTHERLAND J. G., *Discussion of paper [AYRE R. S., JACOBSEN L. S., 1950],* J. Applied Mechanics, Trans. ASME, 73, 217-218, (1951)

GUILD F. J., ADAMS R. D., *A New Technique for the Measurement of the Specific Damping Capacity of Beams in Flexure*, J. of Physics, E: Scientific Instruments, 14, 355-363, (1981)

HERRMANN G., *Forced Motions of Timoshenko Beams*, J. Applied Mechanics, Trans. ASME, 76, 221-224,(1955)

HUANG T. C., *The Effect of Rotatory Inertia and of Shear Deformation on the Frequency and Normal Mode Equations of Uniform Beams With Simple End Conditions*, J. Applied Mechanics (vol 28), Trans. ASME, 83 (E), 571-584, (1961)

HUANG T. C., HUANG C. C., *Free Vibration of Viscoelastic Timoshenko Beams*, J. Applied Mechanics, Trans. ASME, 38, 515-521, (1971)

JAMES W. L., *Calculation of Vibration Damping in Sandwich Construction from Damping Properties of the Cores and the Facings*, Report No. 1888, Forest Products Laboratory, Madison, Wisconsin, (1962)

KEER L., LAZAN B. J., *Damping and Fatigue Properties of Sandwich Configurations in Flexure*, ASD Technical Report 61-646, U.S. Air Force, Wright-Patterson Air Force Base, Ohio, (1961)

KULKARNI S. V., PAGANO N. J., *Dynamic Characteristics of Composite Laminates*, J. Sound and Vibration, 23 (1), 127-143, (1972)

LANTZ R.B., *Boron Epoxy Laminate Test Methods*, J. Composite Materials, 3, 642-650, (1969)

LAZAN B.J., *Energy Dissipation Mechanisms in Structures, with Particular Reference to Material Damping*, Structural Damping, Ed. RUZICKA J.E., Pergamon Press, London, (1960)

LAZAN B.J., *Damping of Materials and Members in Structural Mechanics*, Pergamon Press, London, (1968)

LIN D. X., NI R. G., ADAMS R. D., *Prediction and Measurement of the Vibrational Damping Parameters of Carbon and Glass Fibre-Reinforced Plastics Plates*, J. Composite Materials, 18, 132-152, (1984)

LIN D. X., ADAMS R. D., *Determination of Dynamic Characteristics of Structures by Transient Testing Using Zoom-FFT*, J. de Physique, 44, C9:363-369, (1984)

MARKUS S., VALASKOVA O., *On Eigenvalue Boundary Problems of Transversely Vibrating Sandwich Beams*, J. Sound and Vibration, 23 (4), 423-432, (1972)

MEAD D. J., *The Damping Properties of Elastically Supported Sandwich Plates*, J. Sound and Vibration, 24 (3), 275-295, (1972)

MEAD D. J., *A Comparison of Some Equations for the Flexural Vibration of Damped Sandwich Beams*, J. Sound and Vibration, 83 (3), 363-377, (1982)

MEAD D. J., MARKUS S., *The Forced Vibration of a Three-Layer, Damped Sandwich Beam With Arbitrary Boundary Conditions*, J. Sound and Vibration, 10 (2), 163-175, (1969)

MEAD D. J., MARKUS S., *Loss Factors and Resonant Frequencies of Encastré Damped Sandwich Beams*, J. Sound and Vibration, 12 (1), 99-112, (1970)

MIKLOWITZ J., *Flexural Wave Solution of Coupled Equations Representing the More Exact Theory of Bending*, J. Applied Mechanics, Trans. ASME, 75, 5111-514, (1953)

MINDLIN R. D., *Influence of Rotatory Inertia and Shear on Flexural Motions of Isotropic, Elastic Plates*, J. Applied Mechanics, 18, 31-38, (1951)

MINDLIN R. D., DERESIEWICZ H., *Timoshenko's Shear Coefficient for Flexural Vibrations of Beams*, Proc. 2nd U.S. Natl. Cong. Aplld. Mechs., 171-178, (1955)

NI R. G., ADAMS R. D., *The Damping and Dynamic Moduli of Symmetric Laminated Composite Beams - Theoretical and Experimental Results*, J. Composite Materials, 18, 104-121, (1984)

NI R. G., LIN D. X., ADAMS R. D., *The Dynamic Properties of Carbon-Glass Fibre Sandwich Laminated Composites: Theoretical, Experimental and Economic Considerations*, Composites, 15 (4), 297-304, (1984)

NG C.F., WHITE R.G., *The Dynamic Behaviour of Postbuckled Composite Plates under Acoustic Excitation*, Composites Structures, 9, 19-35, (1988)

NORDBY G. M., CRISMAN W. C., BERT C. W., *Dynamic, Elastic, Damping, and Fatigue Characteristics of Fiberglass-Reinforced Sandwich Structure*, USAAVLABS Technical Report 65-60, Contract DA 44-177-AMC-164(T), University of Oklahoma Research Institute, (1965)

PAGANO N. J., *Exact Solutions for Rectangular Bidirectional Composites and Sandwich Plates*, J. Composite Materials, 4, 20-34, (1970)

PAGANO N.J., HALPIN C. J., *Influence of End Constraint in the Testing of Anisotropic Bodies*, J. Composite Materials, 2, 18-31, (1968)

RAVILLE M. E., UENG E. S., LEI M. M., *Natural Frequencies of Vibration of Fixed-Fixed Sandwich Beams*, J. Applied Mechanics, Trans. ASME, 83 (E), 376-381, (1961)

REISSNER E., *The effect of Transverse Shear Deformation on the Bending of Elastic Plates* , J. Applied Mechanics, 12 (2), Trans. ASME, 67, A-69-77, (1945)

RITCHIE I. G., *Improved Resonant Bar Techniques for the Measurement of Dynamic Elastic Moduli and a Test of the Timoshenko Beam Theory*, J. Sound and Vibration, 31 (4), 453-468, (1973)

RITCHIE I. G., ROSINGER H. E., SHILLINGLAW A. J., FLEURY W. H., *The Dynamic Elastic Behaviour of Fibre-Reinforced Composite Sheet: I. The Precise Experimental Determination of the Principal Elastic Moduli*, J. Physics, D: Applied Physics, 8, 1733-1749, (1975)

SOOVERE J., *Dynamic Properties of Graphite Fibre Honeycomb Panels*, AIAA Paper No. 73-326, (1973)

SOOVERE J., *Dynamic Response of Acoustically Excited Stiffened Composite Honeycomb Panels*, Ph.D. Thesis, I.S.V.R., University of Southampton, (1984)

SOOVERE J., DRAKE M.L., *Aerospace Structures Technology Damping Design Guide*, AFWAL-TR-84-3089 Volume 1, (1985)

SUN C. T., WHITNEY J. M., *Theories for the Dynamic Response of Laminated Plates*, AIAA J., 11, 178-183, (1973)

TETI R., CAPRINO G., *Mechanical Behaviour of Structural Sandwiches*, Proc. 1st. Int. Conf. on Sandwich Constructions, Stockholm, Eng. Materials Advisory Services Ltd., U.K., (1989)

TIMOSHENKO S. P., *On the Correction for Shear of the Differential Equation for Transverse Vibrations of Prismatic Bars*, Philosophical Magazine, 41, 744-746, (1921)

TIMOSHENKO S. P., *On the Transverse Vibrations of Bars of Uniform Cross-Sections*, Philosophical Magazine, 43, 125-131, (1922)

TIMOSHENKO S., *Vibration Problems in Engineering (3rd Ed.)*, Macmillan & Company, Ltd., London, (1955)

TIMOSHENKO S., GOODIER J.N., *Theory of Elasticity (2nd Ed.)*, McGraw-Hill Book Company, London, (1951)

WALTON D., *Torsion of Prismatic Bars of Orthotropic Materials*, Internal Report, Dept. Mech. Eng., University of Bristol, (1973)

WHITE R.G., ABDIN E.M.Y., *Dynamic Properties of Aligned Short Carbon Fibre-Reinforced Plastics in Flexure and Torsion*, Composites, 16 (4), 293-306, (1985)

WHITE R.G., MOUSLEY R.F., *Dynamic Response of CFRP Plates under Action of Random Acoustic Loading*, Composite Structures 4, 1, Elsevier Applied Science , London, 1.519-1.535, (1987)

WHITNEY J. M., *Stress analysis of Thick Laminated Composite and Sandwich Plates*, J. Composite Materials, 6, 426-440, (1972)

WHITNEY J. M., *Shear Correction Factors for Orthotropic Laminates Under Static Load*, J. Applied Mechanics, Trans. ASME, 40 (E), 302-304, (1973)

WHITNEY J. M., *Structural Analysis of Laminated Anisotropic Plates*, Technomic Publishing Co. Inc., (1987)

WHITNEY J.M., DAUKSYS R.J., *Flexure Experiments on Off-Axis Composites*, J. Composite Materials, 4, 135-137, (1970)

WHITNEY J. M., PAGANO N. J., *Shear Deformation in Heterogeneous Anisotropic Plates*, J. Applied Mechanics, Trans. ASME, 37 (4), 1031-1036, (1970)

WILKINS D. J., *Analysis of Material Damping in Sandwich Beams*, M.Sc. Thesis, University of Oklahoma, (1965)

WILLWAY T.A., WHITE R.G., *The Effects of Induced Axial Strains on the Damping of Clamped-Clamped Unidirectional CFRP and Resin Rods in Torsion*, Composites Structures, 9, 89-100, (1988)

WREN G. G., KINRA V. K., *On the Effect of an End-Mass on Beam Damping*, 'To appear in Experimental Mechanics' (See following ref.) (1989-a)

WREN G. G., KINRA V. K., *An Experimental Study of the Complex Dynamic Modulus*, Proc. Damping'89, WRDC-TR-89-3116 Vol II, (1989-b)

YU Y.-Y., *A New Theory of Elastic Sandwich Plates - One Dimensional Case*, J. Applied Mechanics, Trans. ASME, 81 (E), 415-421, (1959-a)

YU Y.-Y., *Simple Thickness-Shear Modes of Vibration of Infinite Sandwich Plates* , J. Applied Mechanics, Trans. ASME, 26, 679-681, (1959-b)

Fig. 3.5 Frequency Vs Mode No.

(Test piece : AL1, square section Duralumin beam)

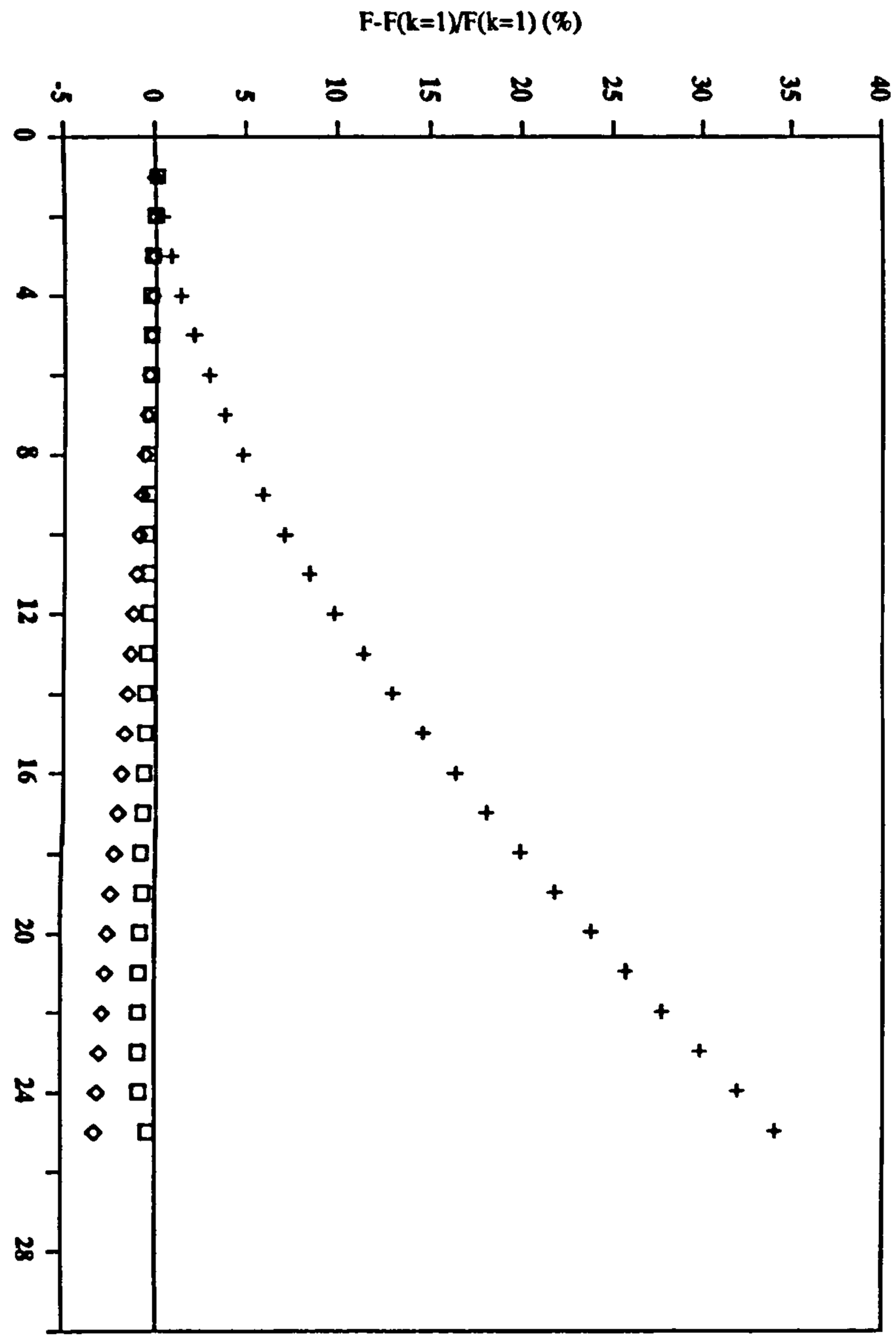

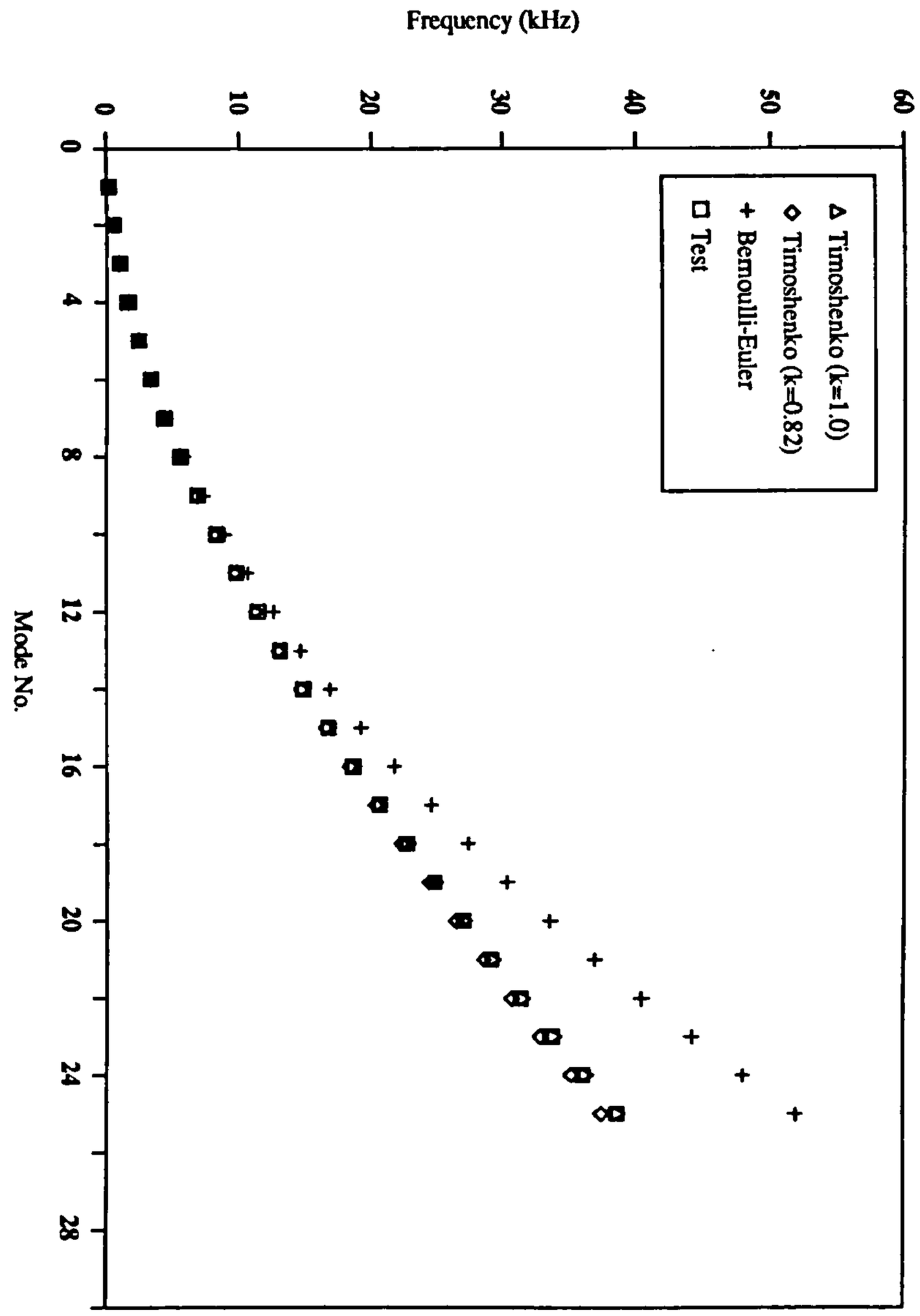

Fig. 3.6 Frequency Vs Mode No.

(Test piece : AL2, rectangular section Duralumin beam)

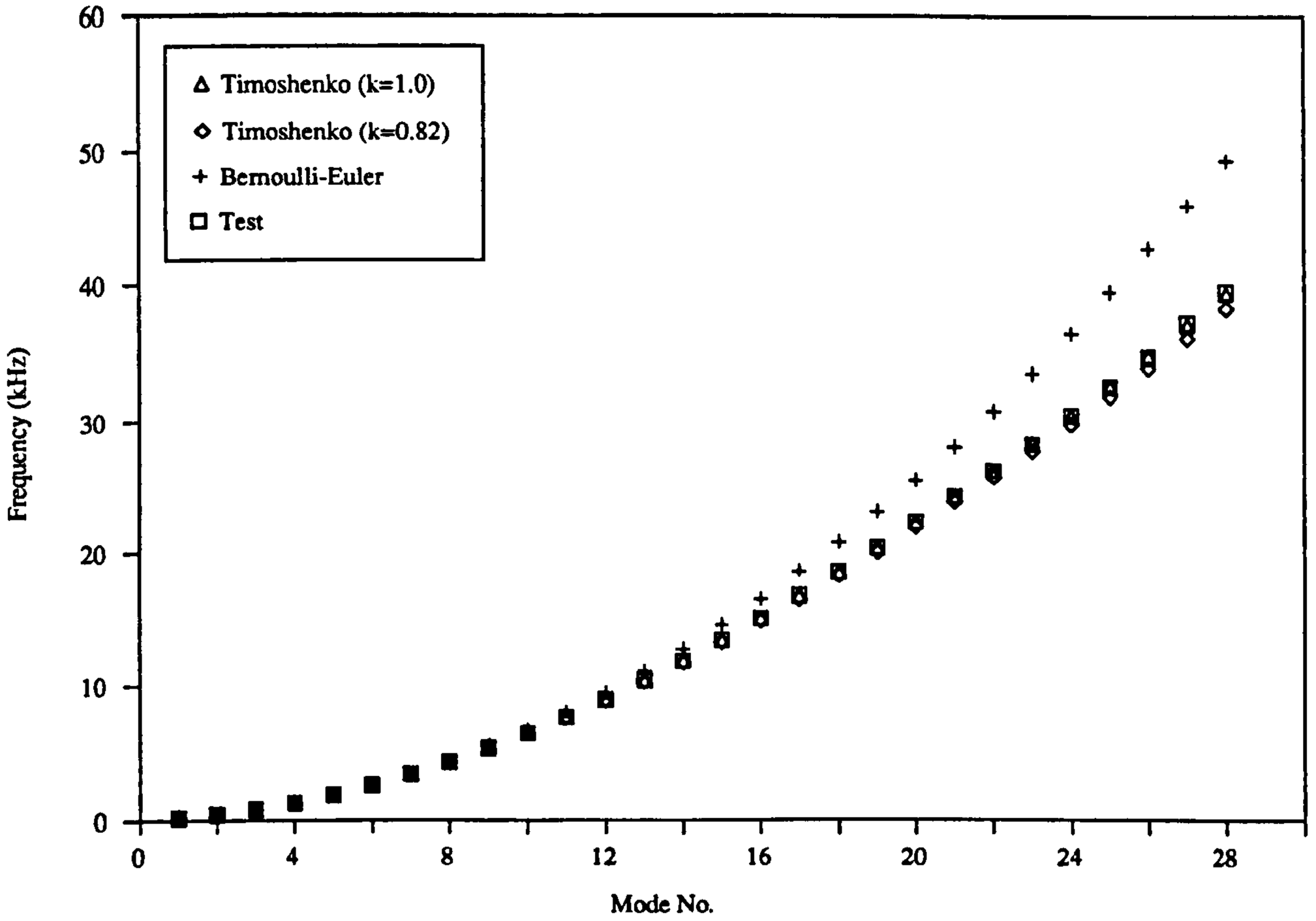

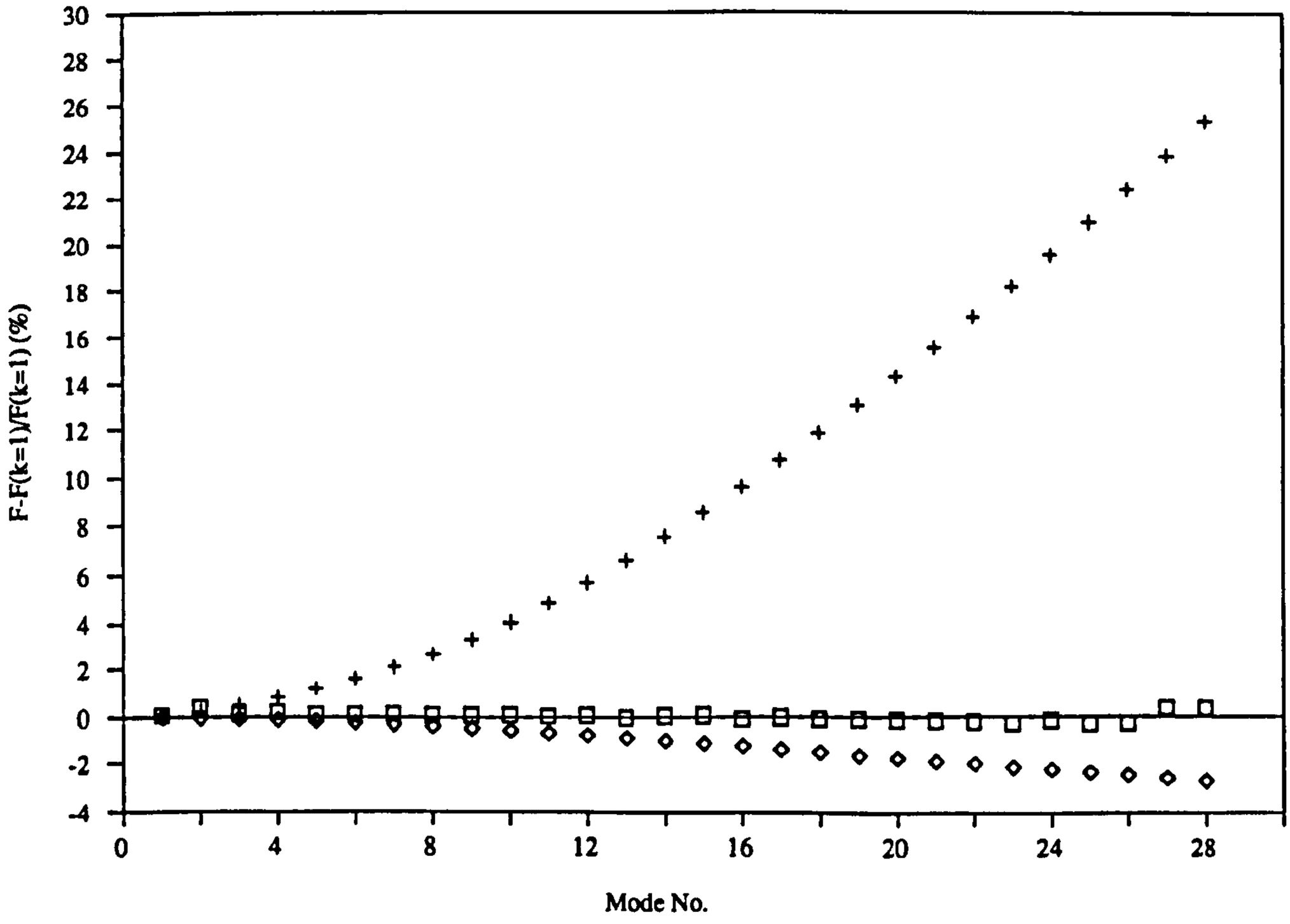

Fig. 3.7 Frequency Vs Mode No.

(Test piece : MS1, square section mild steel beam)

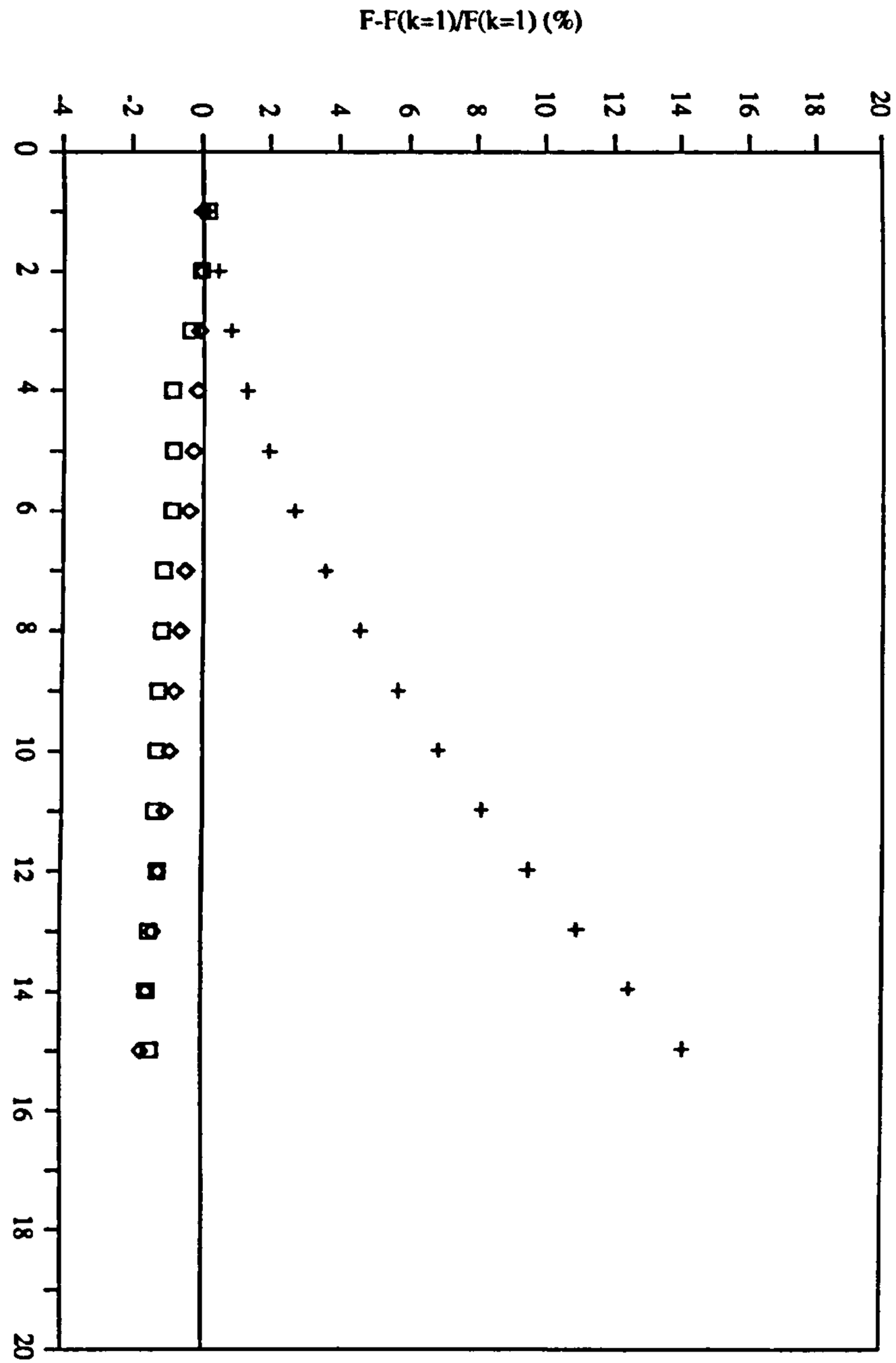

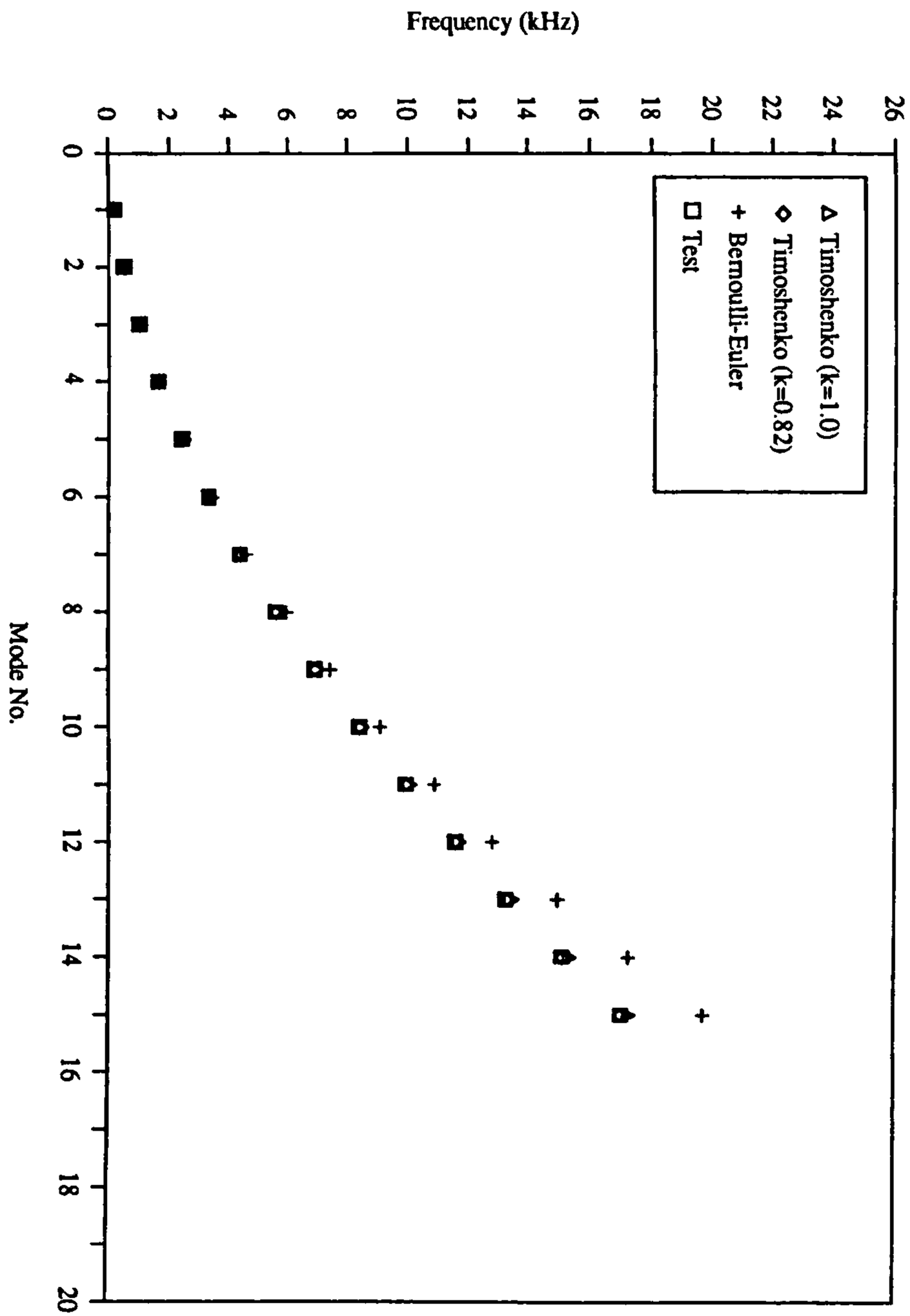

Fig. 3.8 Frequency Vs Mode No.

(Test piece : MS2, rectangular section mild steel beam)

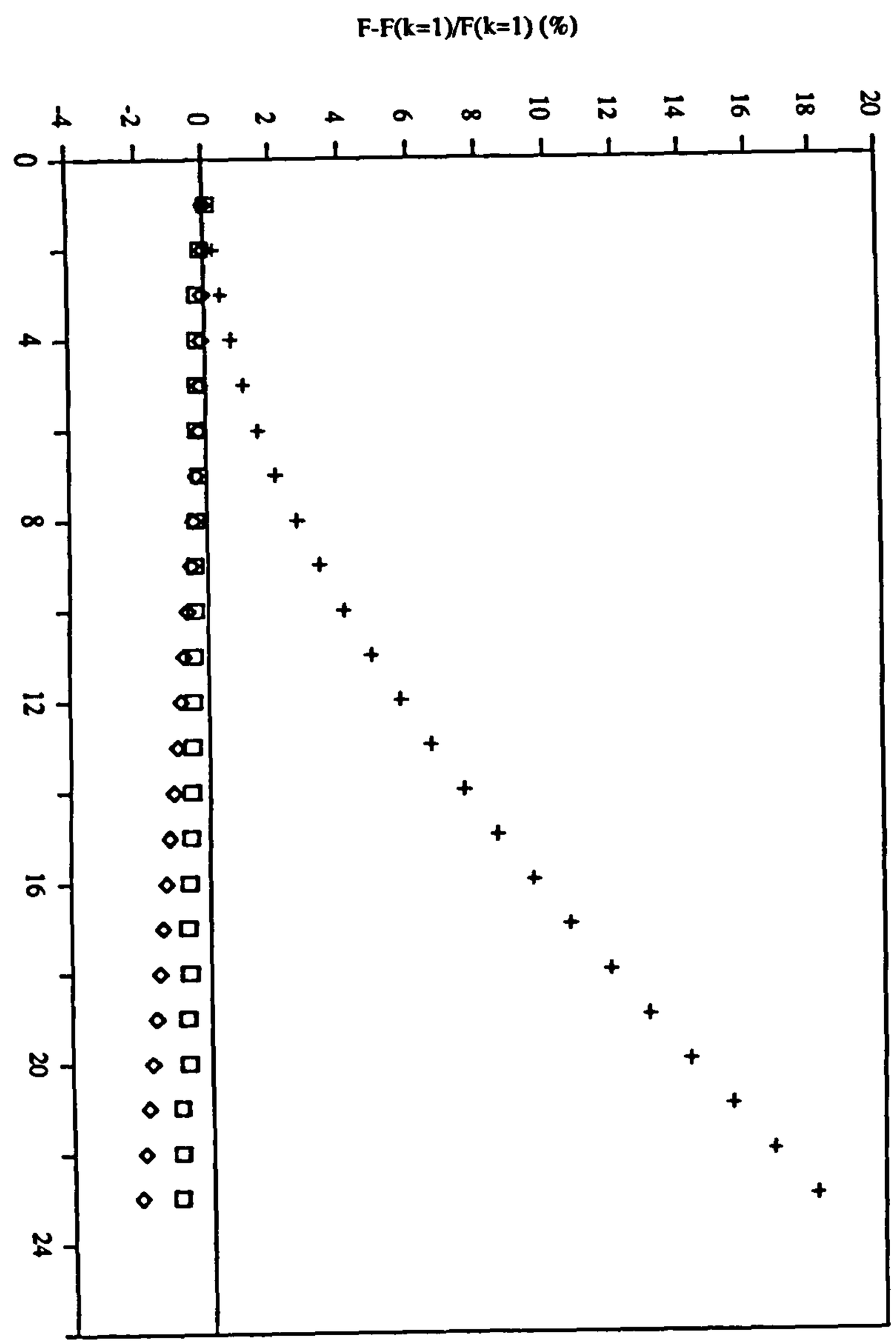

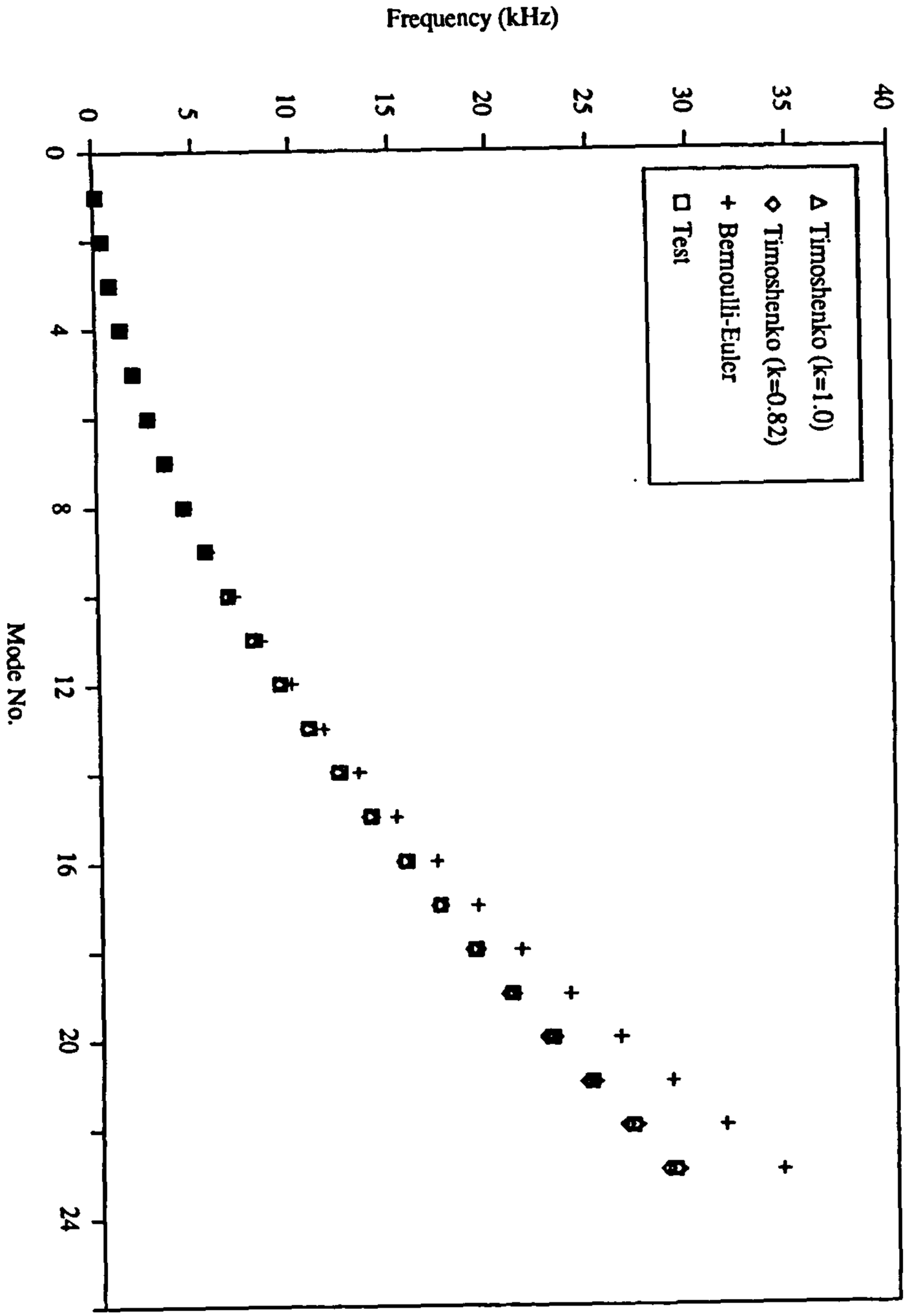

Fig. 3.9 Fundamental natural frequency Vs Thickness/length

(Test piece : AL1, square section Duralumin beam)

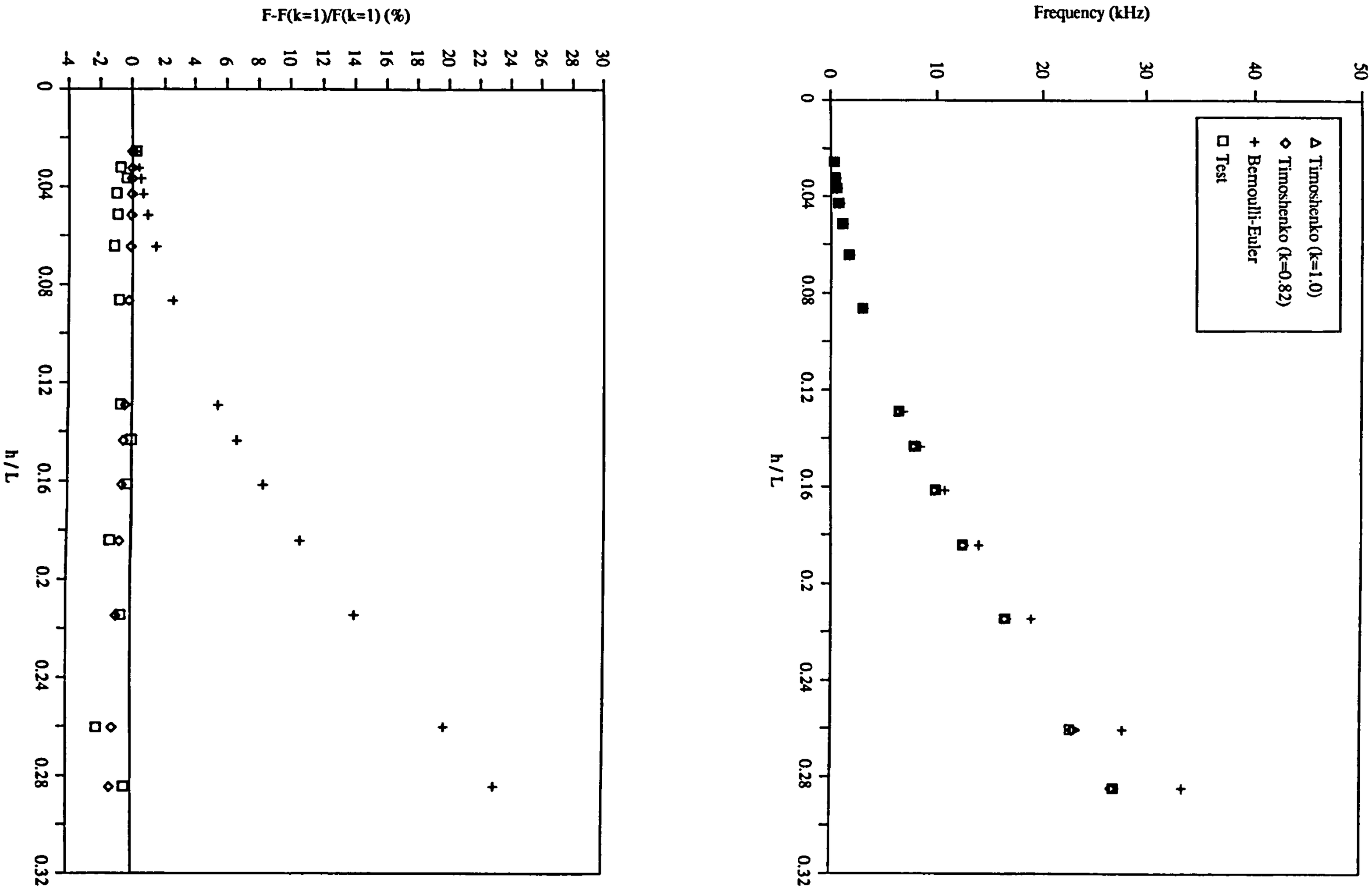

Fig. 3.10 Fundamental natural frequency Vs Thickness/length

(Test piece : AL2, rectangular section Duralumin beam)

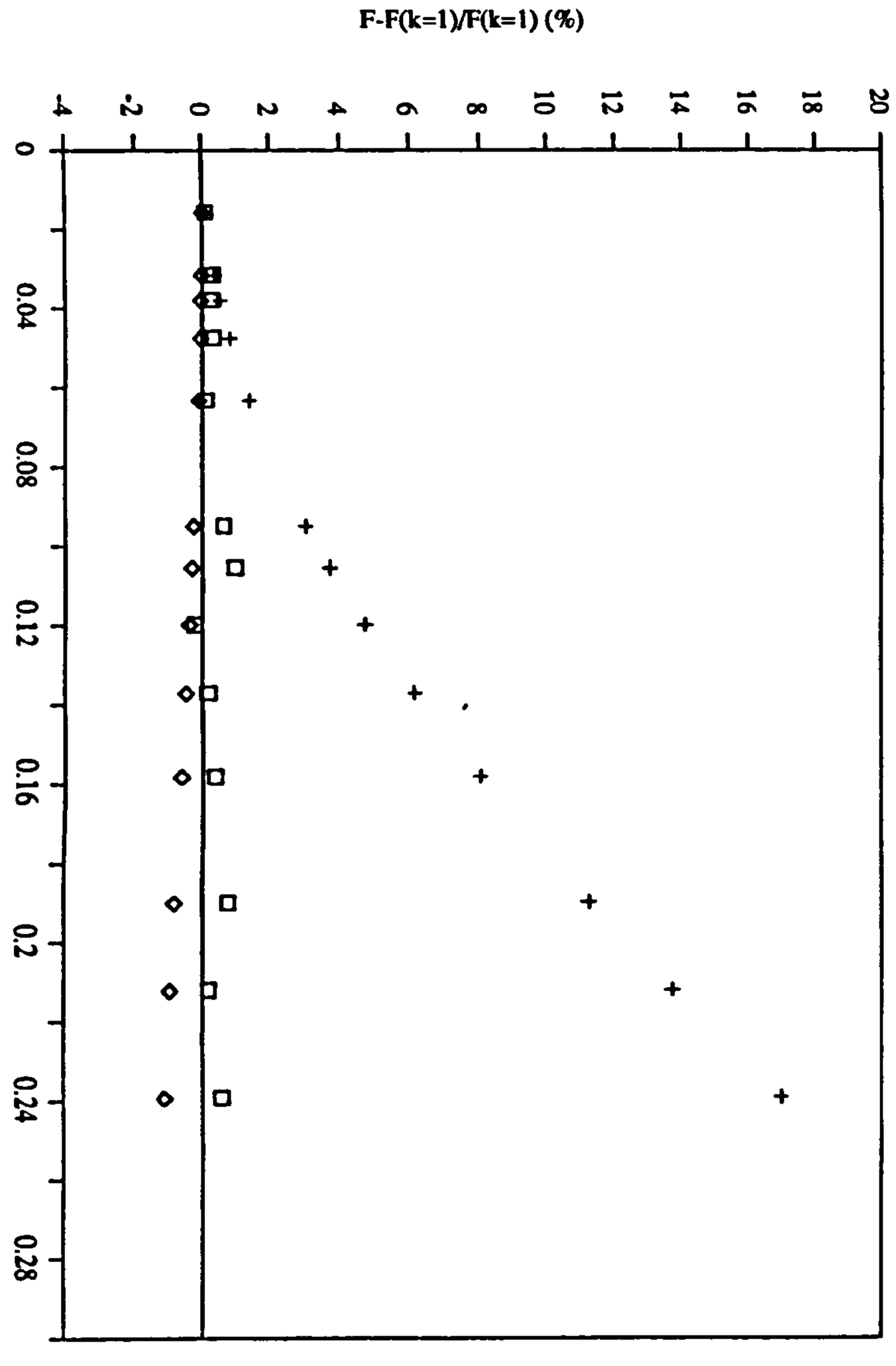

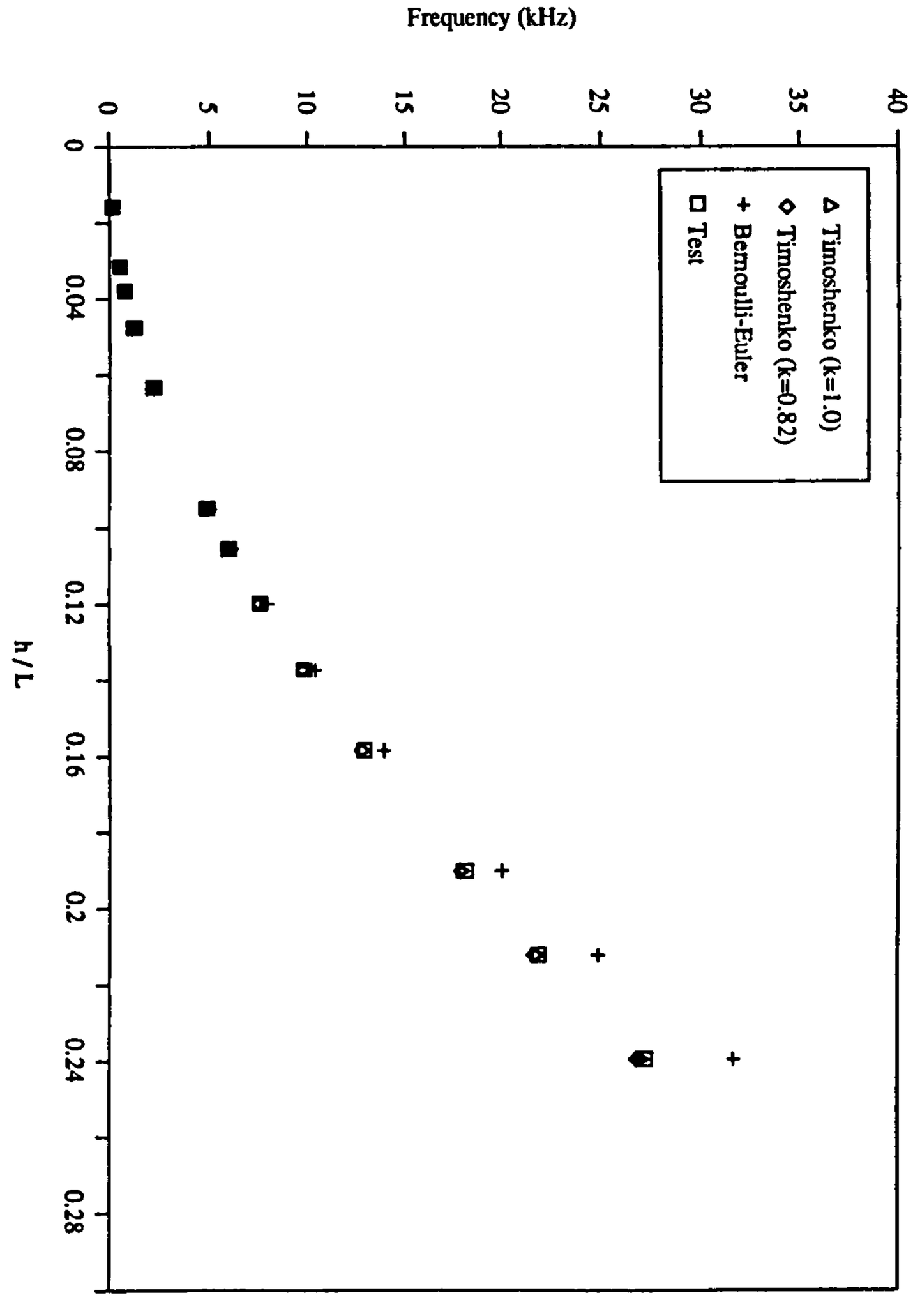

Fig. 3.11 *Fundamental natural frequency Vs Thickness/length*

(Test piece : MS1, square section mild steel beam)

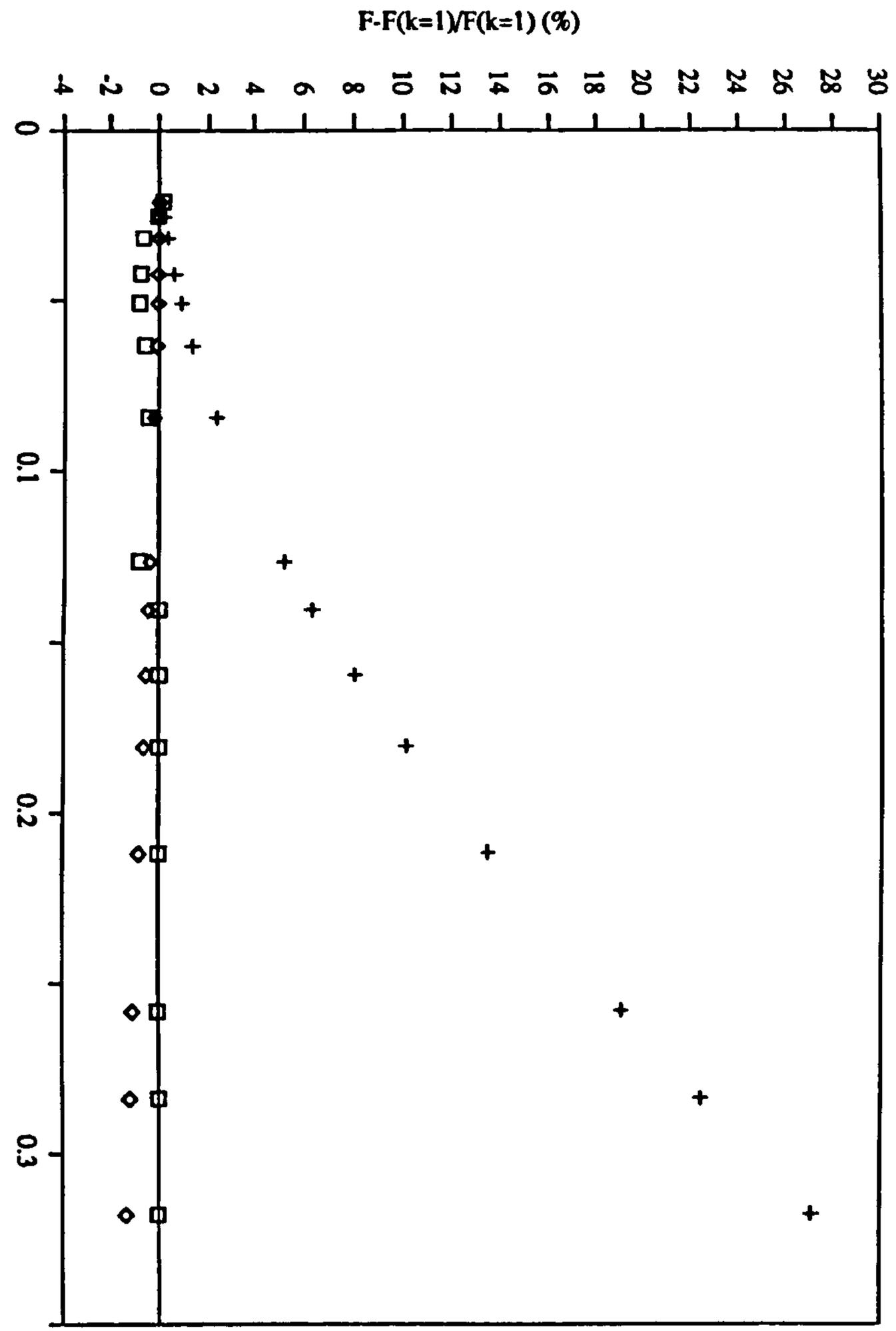

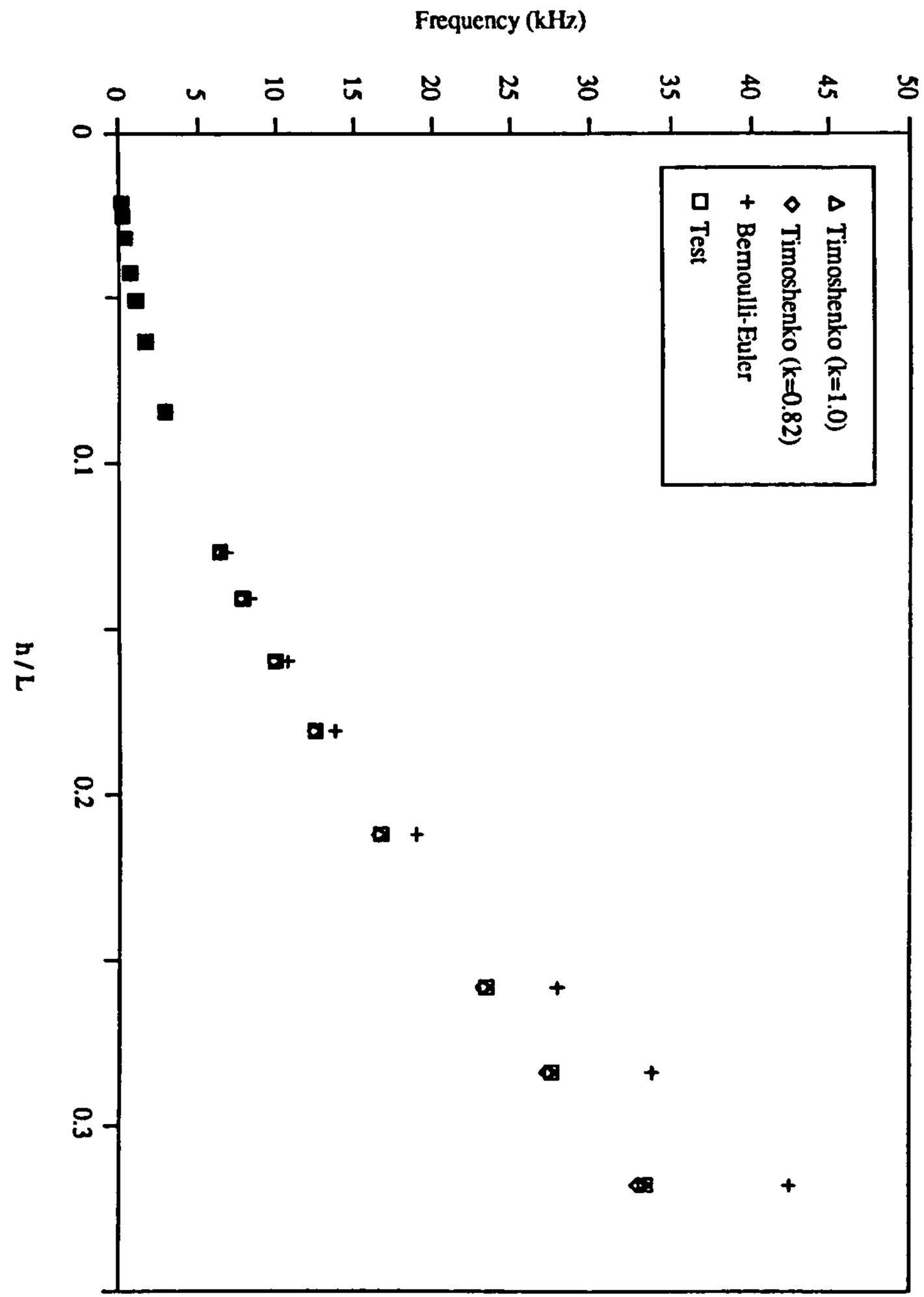

Fig. 3.12 Fundamental natural frequency Vs Thickness/length

(Test piece : MS2, rectangular section mild steel beam)

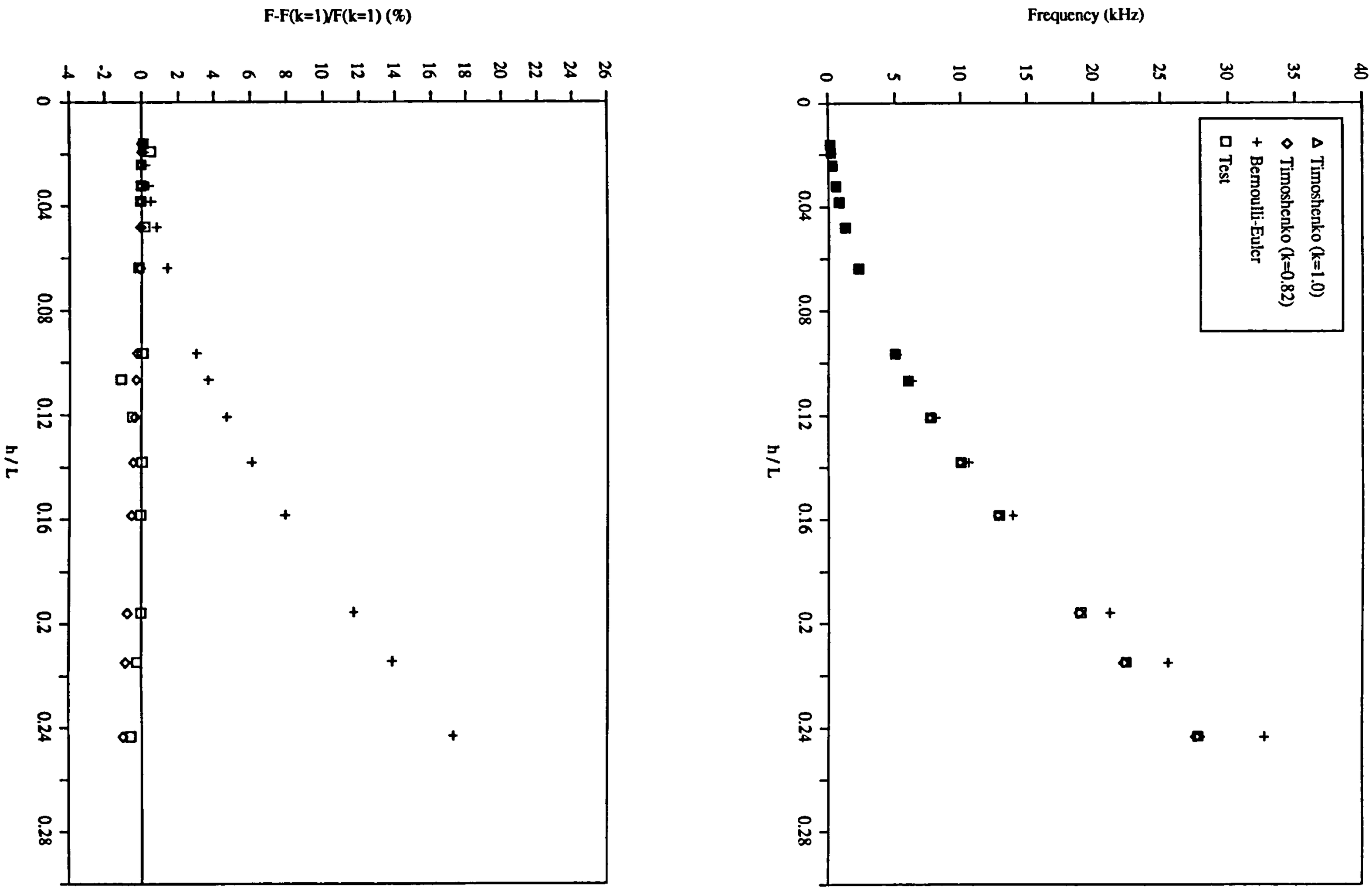

Fig. 3.13 (a) *Frequency Vs Symmetric mode No.*

(Test piece : Centrally-loaded AL2, rectangular section Duralumin beam)

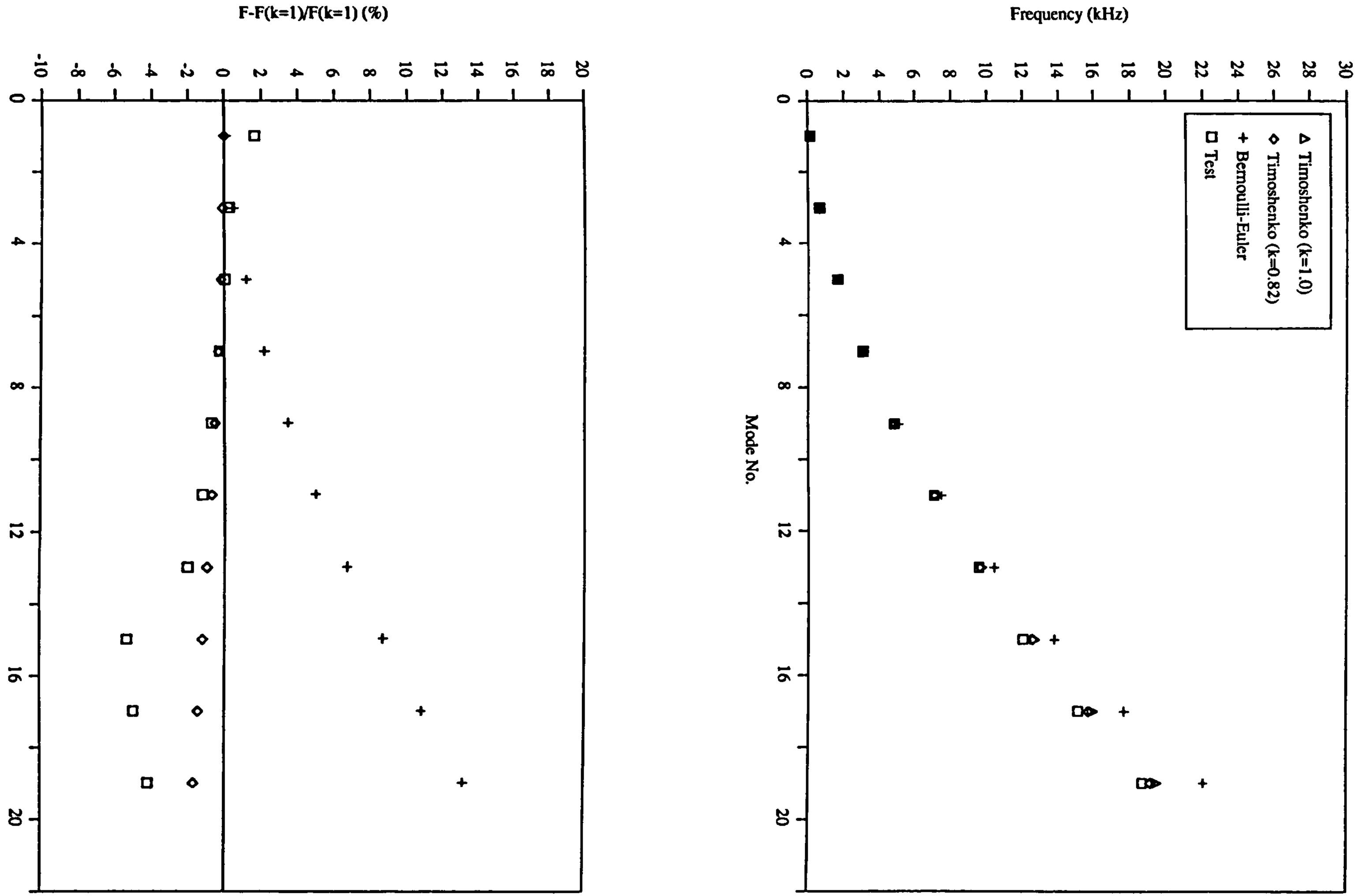

Fig. 3.13 (b) Frequency Vs Anti-symmetric mode No.

(Test piece : Centrally-loaded AL2, rectangular section Duralumin beam)

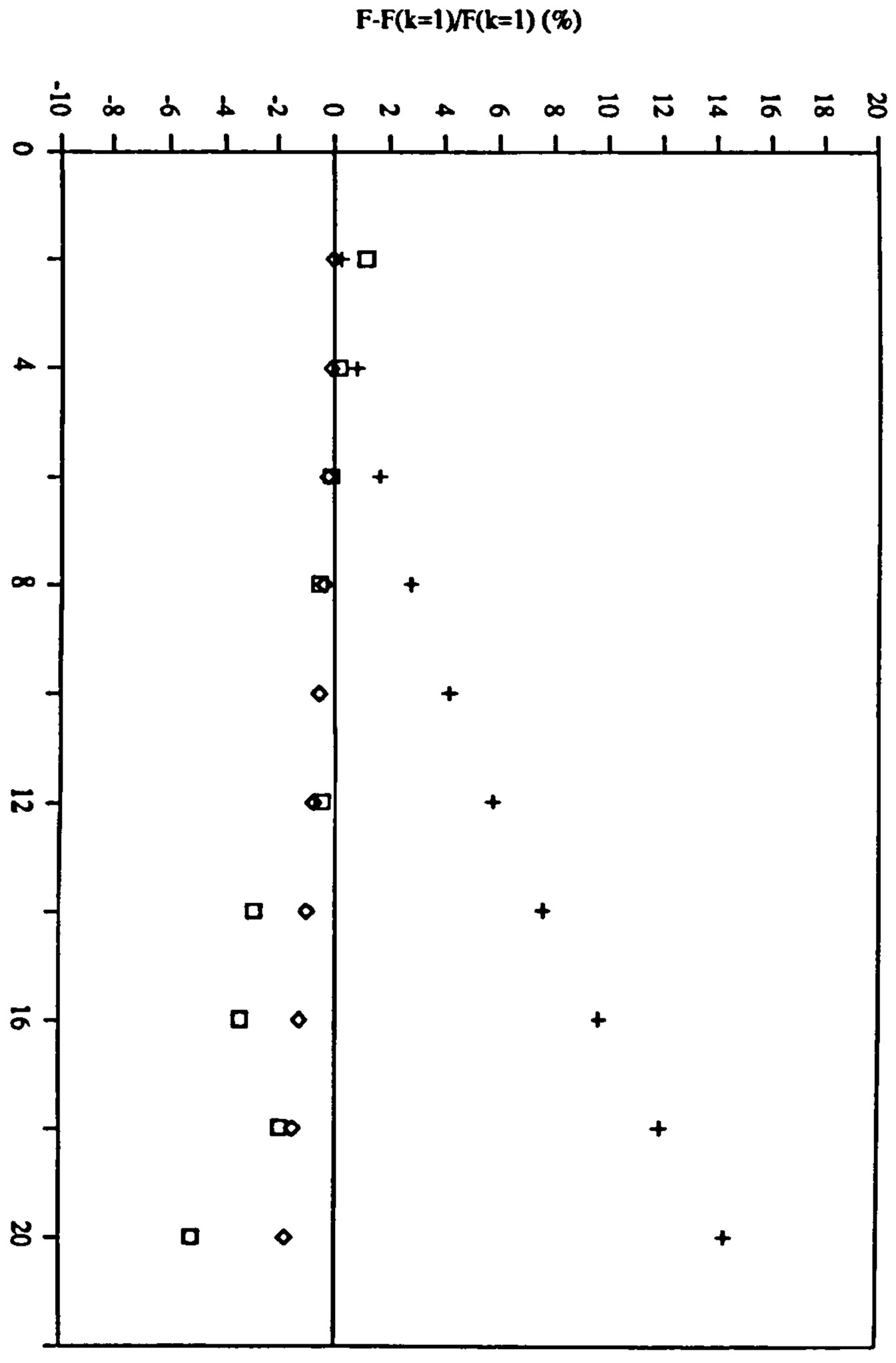

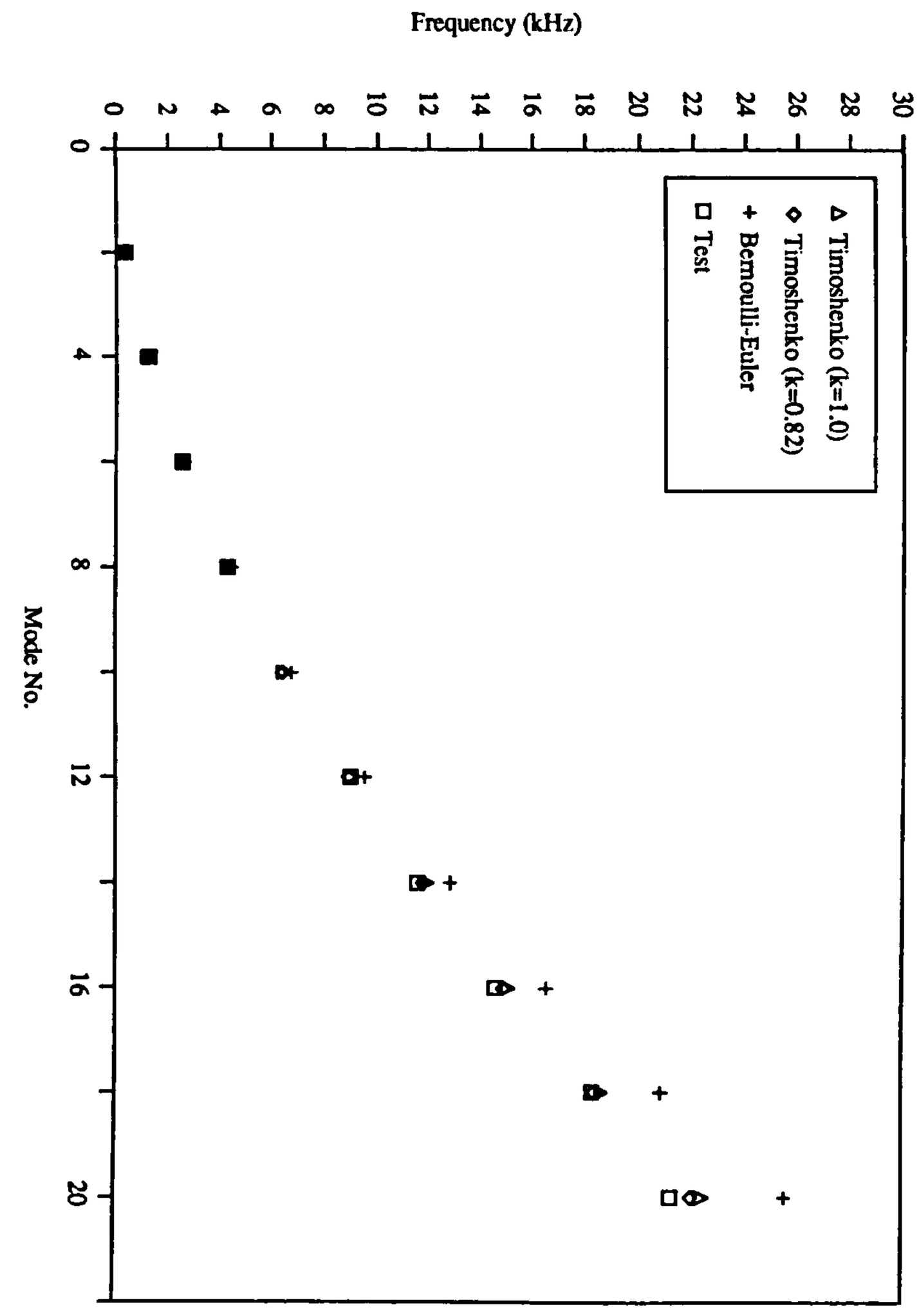

Fig. 3.14 Frequency Vs Mode No.

(Test piece : End-loaded AL2, rectangular section Duralumin beam)

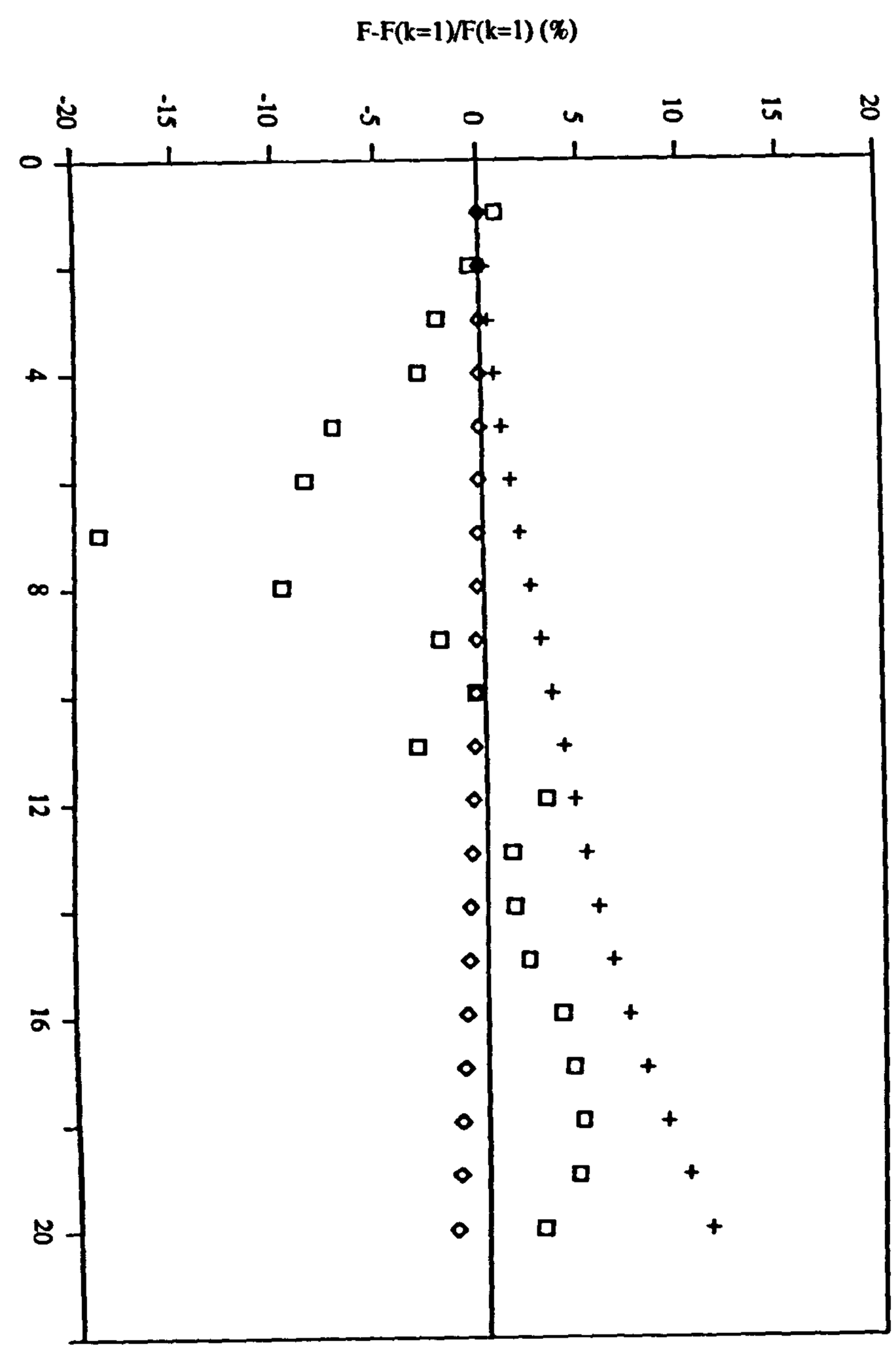

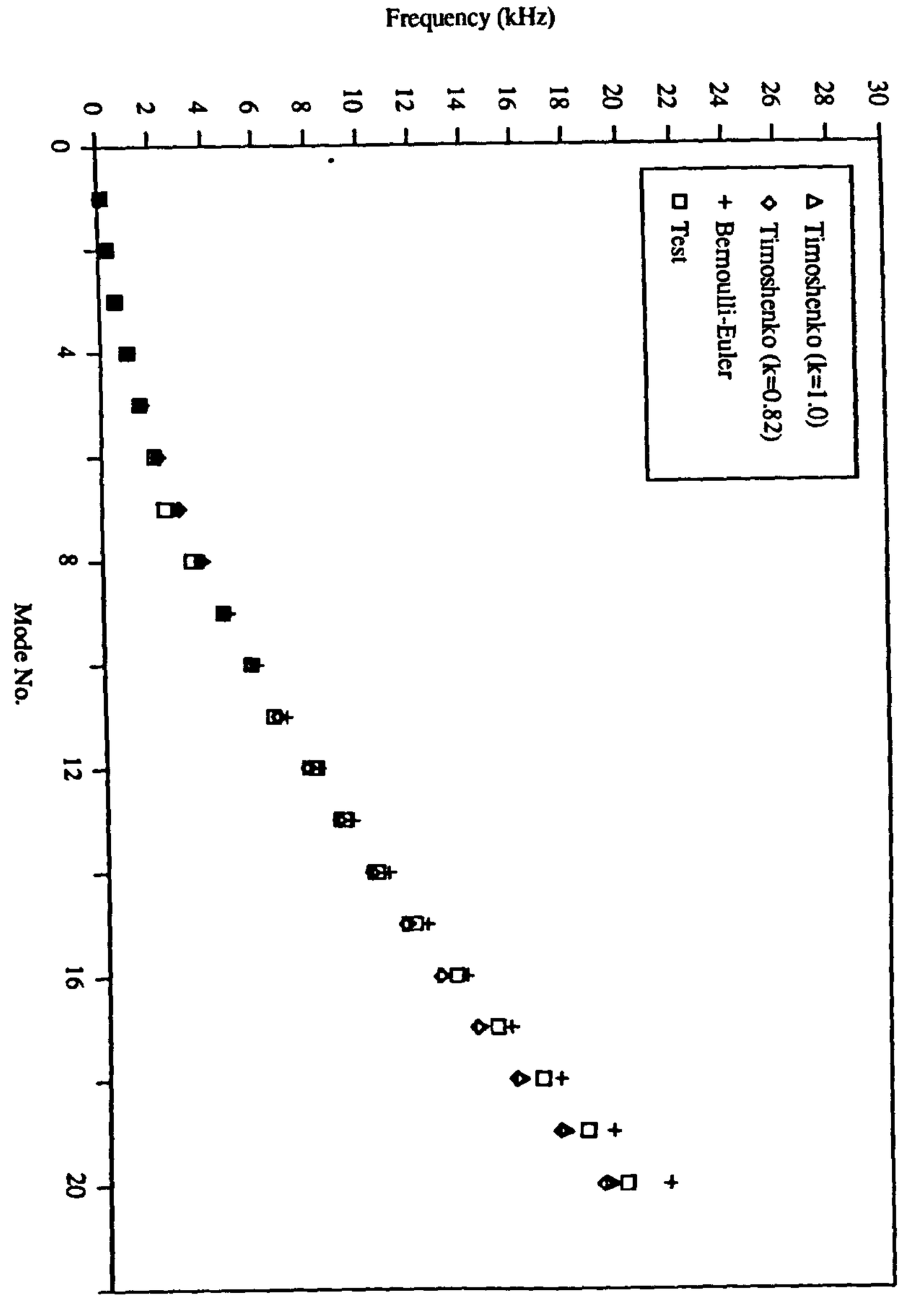

Fig. 3.15 Frequency Vs Mode No.

(Test piece : 2SB1-X, 0.5 in. thick M-Board sandwich beam)

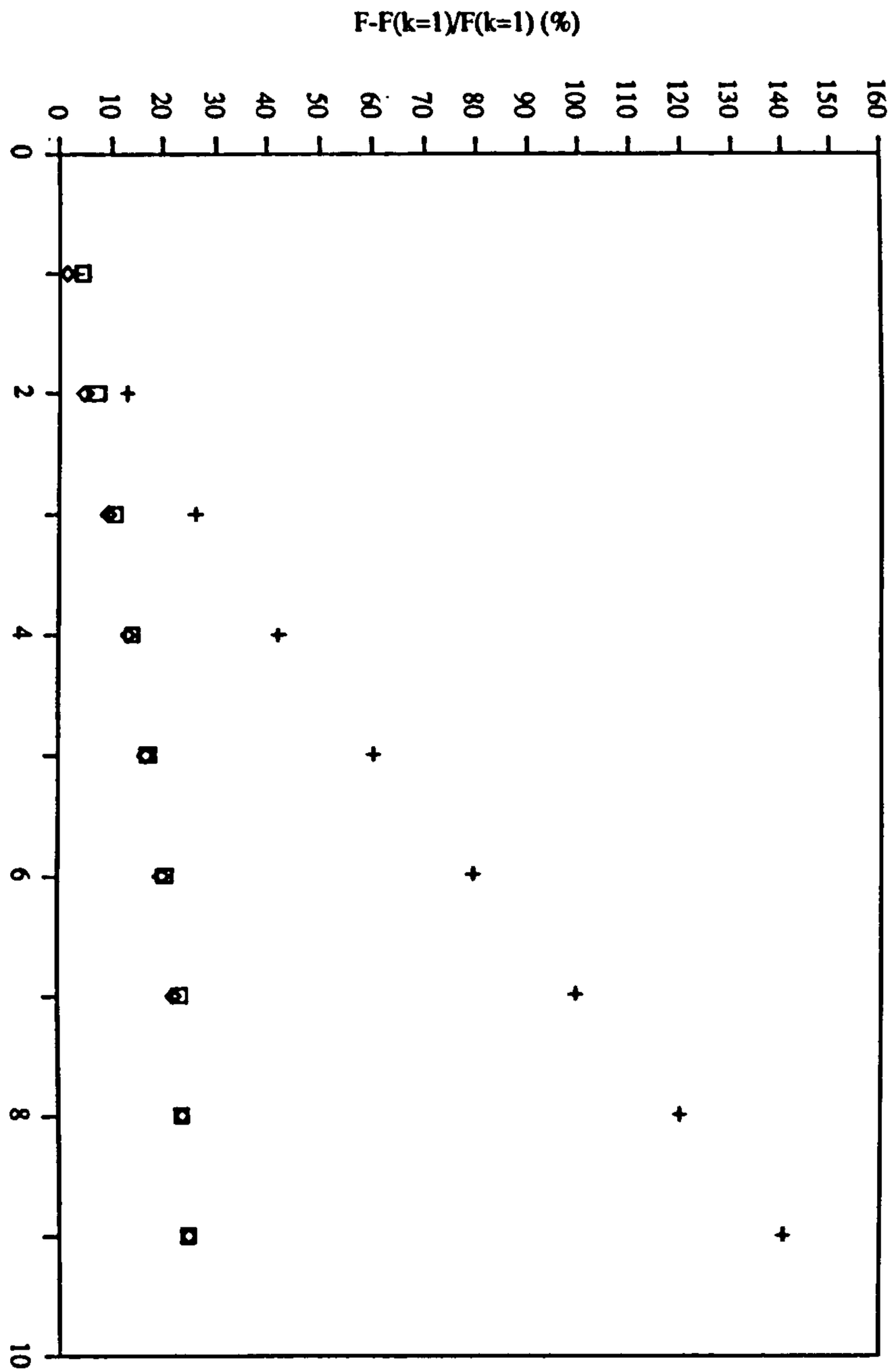

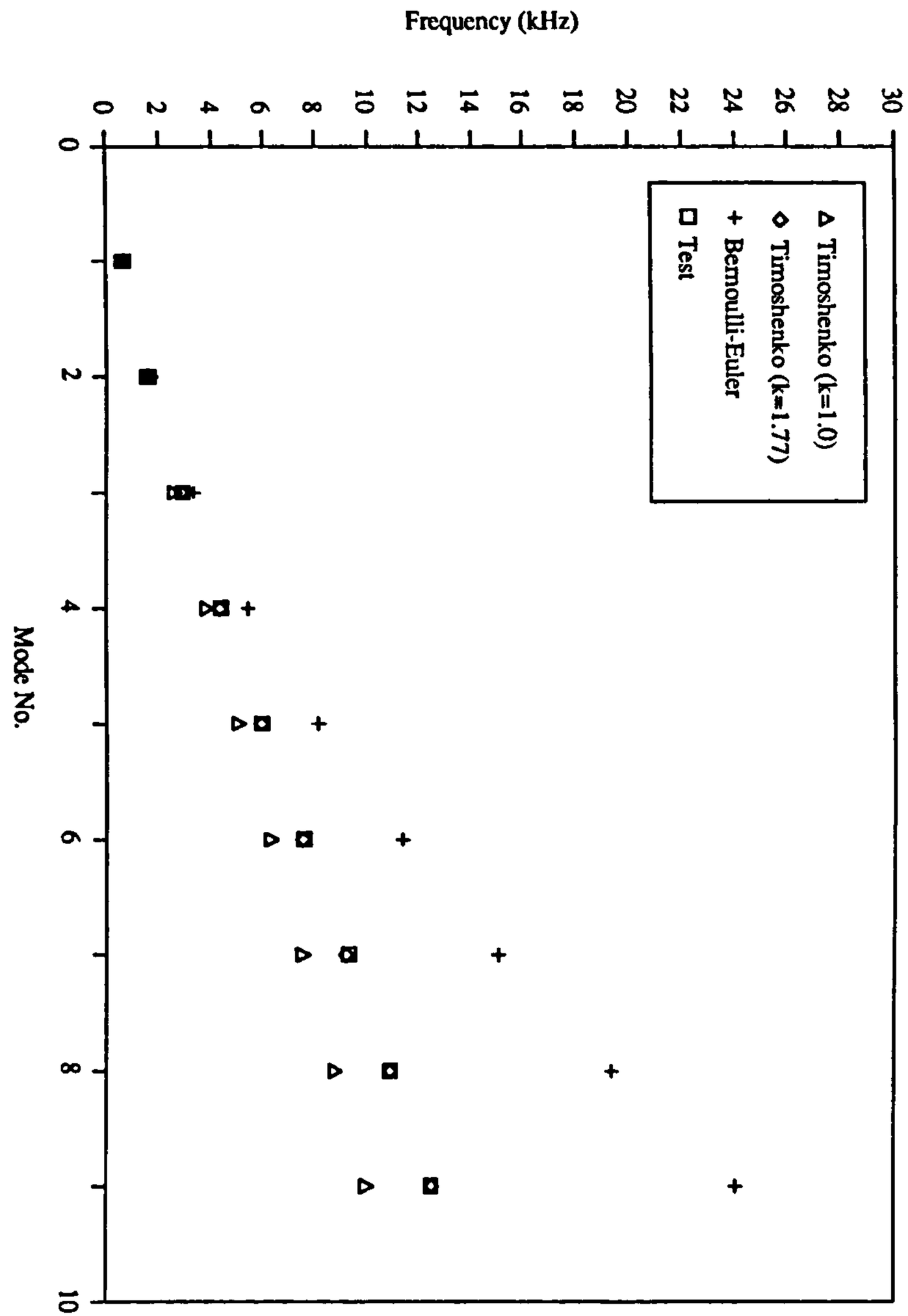

Fig. 3.16 *Frequency Vs Mode No.*

(Test piece : Centrally-loaded 2SB1-X, 0.5 in. thick M-Board sandwich beam)

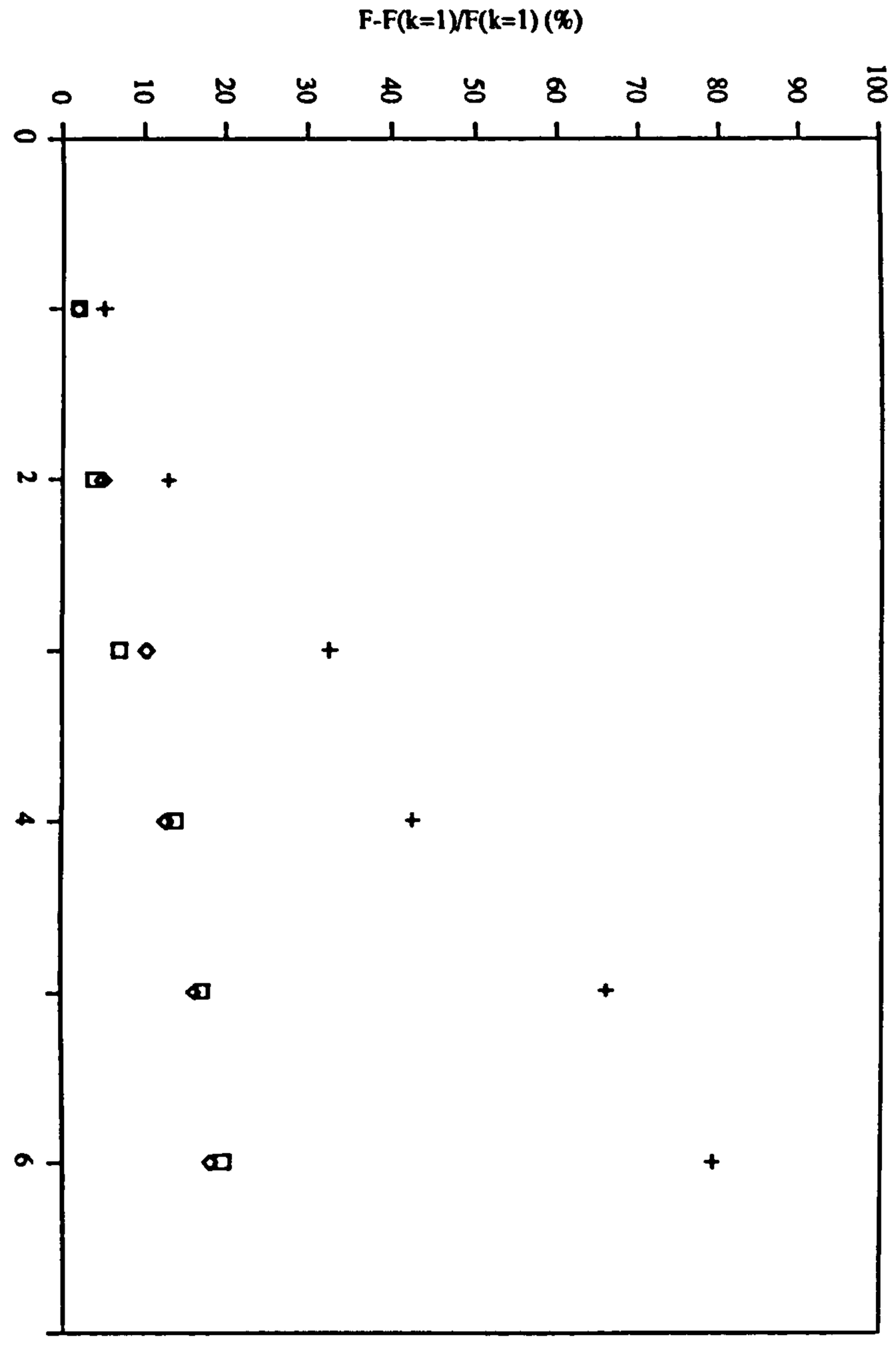

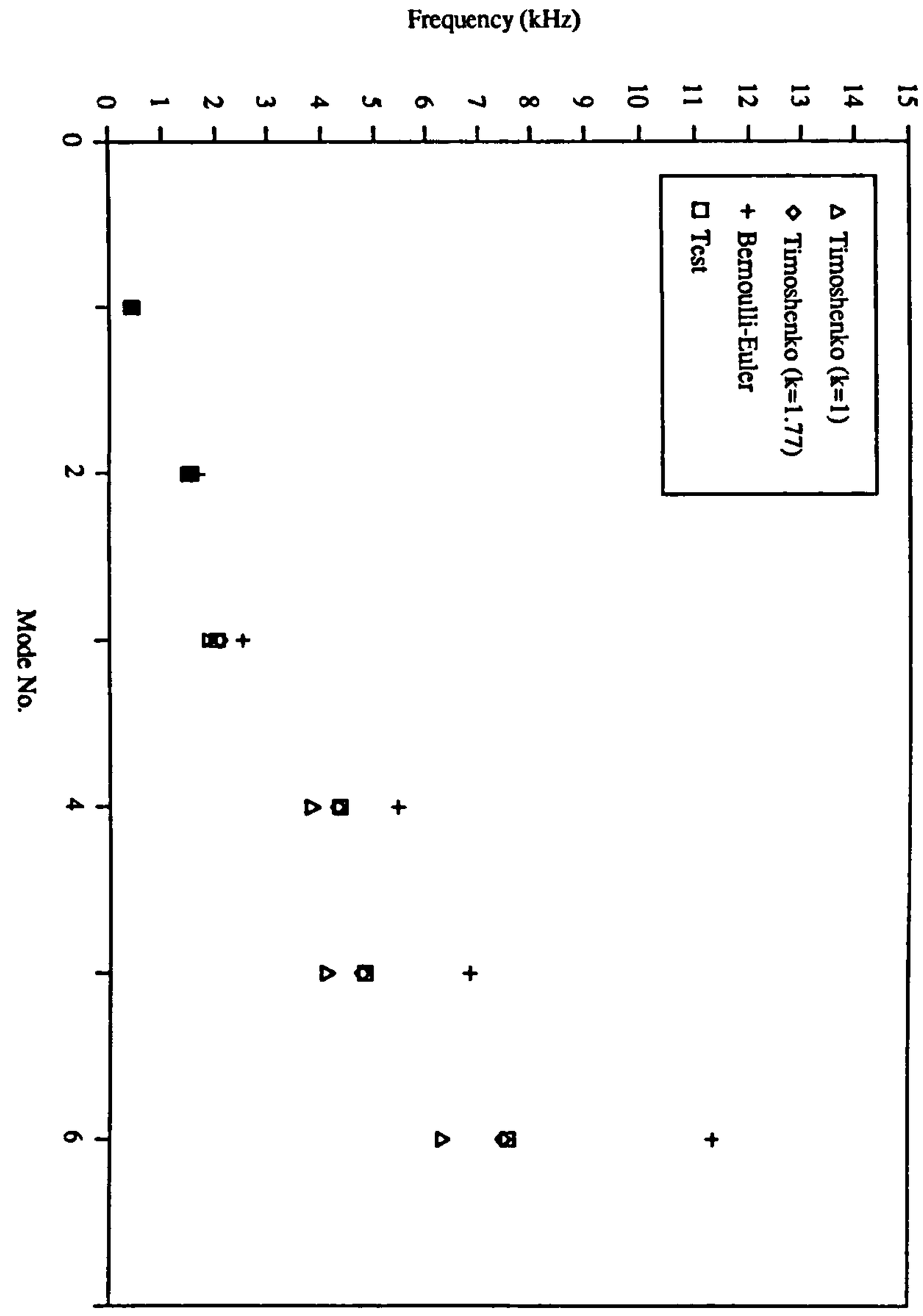

Fig. 3.17 Frequency Vs Mode No.

(Test piece : 2SB2-X, 1 in. thick M-Board sandwich beam)

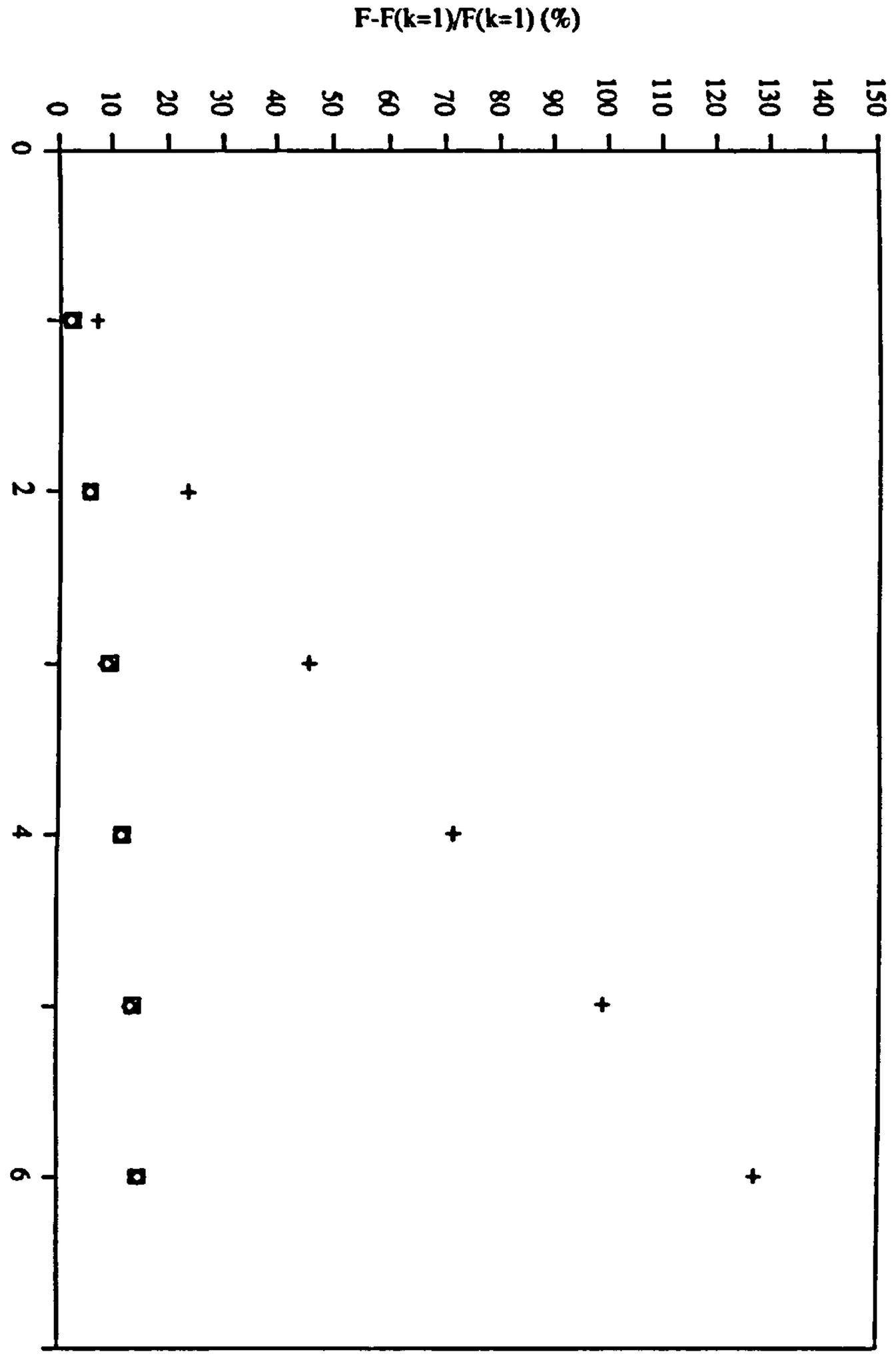

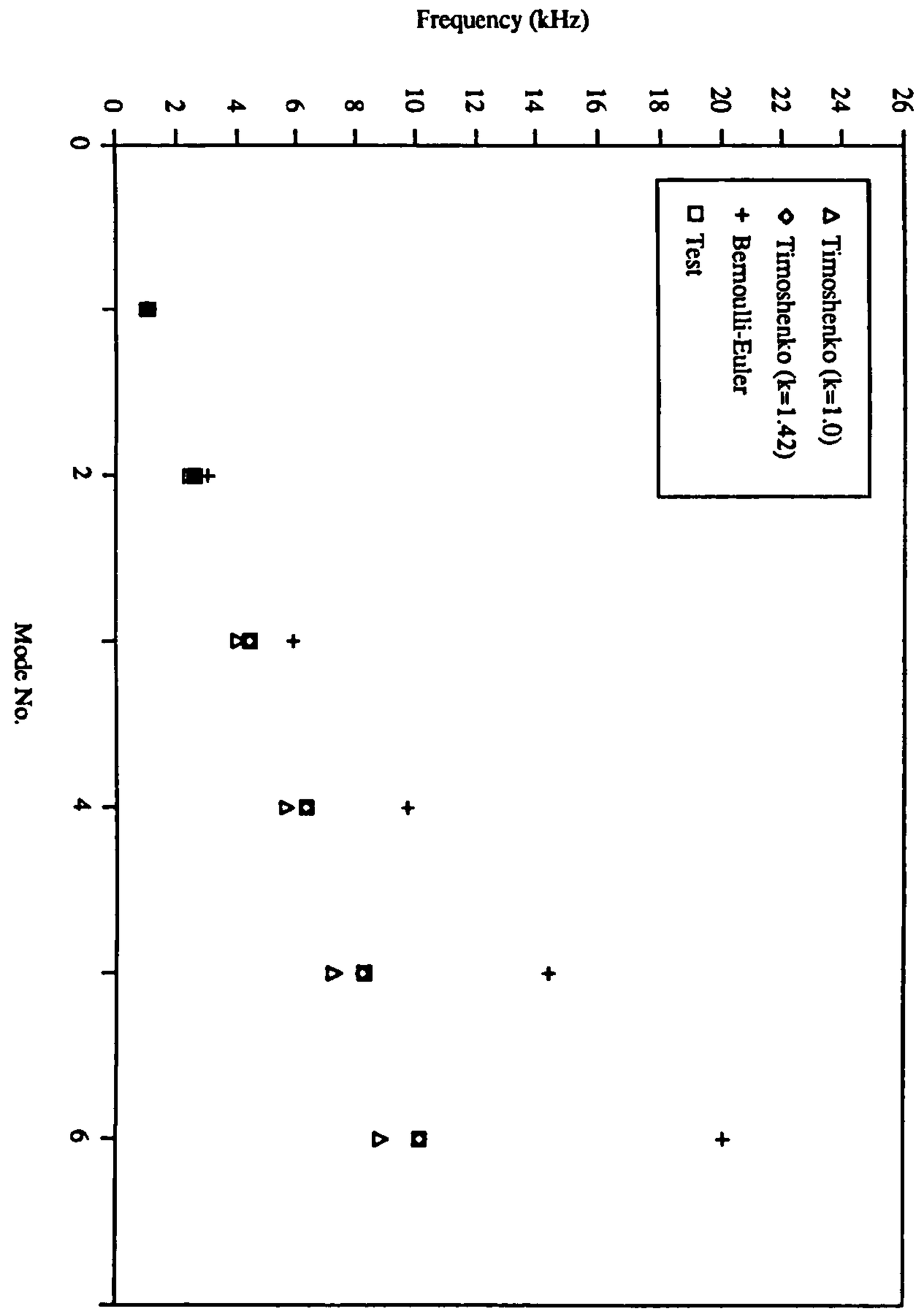

Fig. 3.18 Frequency Vs Mode No.

(Test piece : 2SB3-X, 1.33 in. thick M-Board sandwich beam)

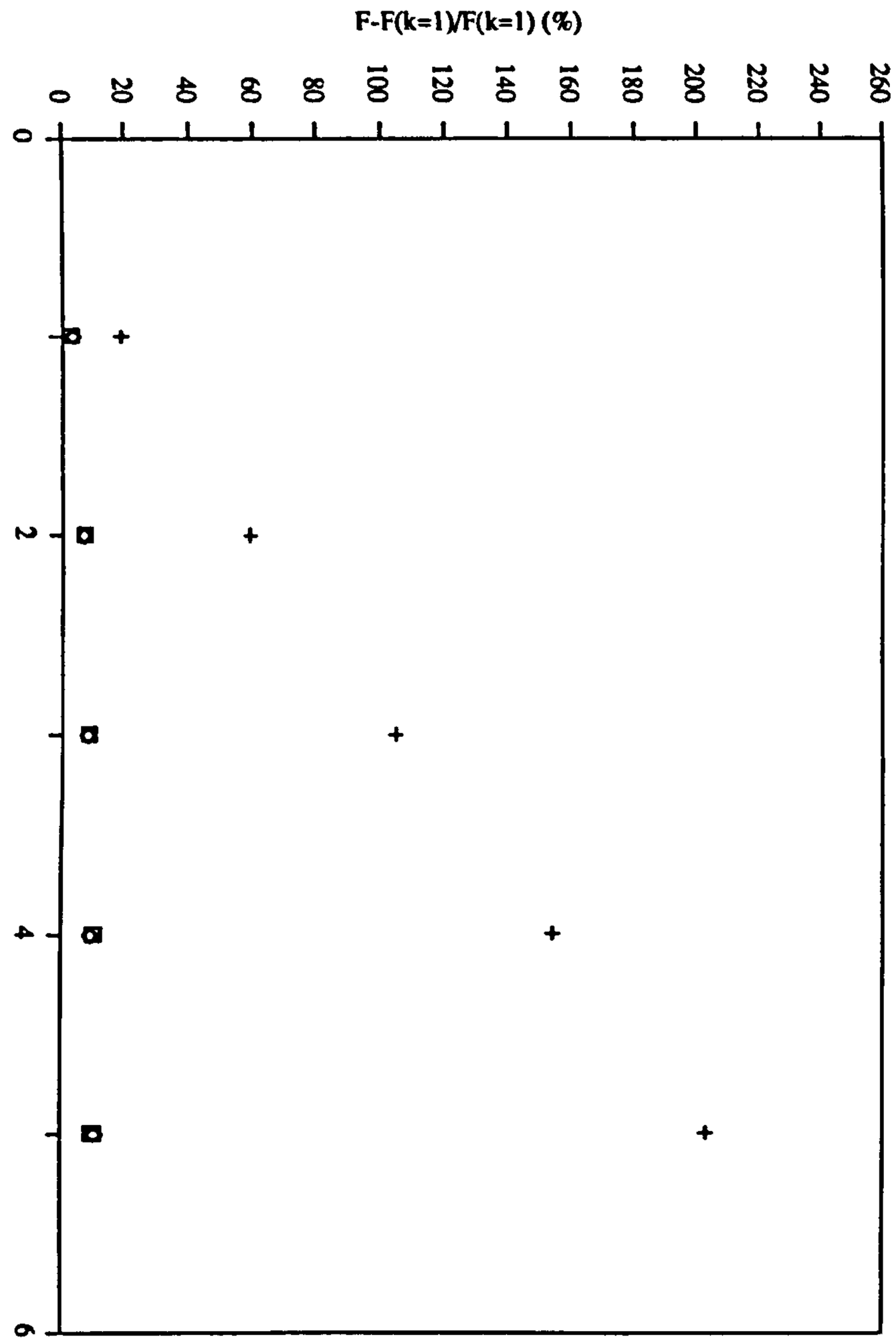

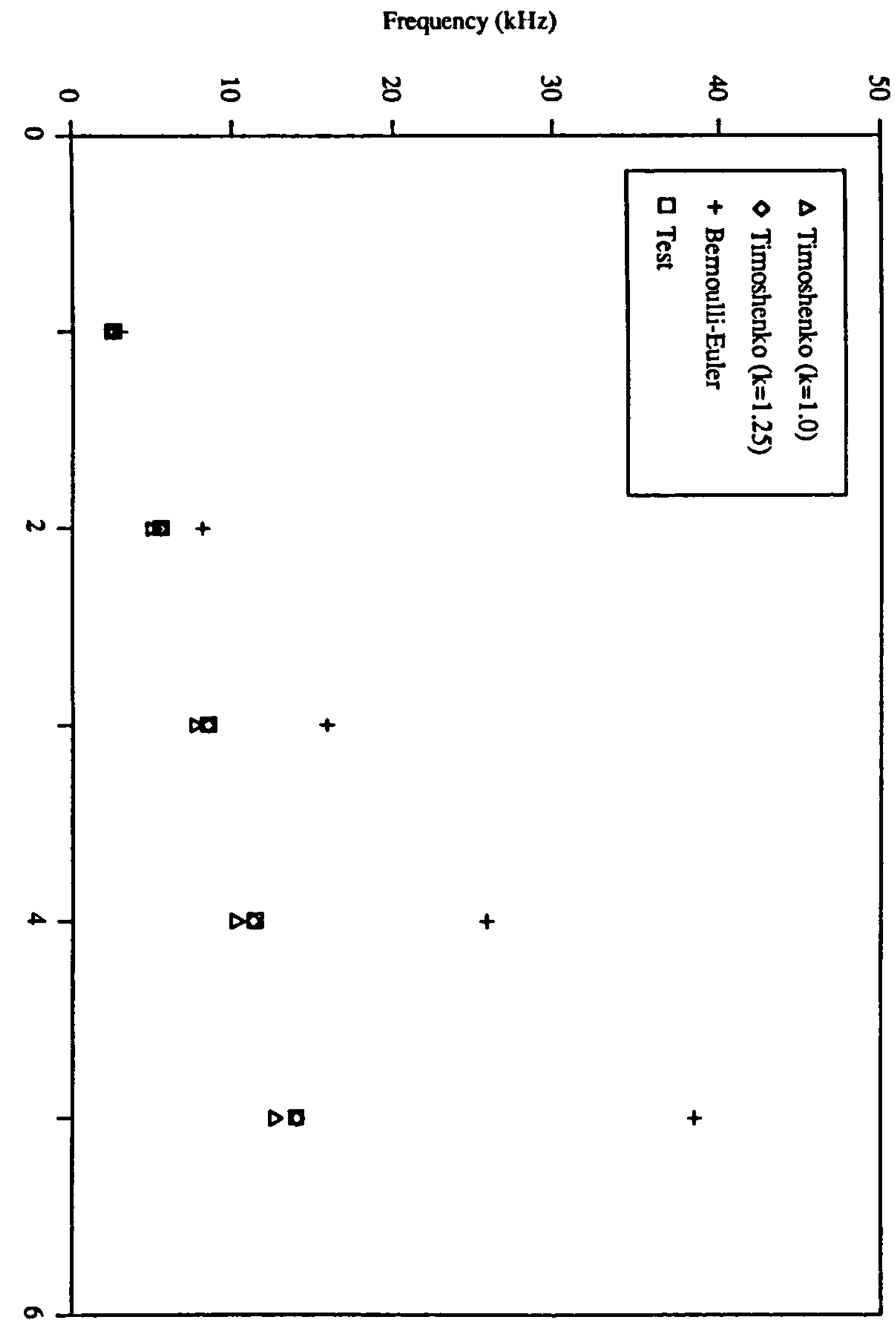

Fig. 3.19 Frequency Vs Mode No.

(Test piece : 2SB4-X, 2 in. thick M-Board sandwich beam)

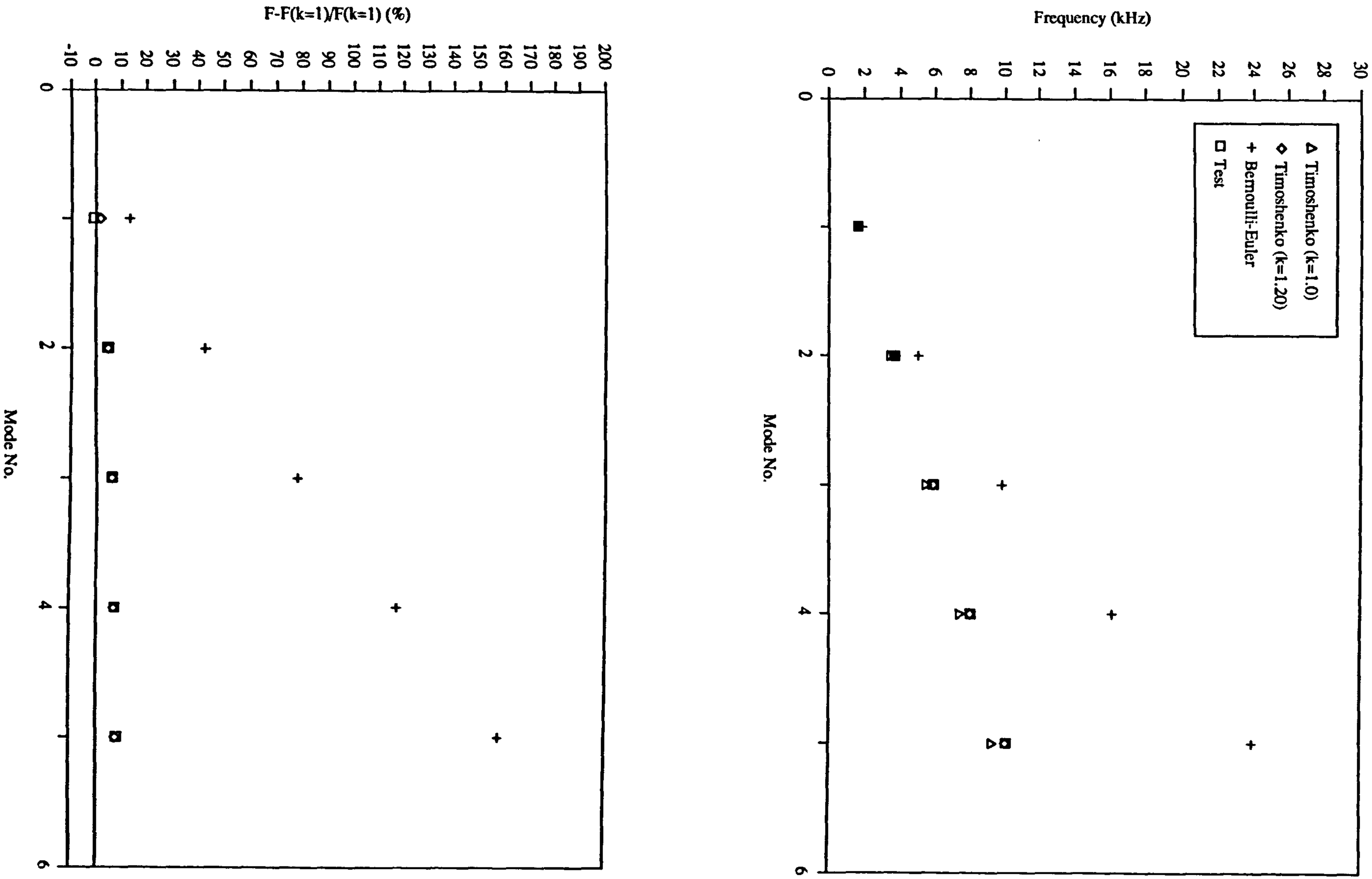

Fig. 3.20 Optimum shear factor Vs Skin/core thickness

(Test piece : 2SB1X to 2SB4X sandwich beams)

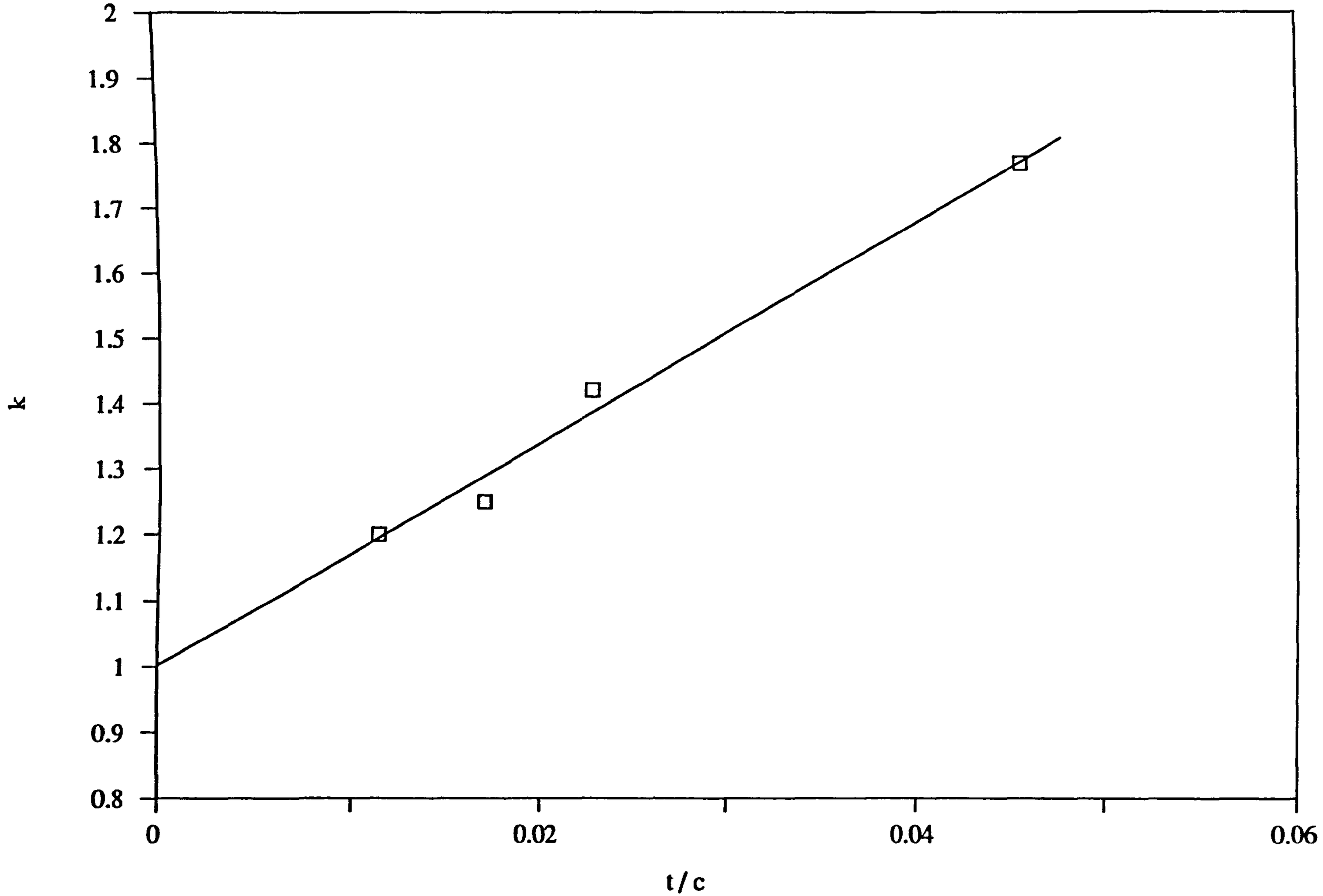

Fig. 3.21 Mode shape of 2SB1-X

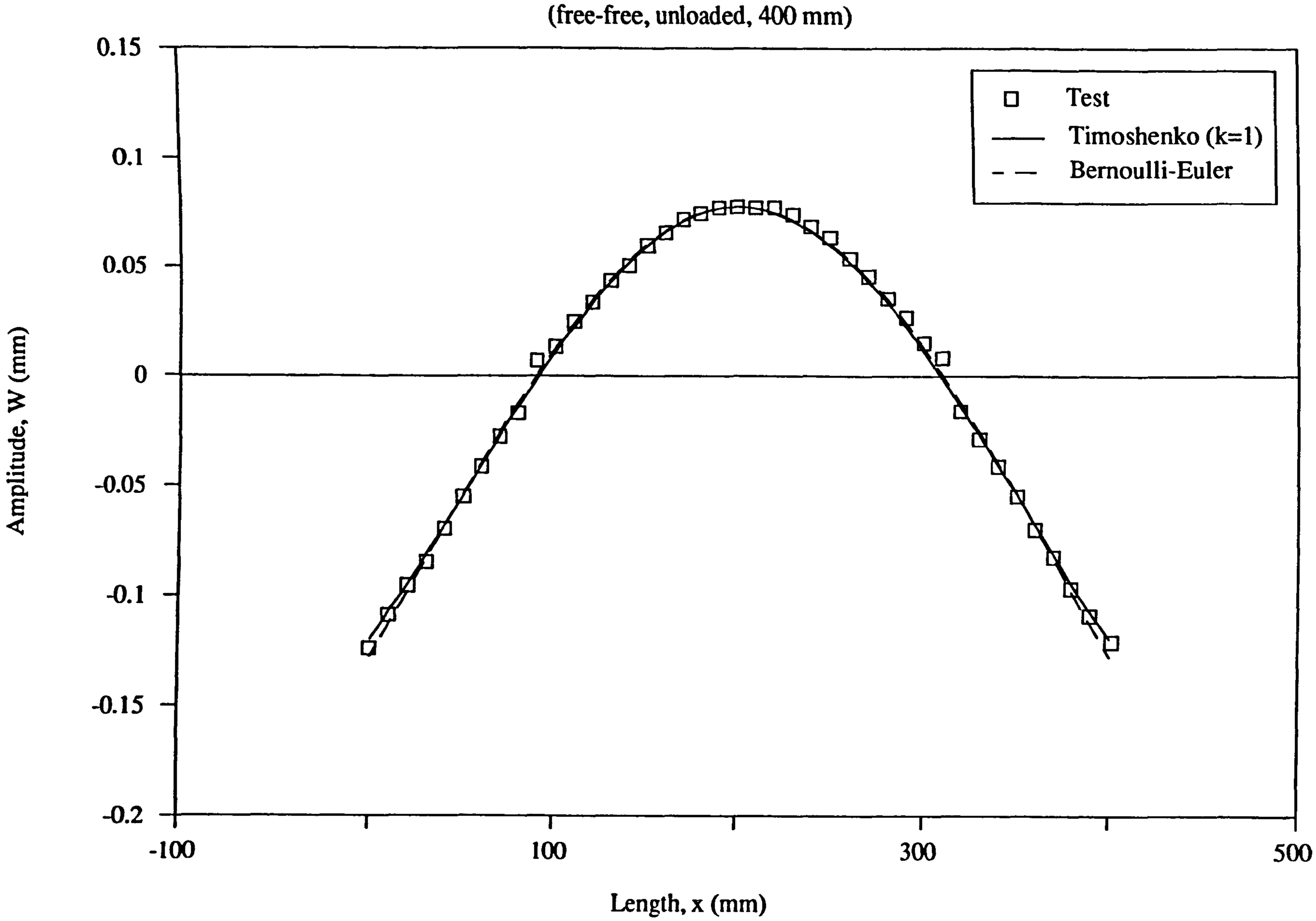

Fig. 3.22 Mode shape of 2SB1-X

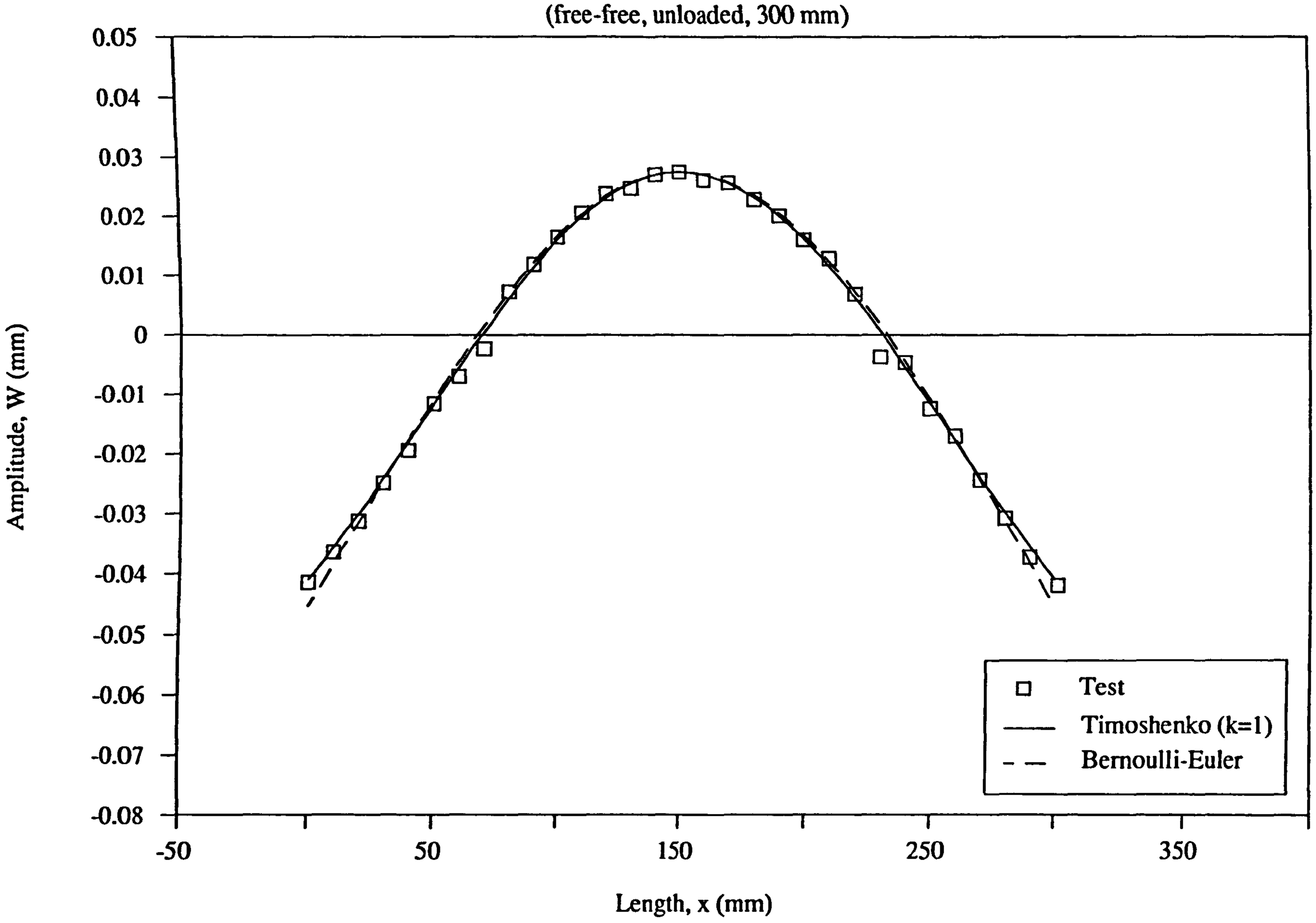

Fig. 3.23 Mode shape of 2SB1-X

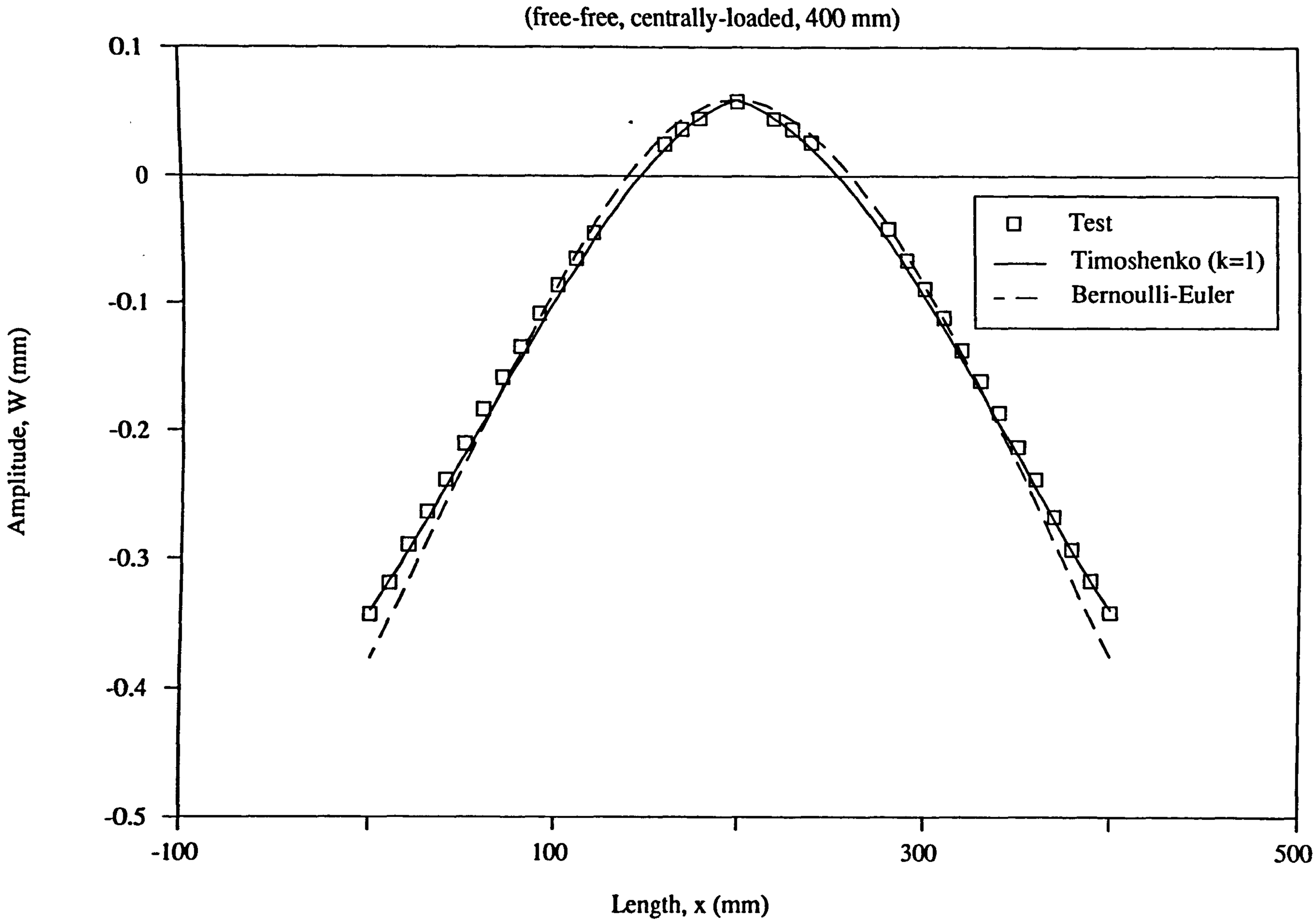

Fig. 3.24 *Mode shape of 2SB1-X*

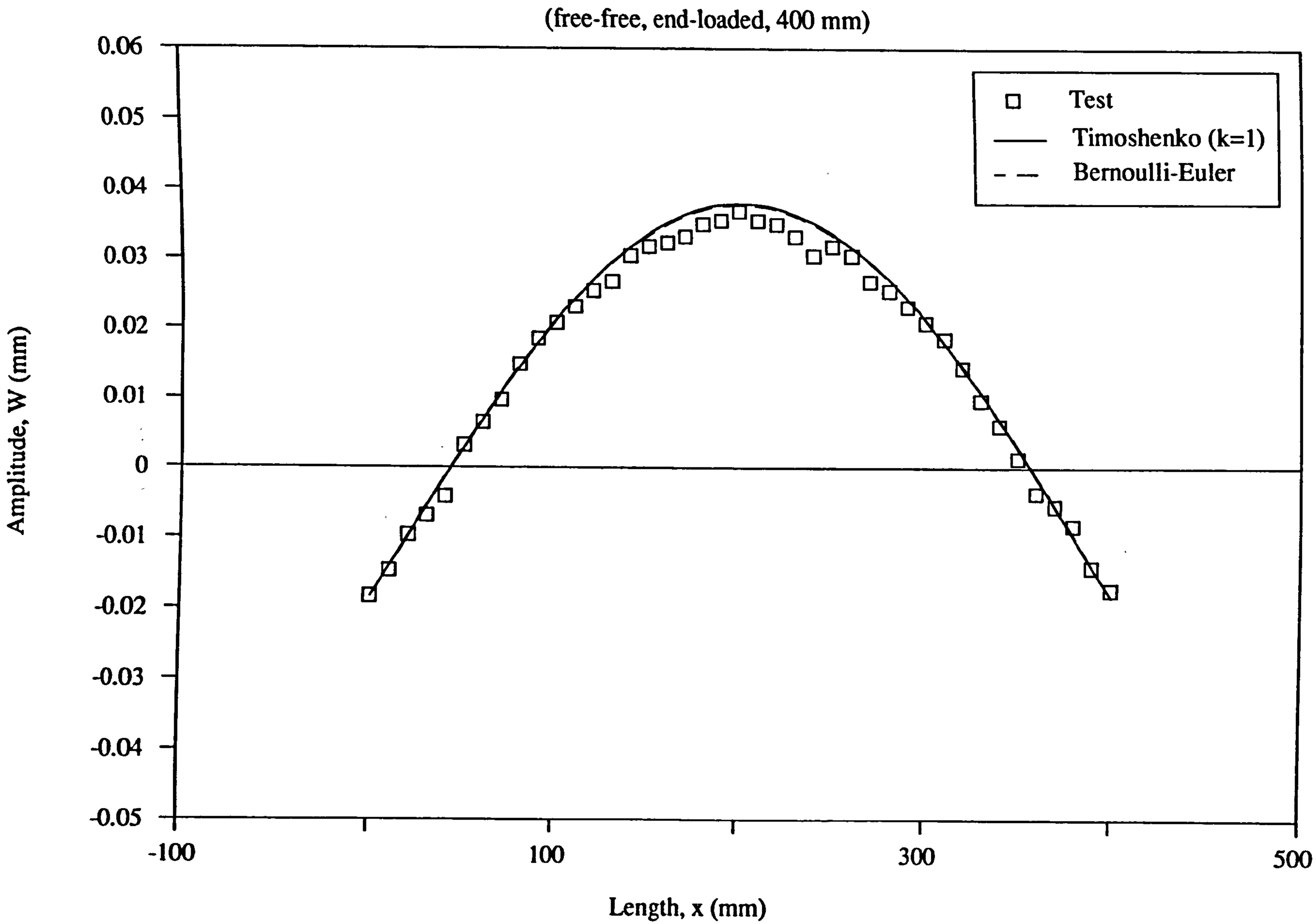

Fig. 3.25 *Mode shape of 2SB1-X*

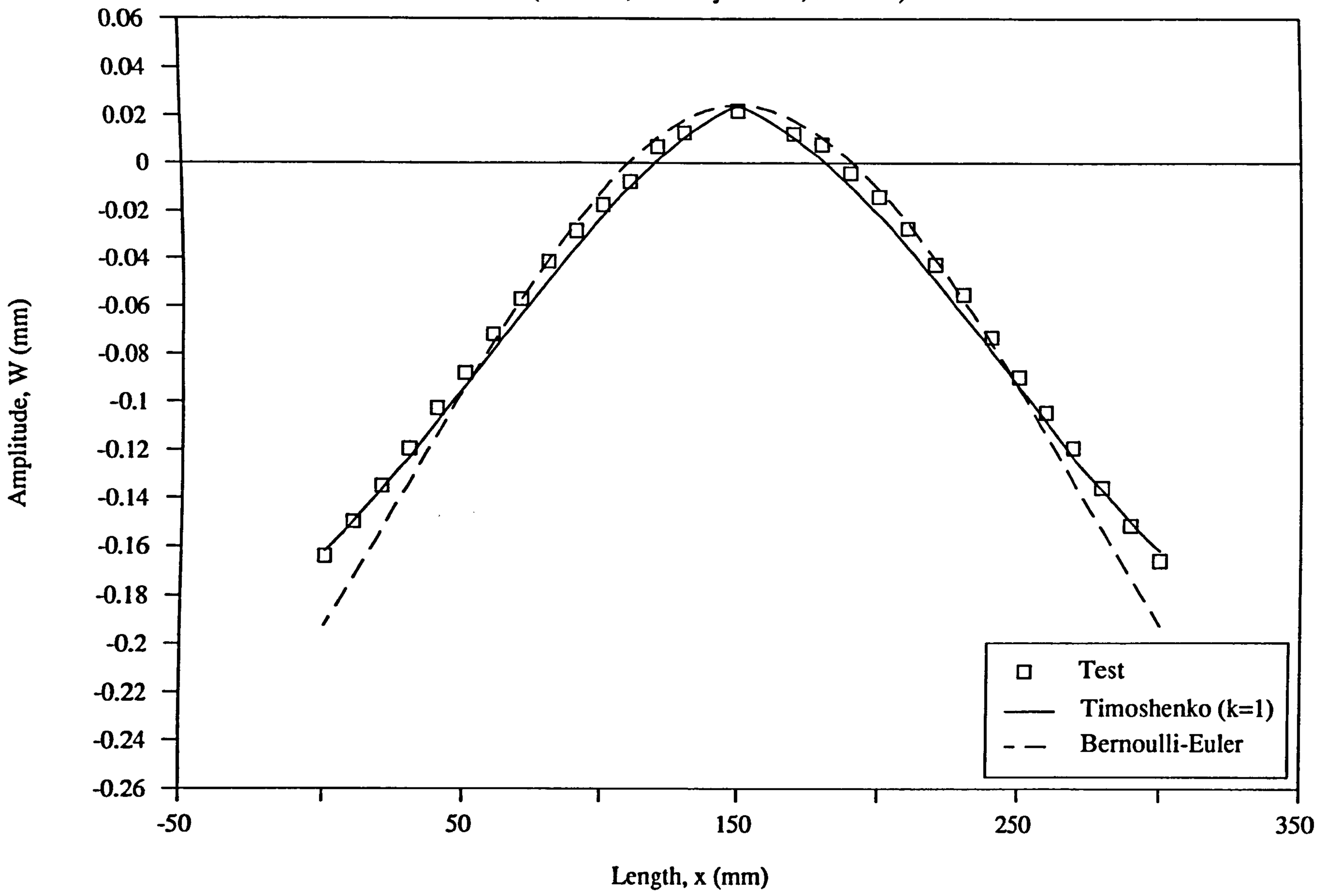

Fig. 3.26 Mode shape of 2SB1-X

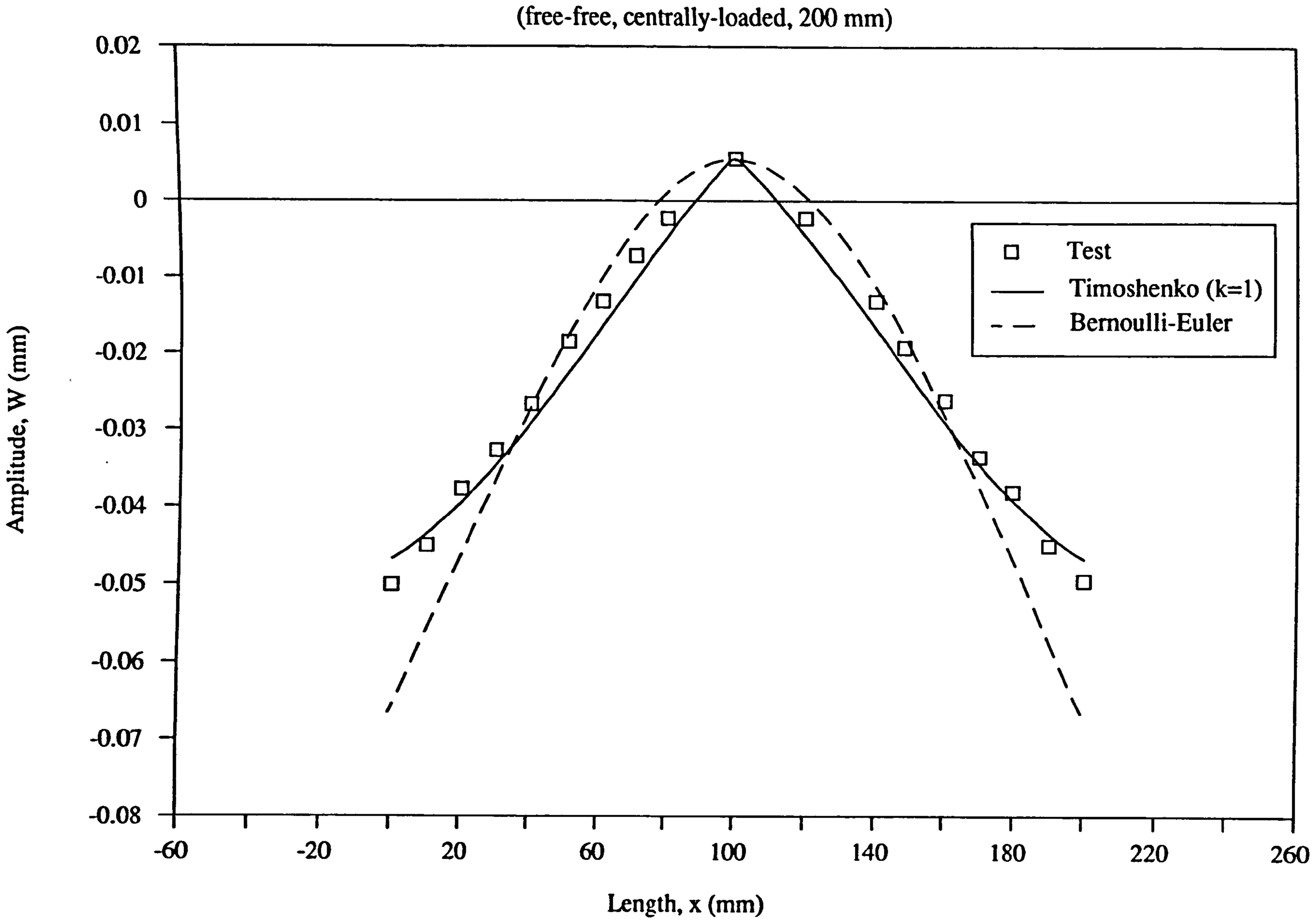

Fig. 4.8 *Honeycomb edge effect : Shear properties Vs Normalised shear area*

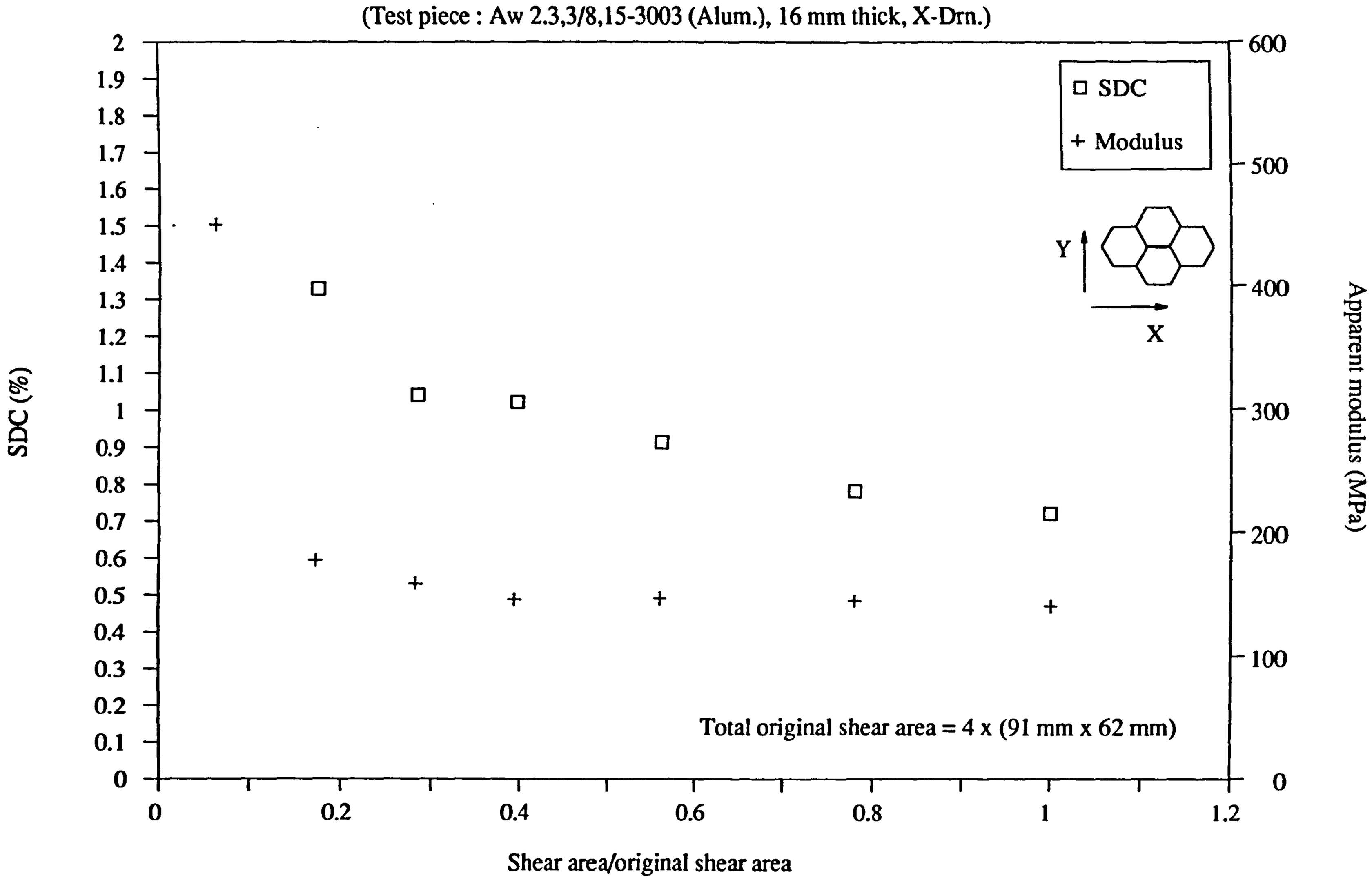

Fig. 4.9 *Honeycomb shear : SDC Vs Stress amplitude*

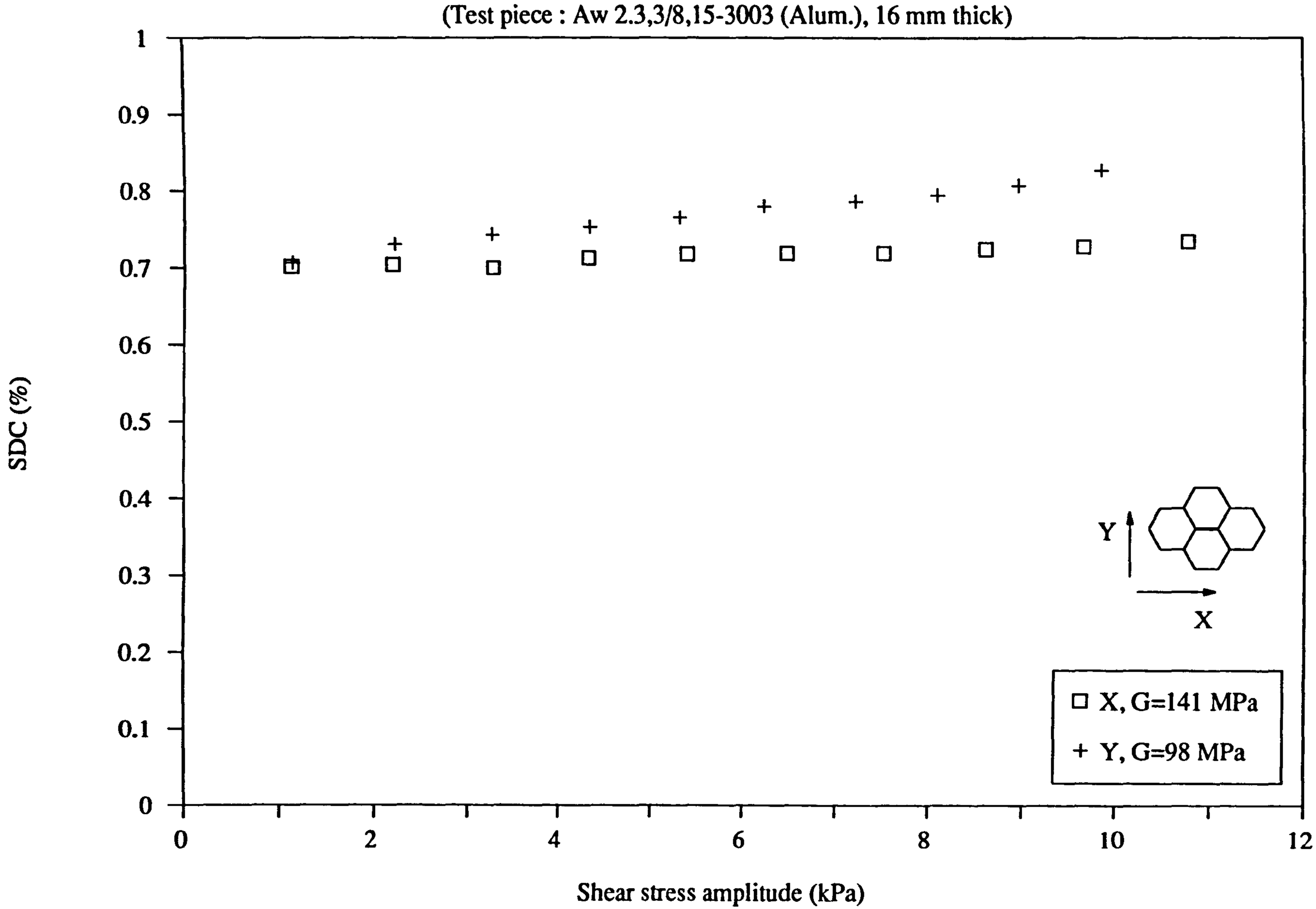

Fig. 4.10 *Honeycomb shear : SDC Vs Stress amplitude*

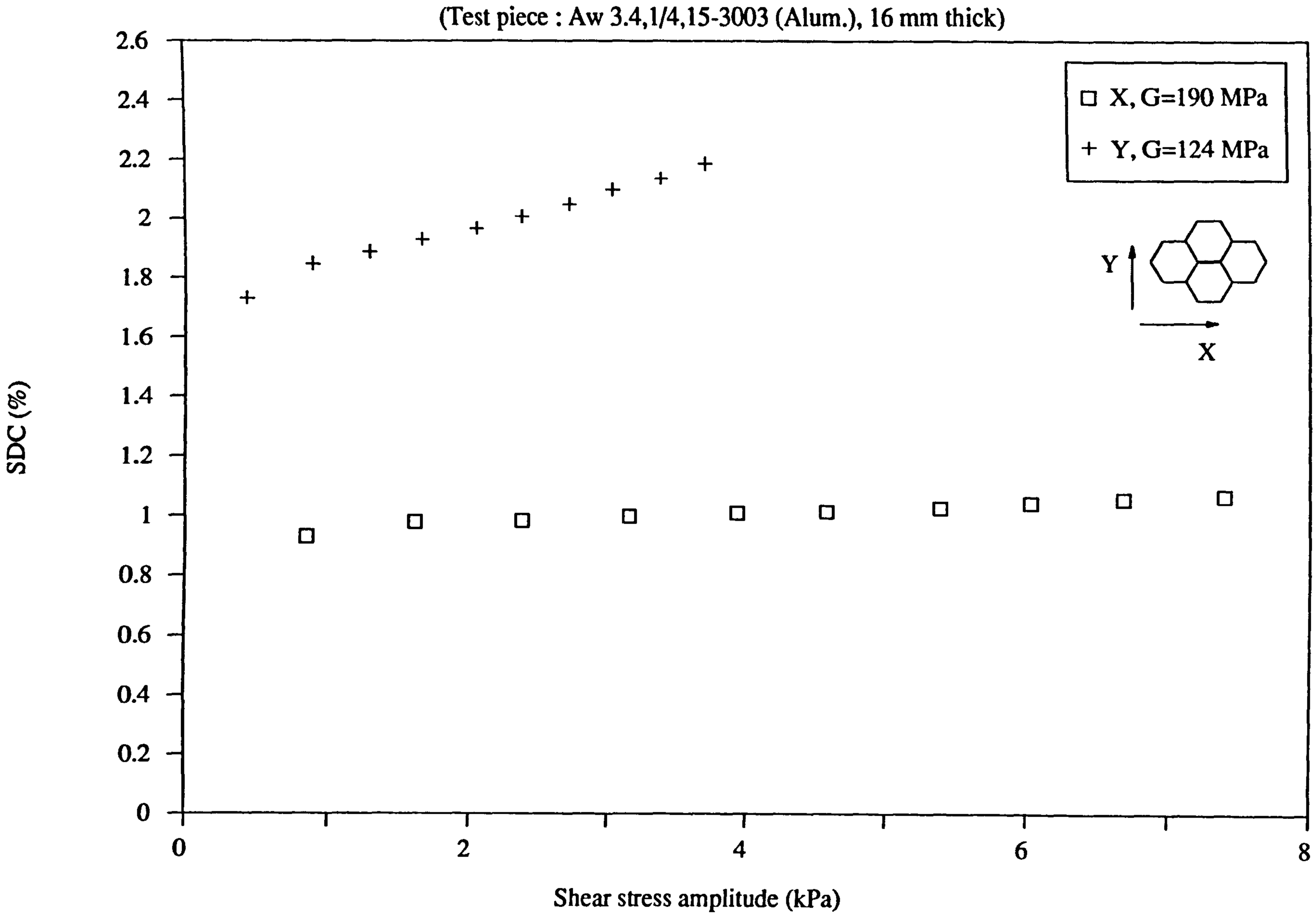

Fig. 4.11 *Honeycomb shear : SDC Vs Stress amplitude*

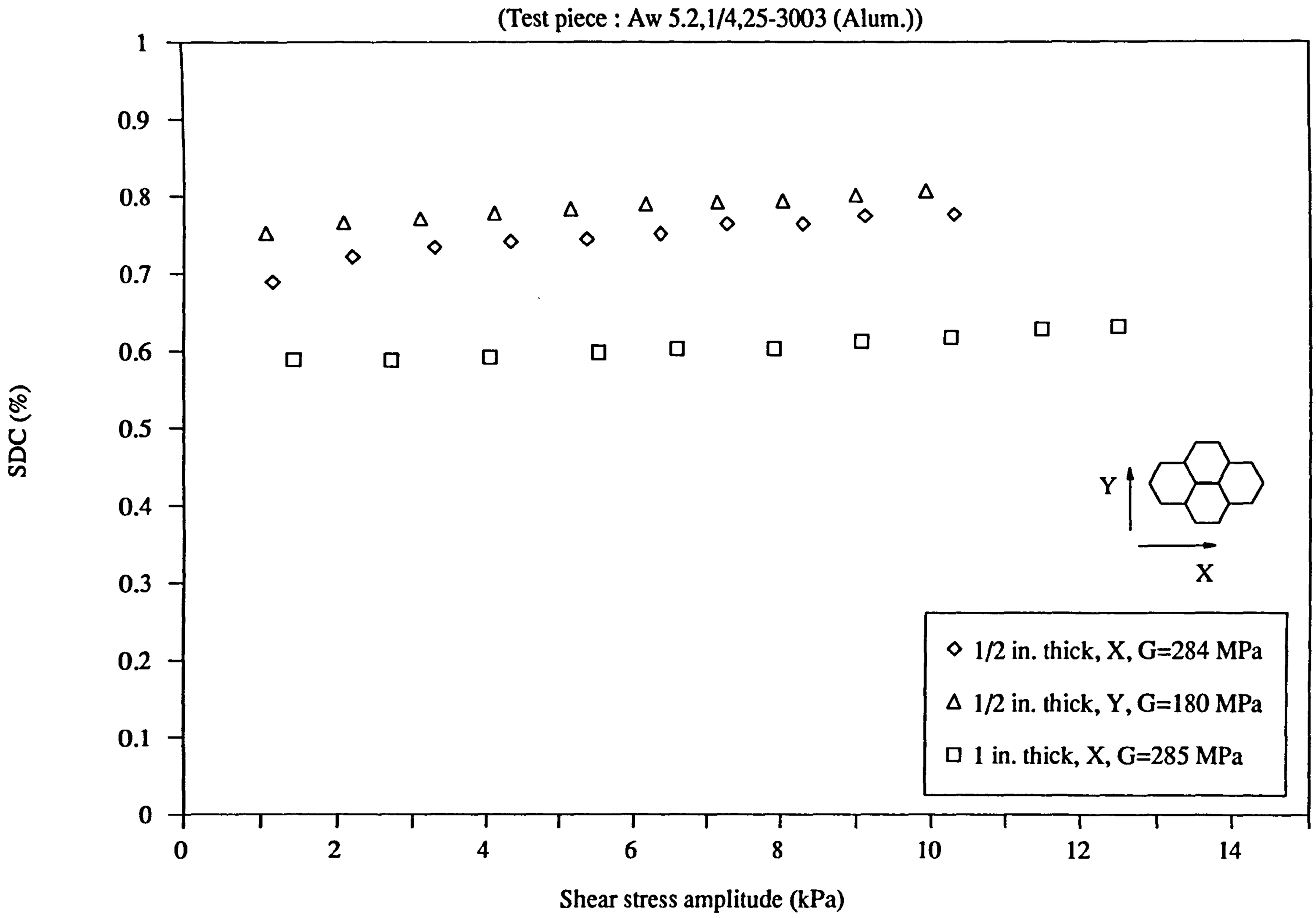

Fig. 4.12 Honeycomb shear : SDC Vs Stress amplitude

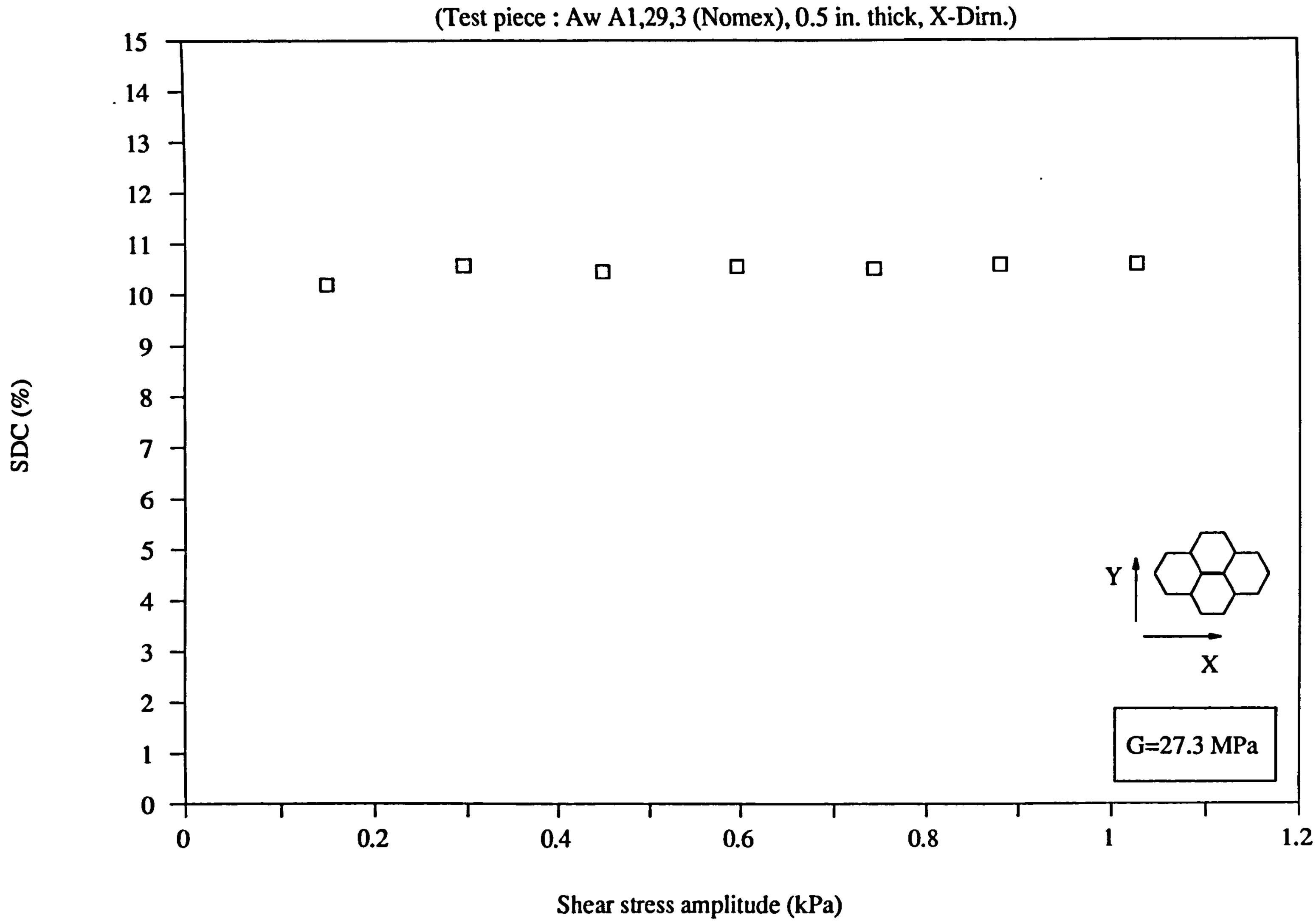

Fig. 4.13 *Honeycomb shear : SDC Vs Stress amplitude*

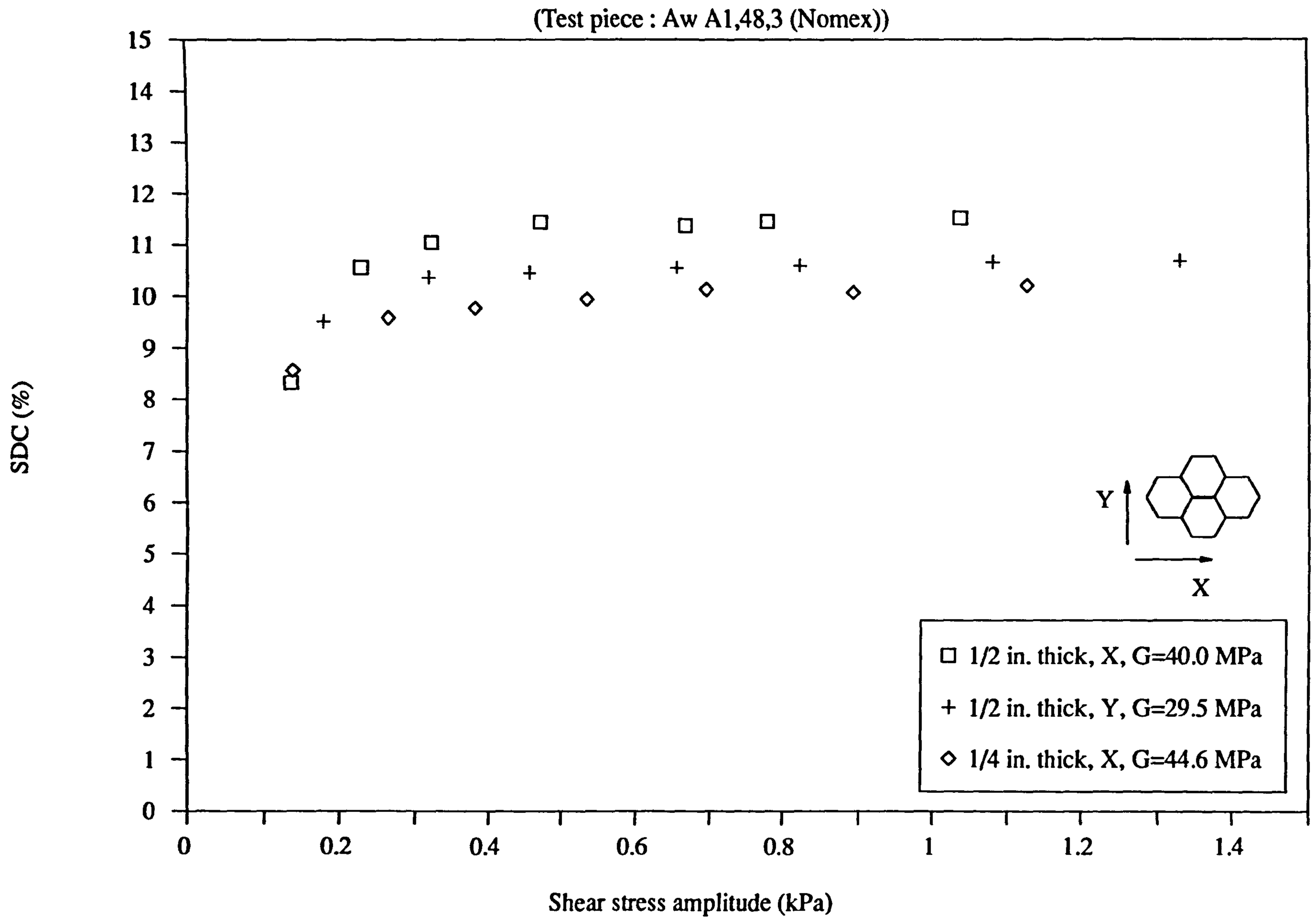

Fig. 4.14 *Honeycomb shear : SDC Vs Stress amplitude*

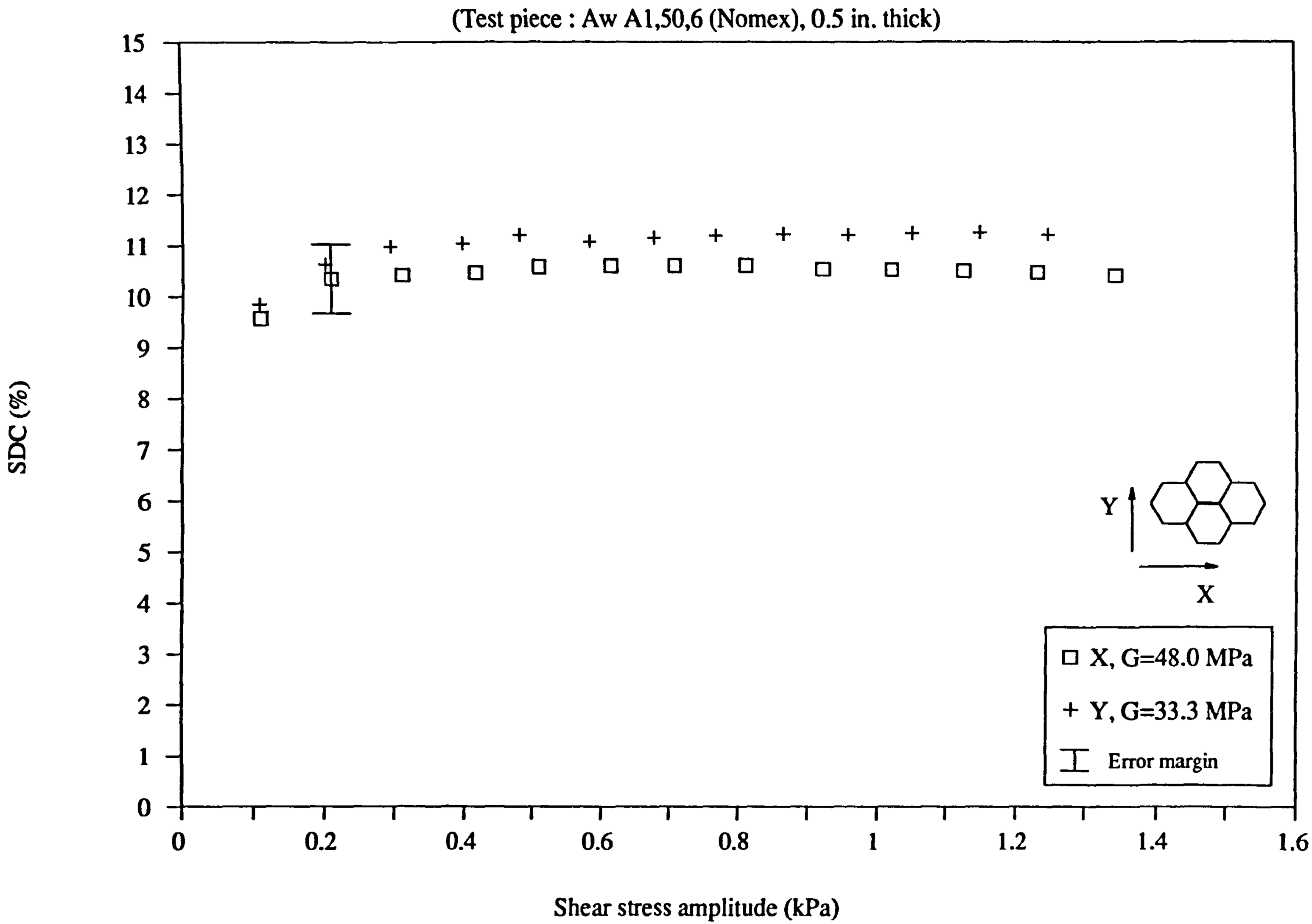

Fig. 4.15 Honeycomb shear : SDC Vs Stress amplitude

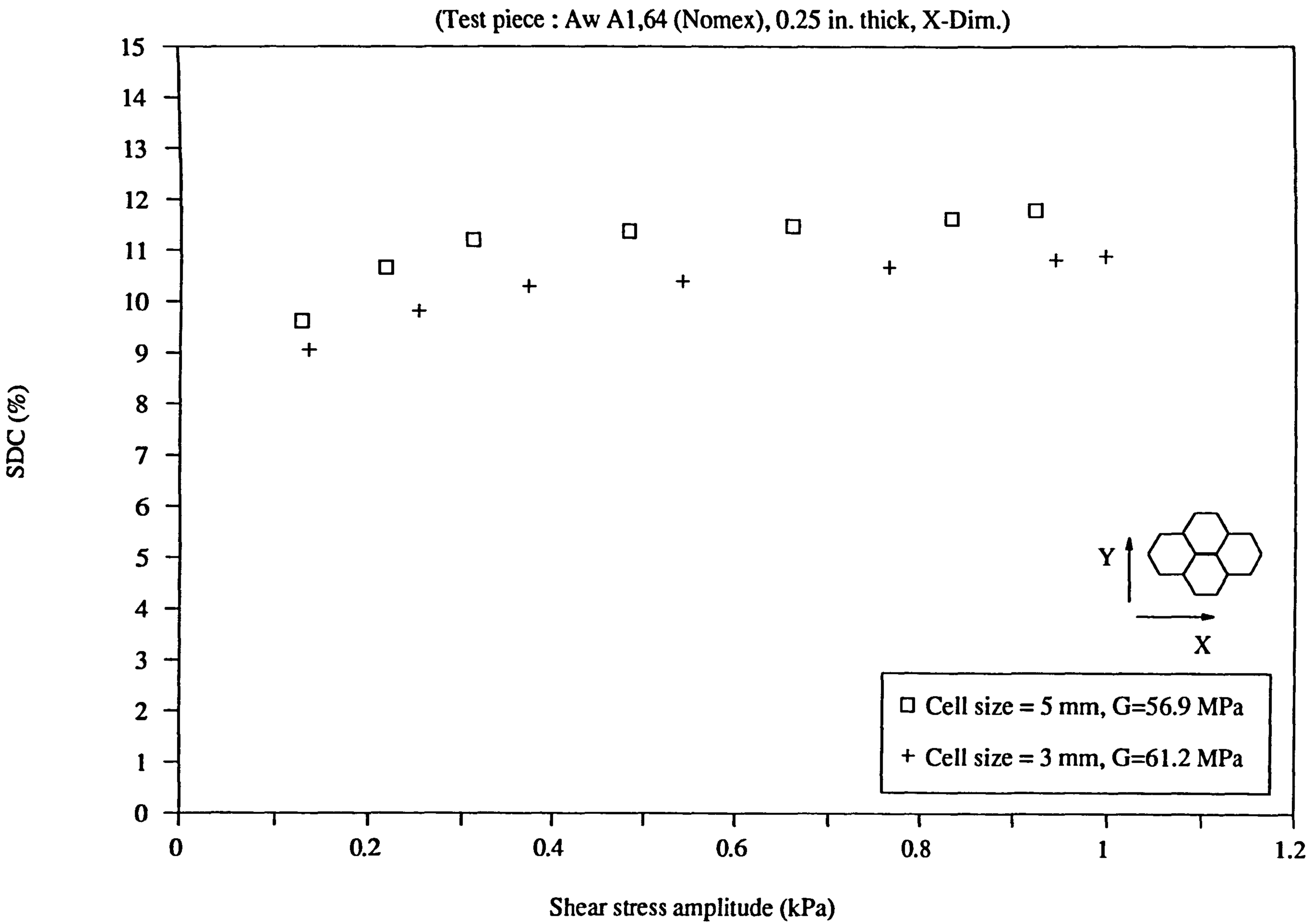

Fig. 4.16 *Honeycomb shear : SDC Vs Stress amplitude*

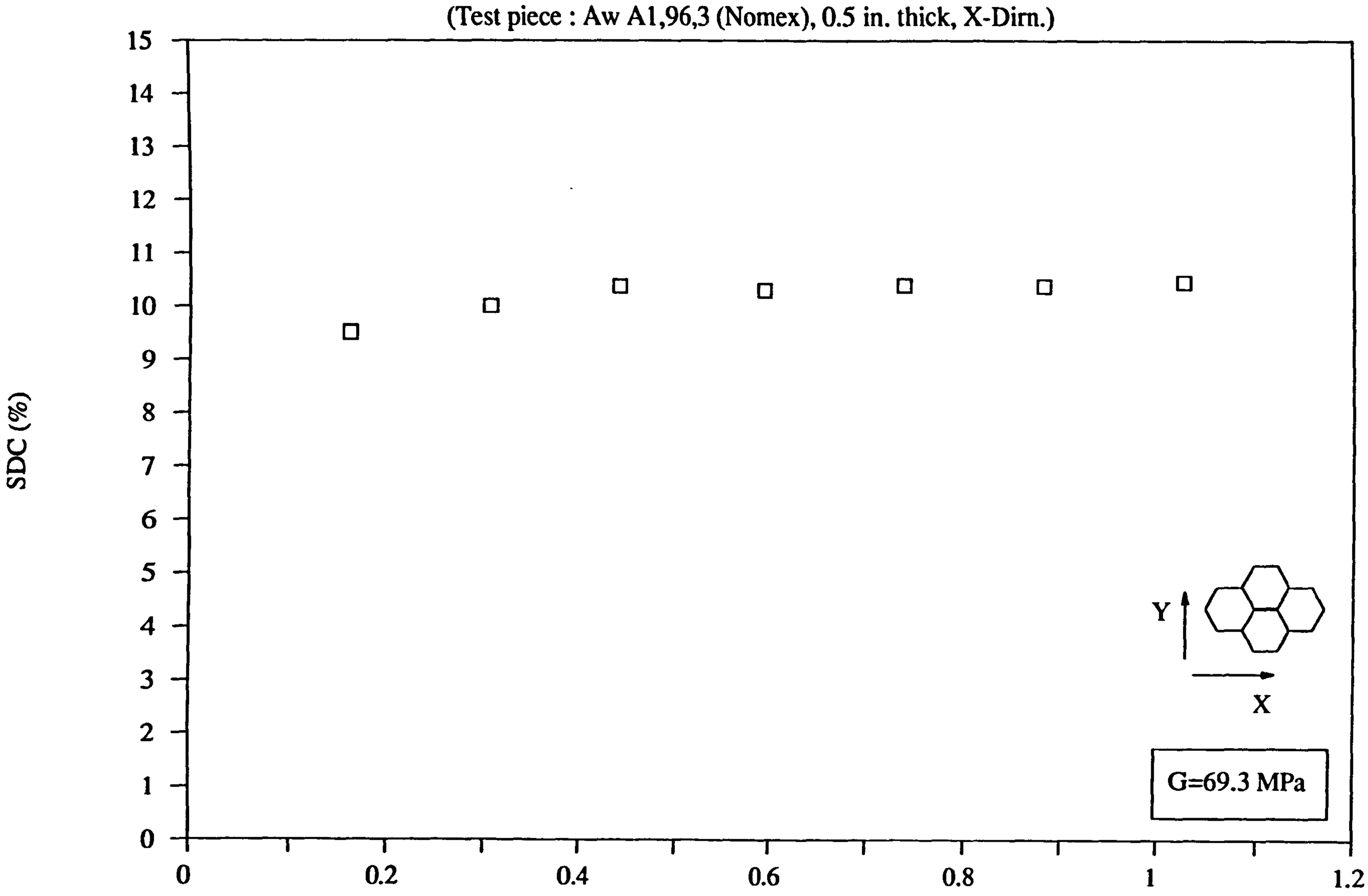

Fig. 4.17 *Honeycomb shear properties Vs Density*

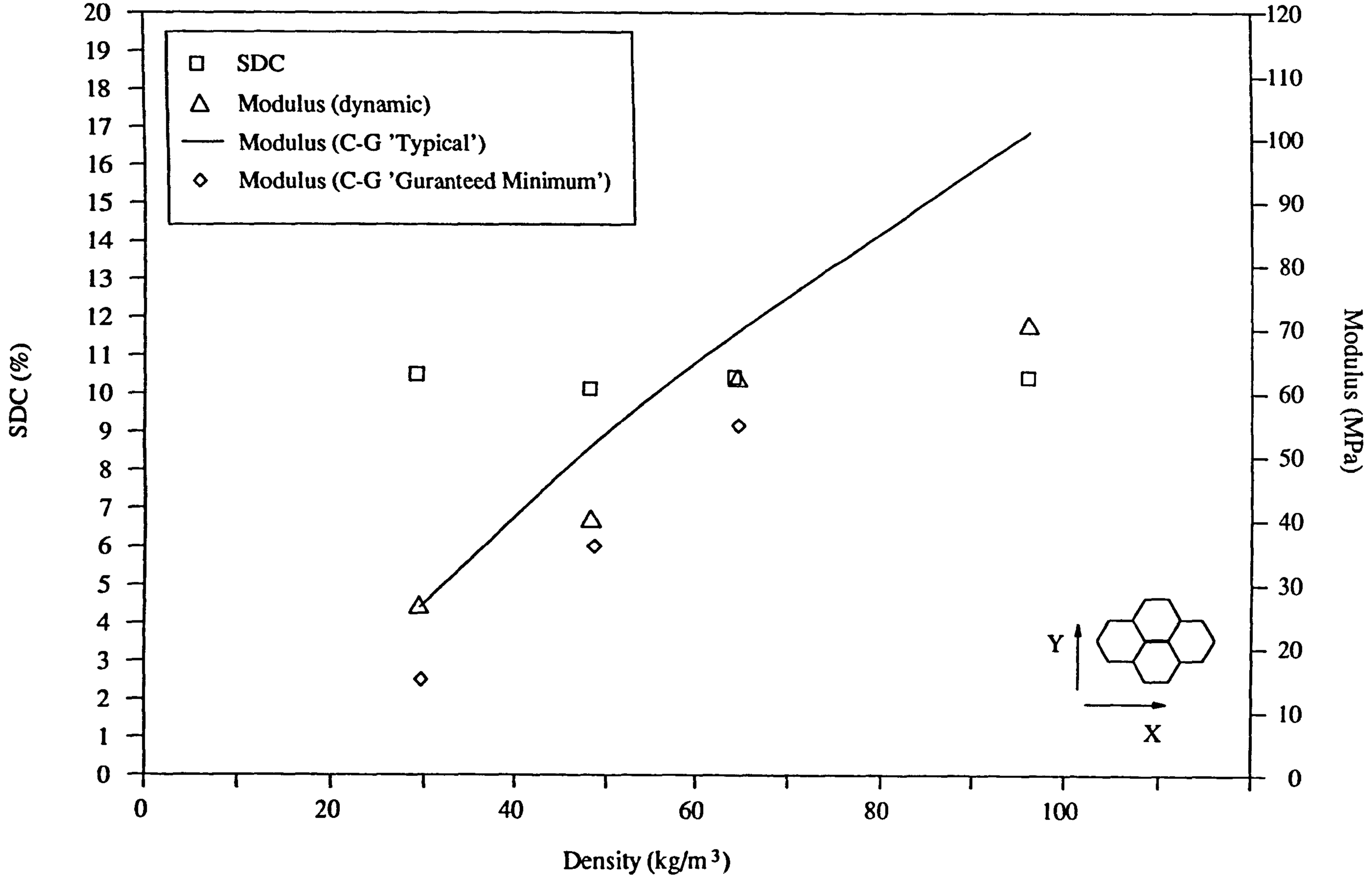

Fig. 5.2 *SDC Vs Displacement amplitude*

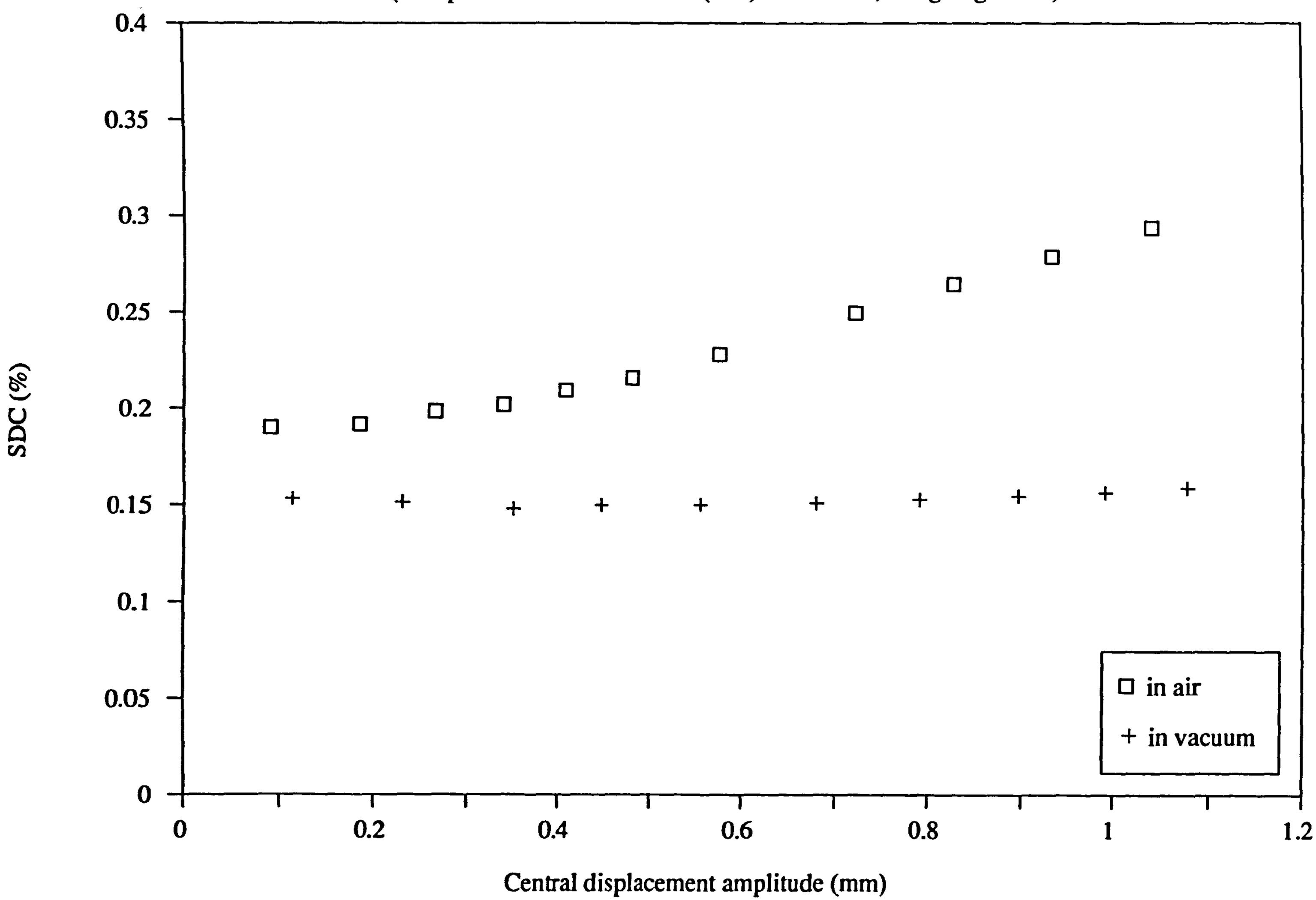

Fig. 5.3 *SDC Vs Displacement amplitude*

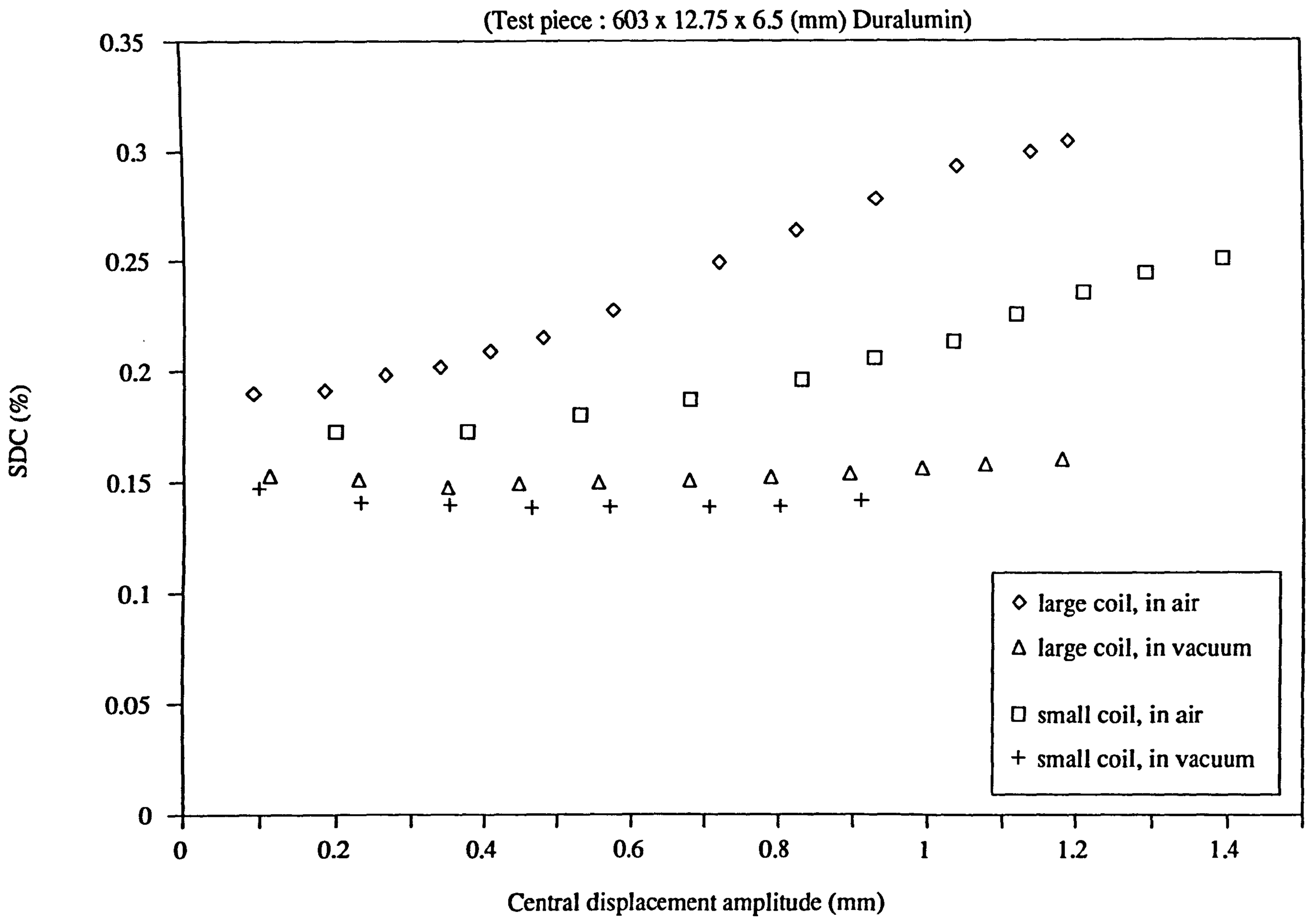

Fig. 5.4 *SDC Vs Displacement amplitude*

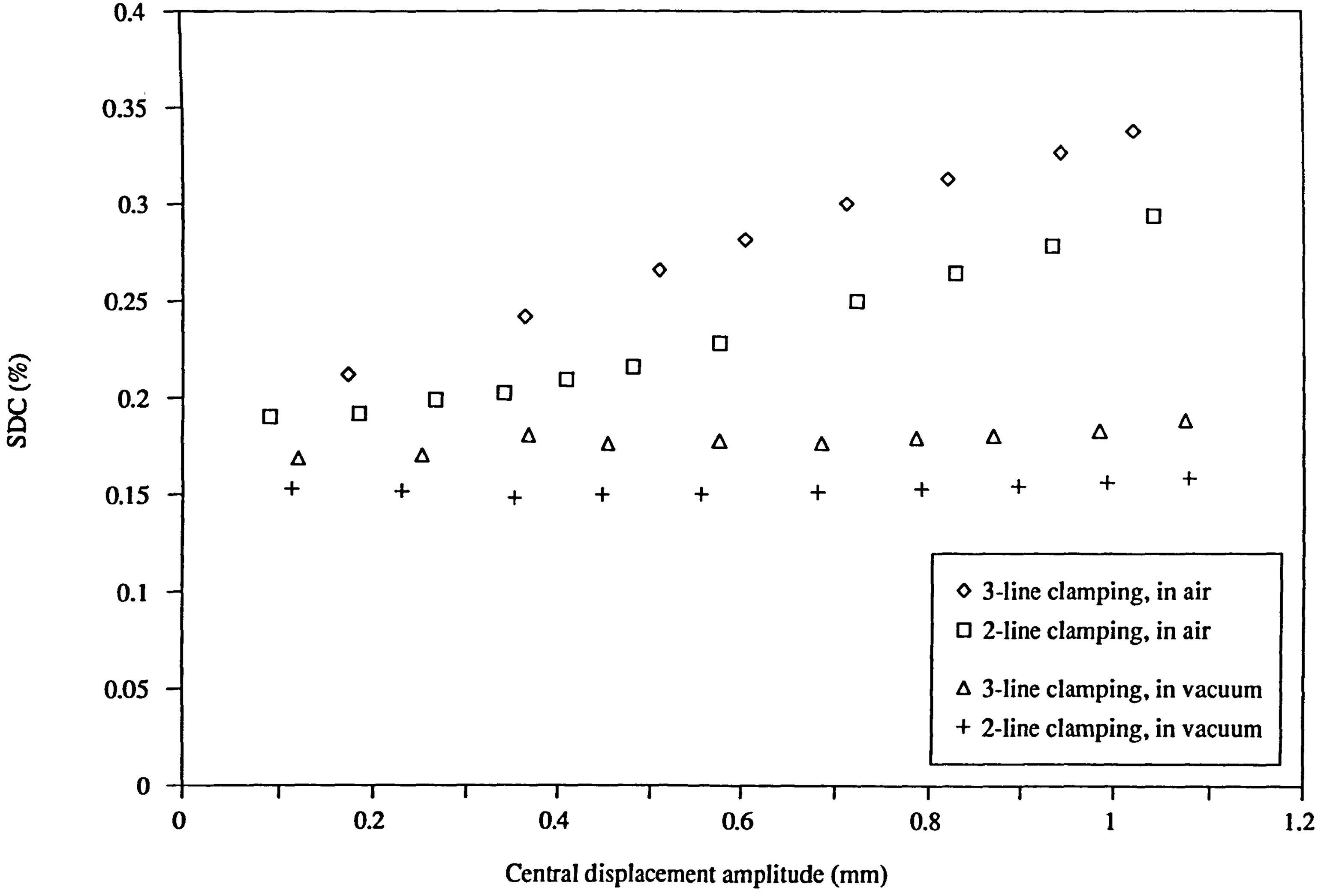

Fig. 5.5 *SDC Vs Skin stress amplitude*

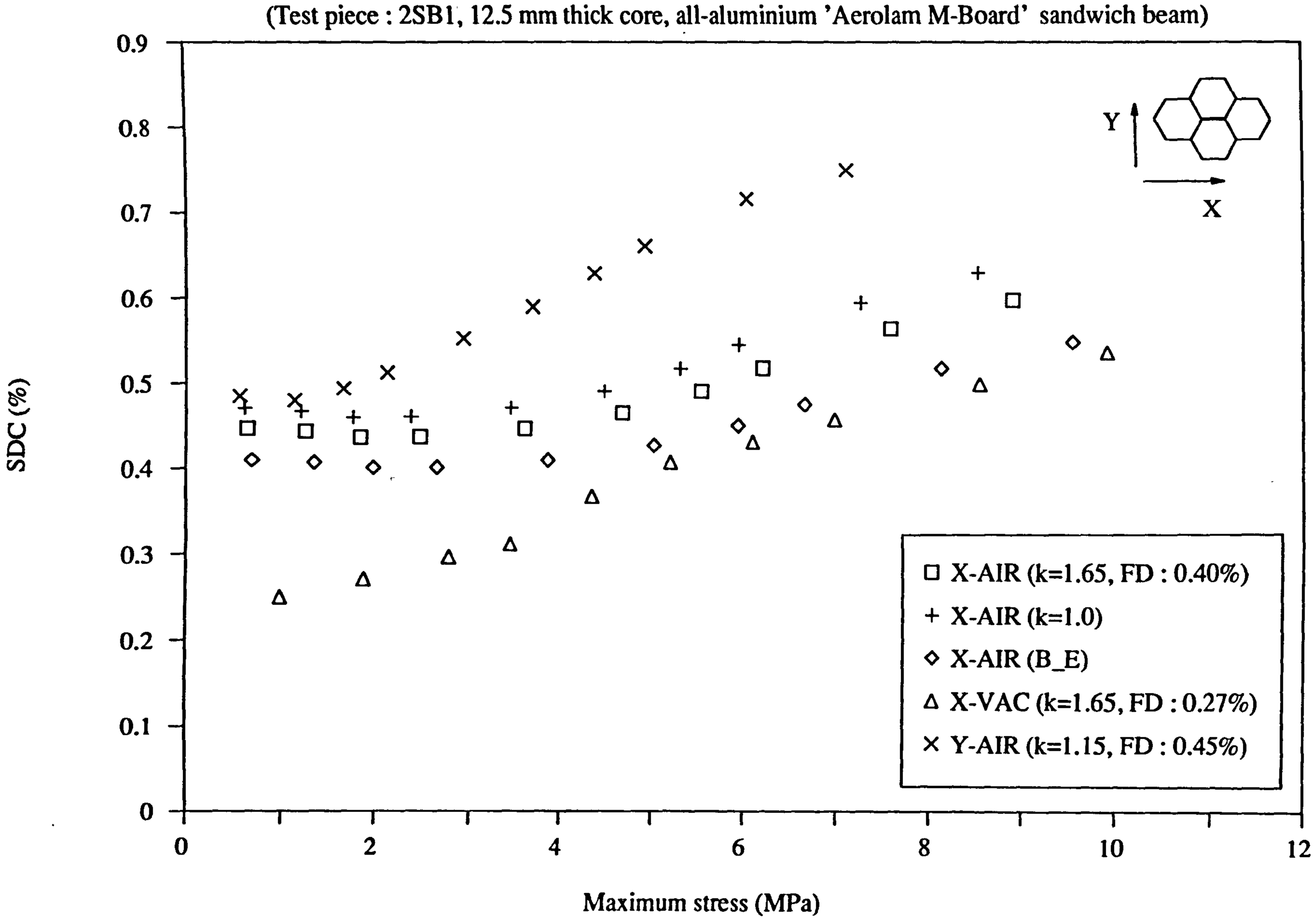

Fig. 5.6 *SDC Vs Skin stress amplitude*

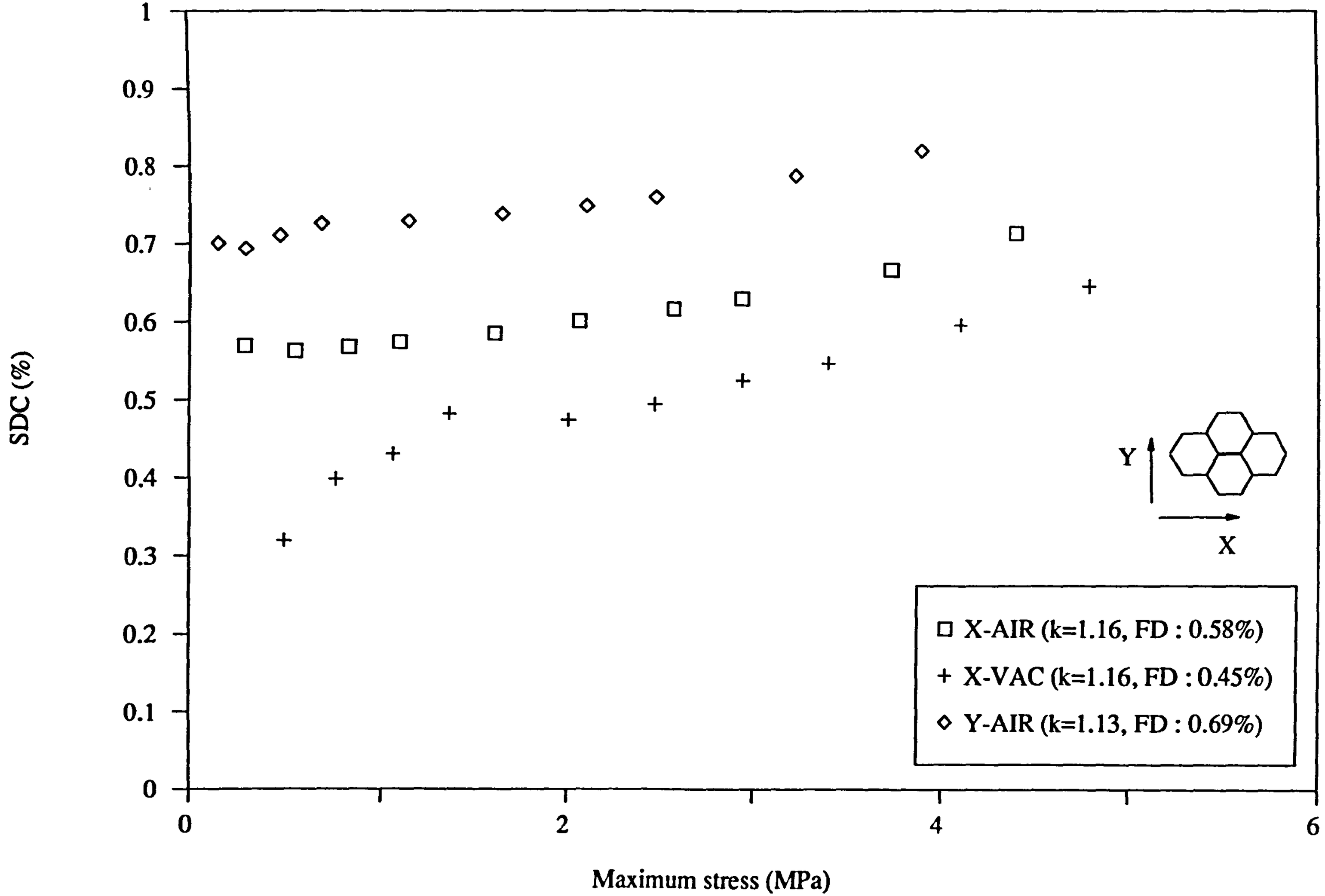

Fig. 5.7 *SDC Vs Skin stress amplitude*

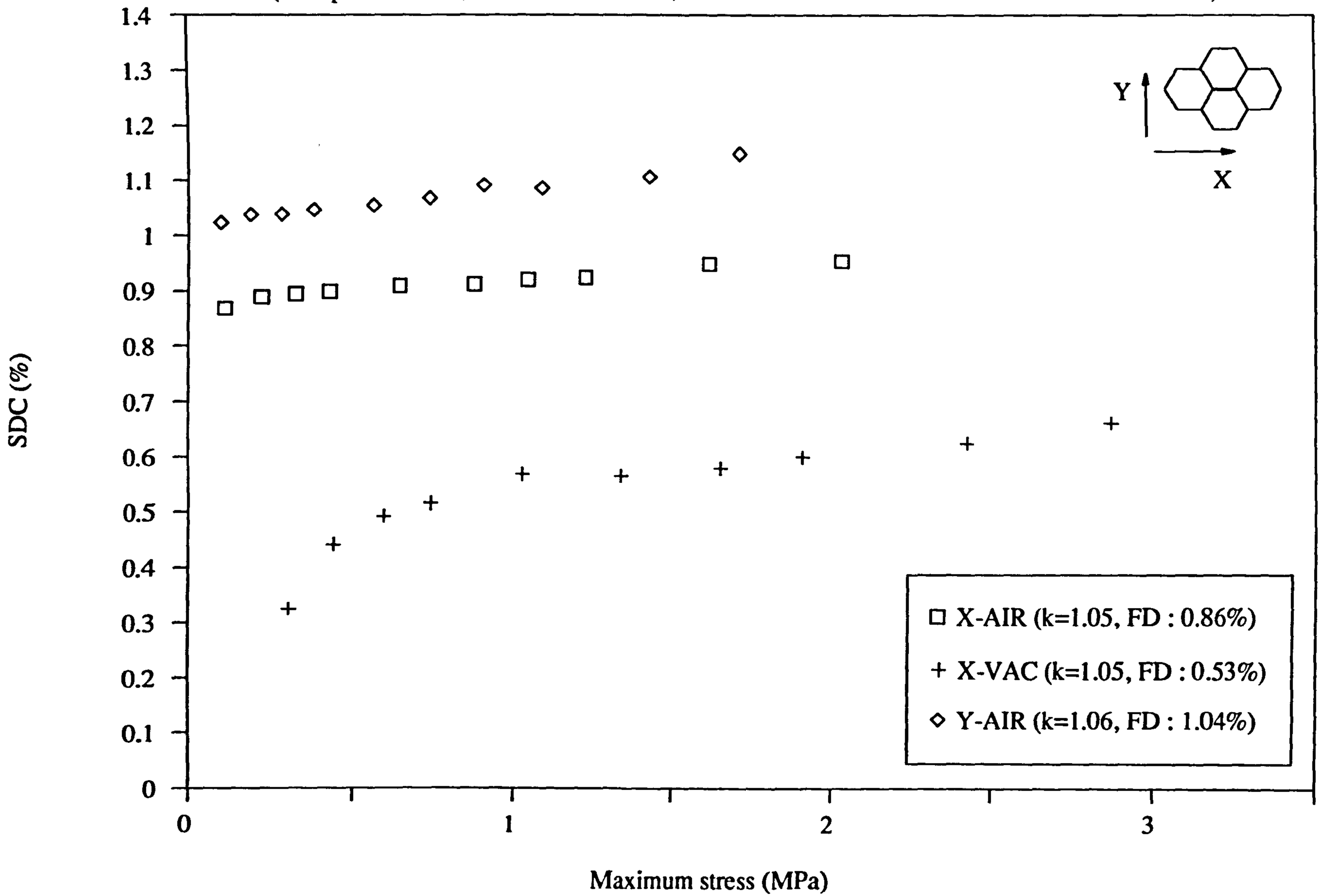

Fig. 5.8 *SDC Vs Core thickness*

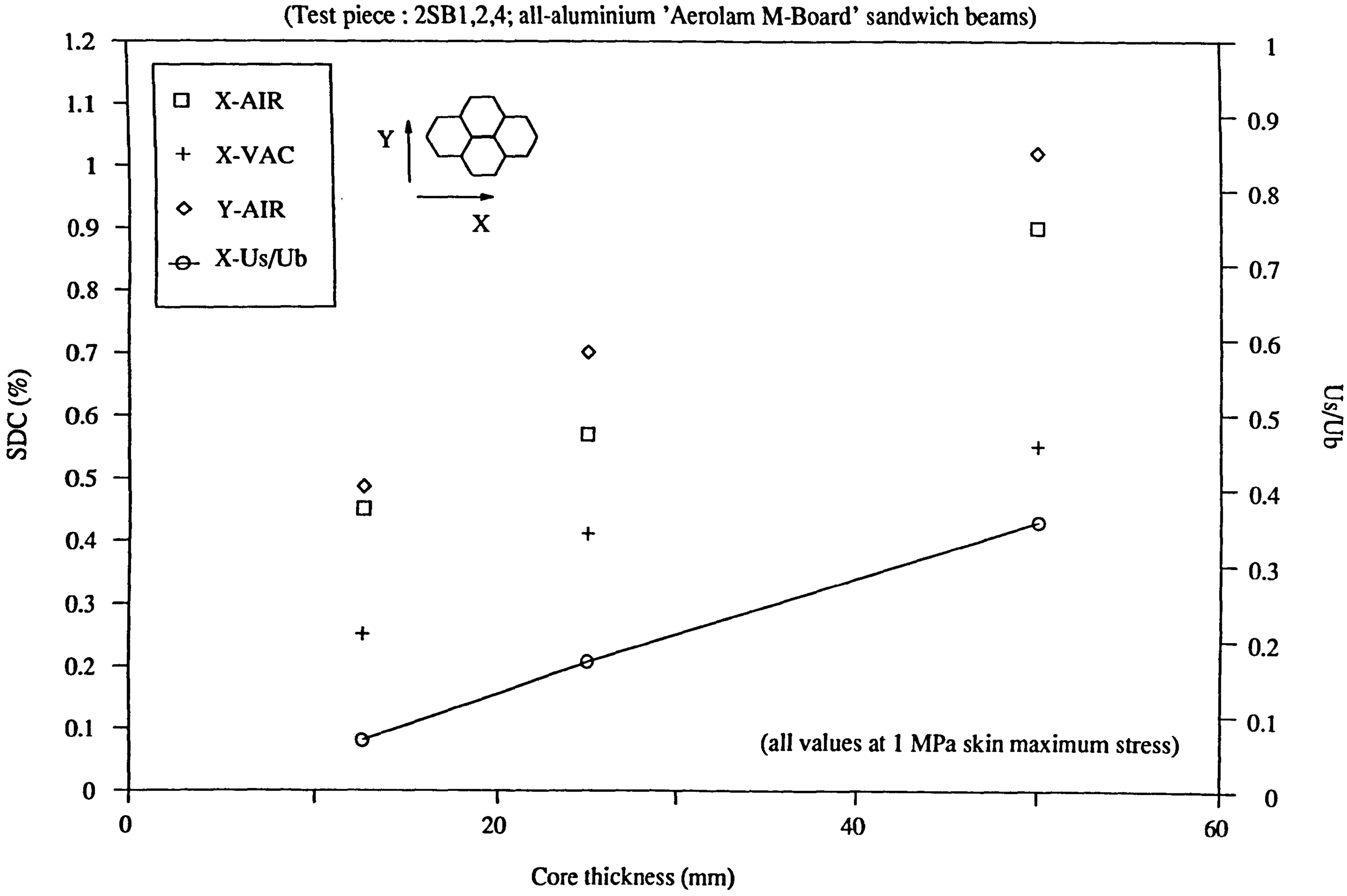

Fig. 5.9 *Strain energy Vs Displacement amplitude*

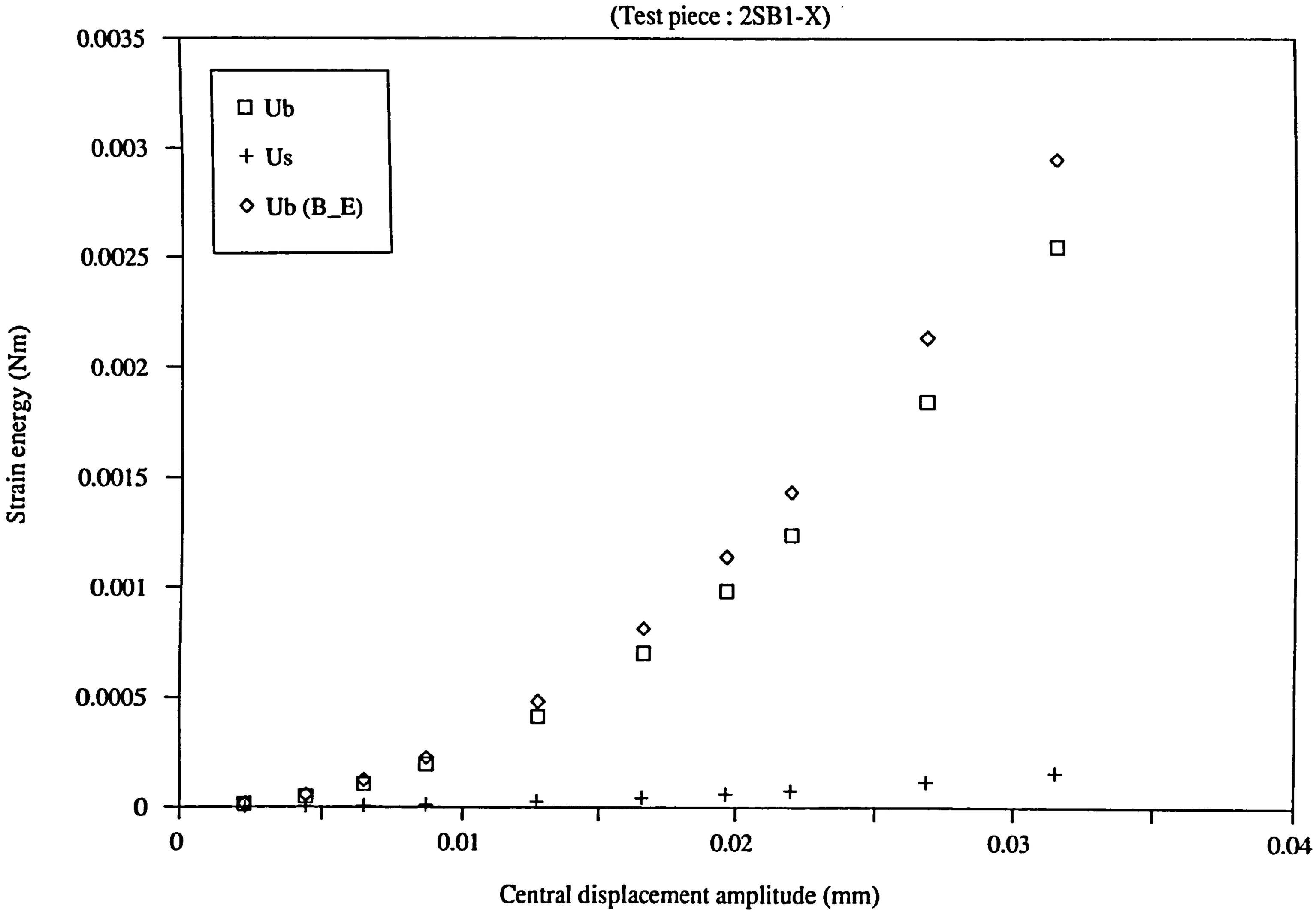

Fig. 6.2 Modulus Vs Fibre orientation

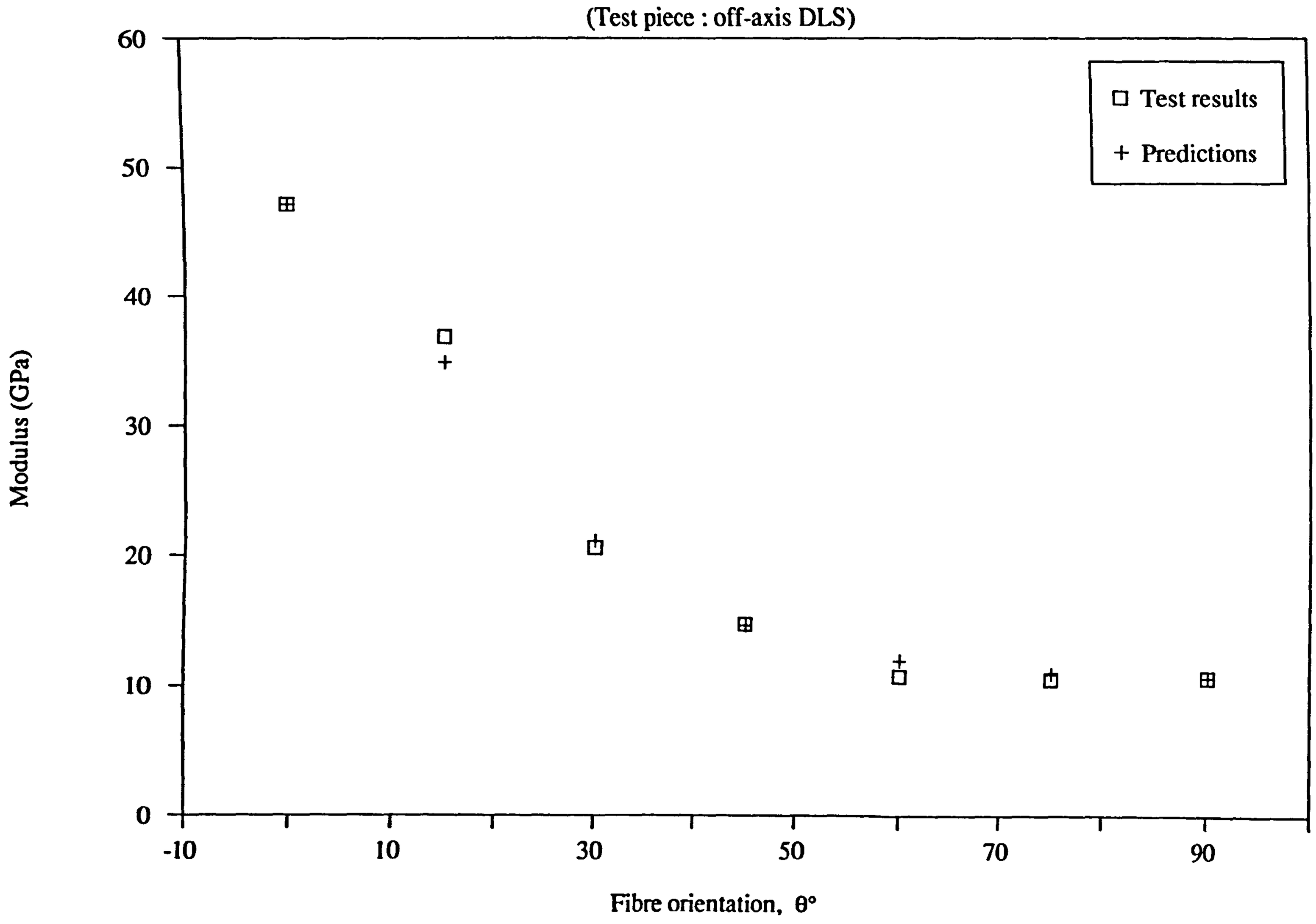

Fig. 6.3 *Modulus Vs Fibre orientation*

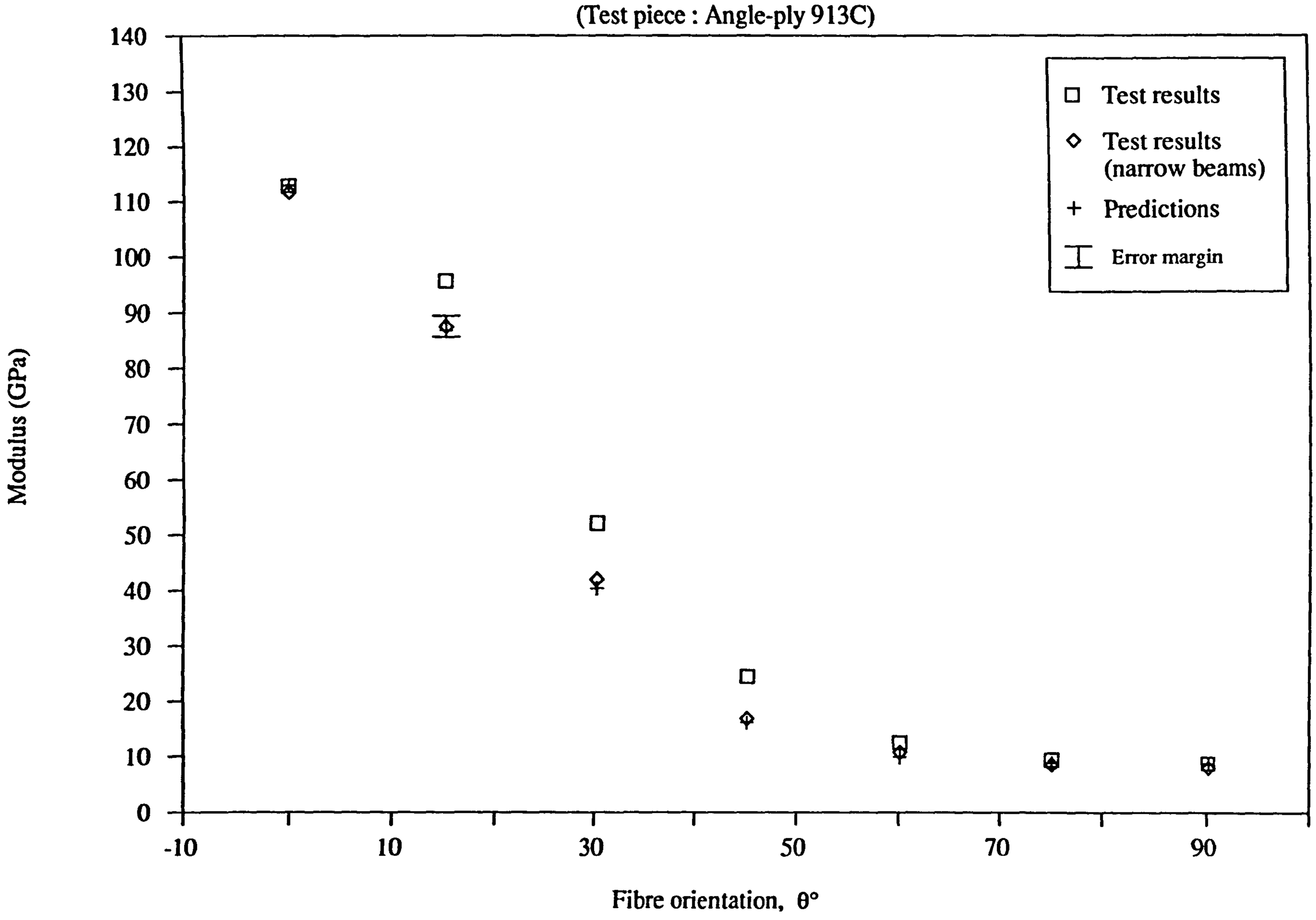

Fig. 6.4 Modulus Vs Fibre orientation

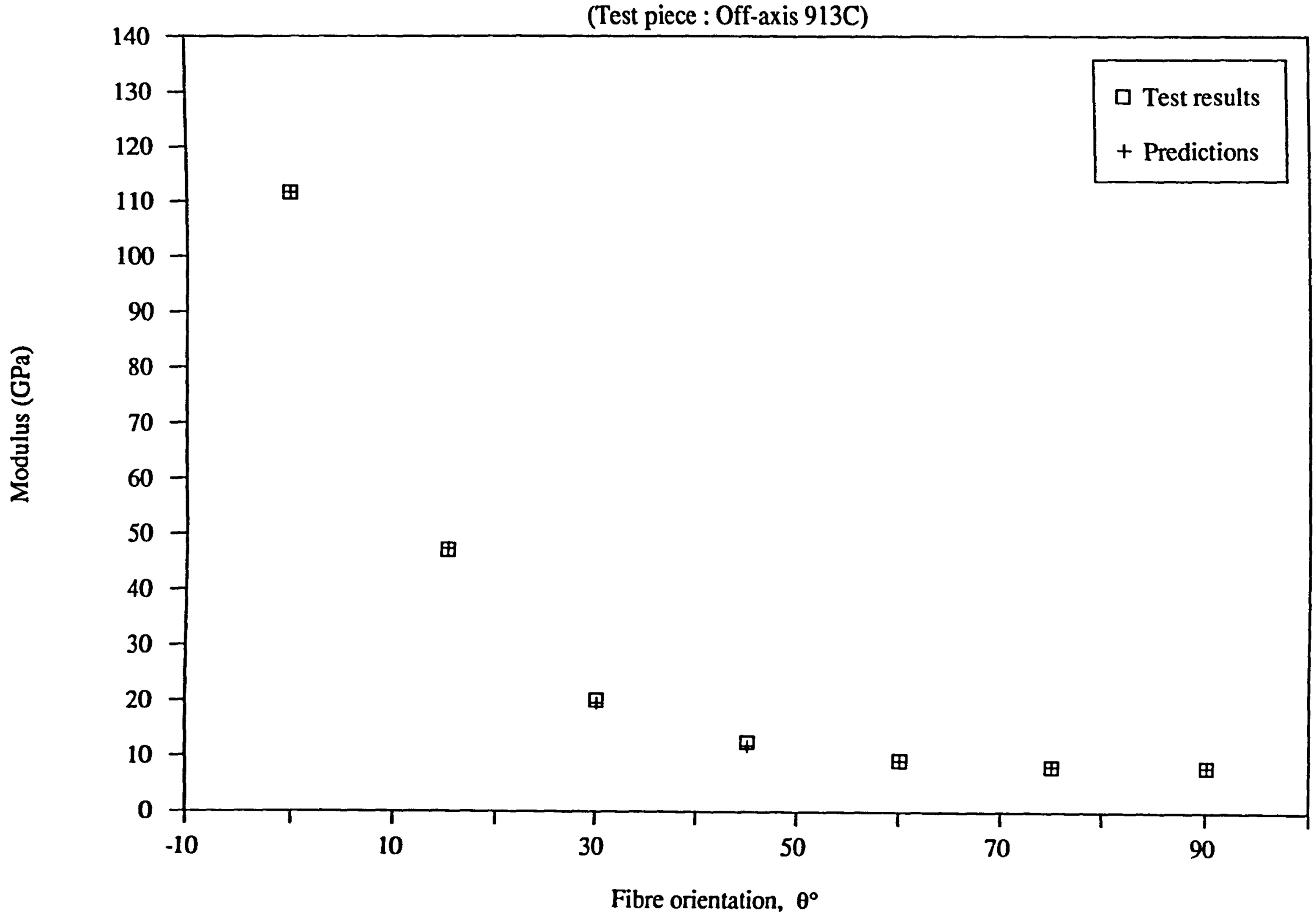

Fig. 6.5 Modulus Vs Fibre orientation

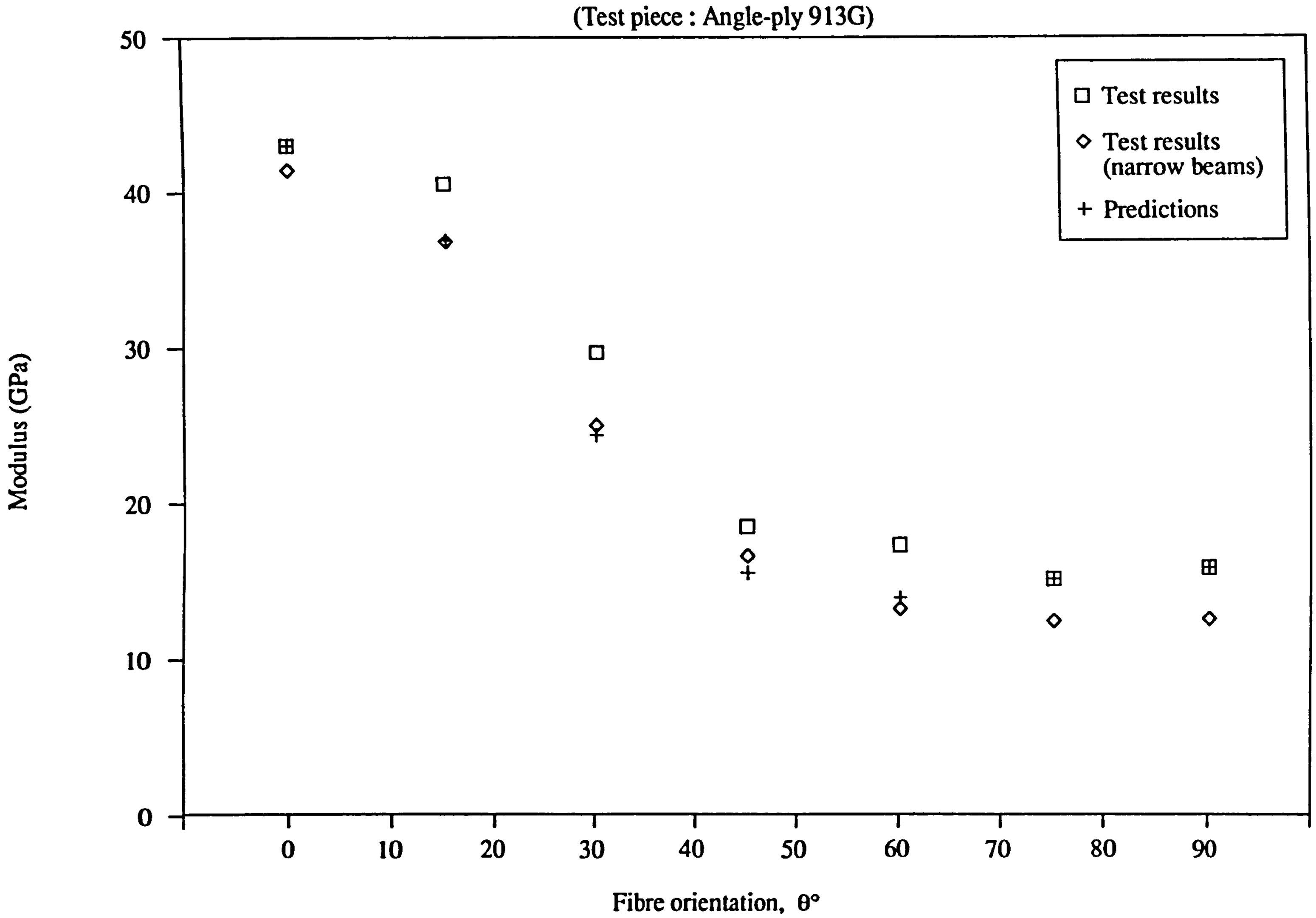

Fig. 6.6 Modulus Vs Fibre orientation

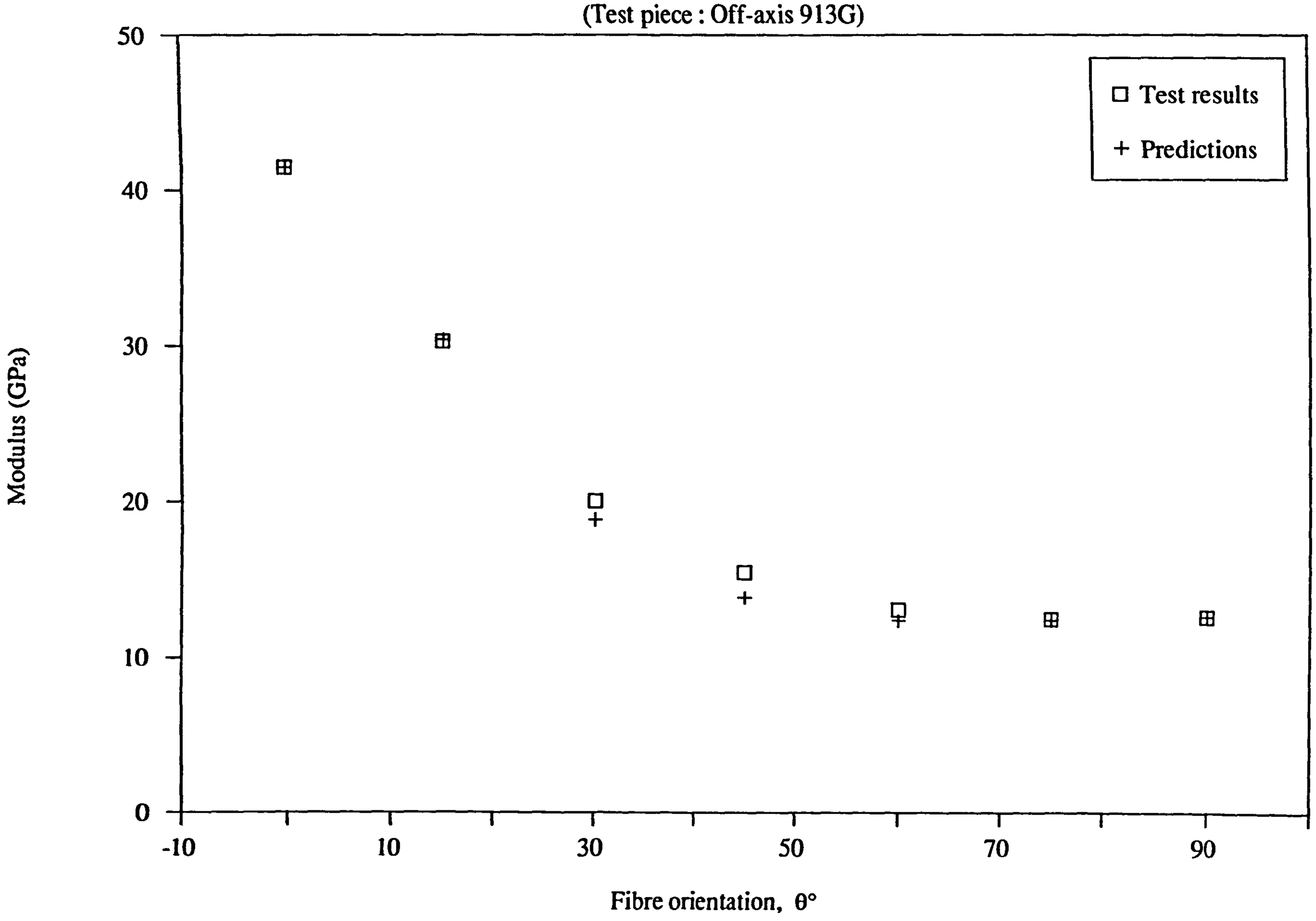

Fig. 6.7 SDC Vs Stress amplitude

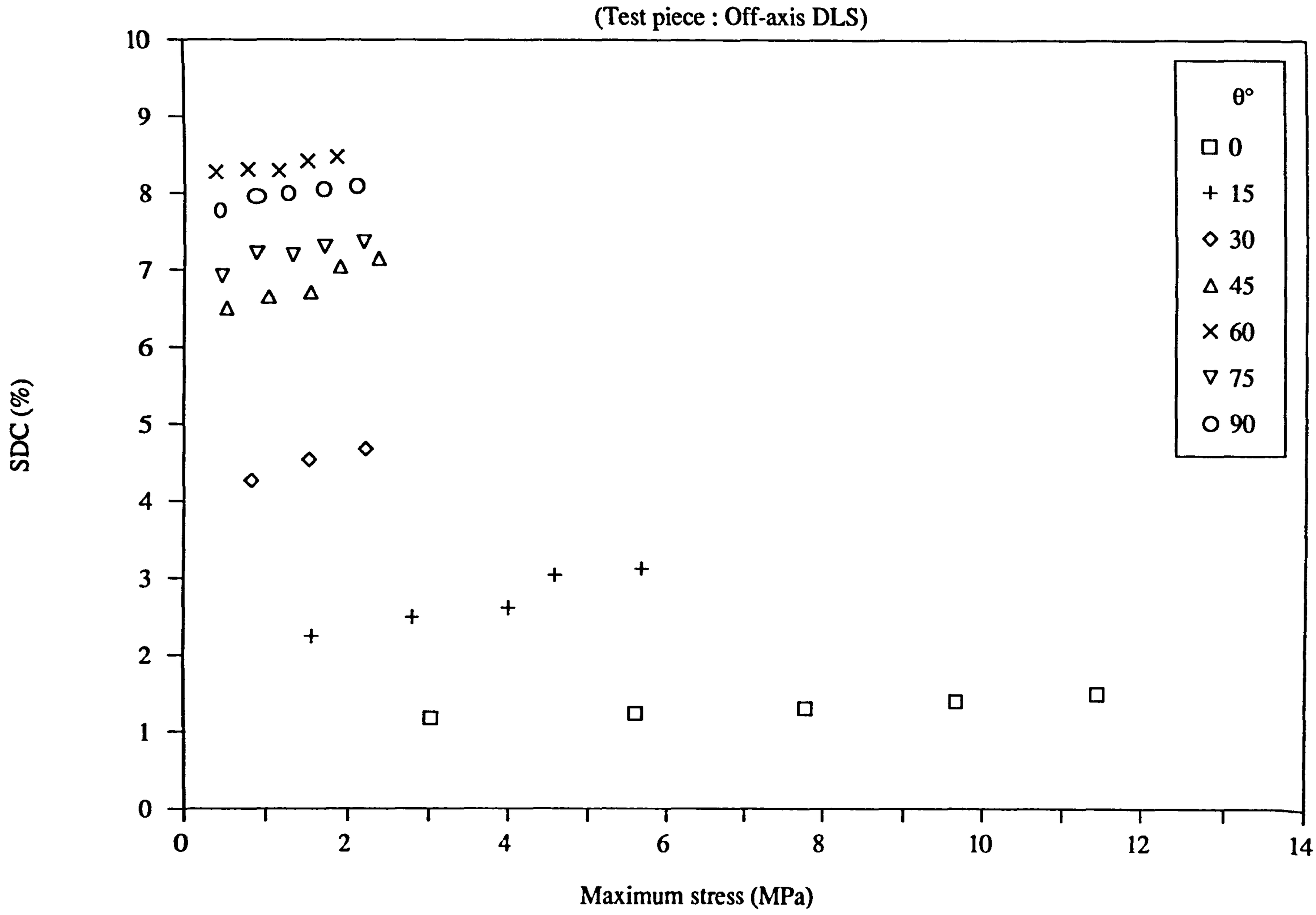

Fig. 6.8 SDC Vs Stress amplitude

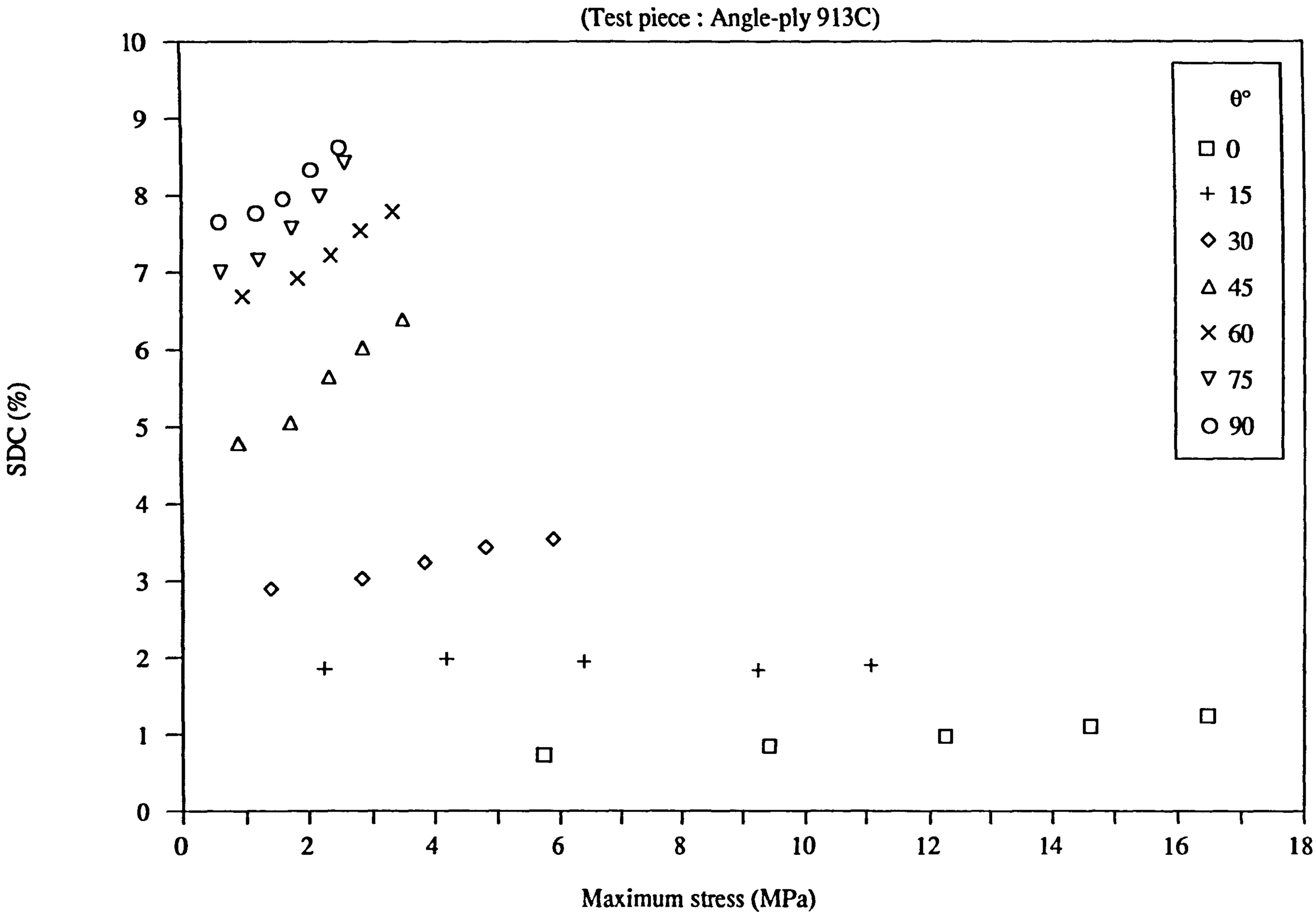

Fig. 6.9 SDC Vs Stress amplitude

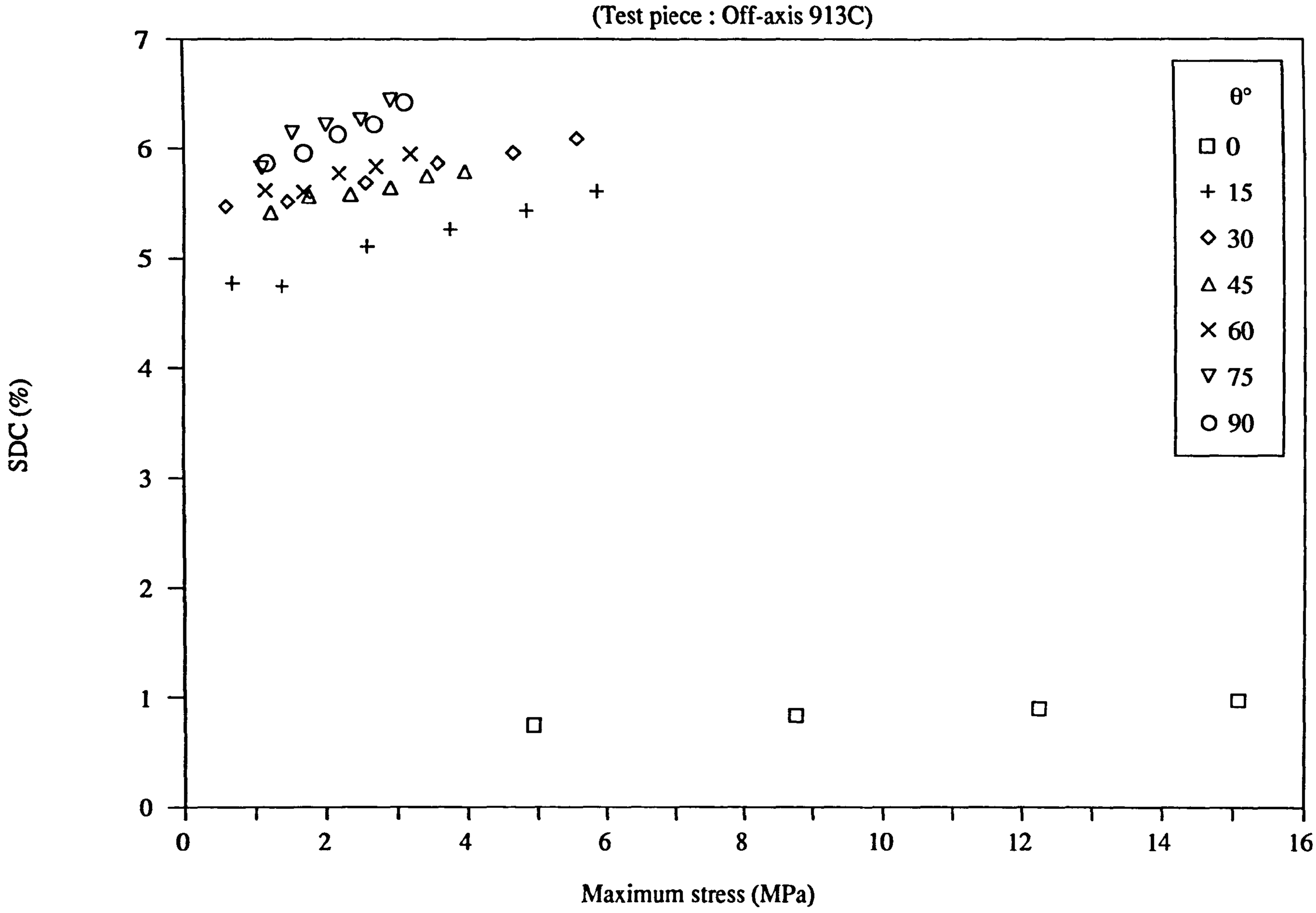

Fig. 6.10 SDC Vs Stress amplitude

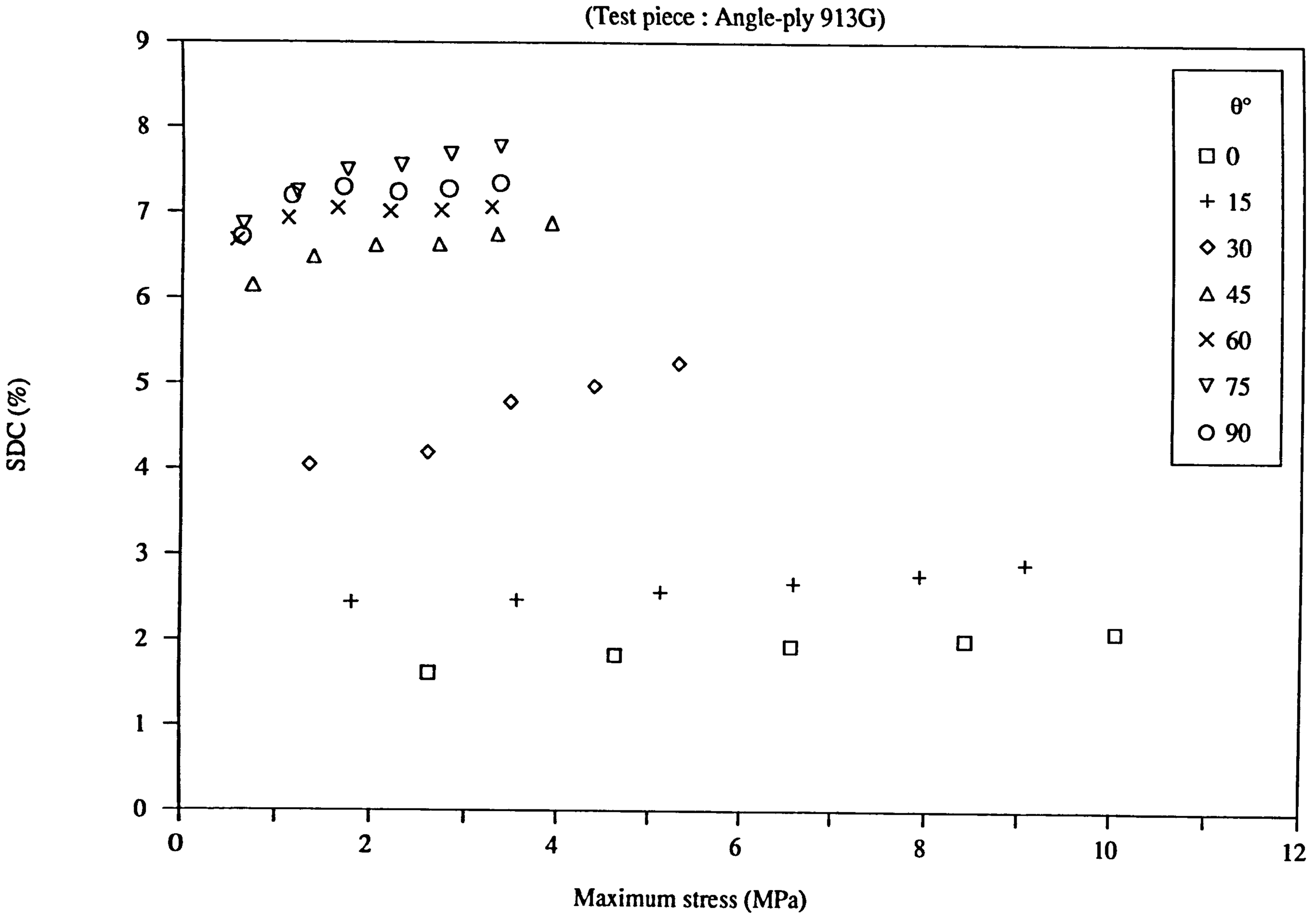

Fig. 6.11 SDC Vs Stress amplitude

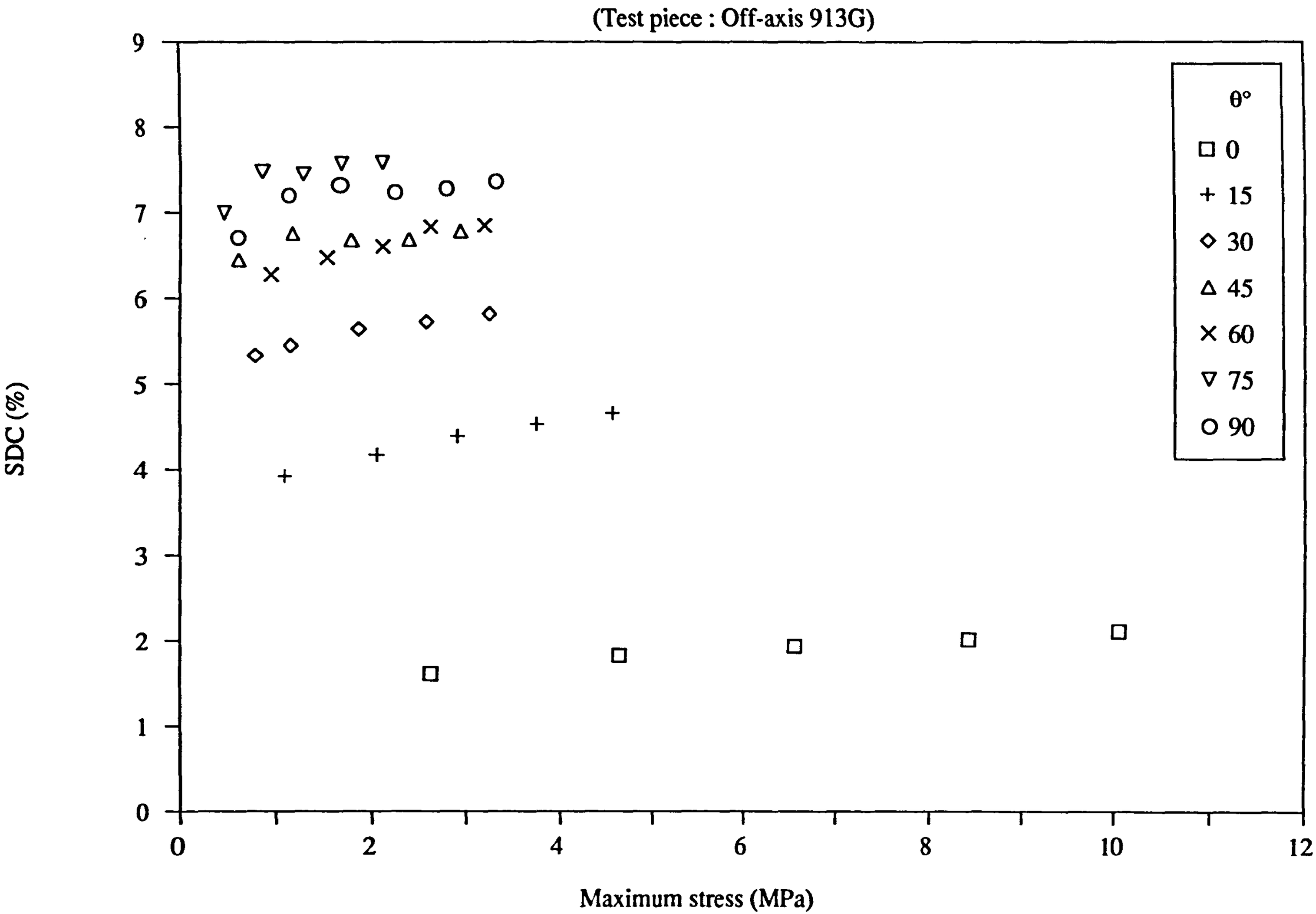

Fig. 6.12 SDC Vs Fibre orientation

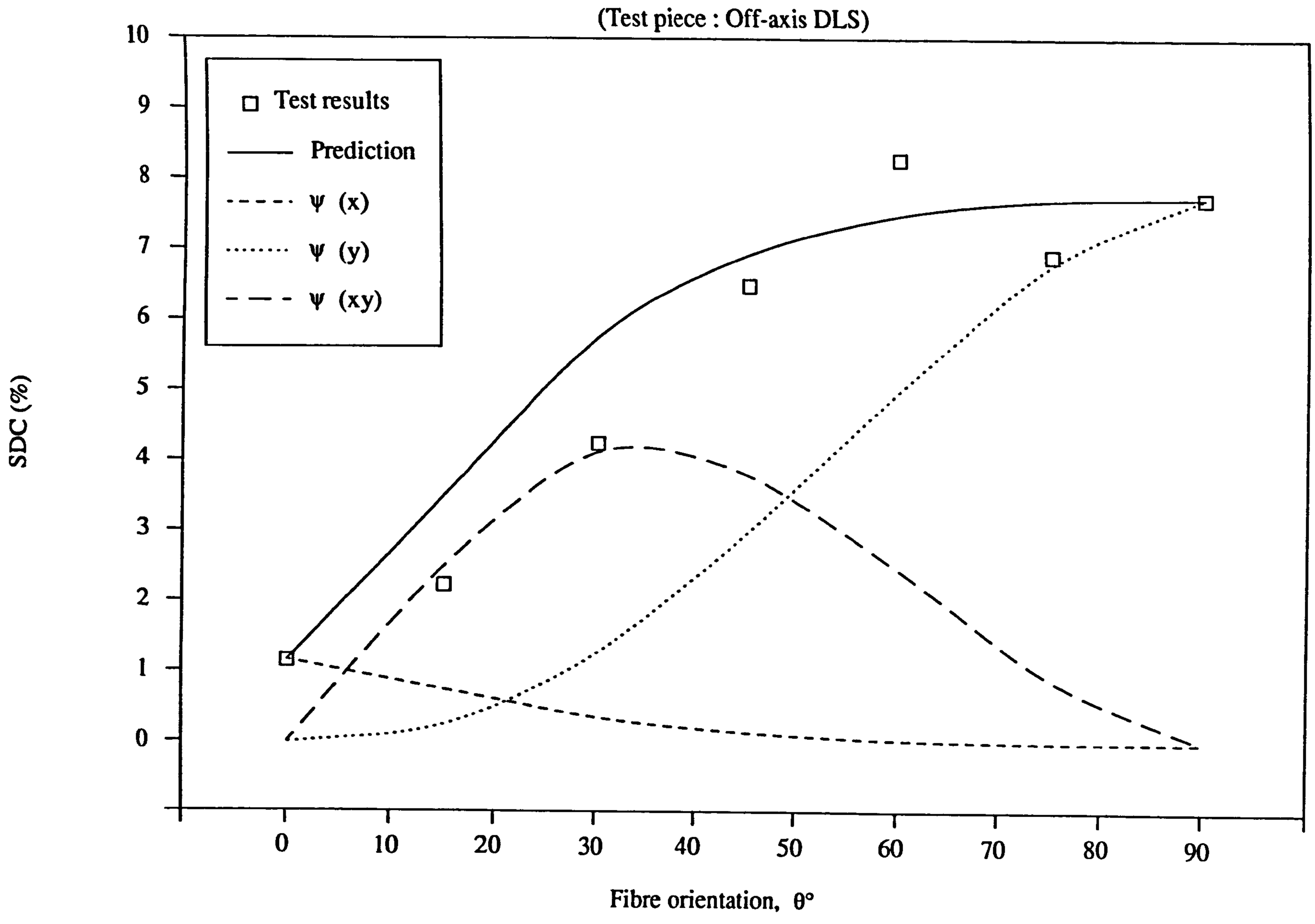

Fig. 6.13 SDC Vs Fibre orientation

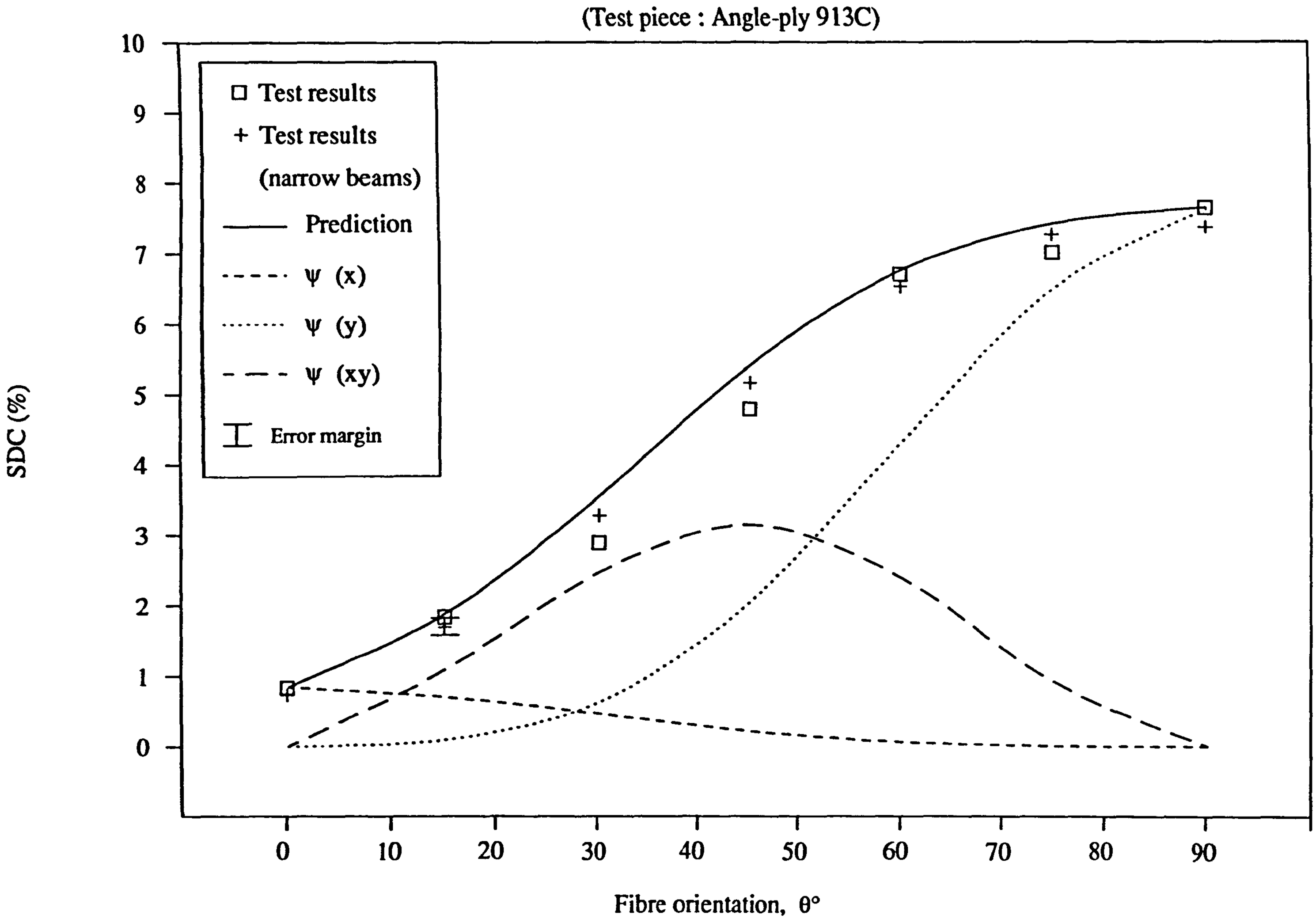

Fig. 6.14 SDC Vs Fibre orientation

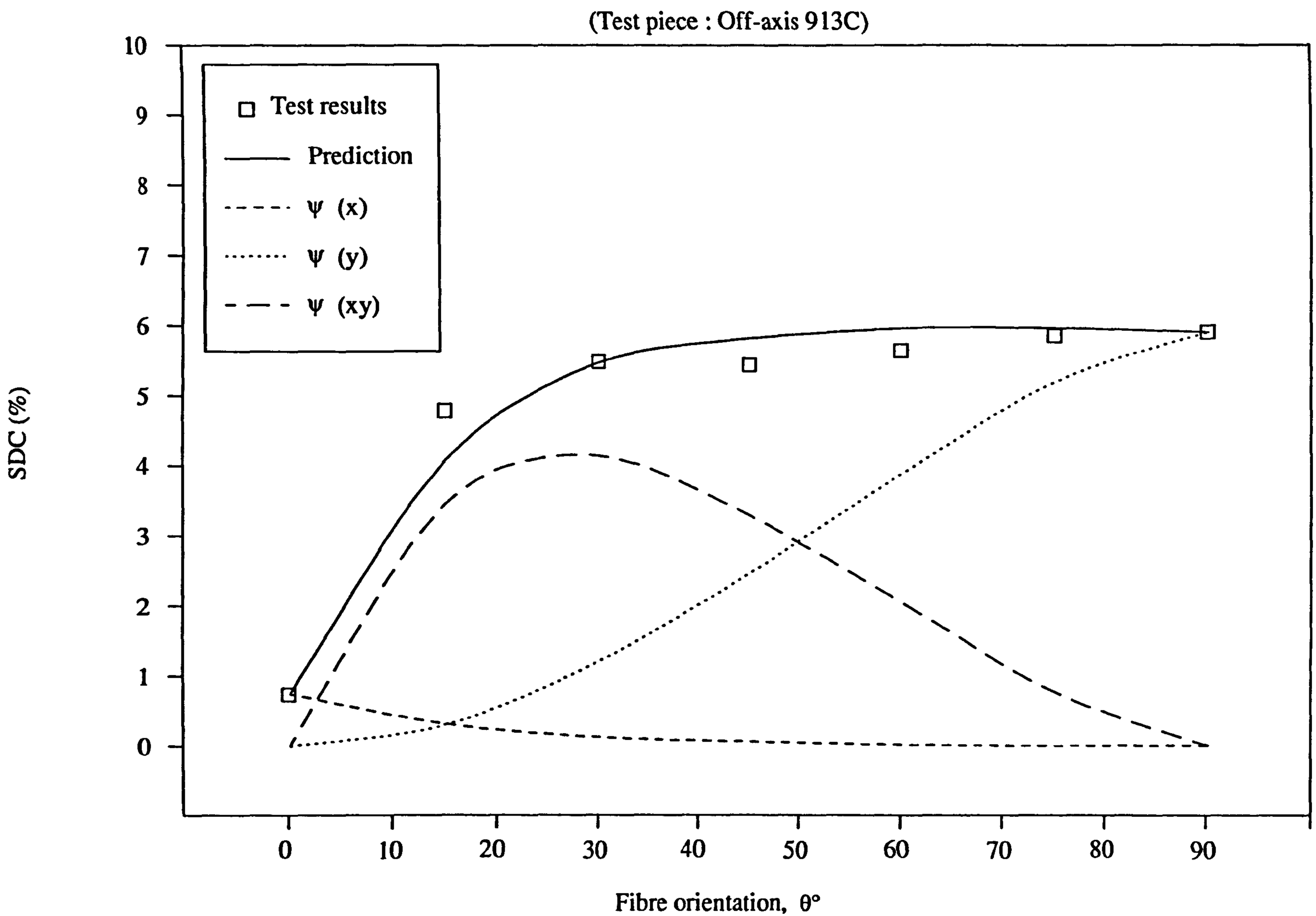

Fig. 6.15 SDC Vs Fibre orientation

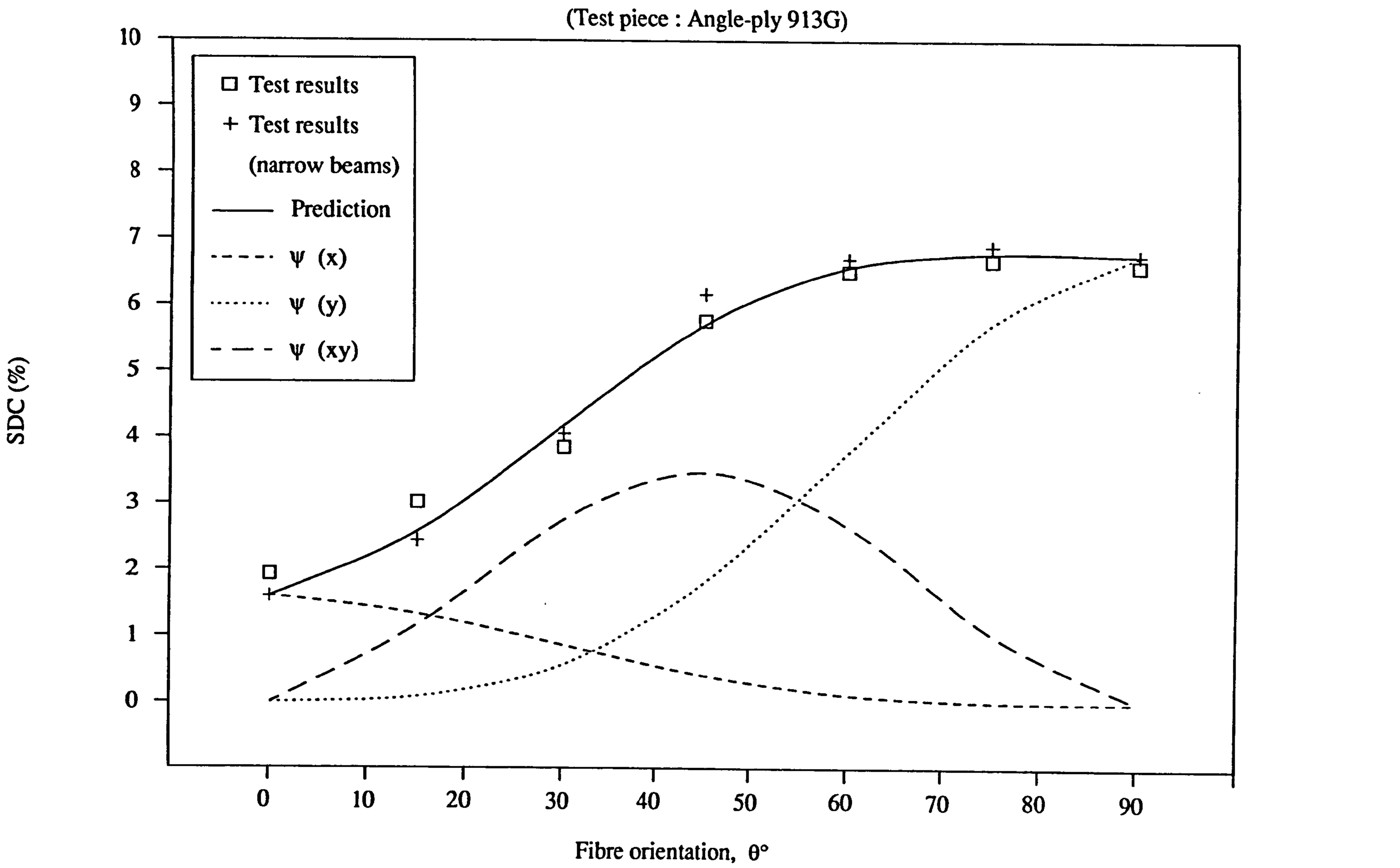

Fig. 6.16 SDC Vs Fibre orientation

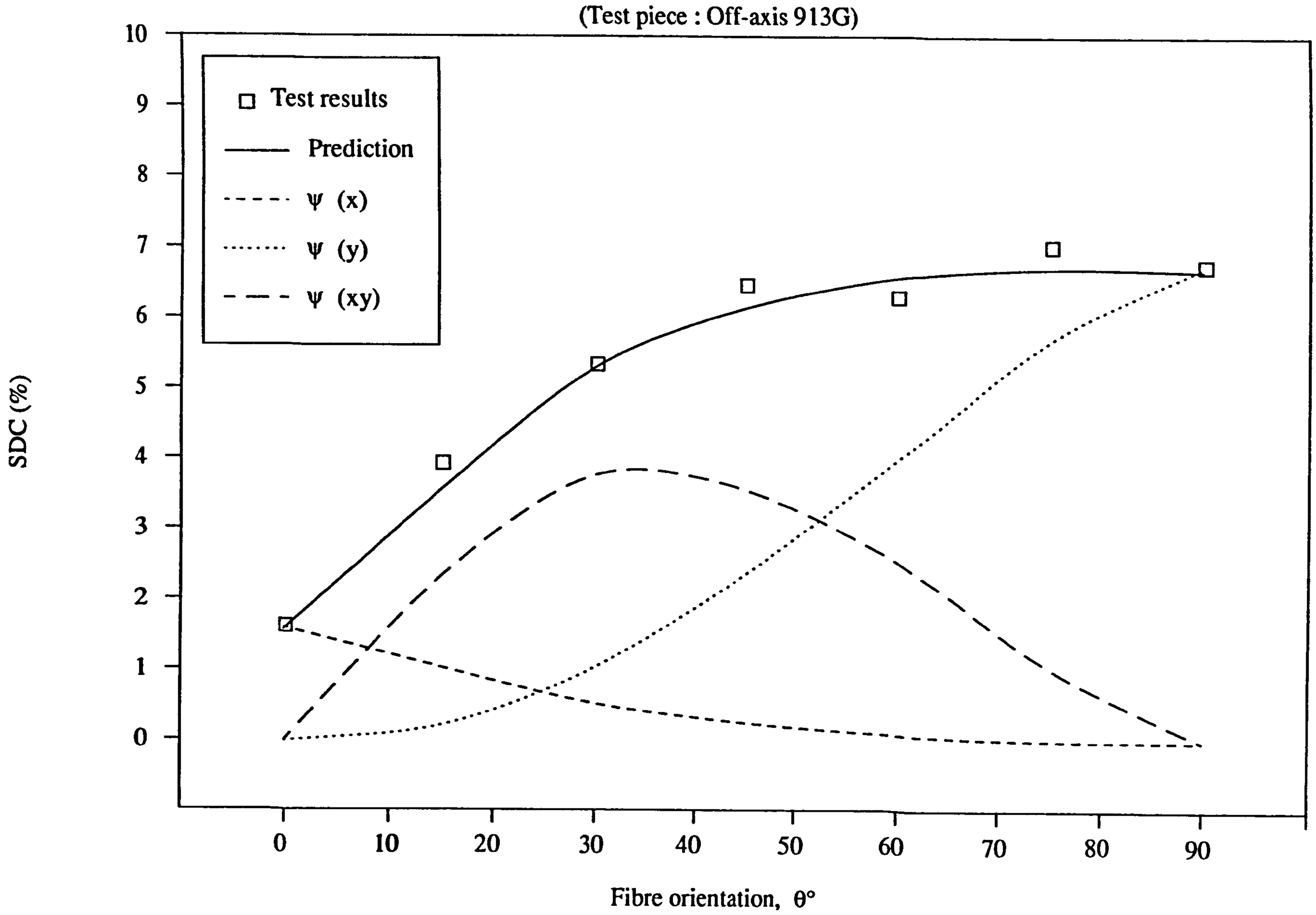

Fig. 6.17 Frequency Vs Mode No.

(Test piece : Unloaded free-free 0 Deg. 913C/Alum.)

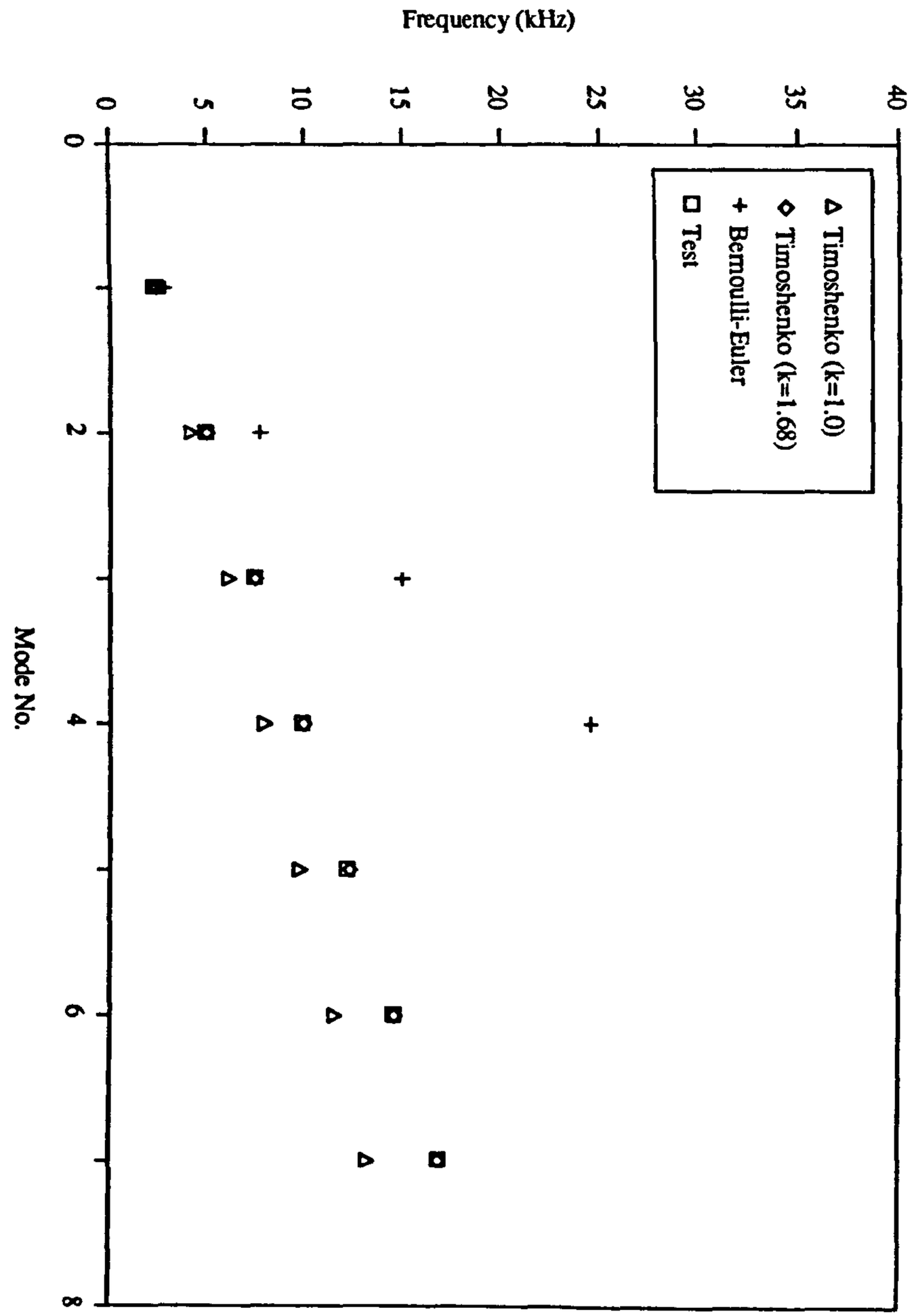

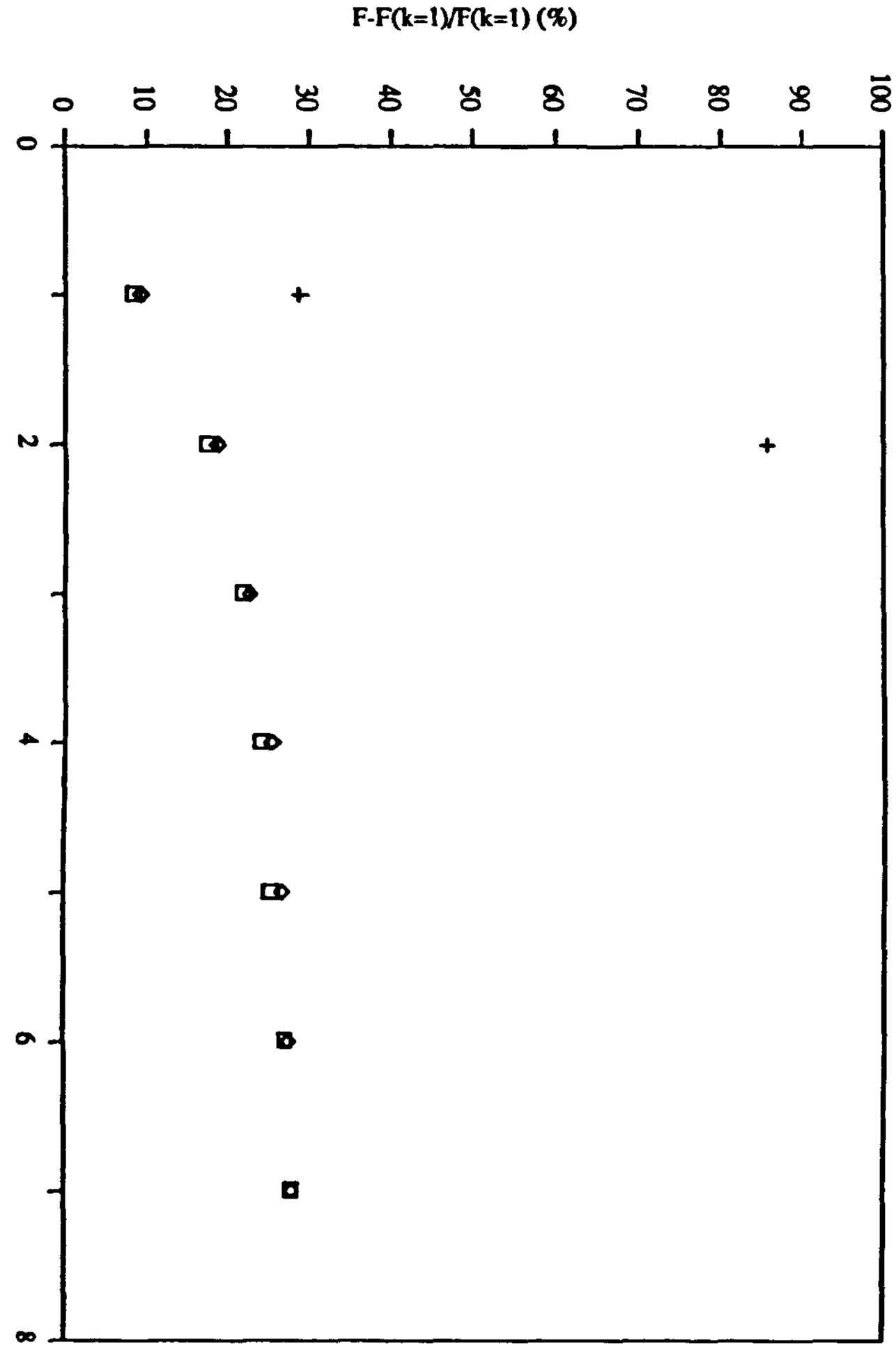

Fig. 6.18 Frequency Vs Mode No.

(Test piece : Unloaded free-free 0 Deg. 913C/Nomex)

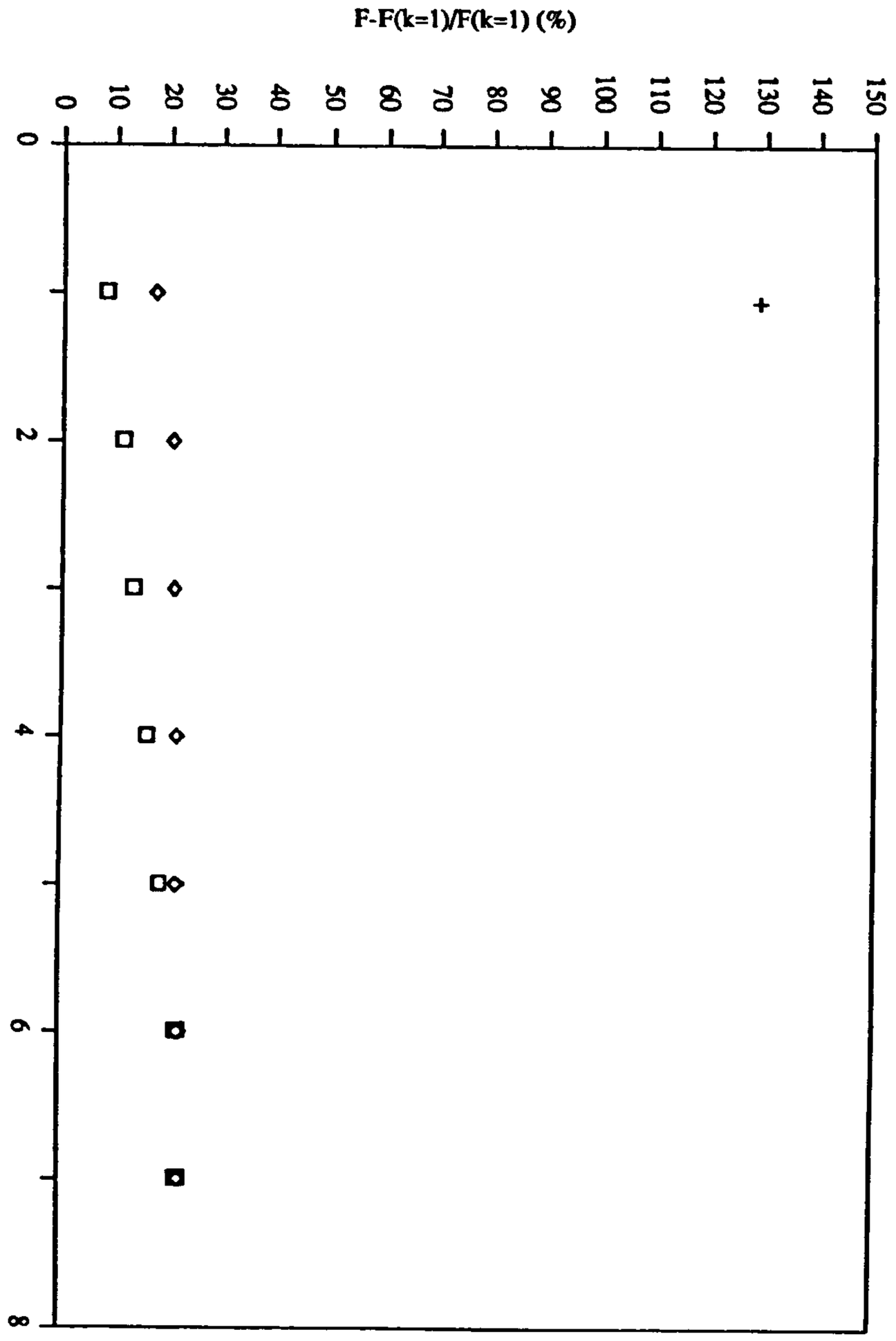

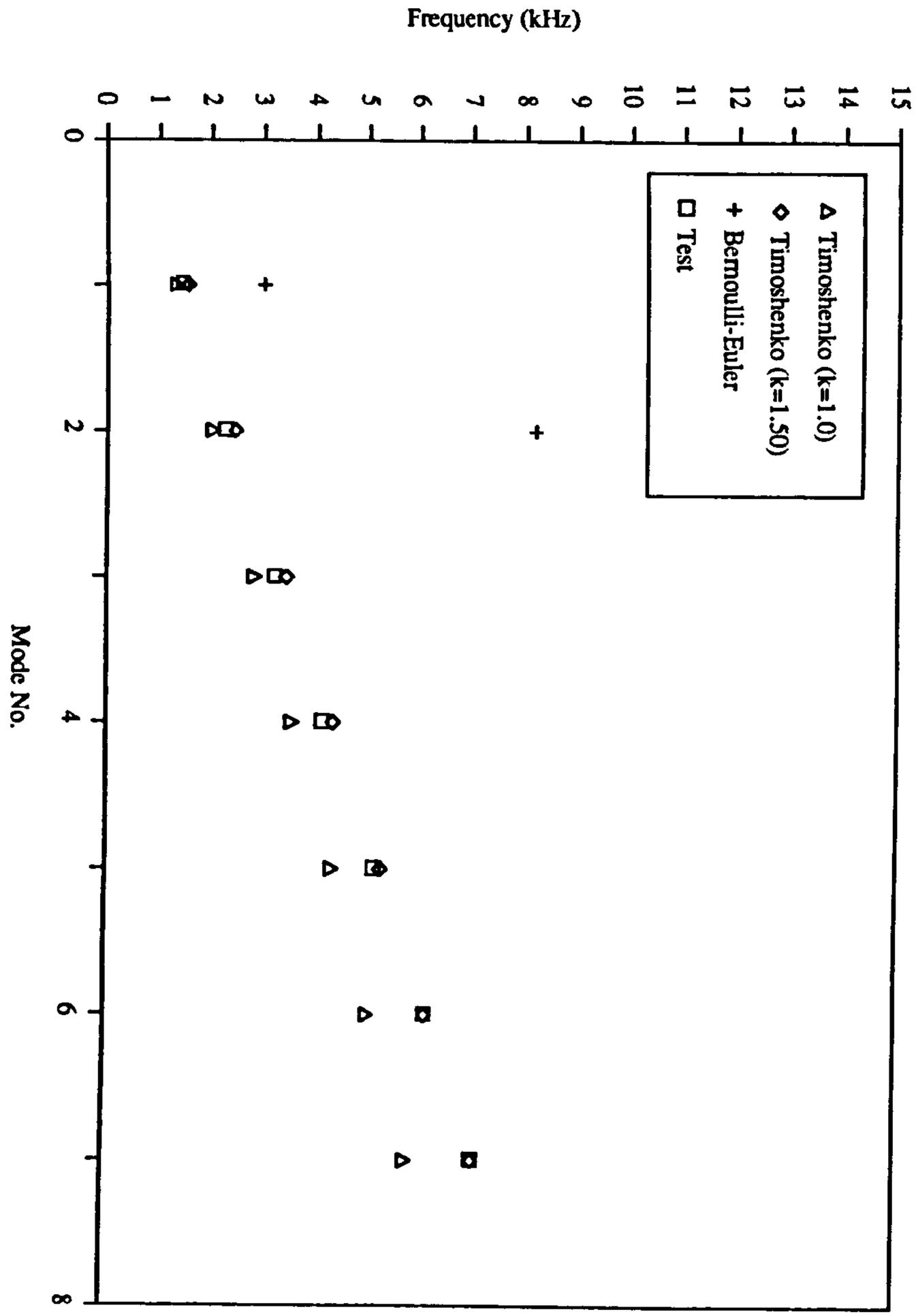

Fig. 6.19 Theoretical SDC Vs Skin fibre orientation

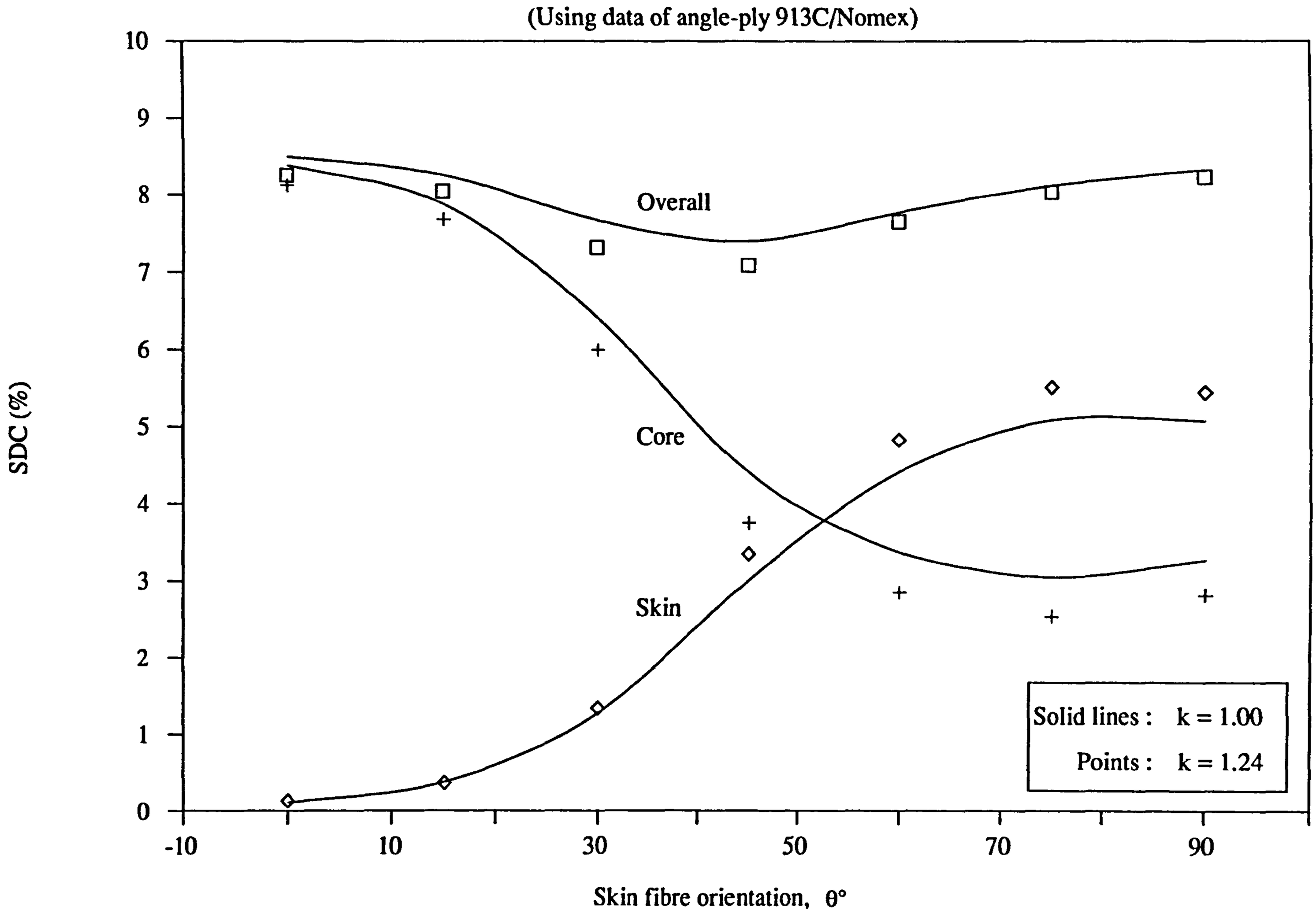

Fig. 6.20 Modulus Vs Skin fibre orientation

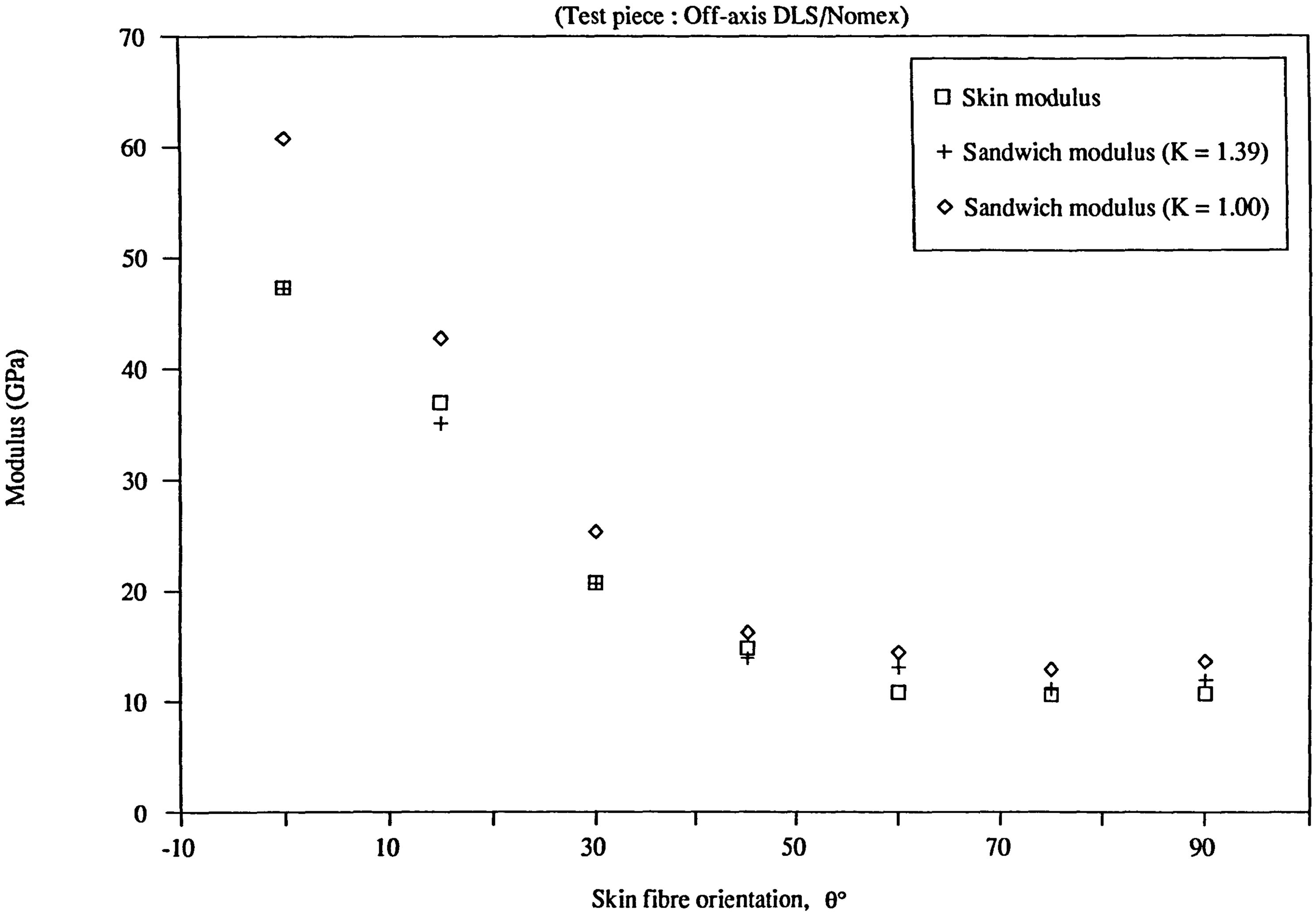

Fig. 6.21 Modulus Vs Skin fibre orientation

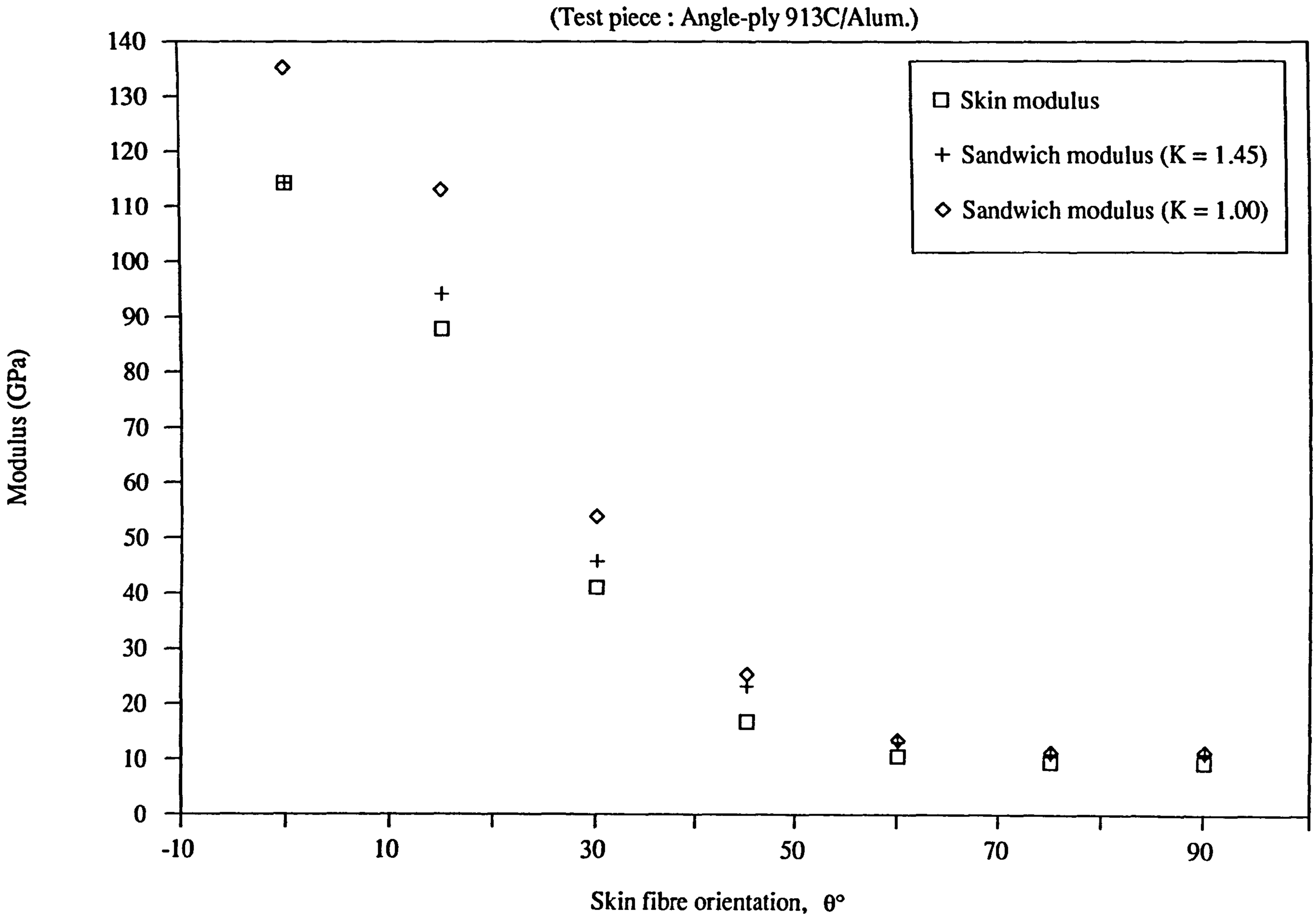

Fig. 6.22 Modulus Vs Skin fibre orientation

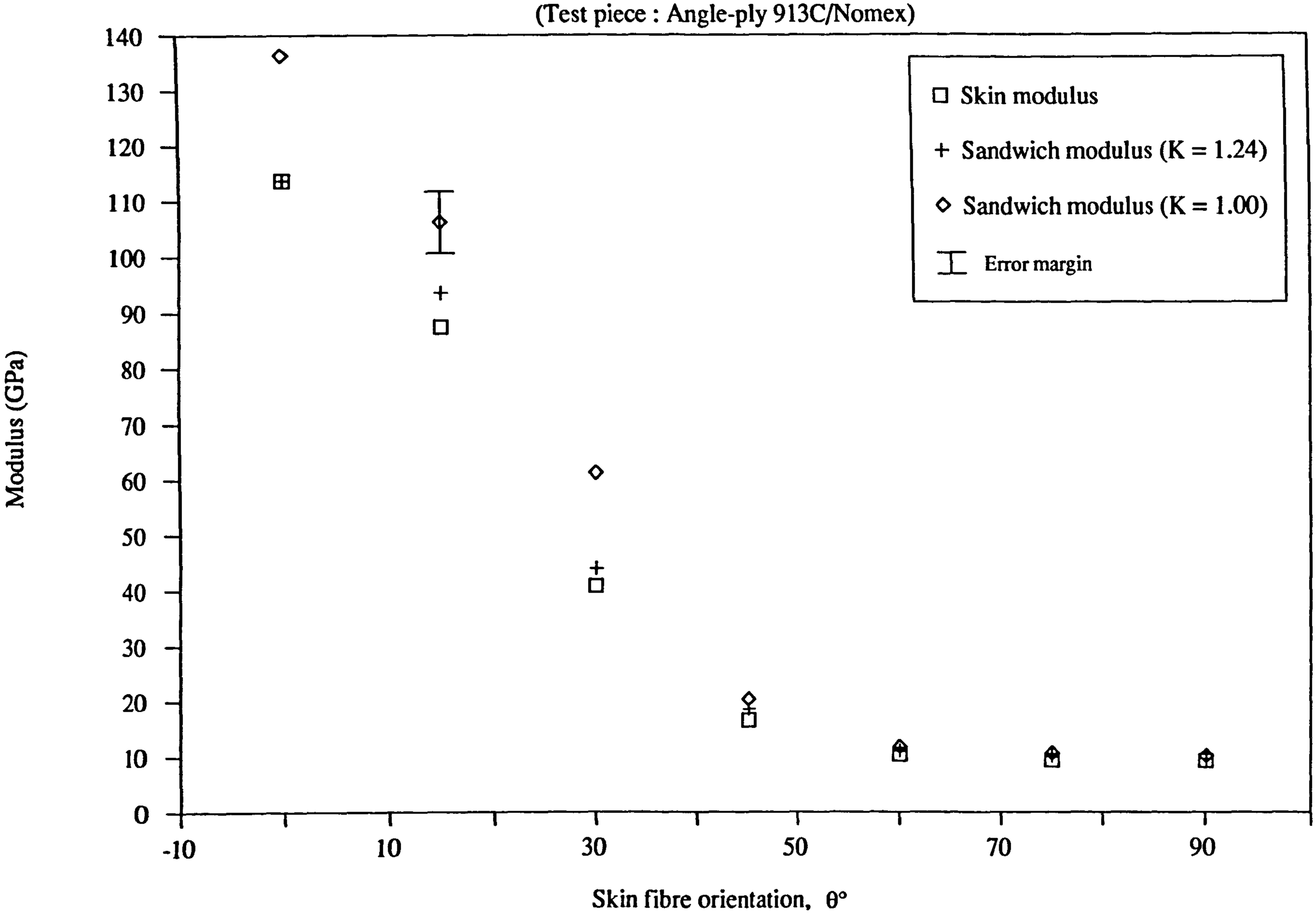

Fig. 6.23 Modulus Vs Skin fibre orientation

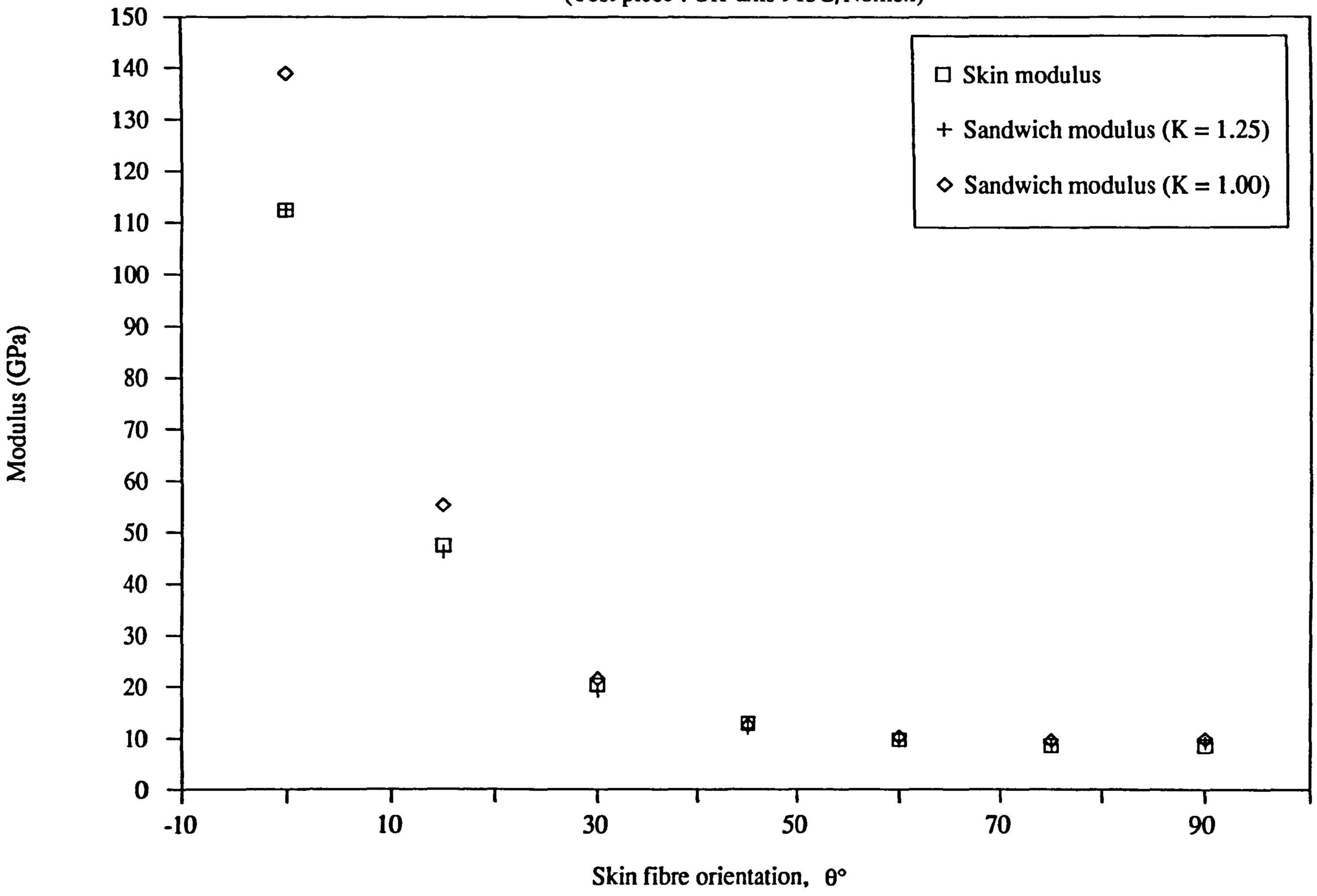

Fig. 6.24 Modulus Vs Skin fibre orientation

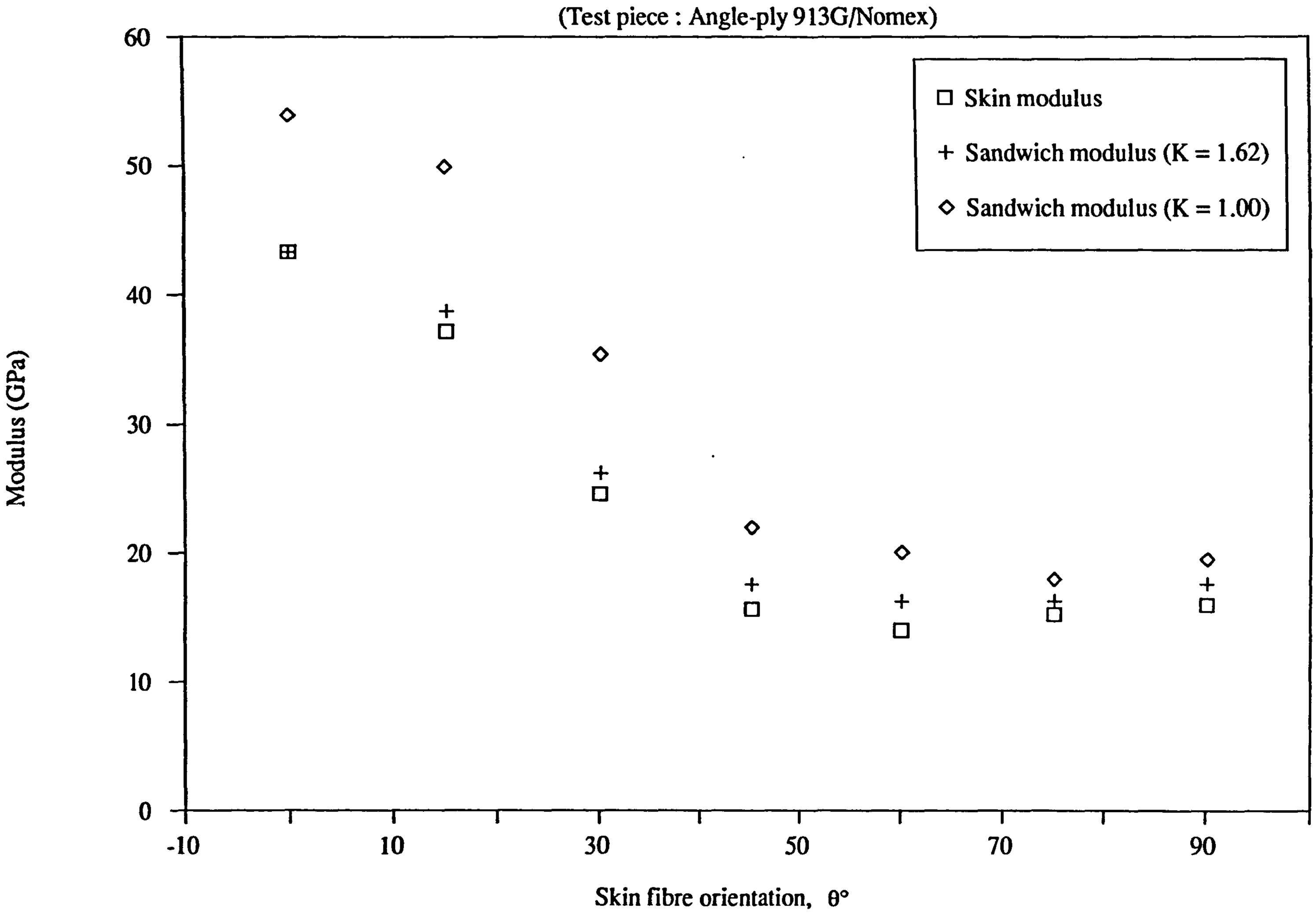

Fig. 6.25 SDC Vs Skin stress amplitude

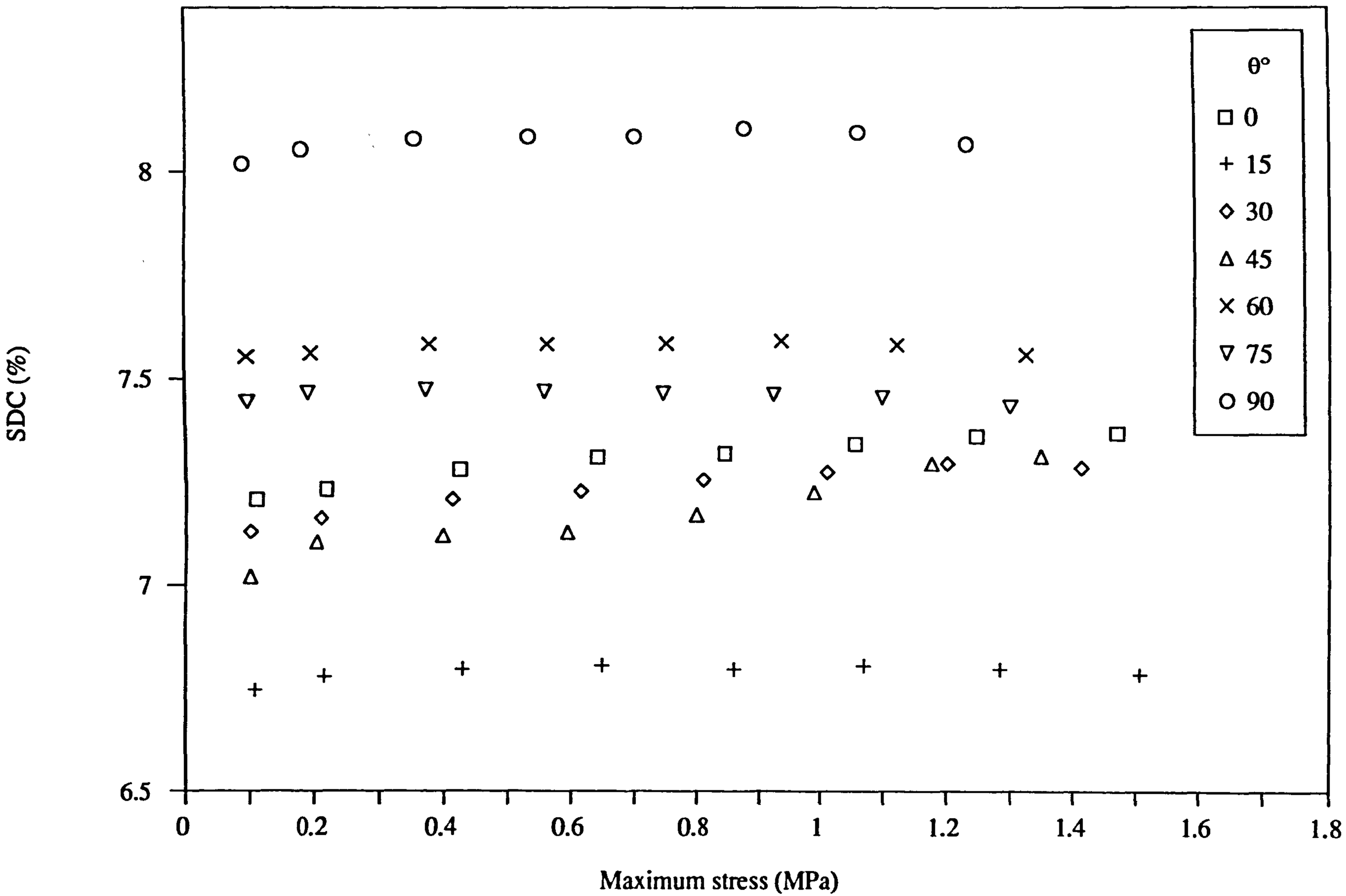

Fig. 6.26 SDC Vs Skin stress amplitude

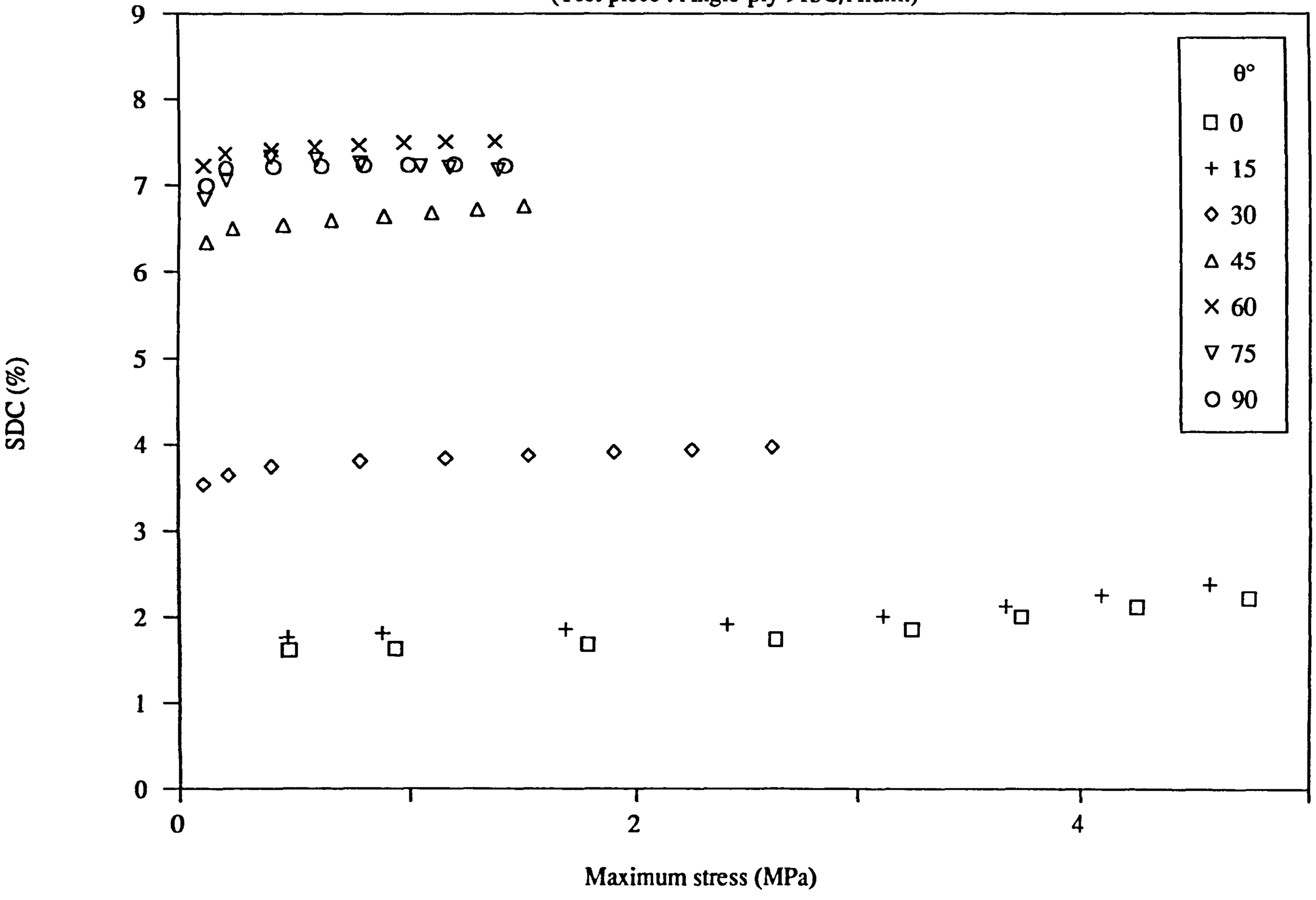

Fig. 6.27 SDC Vs Skin stress amplitude

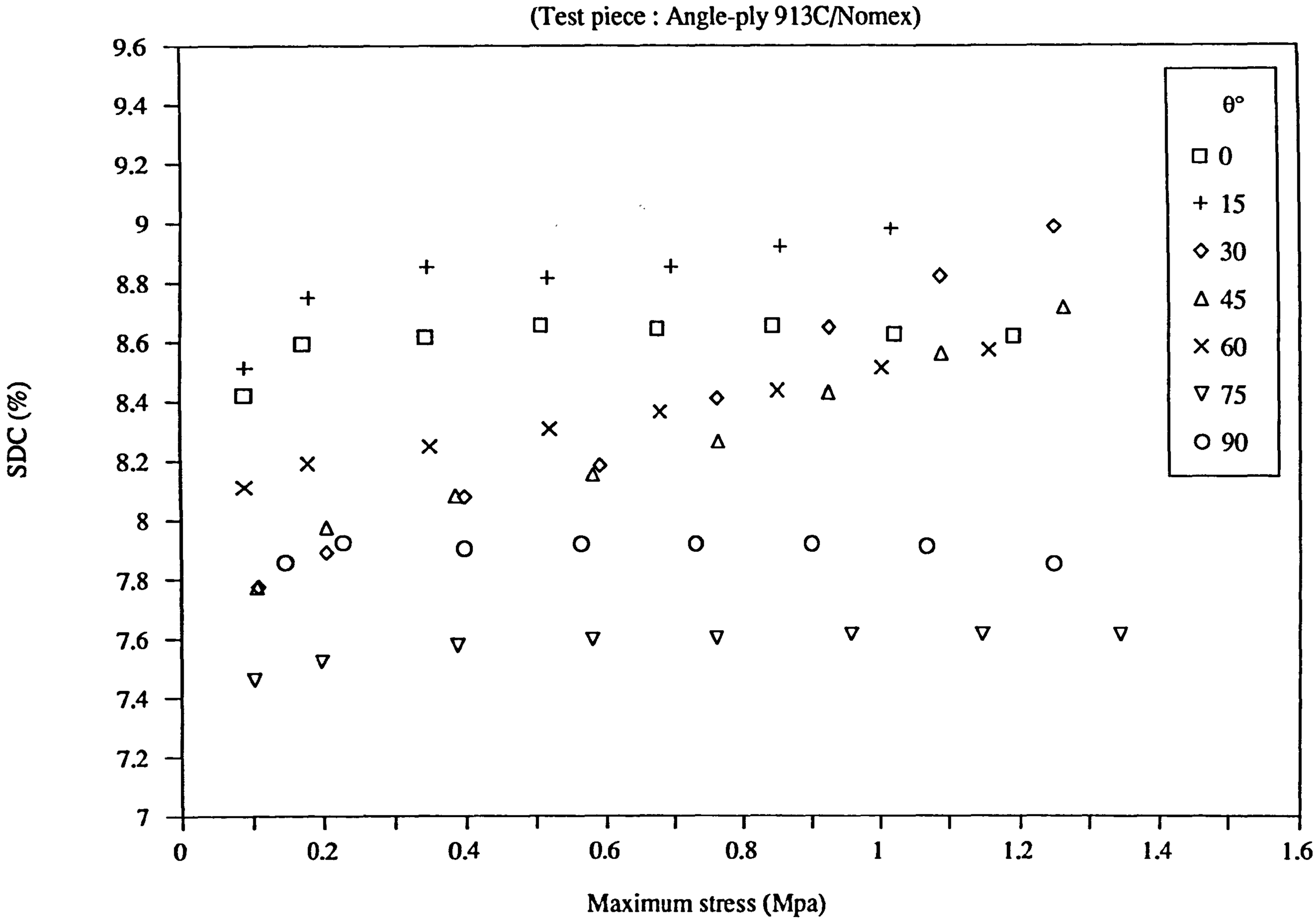

Fig. 6.28 SDC Vs Skin stress amplitude

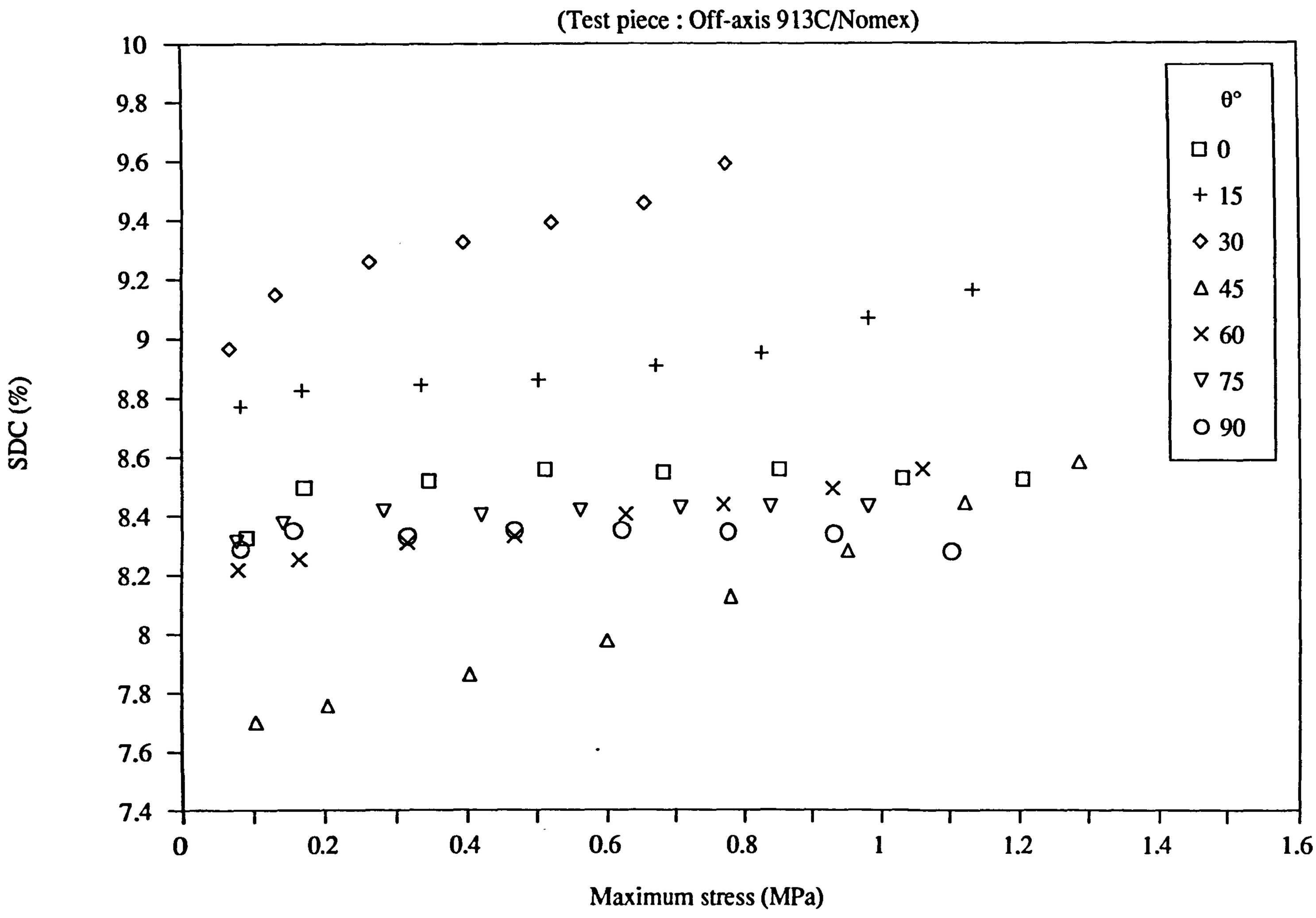

Fig. 6.29 SDC Vs Skin stress amplitude

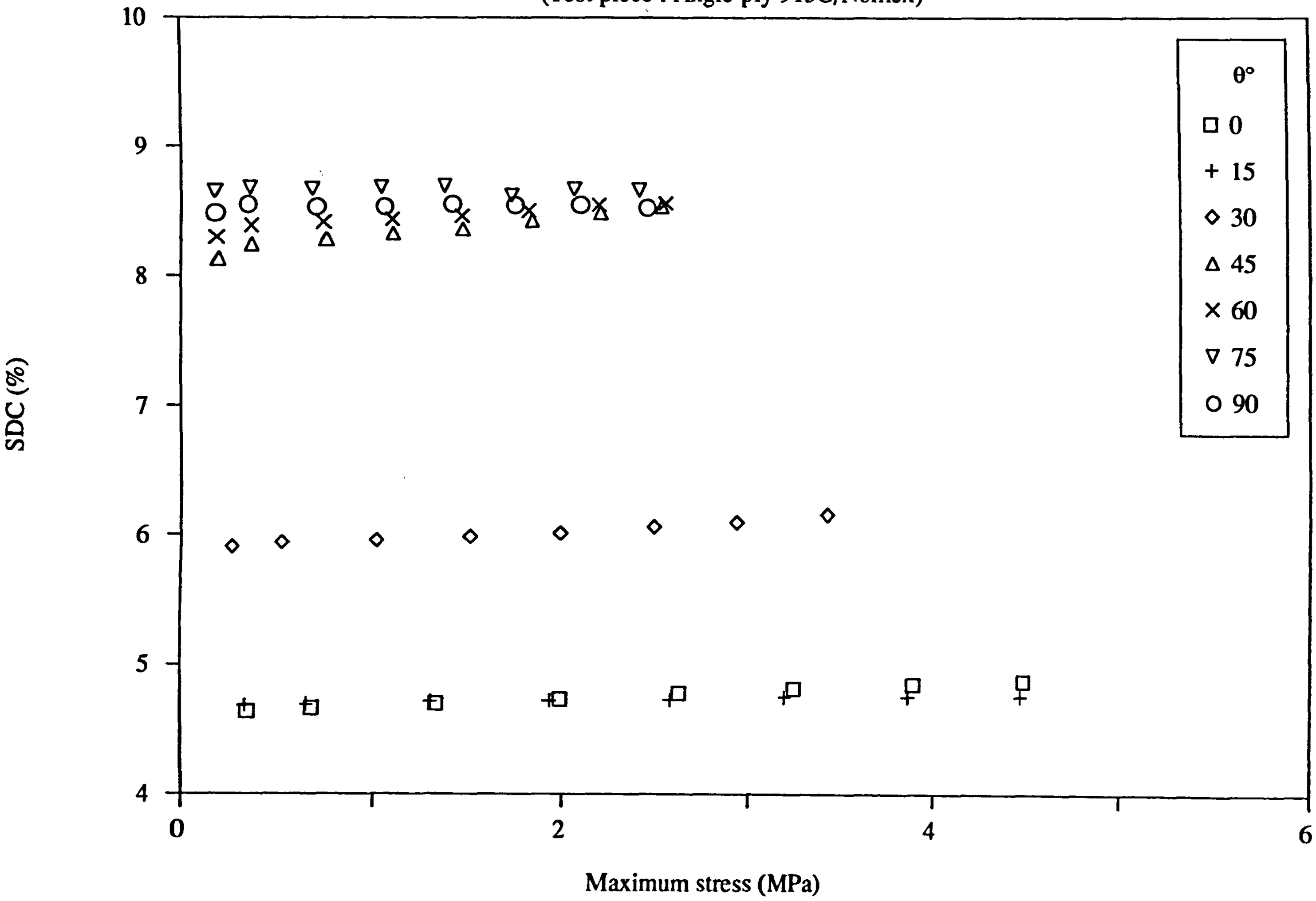

Fig. 6.30 SDC Vs Core stress amplitude

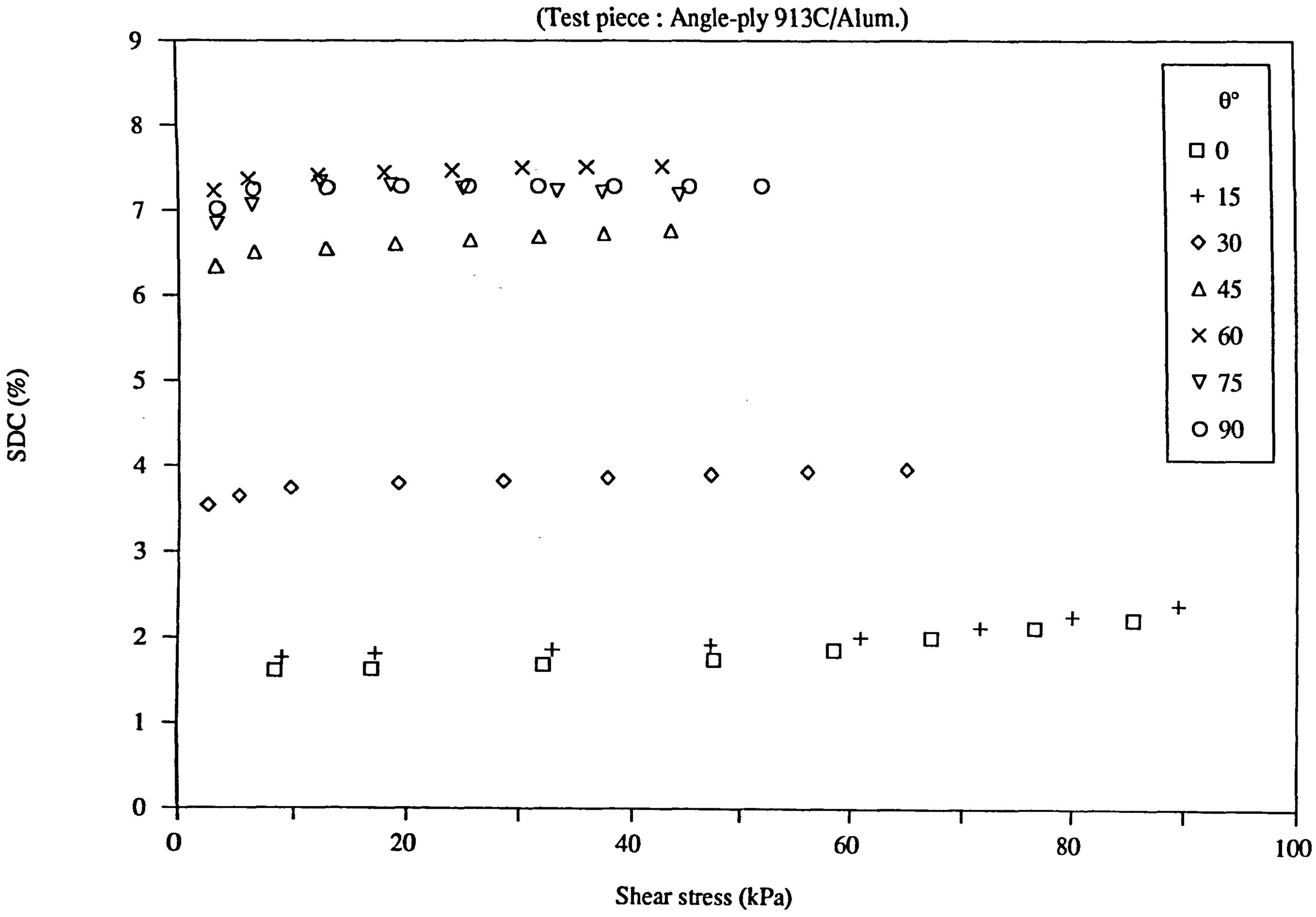

Fig. 6.31 SDC Vs Skin fibre orientation

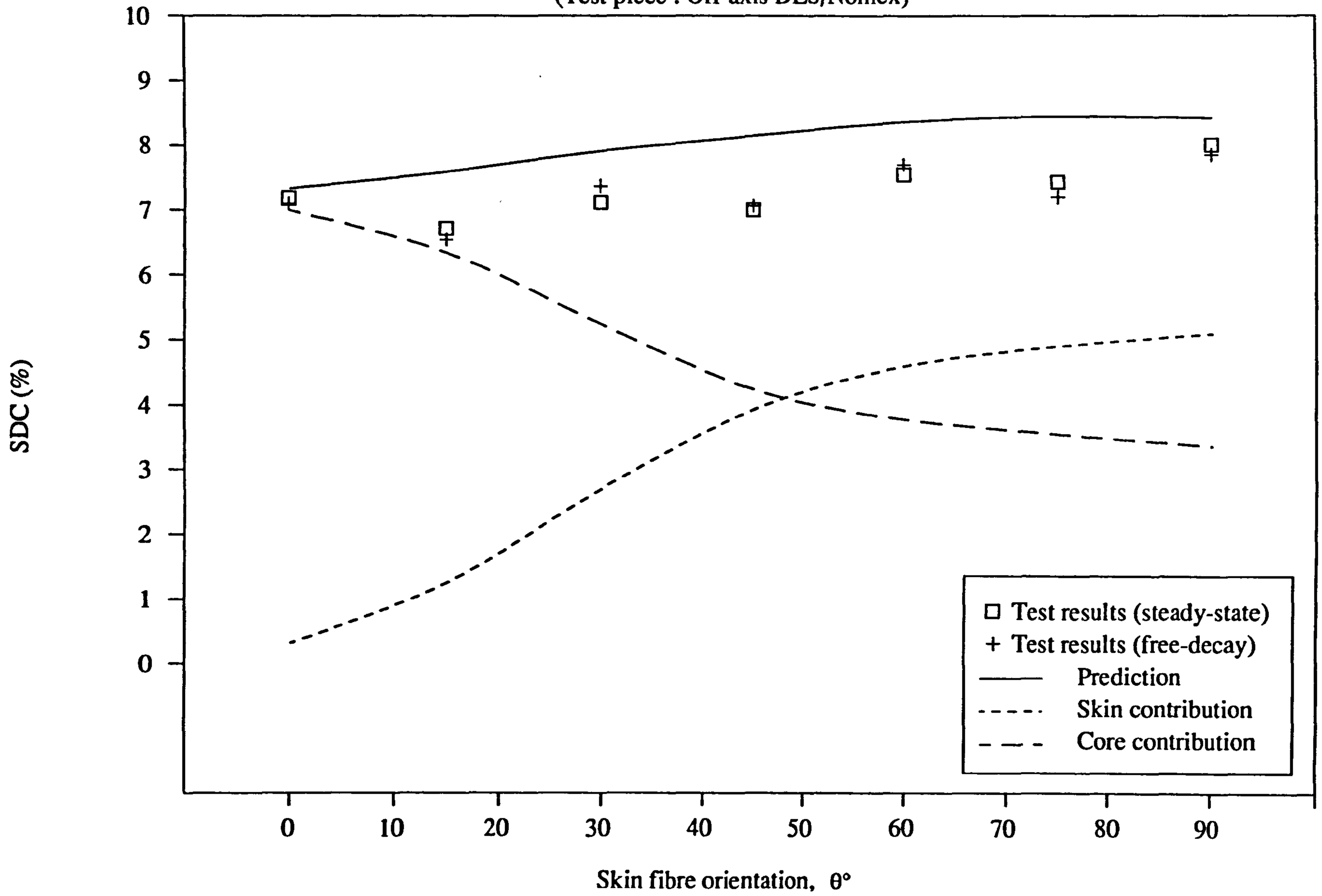

Fig. 6.32 SDC Vs Skin fibre orientation

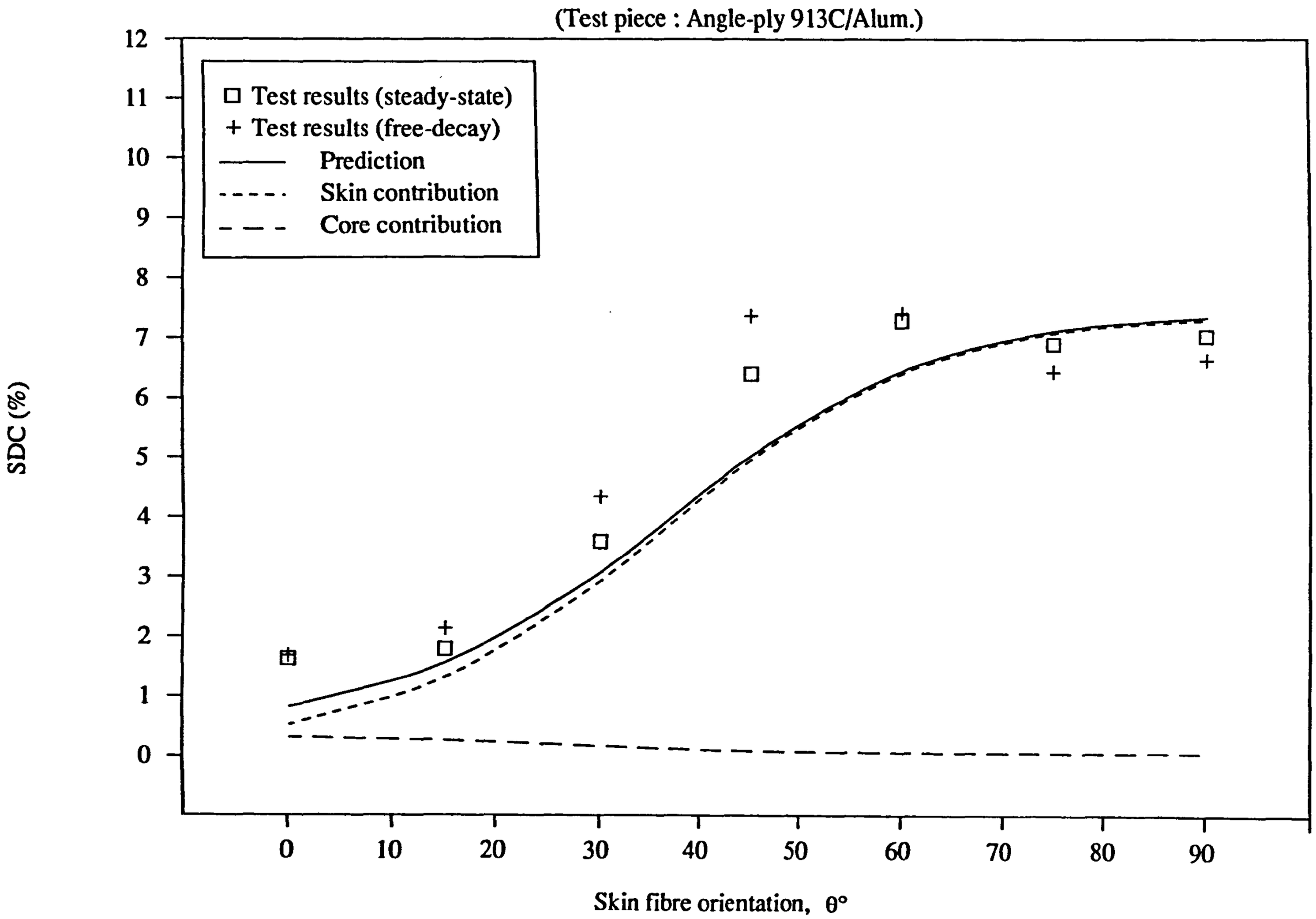

Fig. 6.33 SDC Vs Skin fibre orientation

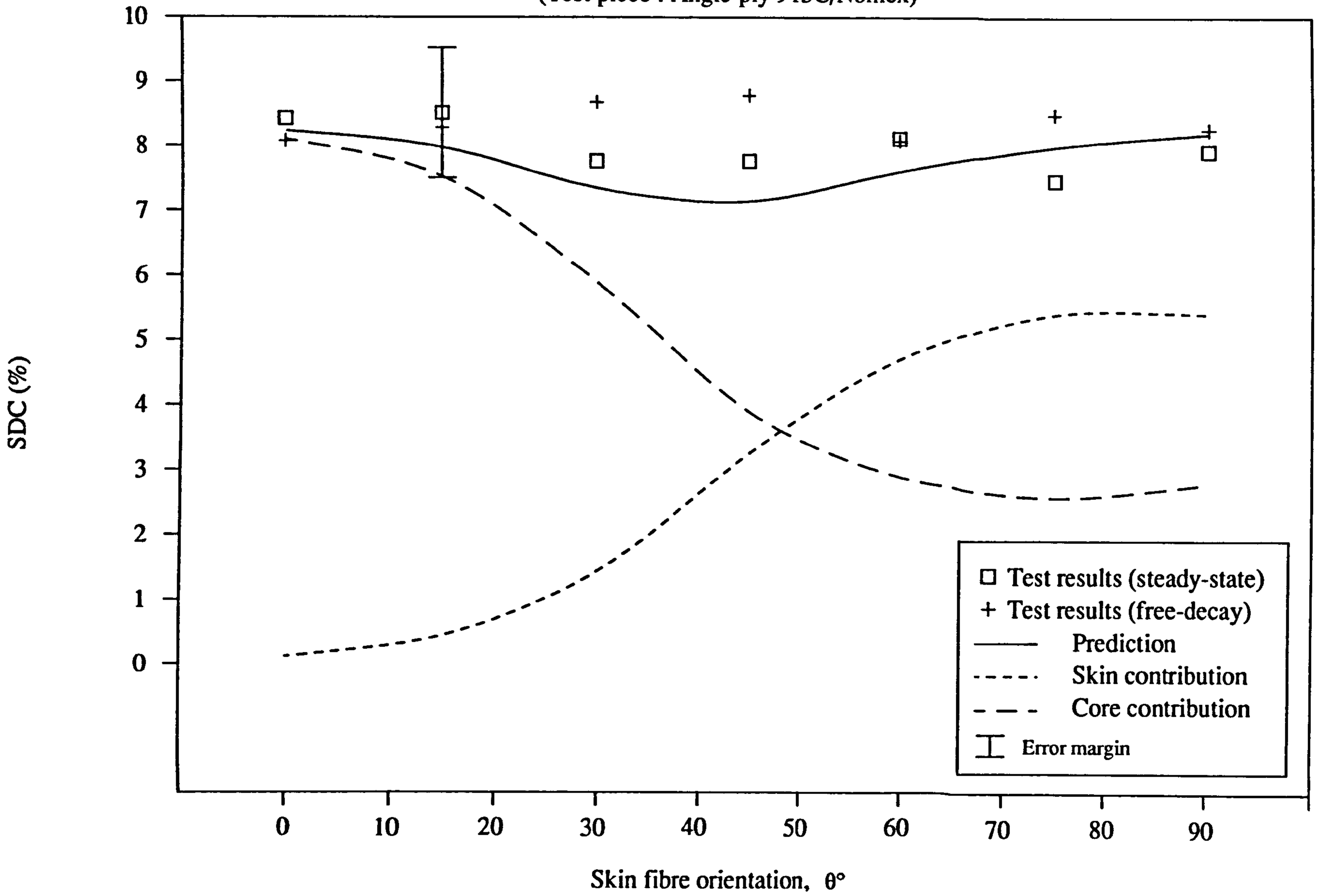

Fig. 6.34 SDC Vs Skin fibre orientation

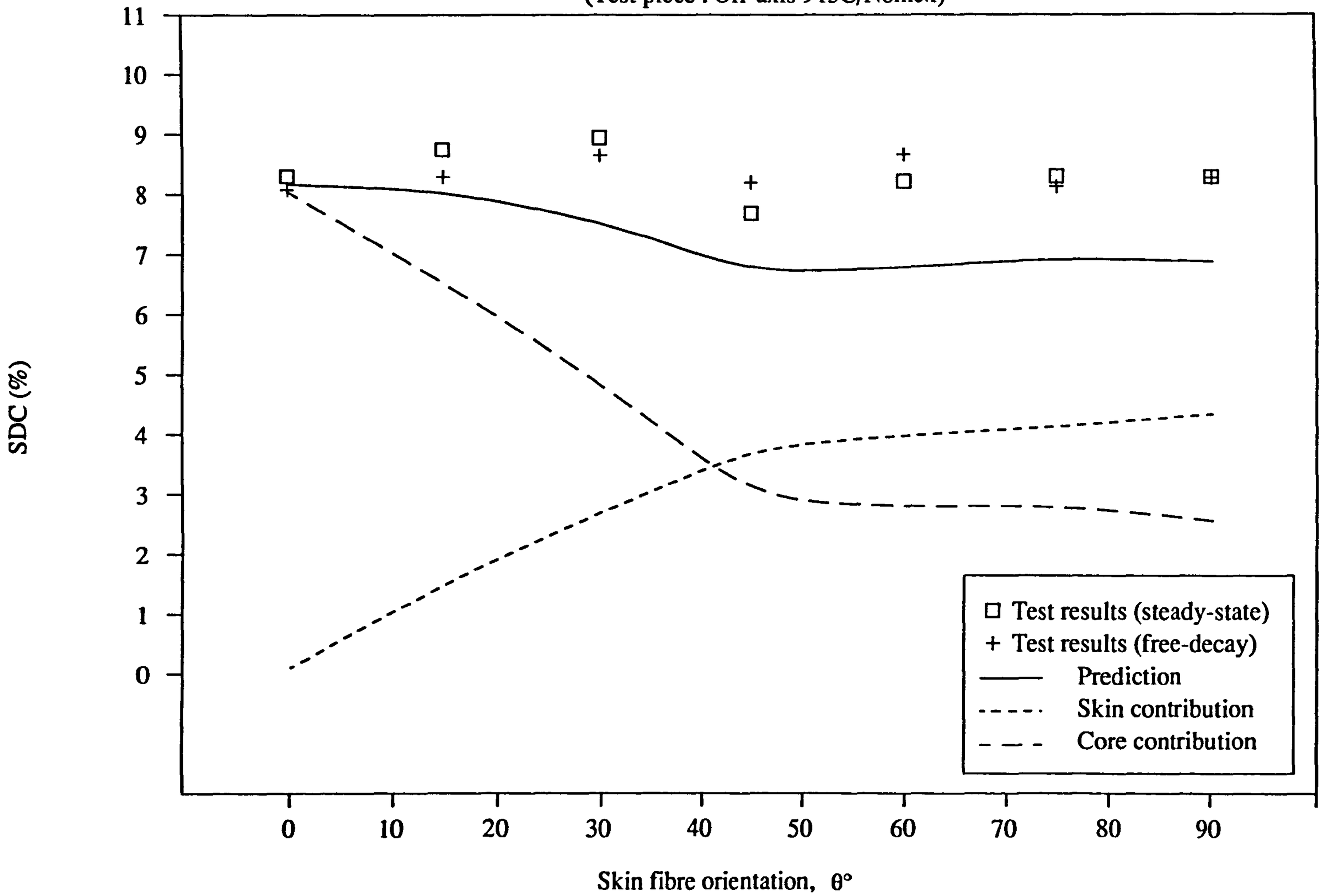

Fig. 6.35 SDC Vs Skin fibre orientation

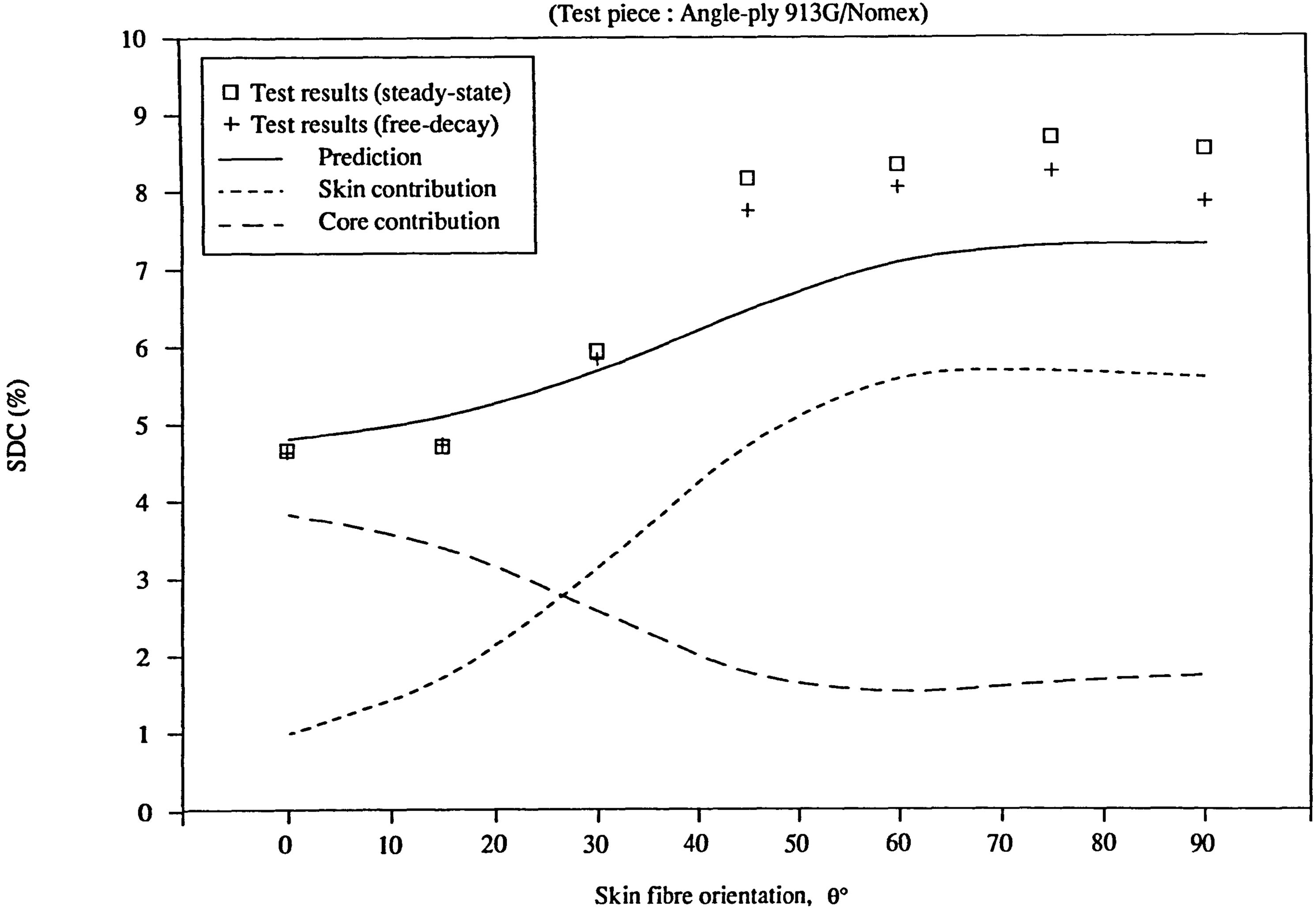

Fig. 6.36 Theoretical SDC Vs Mode No.

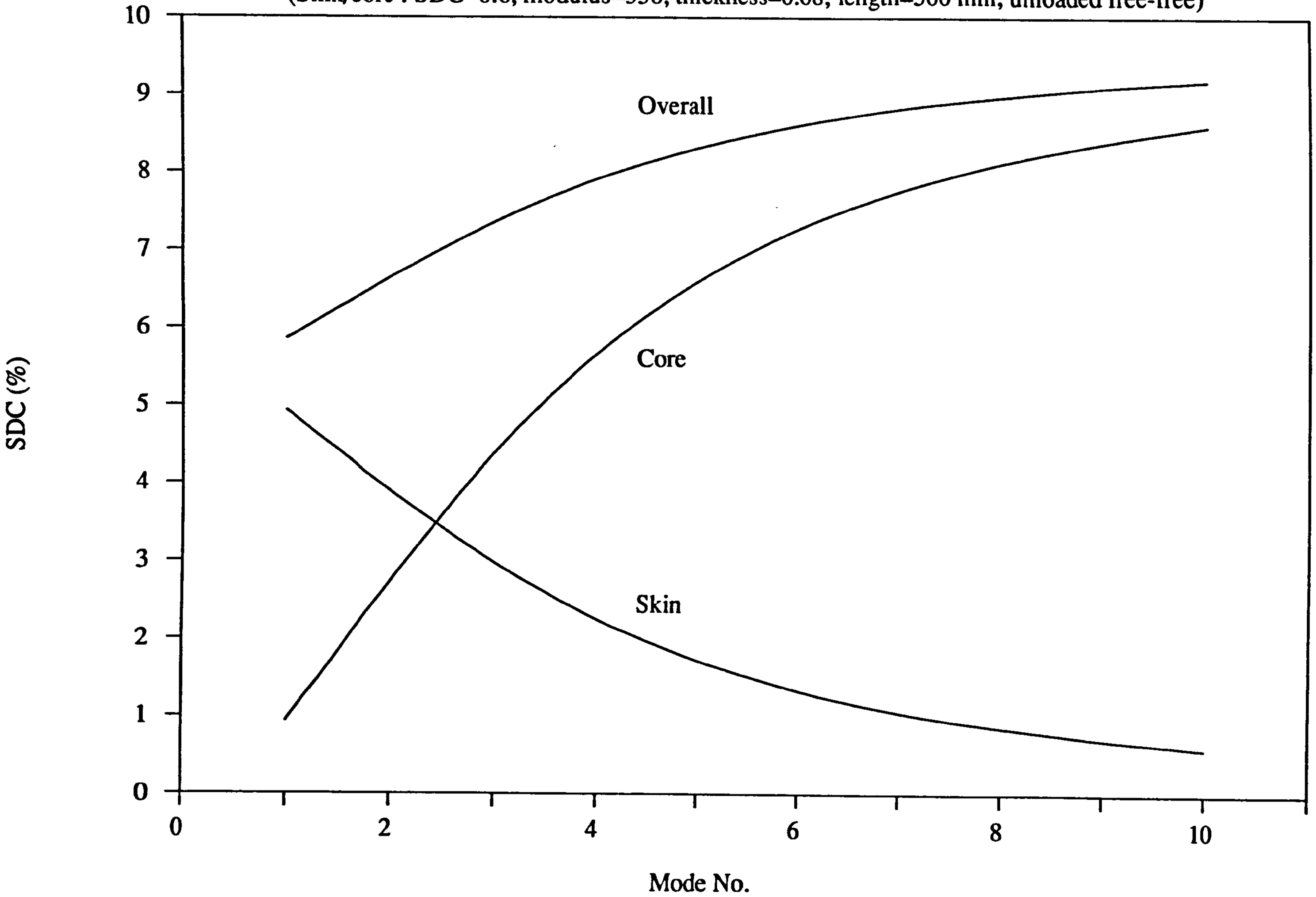

Fig. 6.37 Theoretical SDC Vs Core depth/length

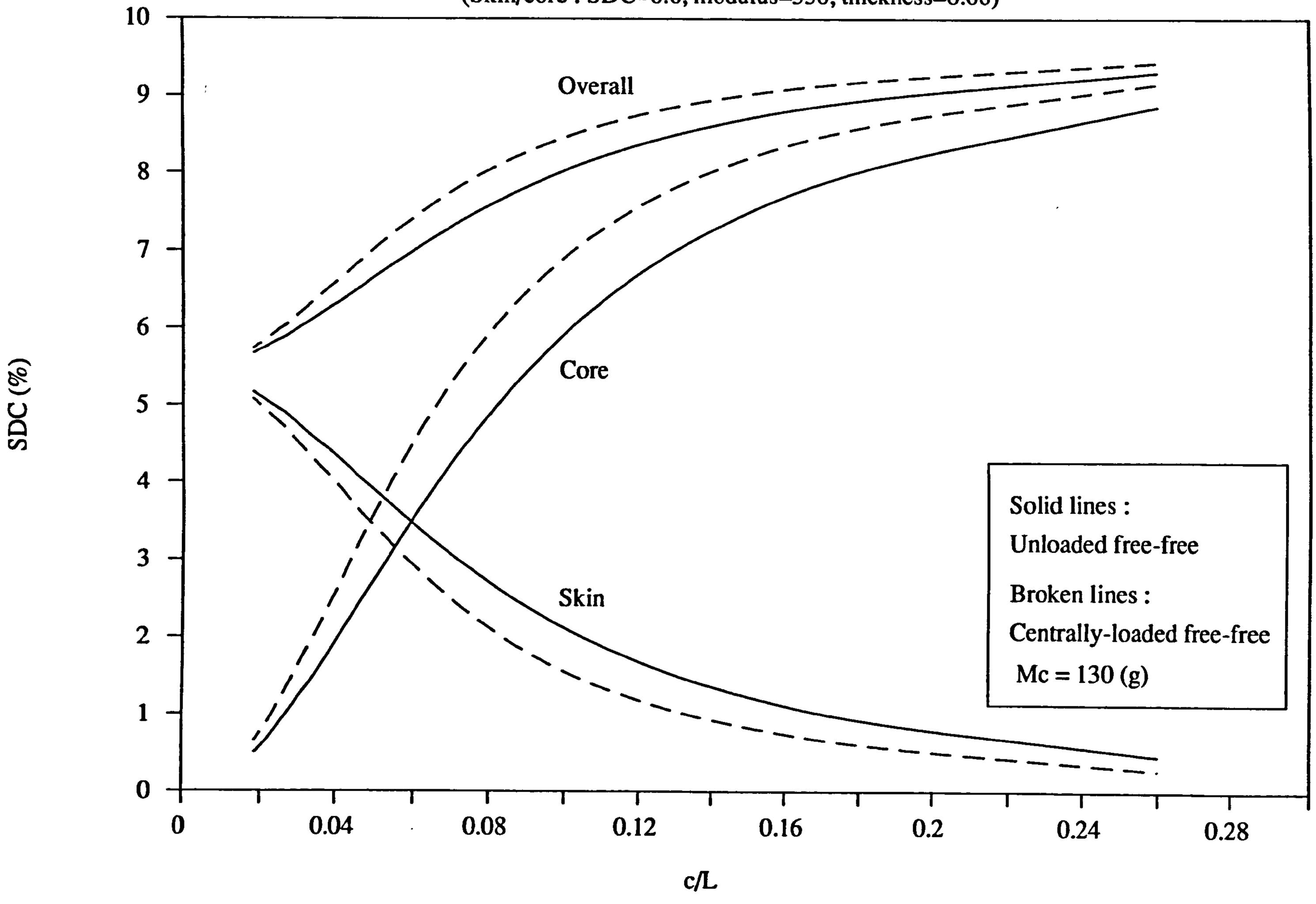

Fig. A.1 Voltage Vs Velocity

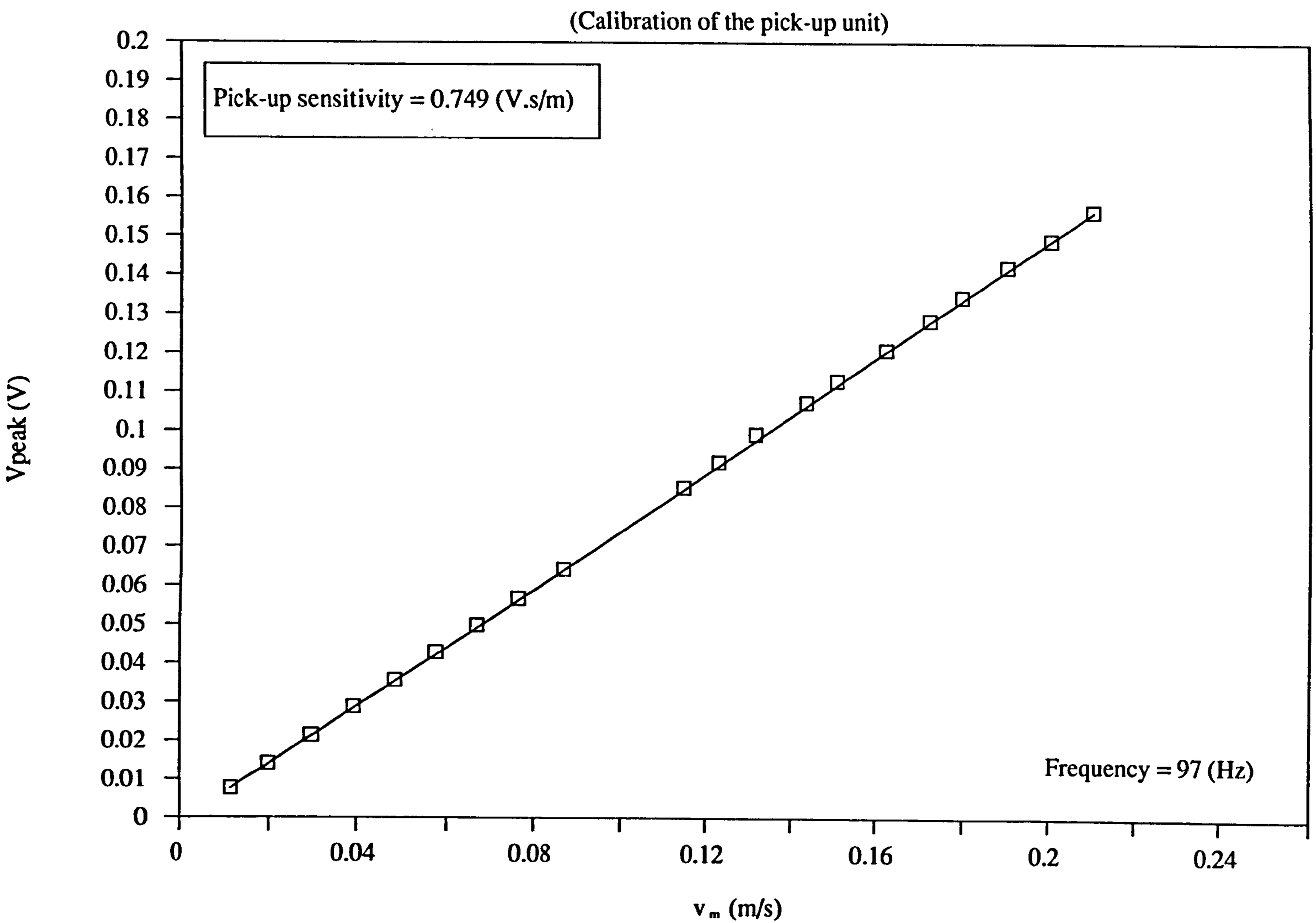

Fig. A.2 Voltage Vs Velocity

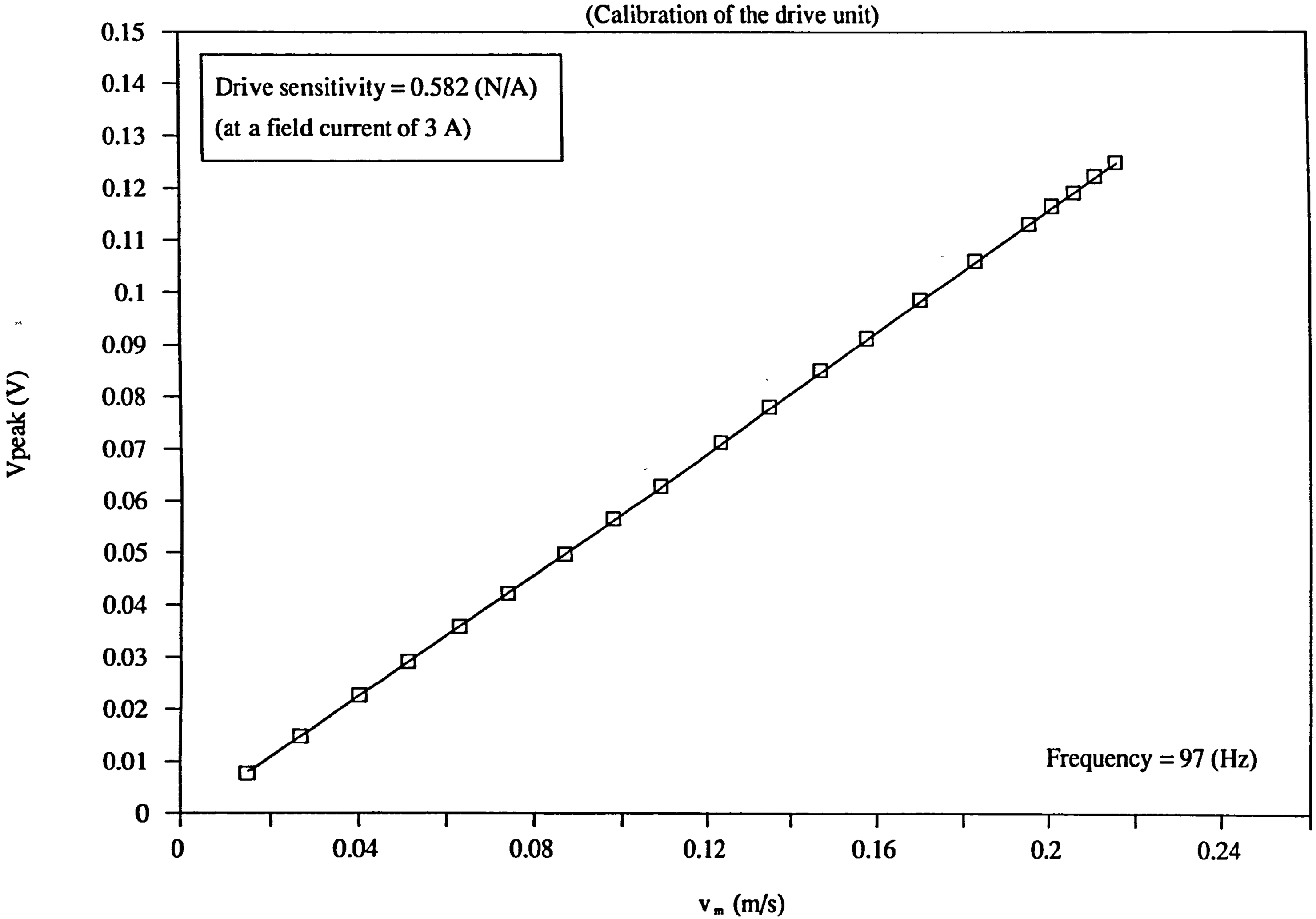

Fig. A.3 Sensitivity Vs Field current

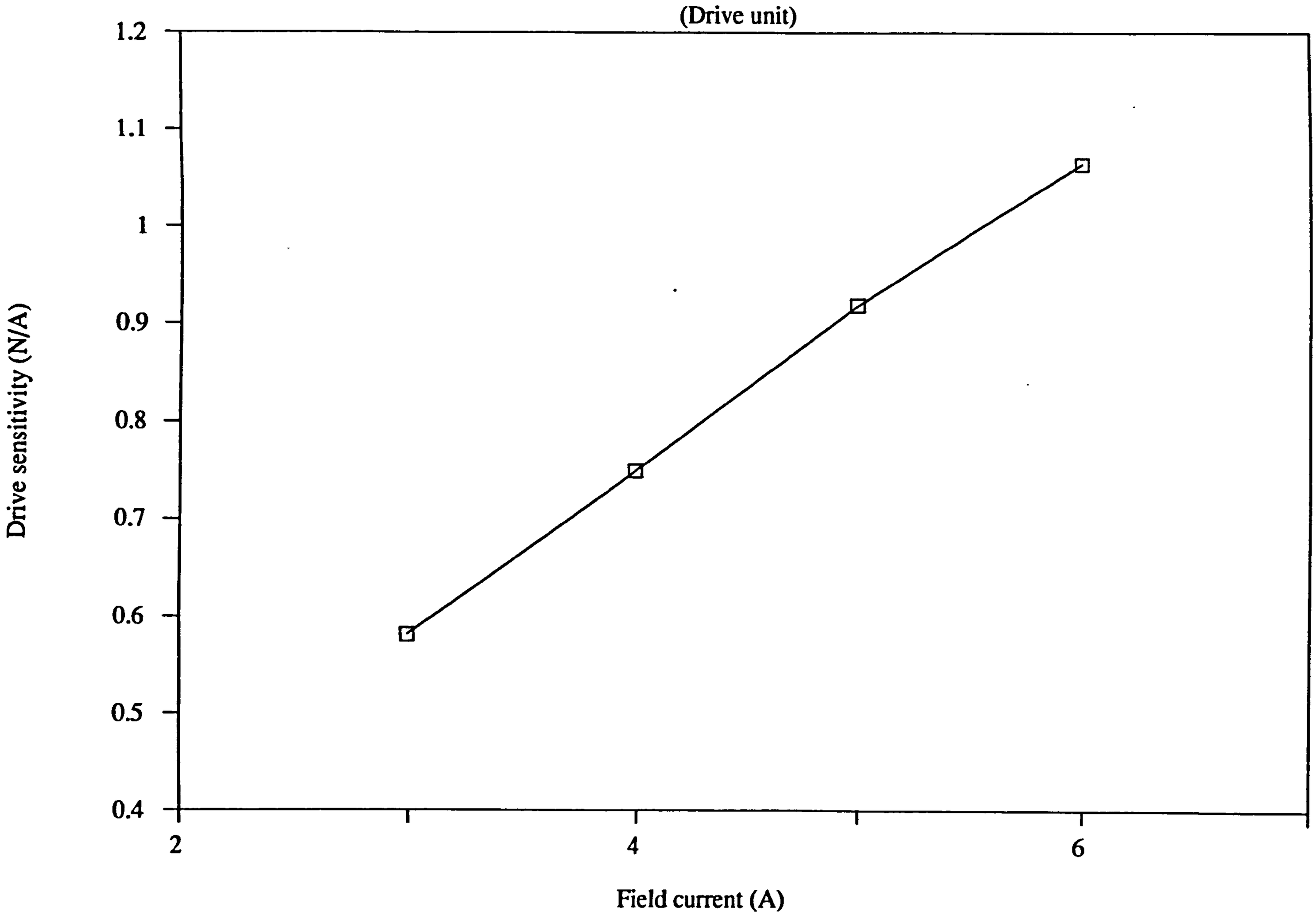

Fig. B.2 Longitudinal shear : SDC Vs Stress amplitude

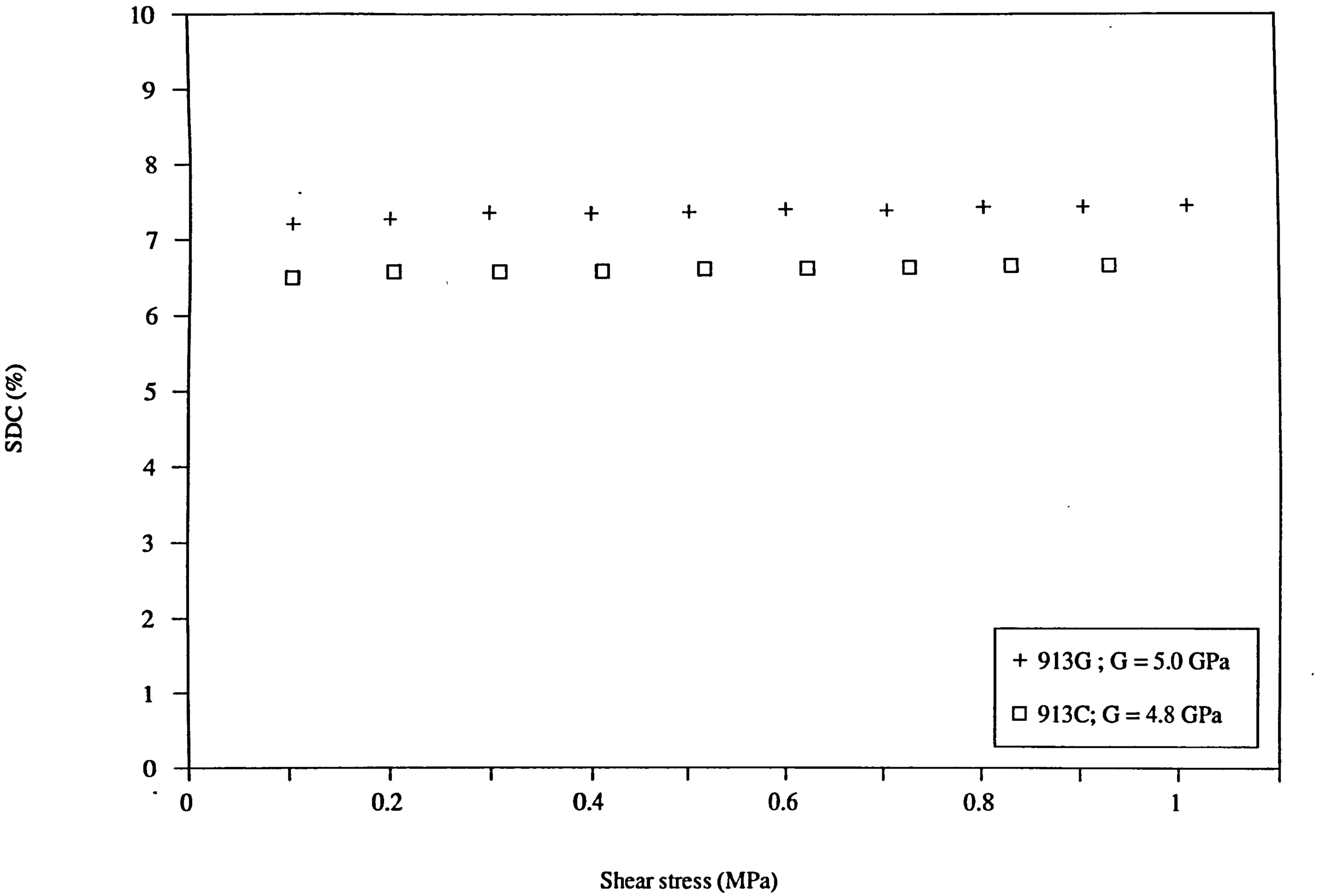

Fig. B.3 Longitudinal shear : SDC Vs Stress amplitude